The Erosion-Corrosion Behaviour of Copper-Nickel Alloys.

By

George E. Vassiliou

Vol. I

A Thesis submitted to

The Department of Mechanical Engineering

University of Glasgow

UNIVERSITY
of
GLASGOW

in fulfilment of the requirement for

The Degree of Doctor of Philosophy

November 2001

ABSTRACT

This research focuses on an investigation of the erosion-corrosion behaviour of Cu-Ni-base alloys in aqueous environments. The principal objectives of the research were to examine the fundamental mechanisms of the erosion-corrosion attack.

The work was focused on a standard *Cu-10%Ni* alloy that is used extensively in a variety of marine industries and on *Marinel* alloy, which is a high strength precipitation-hardened copper-nickel alloy. Erosion-corrosion tests were carried out for exposure times up to 72 hours, in a solid free 3.5% NaCl solution impinging at velocities of 2.38-86 m/sec, (R_e=4500-86000), at temperatures of 19°C and 35°C.

The overall erosion-corrosion behavior and the direct corrosion component were monitored using gravimetric and electrochemical-monitoring techniques. Contributions from mechanical erosion were assessed by cathodically protecting specimens under impingement conditions. The research also considered the influence of various parameters such as temperature, time, velocity, salinity variations, and impingement angle. The extent and morphology of material deterioration and protective film formation under various environmental conditions were assessed, utilizing surface profiling equipment and light optical and scanning electron microscopy.

The work has quantified the complex contributions of corrosion, erosion and synergy to the overall erosion-corrosion material loss. An important finding was the substantial superior erosion-corrosion resistance of Marinel compared to the standard Cu-10%Ni, with interesting effects of impinging velocity and time of exposure being observed. Also this work provided some clear evidence of significant potential benefits in terms of erosion-corrosion resistance, obtained by the exposure of Marinel at the elevated temperature.

CONTENTS

List of Figures.

Figure 6.102. Marinel, V=86m/s, 8 hours, T.W.L., Surface profile with R_a=0.16μm for the entire surface.

Figure 6.103. Marinel, V=86m/s, 8 hours, T.W.L., Central region of the specimen, with a thick yellow film.

Figure 6.104. Marinel, V=86m/s, 8 hours, T.W.L., The grain structure is evident under the jet.

Figure 6.105. Marinel, V=86m/s, 8 hours, T.W.L., Intense pitting attack underneath the thick film outside the central zone.

Figure 6.106. Marinel, V=86m/s, 8 hours, T.W.L., Surface profile under the jet with R_a=020μm.

Figure 6.107. Marinel, V=86m/s, 8 hours, C.P., A discontinuous film under the jet.

Figure 6.108. Marinel, V=86m/s, 8 hours, C.P., The grain structure at the uncovered bits is almost apparent under the jet.

Figure 6.109. Marinel, V=86m/s, 8 hours, C.P., The outside area looks like a ring at the left of the Figure.

Figure 6.110. Marinel, V=86m/s, 8 hours, C.P., The outside area was covered by a thick yellow ring.

Figure 6.111. Marinel, V=86m/s, 8 hours, A.P., A discontinuous film was evident under the jet.

Figure 6.112. Marinel, V=86m/s, 8 hours, A.P., Under the film of above Figure, severe pitting was revealed at high mag.

Figure 6.113. Marinel, V=86m/s, 8 hours, A.P., A ring zone covered by a thick yellow film.

Figure 6.114. Marinel, V=86m/s, 8 hours, A.P., The etched structure with severe pitting covered the rest of the surface.

Figure 6.115. Marinel, V=17m/s, 1 hours, A.R., Surface profile for the entire surface with R_a=0.33• m.

Figure 6.116. Marinel, V=17m/s, 1 hours, A.R., The etched structure with some pits were evident everywhere.

Figure 6.117. Marinel, V=17m/s, 8 hours, A.R., A thicker black-yellow film covered the entire surface.

Figure 9.14. a) Figure similar to Figure 6.22, b) Constant instantaneous corrosion rate between 30mins and 4 hours, at the 4-hour value, c) Constant instantaneous corrosion rate for the whole 4-hour exposure, at the 4-hour value.

Figure 9.15. Anodic and Cathodic polarisation plots of Cu-10%Ni after exposure of 4 hours under a 4mm impinging jet at 4.5m/s. i_{corr}=8.5 $\mu A/cm^2$. The ⊗ indicates the necessary i_{corr} value for the total weight loss to be dominated by the direct corrosion.

List of Tables.

Nomenclature

F.....Faraday's Constant

n.....Number of Electrons

E_o.....Equilibrium electrode potential

I.....Corrosion Current

i.....Corrosion Current Density

β_α.....Tafel Constant

η.....Over Potential

D_z.....Diffusion Coefficient

C_B.....Concentration of ions in bulk solution

δ.....Diffusion layer thickness

G.....Free Energy

Re.....Reynolds number

R.....Universal Gas Constant

Acknowledgements

At the end of my thesis I would like to thank all those people who made this thesis possible and an enjoyable experience for me.

First of all I would like to thank Dr. Trevor Hodgkiess for his supervision, for all the insightful, voluminous comments, and for the amount of time he spent during the writing part of my work. I am also grateful to Dr. Clive Tuck from Langley Alloys for providing the material for this research.

Special thanks go to Prof. John Hancock for his attention and his confidence in the progress of my work, and to Prof. Rex Whitehead for his support and his advises throughout my postgraduate studies.

I wish to express my regards to the technicians of the department for the constant maintenance of the rigs. I am very grateful to the secretaries, Mrs. Fiona Downie, Mrs. Pauline Kyriacou and Miss Jane Livingston for the fruitful exchange of ideas on practical issues. My appreciation is also extended to the guards-janitors, Michael, Jim and Jimmy, for their patience with these envelopes-parcels arriving so often in my pigeon hall.

I would like to express my gratitude to Miss. E.Ford, Mrs. I.Cavoura and Mr. P.McHolland for guiding me during my first year in Glasgow University. The discussions, co-operations and social activities with all of my colleagues have contributed substantially to this work: Pier, Dani, Jorge, and Dimitris have bravely upheld the vision of friendship, laying a sound basis for all future development.

I am indebted to Mr. Socrates Tsihlias, Mrs. Georgia Lemou and Mr. Nikos Kazantzakis, who have not only been a source of enthusiasm and encouragement over many years, but especially for teaching me the joy of writing.

Additional regards go to my teachers, eponymous and anonymous, for passing their knowledge to me, shaping my mind during many technical and non-technical discussions along the way.

Finally, I owe special gratitude to my family for the continuous and unconditional support in order to make all this possible.

To Rania Kakani

Chapter 1

Introduction and Outline of Thesis

1.1 Introduction.

Corrosion when combined with erosion can lead to component failure in a variety of industrial environments including offshore oil and gas, mineral processing and mining. Corrosion on its own can be accentuated by temperature, velocity and salinity while erosion can be influenced by solid content, geometry, velocity and shape of erodent. When the two, corrosion and erosion, are combined, additional interactive or synergistic deterioration can occur. The research described in this thesis was concerned with the erosion-corrosion behaviour of copper-nickel base alloys in saline environments.

These materials are known to possess a long history of use in marine applications, because of their good heat transfer properties, their ease of fabrication and their good resistance to corrosion and biofouling in sea water service; but in erosion-corrosion conditions their ability to resist deterioration reduces.

Much is already known about the erosion-corrosion behaviour of the conventional copper-nickel alloys containing 10% or 30%Ni with and without iron and manganese additions. In this respect, considerable previous effort has been undertaken on erosion-corrosion conditions relevant to the use of these materials in condensers.

Set against the above background the main objectives of the research described in this thesis were twofold.

First, to conduct further investigations of the erosion-corrosion of a standard Cu-10%Ni-Fe-Mn alloy; the emphasis was to learn more about the detailed fundamental mechanisms of attack. The impetus in this respect was to assess the newly found, (and established), information on Cu/Ni alloys against the advances in the understanding of erosion-corrosion phenomena, over a range of engineering materials which have become available in recent years.

Second, to study a fairly-new, high-strength, precipitation-hardened copper-nickel alloy (Marinel), containing about 19% nickel and 4% manganese and strengthened by additions of aluminium, chromium, iron and niobium. In addition to yielding basic

erosion-corrosion data for this alloy, this part of the work comprised a comparison under erosion-corrosion conditions between the two copper nickel alloys. This involved assessing the possible influence of the higher strength properties of Marinel, on the erosion resistance, as well as the other components of its erosion corrosion resistance - the direct corrosion and the synergy.

1.2 Outline of Thesis.

The structure of this thesis is such that Chapter 2 contains all the relevant theory of corrosion and erosion-corrosion subsequently used throughout the thesis.

Chapter 3 introduces the history and use of copper nickel alloys.

Chapter 4 reviews the current literature on the erosion-corrosion behaviour of Cu and Cu-base materials in general, followed by a review in detail, of the current literature, on the erosion-corrosion behaviour of Cu-Ni alloys.

Chapter 5 details of materials studied, experimental equipment, procedures used in this thesis, and any post experiment analysis.

Chapter 6 presents the results related to the effect of velocity and time on erosion-corrosion of Cu-10%Ni and Marinel.

Chapters 7 and 8 continue with the two alloys presenting results on the effect of other parameters on erosion-corrosion tests, and analysing findings on concentric specimens.

Chapter 9 provides a discussion of all the results presented, drawing on major findings and comparing with those in the literature.

Chapter 10 lists the main conclusions from the work and suggests some topics where further work could be useful.

Chapter 2

Industrial Situation – Basic Corrosion and Erosion-Corrosion Principles.

2.1. Relevance to industrial situation.

Rapidly improving standards of living have brought about a changing economic pattern. The world population is growing and material resources are relatively diminishing. Conservation of raw materials is necessary for sociological reasons and because we simply cannot afford the rising cost of dismantling and replacement the old and rusty with the new, and also the loss of production.

The effect of unchecked corrosion is not only confined to the state of the corroding utility itself but it also influences man and his economic and social welfare.

Corrosion is the attack on a metal or alloy by reaction with the environment, with a consequent deterioration of its properties. Deterioration as a result of corrosion has come to be accepted as an unavoidable fact of life whenever metals are used.

Currently the prime motive for research in corrosion is provided by the economic factor. Losses sustained by industry and by the military, amount to many billions of pounds annually.

The economy of a country would be drastically changed if there were no corrosion. For example, ships, oilrigs, desalination plants, pipelines, bridges, would not require coatings or alloys. Proper selection of materials and good design reduces costs of corrosion.

The importance of corrosion studies is threefold [1-2].

The first area of significance is *economic* including the objective of reducing material losses resulting from the corrosion of piping, tanks, metal components of machines, ships, bridges, marine structure, etc.

The second area is *improved safety* of operating equipment which, through corrosion, may fail with catastrophic consequences. Examples are pressure vessels,

boilers, metallic containers for radioactive materials, turbine blades and rotors, bridge cables, aeroplane components, automotive steering mechanisms.

Third is *conservation*, applied primarily to metal resources – the world's supply of these is limited, and the wastage of them includes corresponding losses of energy and water reserves associated with the production and fabrication of metal structure.

Not least important is the accompanying conservation of human effort used in the design and rebuilding of corroded metal equipment, otherwise available for socially useful purposes.

It is quite important to clarify the economic losses as *direct* and *indirect* ones [1].

Direct losses are those for protection, maintenance and replacement of the materials of construction. Direct losses include the extra cost of using corrosion-resistant metals and alloys instead of carbon steel where the latter has adequate mechanical properties but not sufficient corrosion resistance; there are also the costs of galvanising or nickel plating of steel, of adding corrosion inhibitors to water, or of dehumidifying storage rooms for metal equipment.

Indirect losses are more difficult to assess, but a few examples are as follows:

a) *Loss of production.*

The replacement or repair of a corroded piece of equipment may cost little but while the equipment is being repaired the whole plant may shut down for some time, with loss of production.

b) *Reduction in efficiency.*

The accumulation of corrosion products can reduce the efficiency of operating plant. An example is the loss of efficiency due to reduction of heat transfer through accumulated corrosion products.

c) *Product contamination.*

Food processing industries cannot afford to pick-up even small quantities of metal ions in their product. A small amount of copper picked up by slight corrosion of copper piping or of brass equipment that is otherwise durable may damage an entire batch of soap. Copper salts accelerate rancidity of soaps and shorten the time they can be stored before use. Traces of metals may similarly alter the color of dyes. So plants

need to use corrosion-resistant metals and alloys, which puts the capital cost of the plant, due to the necessity to avoid corrosion, much higher.

d) Overdesign.

When a plant is overdesigned, sections used are much thicker than would normally be required for mechanical strength to allow for corrosion. In water treatment and oil industries corrosion allowances of between 50% and 100% are made on susceptible areas of plant. This approach to design results in the need for extra material and goes against the concept of conservation.

e) Maintenance of standby plant and equipment.

Regular shutdowns cannot be tolerated in large integrated factories and replacement sections of plant have to be maintained in readiness to operate when corrosion failure occurs. So this leads to a considerable increase in capital investment.

f) General losses.

The unpredictable failure of critical parts of industrial equipment, aircraft or other means of transport can cause accidents wasting both lives and money. The degree of corrosion involved may be very slight, such as pitting or crevice corrosion.

A hole due to pitting corrosion in a heat exchanger tube could result in the shutdown of a power station, and as a result a whole city may be left without electricity or heating.

Usually when an engineer designs a plant and overdesigns it for corrosion effects he should take into account, when choosing the metal materials, not only general corrosion, which is predictable, but also localised forms of corrosion, which can lead to catastrophic results [3].

An analytical presentation of the basic corrosion principals and the localised types of corrosion damage, like the erosion-corrosion attack, is presented in the following section.

2.2. Basic corrosion principles.

2.2.1. Corrosion in aqueous environments.

The electrochemical mechanism of corrosion can be demonstrated in the set-up shown in Figure 2.1., which illustrates a kind of corrosion referred to as galvanic, (or bimetallic) corrosion. Galvanic corrosion results from the reaction which occurs when two, (or more), dissimilar metals are in contact or are otherwise electrically connected in a conductive solution. Because of the difference in the electrical potentials of the dissimilar metals of the couple, a galvanic current is generated. The *anode*, the more active, i.e. more electronegative metal of the couple, corrodes more rapidly than it would if it were uncoupled in the same medium. The less active, i.e. less electronegative metal, the *cathode*, generally corrodes less than would be the case if it was uncoupled in the same medium. This combination of the two electrical conductors (electrodes), M_1 and M_2, immersed in an electrolyte is called a galvanic cell in honour to Luigi Galvani, a physician in Bologna, Italy who published his studies of electrochemical action in 1791.

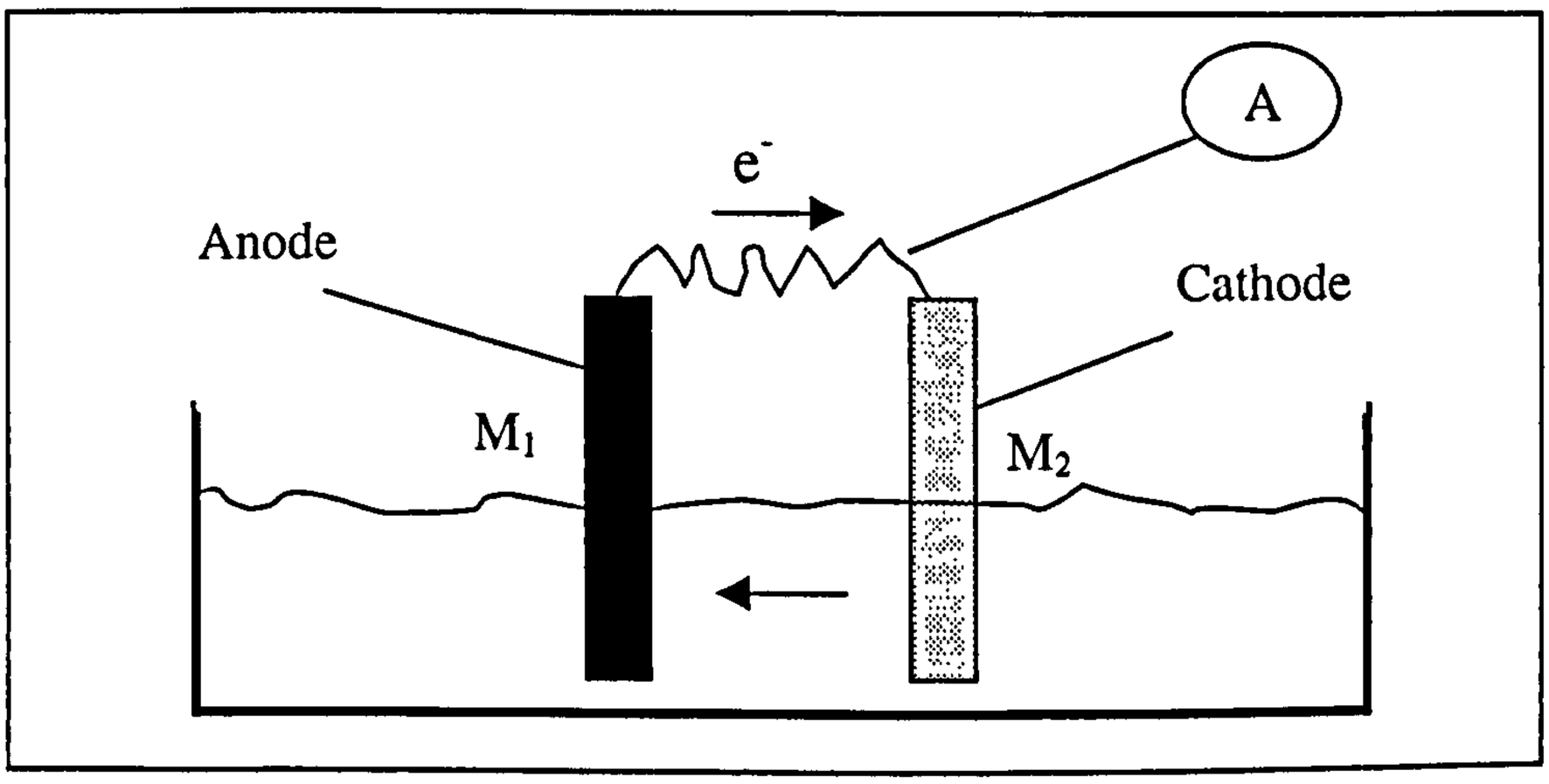

Figure 2.1. Electrochemical cell involving two different metals, (schematic).

There is clearly an association between corrosion on M_1 and flow of current, which can be measured through an ammeter, A. M_1 acts as anode, (supports electron producing reactions) and M_2 acts as cathode, (supports electron consuming reactions). The larger the current flow is, the more severe is corrosion on M_1.

Virtually all metals are basically unstable and have a tendency to revert to their more stable states by combining with other elements present in the surrounding environment, so that their free energy is lowered.

Metals corrode in aqueous environments by an electrochemical process, in which the actual metal loss occurs by dissolution of charged metal ions, M^{n+} (where "n" is the valency), and the production of electrons as follows [4],

$$M = M^{n+} + ne^-$$

For example in the case of Cu:

$$Cu = Cu^{2+} + 2e^-$$

Any reaction which 'releases' electrons, as above, is called "A*nodic reaction*".

In order for the corrosion process to continue, the electrons release by the anodic reaction, must be *consumed* by a "*Cathodic reaction*" occurring simultaneously over the metal surface, which involves substances or chemical species present in the surrounding aqueous environment.

An anodic and a cathodic reaction must occur to have corrosion.

The two most common cathodic reactions in aqueous corrosion situations are the following:

a) In acidic environments (pH below 7),

$$2H^+ + 2e^- = 2H_{ads} \begin{cases} \rightarrow H_{2(g)} \\ \rightarrow 2H_{(m)} \end{cases}$$

where H_{ads} represents a hydrogen atom adsorbed on the metal surface and the two arrows are meant to indicate two alternative 'routes' for the absorbed hydrogen atoms. Thus one possibility is that the latter can combine to yield a hydrogen molecule ($H_{2(g)}$) which is

released from the metal surface either as a gas molecule dissolved in the aqueous environment, or combines with other adsorbed hydrogen atoms to form evolved gas bubbles. The alternative is for the adsorbed hydrogen atoms to become absorbed into the metal, i.e. to diffuse into the interior of the metal (indicated by $H_{(m)}$) and where in certain circumstances with some metals, they can cause embrittlement of the metal.

b) In neutral or alkaline conditions (pH around or above 7), the cathodic reaction is the oxygen-reduction reaction, which involves the reduction of oxygen molecules dissolved in the aqueous environment as follows,

$$O_2 + 2H_2O + 4e^- = 4(OH)^-$$

An anodic and a cathodic reaction must occur to have corrosion. The anodic and cathodic reactions have to balance over the entire component surface. The anodic reaction can not occur any faster that the overall cathodic reaction rate.

In most instances of the corrosion of metal components, both the anodic and cathodic reactions occur on the surface of a single component. In other words the corroding metal is acting like a short-circuited electrochemical cell with the aqueous environment completing the circuit between anodic and cathodic sites. (Figure 2.2.)

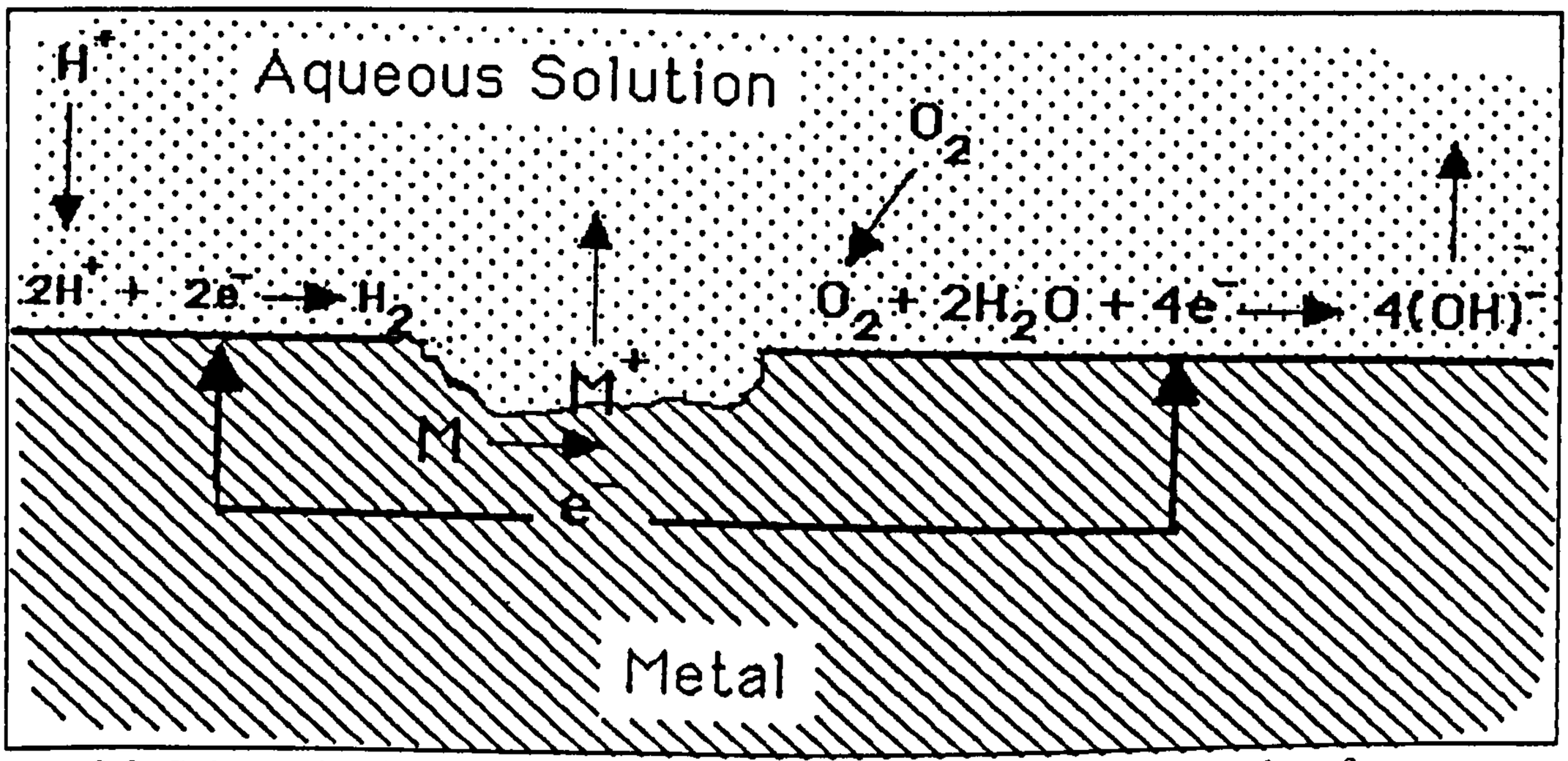

Figure 2.2. Schematic diagram of anodic and cathodic reactions on a metal surface.

When a component is corroding actively, the actual rate of corrosion is often critically dependent upon the progress of the cathodic reaction.

This, in turn, means that in non-acidic environments the supply of dissolved oxygen to the component surface very often controls the corrosion rate. Thus, aqueous environments of high oxygen content are more corrosive than de-oxygenated ones. Another important factor is that the diffusion of dissolved oxygen molecules in water is relatively slow. Consequently, for any given oxygen content, flowing water will cause higher corrosion rates than stagnant conditions because the former situation will facilitate rapid supply of oxygen to the component surface and hence will trigger the oxygen-reduction cathodic reaction.

As with all chemical reactions, there is a change in free energy, ΔG, when these reactions proceed. The free energy change may be associated with an equilibrium electrode potential, E_o, at equilibrium, by the fundamental relationship

$$\Delta G = -n * F * E_o$$

where n is the number of electrons and F is Faraday's constant 96487 coulombs per equivalent. The half-cell reactions, i.e. the anodic and the cathodic, also have free-energy changes analogous to ΔG and corresponding potentials e_a and a_c, (the half cell potentials corresponding to the anodic and cathodic reactions respectively). The algebraic sum of these potentials e_a and e_c is equal to E_o in the equation:

$$E_o = e_a + e_c$$

The potentials e_a and e_c have been called half-cell, single electrode or redox potentials for the corresponding half-cell reactions. It is impossible to measure the absolute value of any half-cell electrode potential. Only cell potentials consisting of two half-cell electrode potentials are measurable, and one must be selected as a primary reference.

2.2.2. Electrochemical Polarisation.

Polarisation is the name given to potential change from a given "reference" potential associated with restricted charge transfer processes at electrodes. In relation to the equilibrium electrode potential, polarisation (η) is the potential change, $E-E_o$. For a cathodic electrode polarisation, η_c, electrons are supplied to the surface, and a build-up in the metal due to the slow reaction rate causes the surface potential, E, to become negative to e_c. For anodic polarisation, η_a, electrons are removed from the metal, a deficiency results in a positive potential change due to the slow liberation from the metal by the surface reaction, hence η_a, is positive.

Polarisation can be classified into two types – activation polarisation and concentration polarisation [5].

2.2.2.1. Activation polarisation.

When the rate of charge flow is controlled by the activation energy required for a particular step, the reaction is said to be under activation or charge-transfer control, and activation polarisation results.

Consider an electrode reaction,

$$O + ne^- \rightleftharpoons R$$

which can occur in either direction.

Let the rate of the cathodic reaction (left→right) controlled by a cathodic current density i_c, and that of the anodic reaction (right→left) by an anodic current density, i_a.

Consider that the reaction is in equilibrium, (with electrode potential, E_o), no net current flows and $i_c=i_a=i_o$, (the exchange current density).

If the potential is shifted from E_o by an amount, η ("overpotential"), a net current, i, flows and $i=i_c=i_a$. The relationship between current and potential for the reaction, in the absence of mass transfer effects, is given by [163]:

$$i = i_o\left[\exp\left(-\frac{\alpha nF\eta}{RT}\right) - \exp\left(\frac{(1-\alpha)nF\eta}{RT}\right)\right]$$

where α is the transfer coefficient, n is the number of electrons associated with the reaction, η is the overvoltage, and F, R, and T have their usual meaning.

The above equation is usually simplified at high overvoltages, where the reverse reaction current can be neglected, to the well known Tafel equation, namely

$$\log i = \log i_o + \frac{\alpha n F \eta}{2.3RT}$$

If the shift in potential from E_o is in the positive (anodic) direction, η_a, then the mathematical equation is

$$\eta_a = \beta_a * \log_{10} \frac{i_a}{i_o}$$

where β_a is known as the "Tafel constant".

The above relationship is illustrated in Figure 2.3.

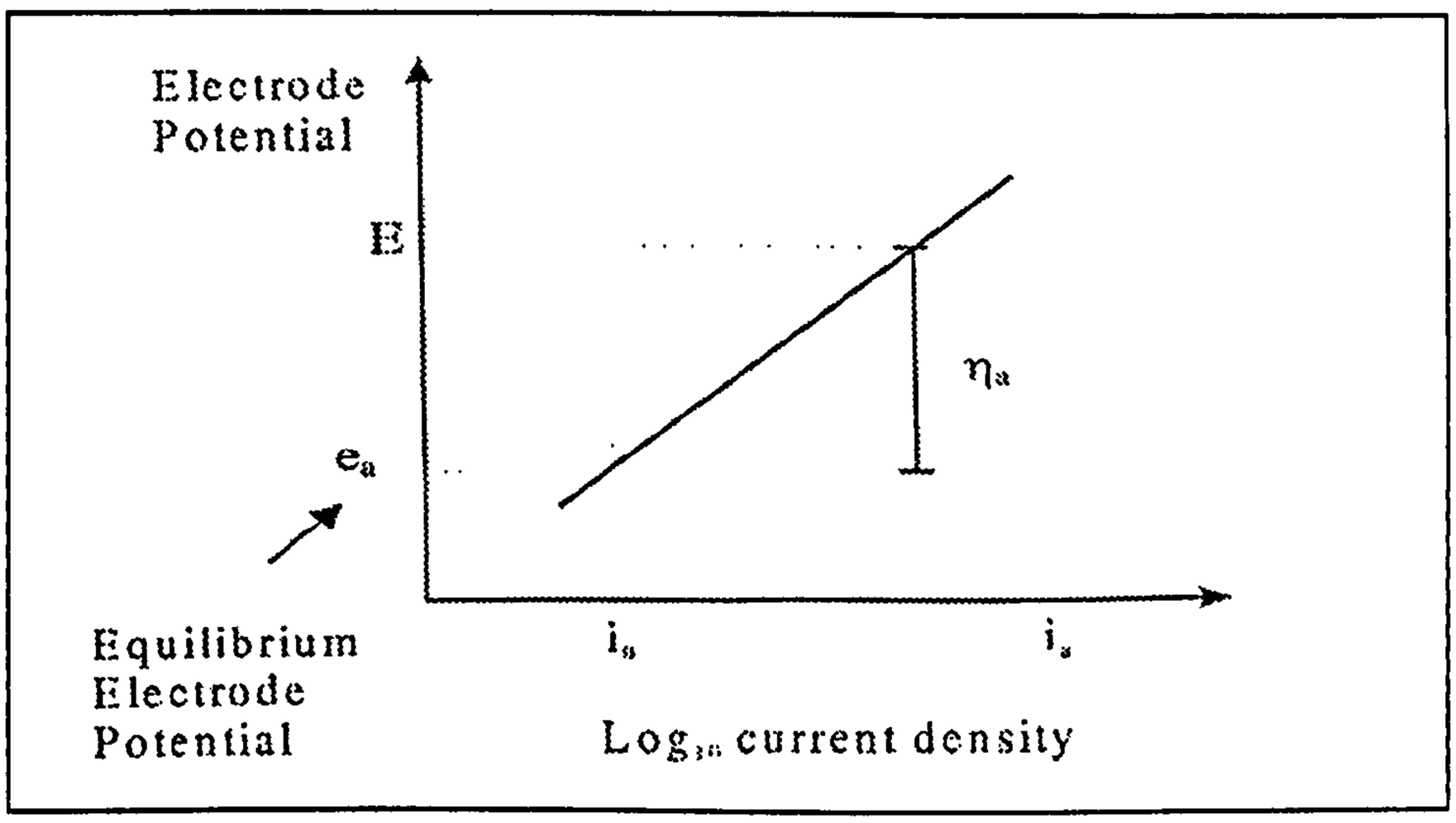

Figure 2.3. i_a/E plot for anodic reaction subject to activation polarisation.

Similarly for a cathodic reaction, the corresponding relationship is :

$$\eta_c = \beta_c * \log_{10} \frac{i_c}{i_o}$$

2.2.2.2. Concentration polarisation.

Concentration polarisation occurs where the progress of an electrode reaction is hindered by the rate of supply of reactants to or removal of products from the surface. For corrosion, concentration polarisation is significant mainly for the oxygen reduction reaction and it is usually negligible for anodic reactions because of the unlimited supply of metal atoms at the interface and the relatively rapid diffusion of metal ions away from the metal surface.

The potential change resulting from concentration polarisation can be expressed as:

$$\eta_{(concentration)} = 2.3 * \frac{R * T}{n * F} * \log \frac{i_L - i}{i_L}$$

where R is the universal gas constant, T is the temperature, η is the number of electrons, F is Faraday's constant, i_L the limited diffusion current density and i is the actual current density. This is shown graphically in Figure 2.4. The limiting current density, i_L, is a measure of the maximum reaction rate that can not be exceeded because of a limited diffusion rate of ions or molecules through the bulk solution where :

$$i_L = \frac{D_Z * \eta * F * C_B}{\delta}$$

D_Z is the diffusion coefficient of the reacting species, in this case oxygen; C_B is the concentration of oxygen in the bulk solution and δ is the thickness of the diffusion layer.

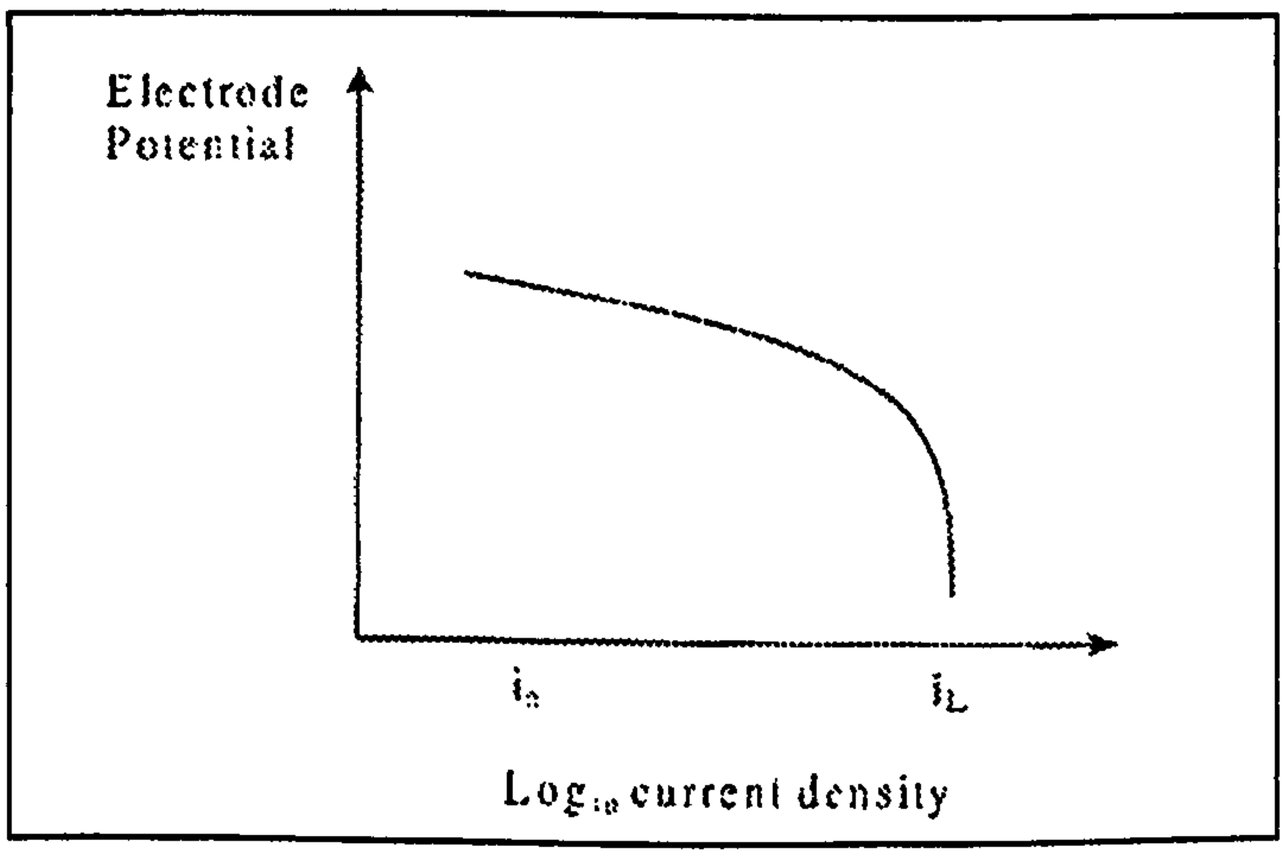

Figure 2.4. Polarisation curve for cathodic reaction undergoing concentration polarisation.

2.2.3. Mixed potential theory.

When the metal is corroding in an aqueous solution, both the anodic

$$M \rightleftharpoons M^{n+} + ne^-$$

and the cathodic

$$2H^+ + 2e^- \rightleftharpoons H_2$$

half cell reactions occur simultaneously on the surface. Each half-cell reaction has its own equilibrium electrode potential, E_o, and exchange current density, i_o, which represents a dynamic equilibrium corresponding to the balance of current caused by the forward and reverse reactions and which cannot exist separately on an electrically conductive surface. Each must polarise or change potential to a common intermediate value, E_{corr}, which is called the corrosion potential.

As the anodic and cathodic reactions polarise on the same surface, the half-cell electrode potentials, (assuming activation polarisation dominates), change according to

$$\eta_a = \beta_a * \log_{10} \frac{i_a}{i_o}$$

and

$$\eta_c = \beta_c * \log_{10} \frac{i_c}{i_o}$$

until they become equal to E_{corr} as shown in Figure 2.5. Also the rate of anodic dissolution, i_a, is identical to the corrosion rate, i_{corr}, in terms of current density, at E_{corr}, as indicated in Figure 2.5.

$$i_c = i_a = i_{corr}$$

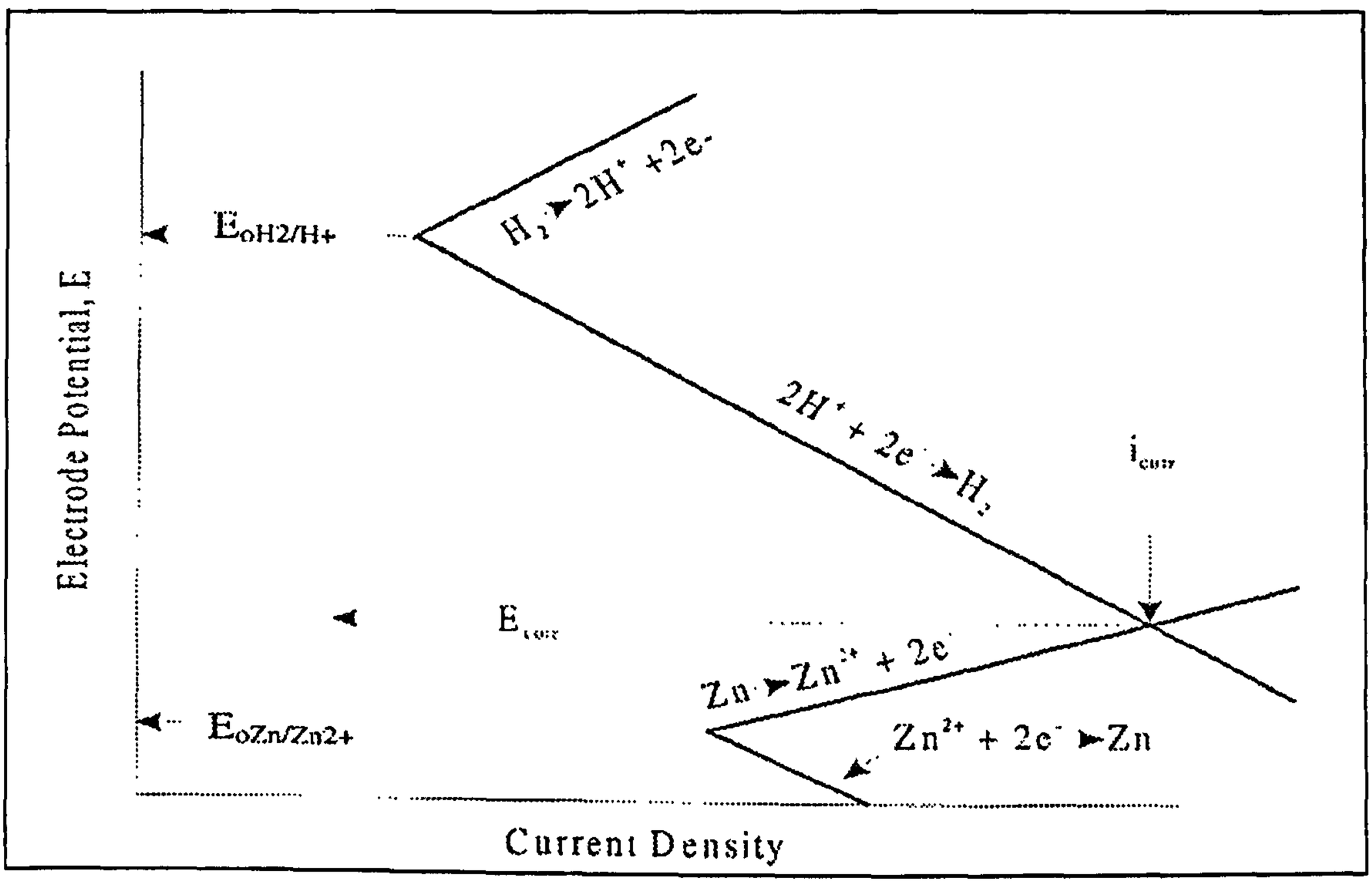

Figure 2.5. Diagram of mixed potential referred to as the free corrosion potential E_{corr}.

2.2.4. Potentiodynamic polarisation.

Polarisation tests involve the polarisation from the free corrosion potential, E_{corr}, by means of a potentiostat, Figure 2.6. A saturated calomel electrode (SCE), which is the reference electrode, provides a relative measure of the potential difference across the specimen. The inert counter electrode, (normally platinum), acts as an electrical connection for current to flow between itself and the specimen when the potential is shifted from E_{corr}.

The potential shift can either be more positive than E_{corr}, in the anodic direction, or a negative shift from E_{corr}, in the cathodic direction and a potential current relationship can be plotted, (Figure 2.7.).

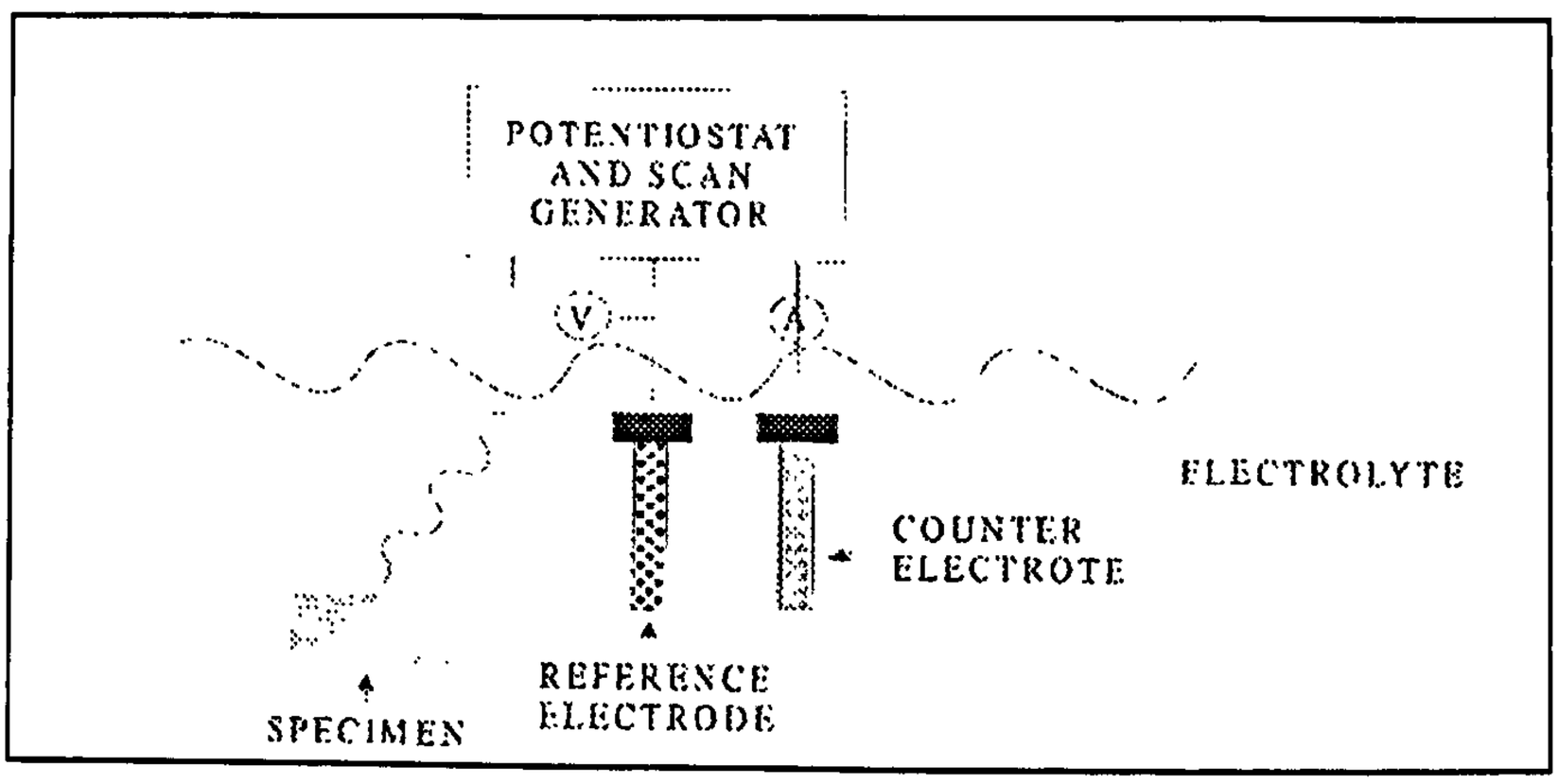

Figure 2.6. Three-electrode cell.

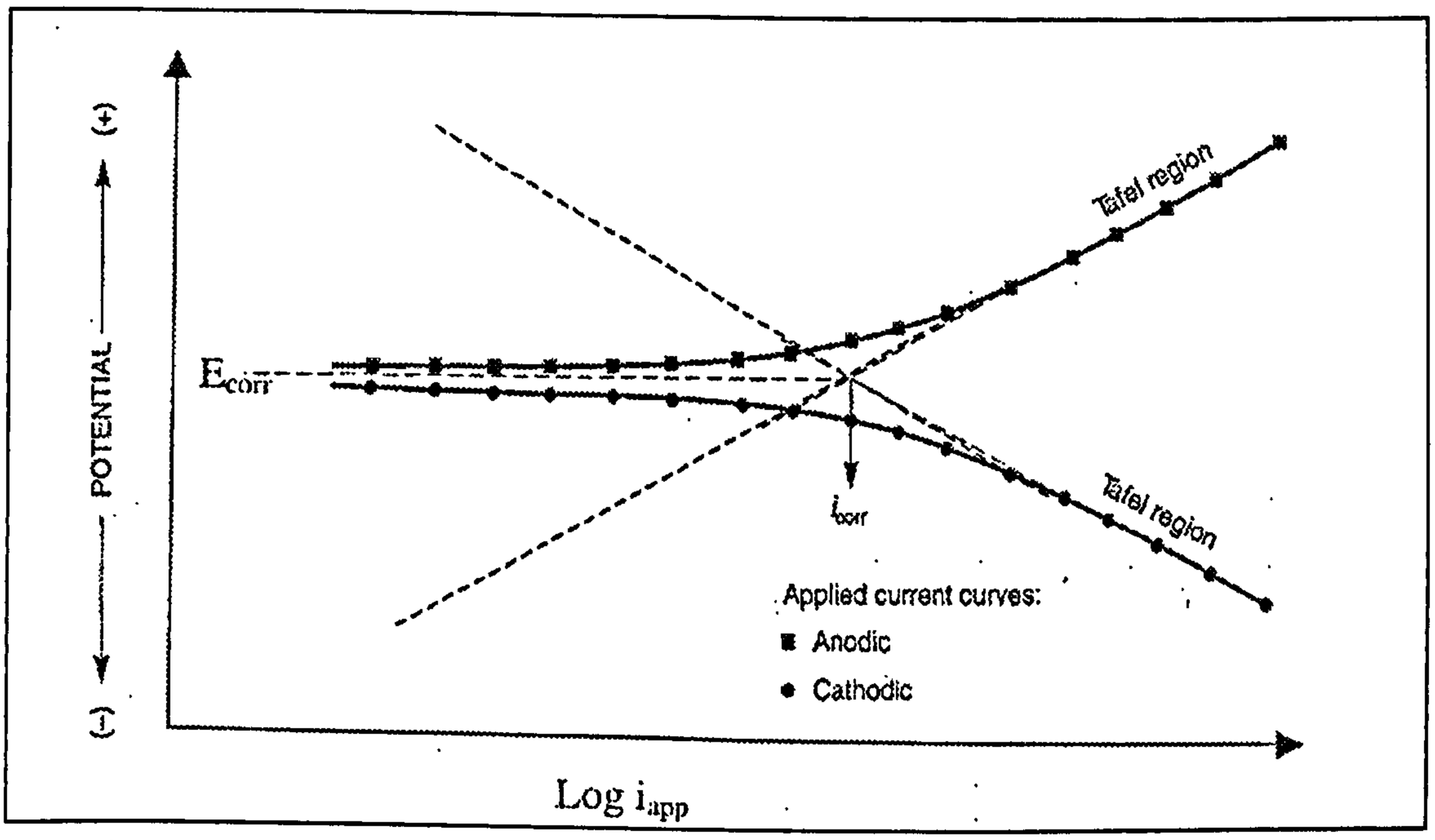

Figure 2.7. Schematic diagram showing anodic and cathodic polarisation.

2.2.5. Cathodic and Anodic polarisation.

When an excess of electron flow (a current density i_{app}), is applied to a corroding metal, (Figure 2.8.), it causes the electrode potential to shift negatively from E_{corr} to E. The negative potential shift, $\varepsilon_c = E - E_{corr}$, is defined as cathodic overpotential. The excess of electrons suppresses the anodic reaction from i_{corr} to i_a and similarly increases the cathodic reduction reaction from i_{corr} to i_c. The difference in the increase in the

cathodic reduction rate and the decrease in the anodic oxidation rate, is equal to the applied current:

$$i_{app} = i_c - i_a$$

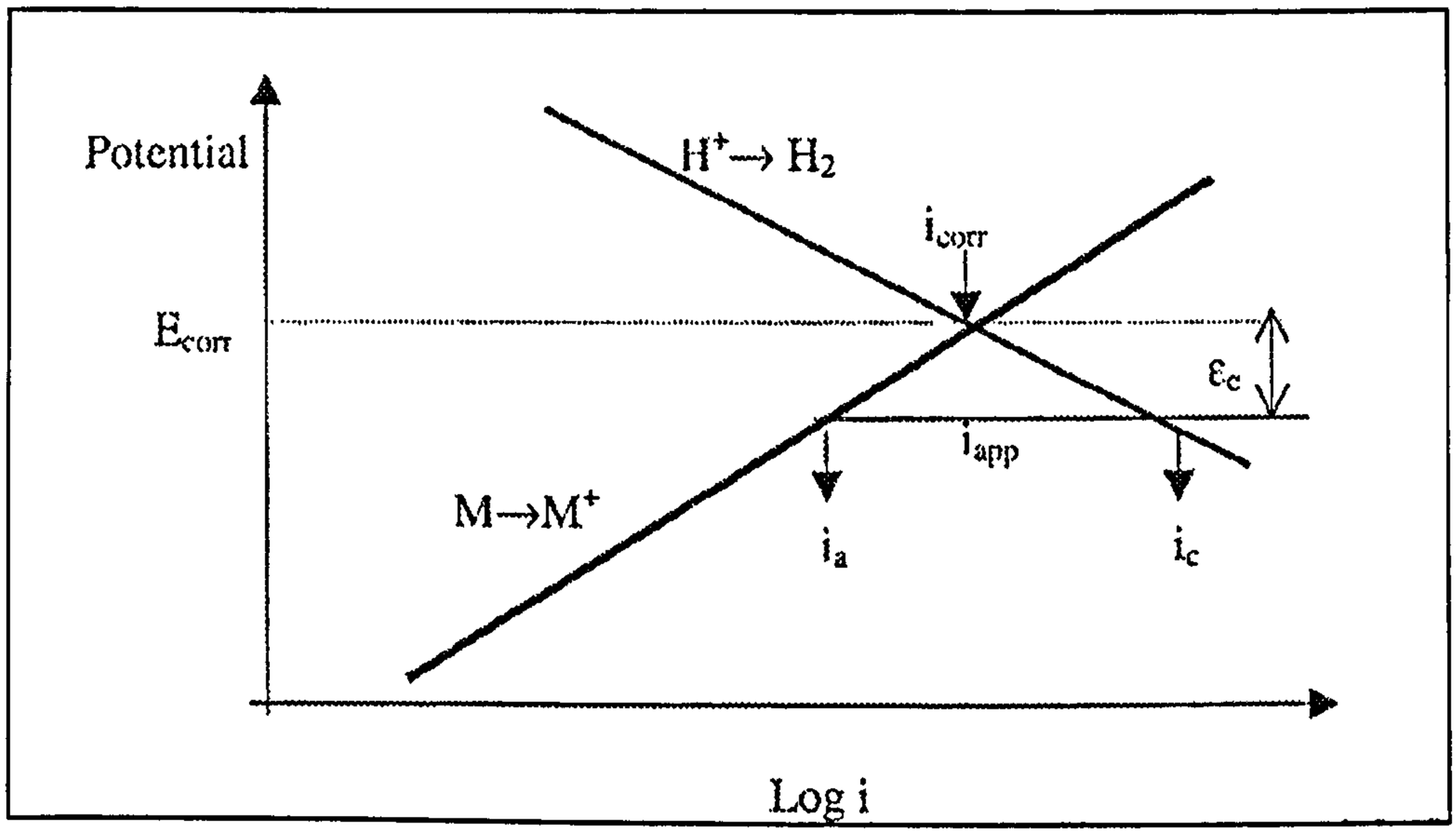

Figure 2.8. Schematic diagram showing cathodic overpotential of ε_c.

Since the dissolution of metal is an anodic reaction, then suppressing this will reduce or prevent corrosion. This method of suppressing the current is the basis of impressed current cathodic protection. Lowering the potential to the reversible potential of the anodic reaction will stop the anodic dissolution. The surface of the cathodically protected object will provide sites for only cathodic corrosion reactions (either hydrogen evolution or oxygen reduction). Cathodic protection can be achieved by impressed current via a potentiostat or through a galvanic couple of a dissimilar metal of a more active metal i.e. sacrificial protection. The galvanic current cathodically protects the more noble metal and preferentially dissolves the more active metal. The electrons flow from the active sacrificial anode to the more noble cathode structure.

At low ε_c, i_c is only slightly higher than i_a, and i_{app} is very low. As ε_c increases, i_c increases while i_a decreases until i_a becomes insignificant compared to i_c. Thus, the simulated cathodic polarisation curve of potential versus i_{app} is curved at low overpotential but becomes linear at higher overpotential, (Figure 2.7.). The linearity on a

semilog plot is termed "Tafel behaviour" named after the German scientist who first discovered it.

Conversely, (Figure 2.9.), when electrons are drawn out of the metal, the deficiency causes the potential to change positively with respect to E_{corr}. The anodic reaction rate, i_a, is increased, while the cathodic reduction rate, i_c, is decreased, so that the applied current density is :

$$i_{app} = i_a - i_c$$

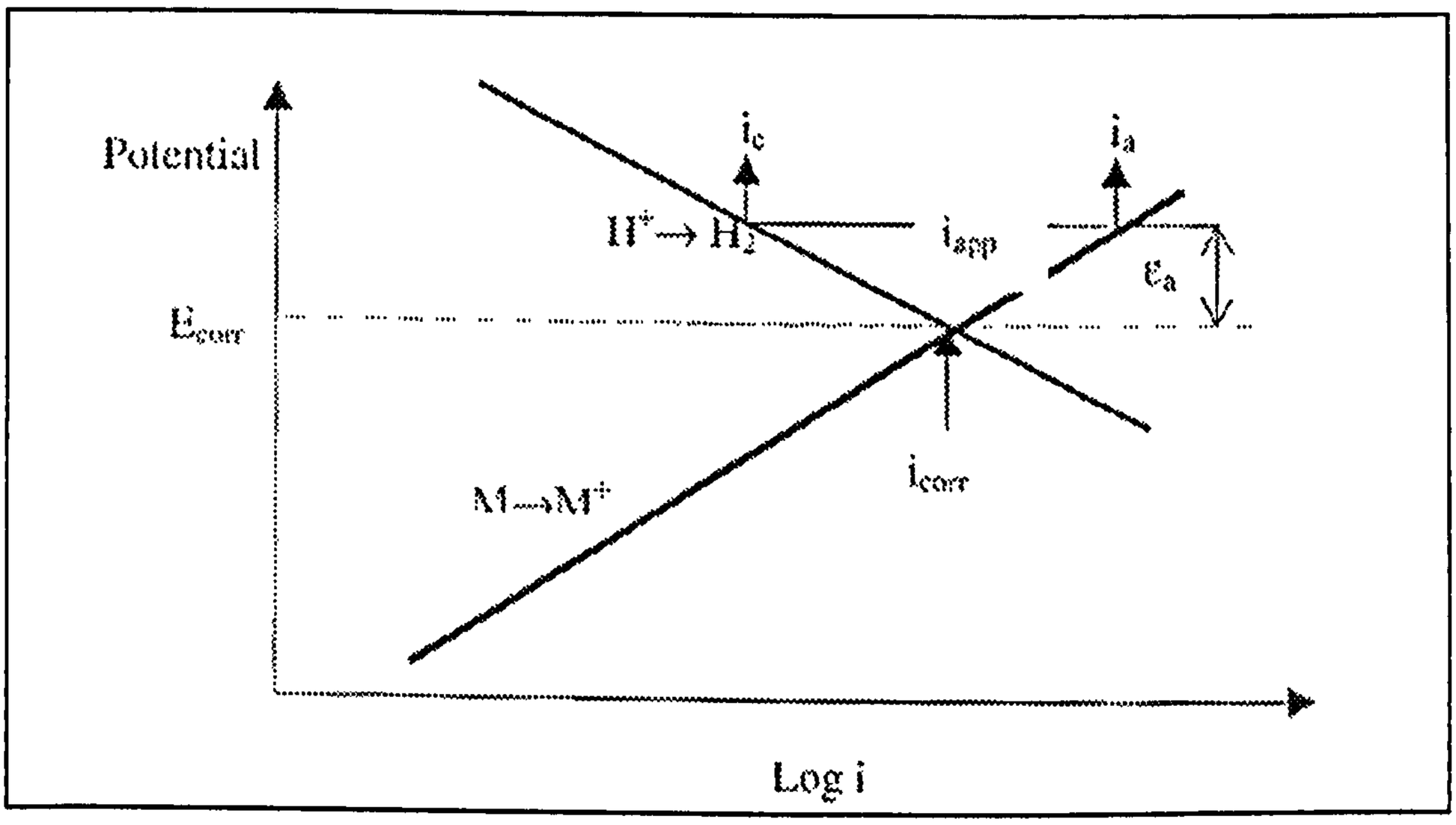

Figure 2.9. Schematic showing anodic overpotential.

As the Tafel regions on the anodic and cathodic polarisation curves, (Figure 2.7.), are extrapolated back, the intersection of the two lines gives the corrosion current density, i_{corr}, from which corrosion rates can be determined.

2.2.6. Types of corrosion damage.

2.2.6.1. General electrochemical corrosion.

General attack, (Figure 2.10.), at a more or less uniform rate, over large areas of the surface of a component, is the most common form of corrosion. The rates of this type of corrosion can vary over very wide ranges. If the products (say M^{n+} ions) of the anodic reaction, $M = M^{n+} + ne^-$, go into solution in the immediately-adjacent environment, then the rate of metal loss may be high-thus leading to serious operational problems.

On the other hand, there may become established on the metal surface an insoluble film (often an oxide or hydroxide). This may be an air-formed film or it may be produced upon exposure to the aqueous environment and, if it is protective, i.e. if it forms as an adherent, non-porous film on the metal surface, it can protect the metal from rapid corrosion. This kind of behaviour, when a protective film forms on the surface is known as "*passivity*".

The nature and properties of the protective oxide films that forms on some metals or alloys are very important from the point of corrosion resistance. The ability of these films to protect the metal depends on the speed or ease with which they form when exposed to the environment, their resistance to mechanical damage or wear, and how good they are in reforming a damaged film.

The strength of an oxide film depends also on the environment that it is going to be in. However, the presence of a dense adherently hard oxide film on a surface of a metal if it breaks down locally, may give rise to highly localised regions of corrosion attack such as pitting [6].

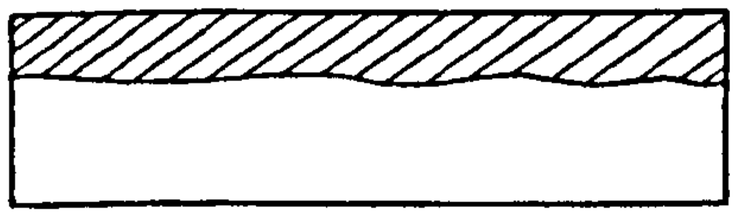

Figure 2.10. General corrosion attack.

2.2.6.2. Local electrochemical corrosion.

The differentiation between local and general electrochemical corrosion is mainly based on practical view-points. If corrosion takes place locally in distinct corrosion cells, metal dissolution may occur in one place and the reduction of the corrosive agent in a second one, whereas the corrosion product, such as rust, is formed in a third site. In such cases, it is unlikely that the corrosion product will give protection against continued attack. If, furthermore, the anode surface is small in comparison to the cathode surface, as when corrosion occurs in a pore, a pit, or a crack in an otherwise protective film, the localised attack may be very strong, even if the total metal loss is small. If, on the other hand, separate anodic and cathodic surfaces do not appear or are of very small dimensions, the attack will be more uniform.

Characteristic features of general and local corrosion as well as some examples of localised attack are listed in the following table[1-2]:

General electrochemical corrosion	*Local electrochemical corrosion*
• Anodes and cathodes not separated • Anode = Cathode = Electrode • Anode potential = cathode potential = Corrosion potential (mixed potential) • Corrosion products may be protective • Results in uniform attack	• Anodes and Cathodes separated • Anode << Cathode • Anode potential < Cathode potential • Corrosion products not protective • Results in localised attack

Table 2.1. Features of general and localised corrosion.

Pitting Corrosion.

This type of corrosion occurs when there is intense attack at localised sites on the free surface of a component whilst the rest of the surface is corroding at a much lower rate.

Once a pit has initiated, (Figure 2.11.), the pit may propagate at a significant rate because of the development of a macrocell, (when the rest of the surface is at a more

positive potential than that inside the pit). As a result, because of the differences in electrode potential between the large area of passive surface, versus the active pit, the pit acts as a small anode and the external surface as a large cathode.

Typical events leading to the initiation of pits on the free surface are:

a) Localised mechanical or chemical damage to a protective oxide film in circumstances preventing its reformation.
b) Localised damage to, or poor application of, a paint coating.
c) Localised breakdown of passive film at sites of non-metallic inclusions.
d) Positive drifts in free corrosion potential.

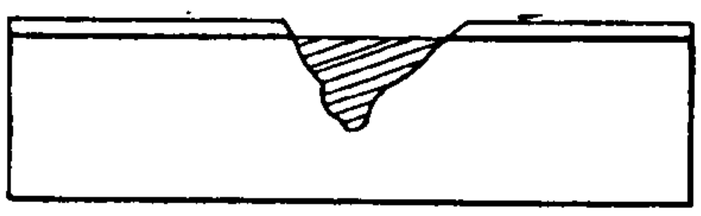

Figure 2.11. Pitting corrosion attack

Crevice Corrosion.

Crevice corrosion, (which as depicted in Figure 2.12, particularly relates to stainless steels), results from local changes in local chemistry, associated with deposits on the metal surface, (weld deposits, or some fouling agent from the water), or at the joint of a bolted assembly. Under such points small amounts of water can collect and become stagnant. Once attack begins within the crevice, its progress is very rapid, and it is frequently more intense in chloride environments.

Crevice corrosion is the attack on a metal in thin crevices between different metallic objects or between a metal and a non-metallic material. In such narrow crevices the replenishment of oxygen is very difficult and it therefore forms an anode, while exposed surfaces of the metal with a good supply of oxygen form cathodes. In a similar manner, *deposit corrosion,* (Figure 2.13), occurs in water and in aqueous solutions under deposits of sand, dead leaves, paper and similar things, which make the replenishment of oxygen to the metal surface difficult.

Typical changes in local chemistry leading to the acceleration of crevice corrosion are:

a) Depletion of inhibitors in crevice.

b) Depletion of oxygen in crevice.

c) Decrease in pH in crevice

d) Built-up of aggressive ion species (e.g. Chloride) in crevice

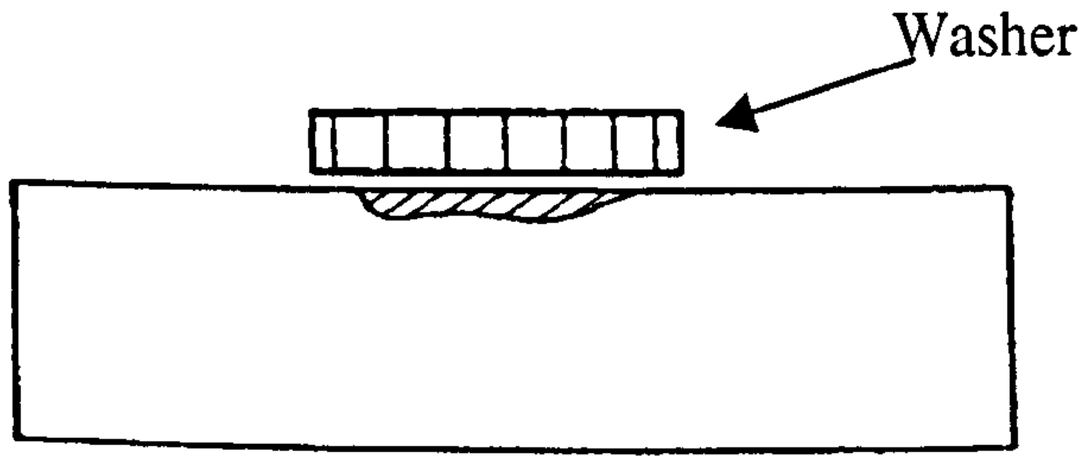

Figure 2.12. Crevice corrosion attack.

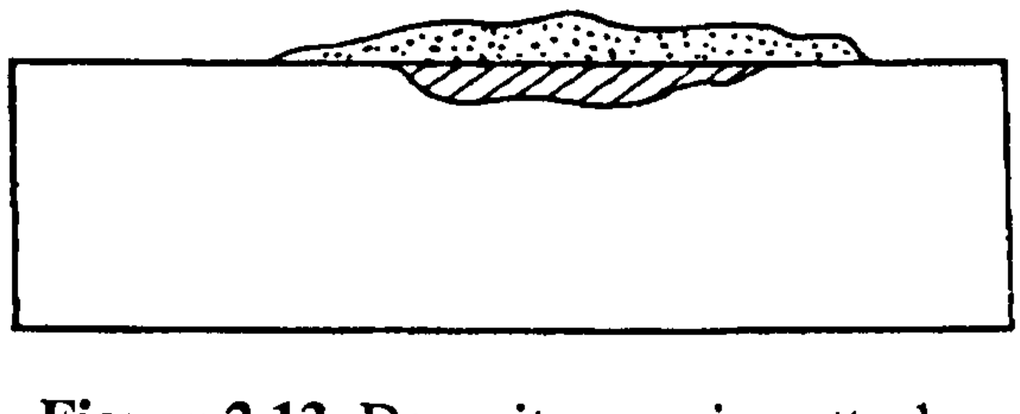

Figure 2.13. Deposit corrosion attack.

Galvanic Corrosion.

When two different metals in contact, (connected by an external wire or by welding or bolting), are exposed to an aqueous environment, an electrochemical cell is constituted, in which the metal, which is the "more-electronegative", becomes the anode, (Figure 2.14.). As a result the corrosion attack is concentrated on this metal.

On the other hand, the other less-electronegative, (or more-noble, or less base), metal provides sites for a cathodic reaction and therefore suffers less corrosion than it would, if located in the same environment in the uncoupled state.

The combination of small anode – large cathode, exemplified by brass bolts in a copper plate, is particularly dangerous in connection with galvanic corrosion. The opposite combination: large anode – small cathode should be aimed at. Screws, bolts,

nuts and welds should therefore always be made from a more noble material. The bolt, weld, etc. will then be cathodically protected.

Copper may cause galvanic corrosion on a more electronegative metal even if it is not in direct contact with the latter. Copper may corrode and dissolved Cu ions, may then diffuse to the light metal and deposit as metallic Cu on the latter, creating small but efficient galvanic cells and severe local attack. This may be called *indirect galvanic corrosion.*

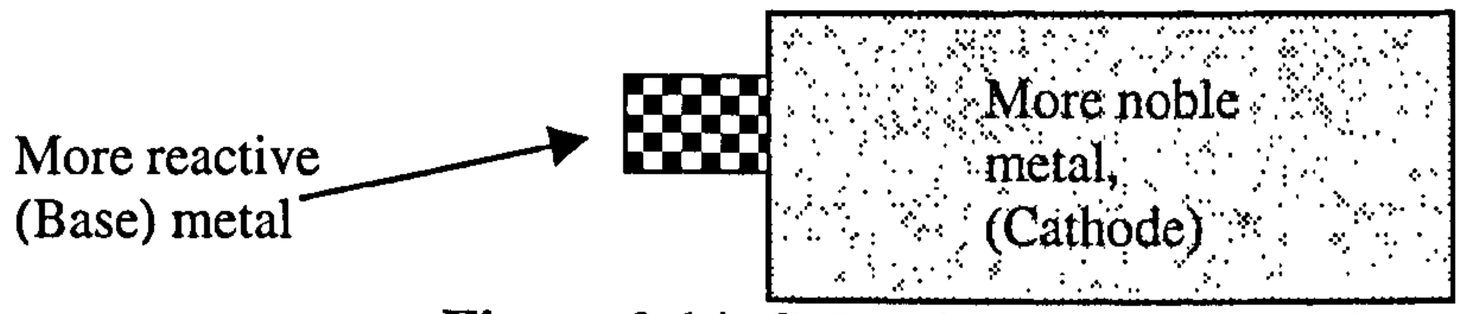

Figure 2.14. Galvanic corrosion attack.

Intergranular Corrosion.

The grain boundaries in a material are sometimes attacked by a corrodent preferentially to the interior of the grain. The attack is usually related to the segregation of specific elements or the formation of a compound in the boundary. Corrosion then occurs by preferential attack on the grain-boundary phase, or in a zone adjacent to it, that has lost an element necessary for adequate corrosion resistance, Figure 2.15a,b. In a severe case of grain-boundary corrosion, entire grains may be dislodged due to complete deterioration of their boundaries, so the metal is transformed to a powder. In any case the mechanical properties of the structure will be seriously affected.

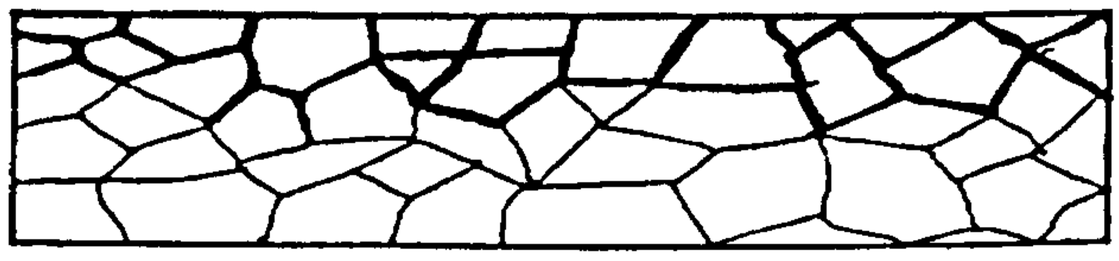

Figure 2.15a. Integranular corrosion attack.

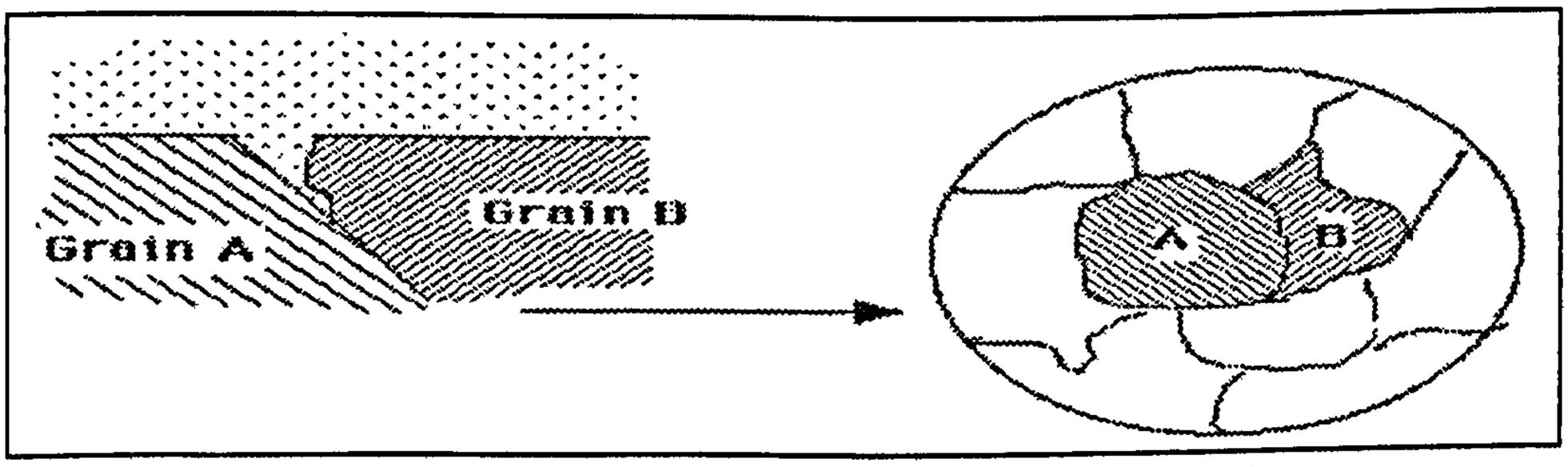

Figure 2.15b. Integranular corrosion attack.

De-alloying or Selective Leaching

In some, relatively rare circumstances, corrosion on an alloy component may take the observed form of one of the major alloying constituents being seemingly "selectively dissolved" leaving other alloy components behind as a kind of spongey mass on the component surface. The detailed mechanisms involved to produce this phenomenon may be rather more complex than simple selective dissolution. Also in selective corrosion (i.e. dissolution of the baser component in a two-component alloy), the process probably starts because of local variations in the composition. Since the more noble metal is retained or re-precipitated, the corrosion process itself generates a galvanic cell, consisting of the more noble metal as the cathode and the alloy as the anode.

Selective corrosion occurs only in alloys, in which two or more metals form a solid solution. In the corrosion process only the less noble component is dissolved to any noticeable extent, while the remainder appears in metallic form even after the corrosion, although with a greatly reduced strength. The corrosion resistance of the alloy is dependent on its composition and it usually increases with increasing concentration of the more noble component of the alloy.

One example of this type of corrosion is mentioned below:

Dezincification of Brass.

The zinc component of the copper-zinc alloy (typically 20-30% in commercial brasses) is lost leaving the copper behind as a usually readily-visible, copper-coloured, porous mass on the surface, Figure 2.16. The resistance of these susceptible brasses to dezincification can be enhanced by the incorporation of a small concentration (typically 0.04%) of arsenic in the brass composition.

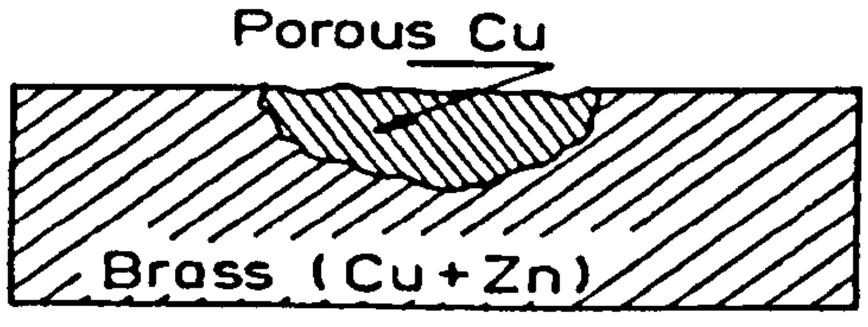

Figure 2.16. De-alloying or selective leaching – e.g. Dezincification of Brass

Other copper-base alloys are susceptible to de-alloying; e.g. "denickelification" of copper-nickel alloys. De–alloying of copper-base alloys is often encountered in marine equipment.

Corrosion Associated with Temperature Effects.

The influence of the temperature of the corrosive medium on corrosion attack is complicated since temperature affects several corrosion factors, such as oxygen solubility, pH, oxide film formation, condensation of moisture etc. in various directions[6].

On the one hand, there is a general tendency for the rates of anodic and cathodic reactions, (and hence corrosion), to be accelerated by increases in temperature – as are most chemical reactions. A general rule of thumb in this respect is a doubling of reaction rate with every 10°C rise in temperature [4].

On the other hand the solubility of dissolved gases in water decreases with increasing temperature and this factor tends to counteract somewhat the above-mentioned accelerating effect of increasing temperature in cases where dissolved gases are involved in the corrosion process, (e.g. the oxygen reduction cathodic reaction).

What all this tends to mean is that one usually observes an increase in corrosion rate up to about 60 – 70°C after which, in systems open to the atmosphere, the decreasing solubility effect starts to come into play and sometimes causes a reduction in corrosion rate at higher temperatures. However, in enclosed systems such as a water pipe from which the dissolved gases can not be eliminated, the corrosion rate can continue to increase with temperature.

Localised Corrosion Associated with Hydrodynamic Effects.

The need to maximise efficiency and minimise costs in handling fluids, demands higher flow rates with the inherent risk of flow-dependent corrosion of engineering equipment [7]. Flow-dependent corrosion occurs on pumps especially as impeller speeds

are increased, on pipes where high intensity turbulence exists in unstreamlined geometry changes or where the flow direction is suddenly changed and on valve seats where high velocities are induced during throttling [8-11].

Many of the types of problems alluded to above are commonly referred to as erosion-corrosion. However, in the general literature, there exist many different detailed definitions and interpretations of the term erosion-corrosion and of general materials degradation in flowing liquids.

Flow-induced corrosion can be defined as a complex form of material deterioration by an electrochemical corrosion reaction, which is accelerated by the relative movement (flow hydrodynamics) between a corrosive fluid and the metal surface [12]. The increased corrosion rate caused by a high-velocity fluid is associated with the transport of species to and from the metal surface, stimulating in that way the oxygen-reduction cathodic reaction.

Rapidly flowing water can have additional mechanical effects, in causing the tearing away of corrosion products, (including a protective oxide film that will result in localised attack at the areas at which the film is removed), and direct mechanical damage to the metal surface [12-13]. In situations where such mechanical damage is involved, the term 'erosion-corrosion' is often used.

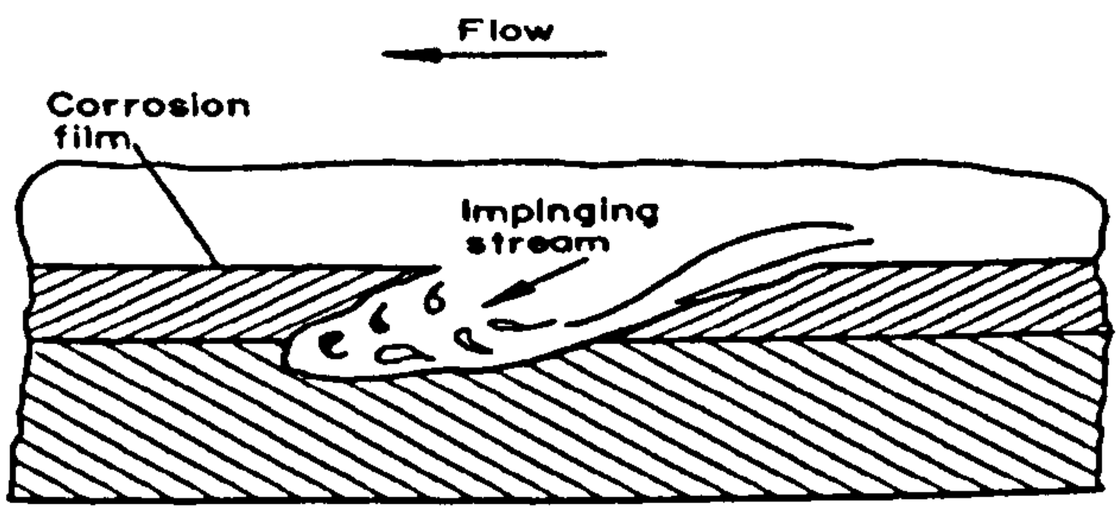

Figure 2.17. Erosion-Corrosion process.

Erosion-corrosion can occur in high-velocity liquids ('liquid erosion-corrosion') and is accelerated in the presence of suspended solids ('solid/liquid erosion-corrosion').

Another form of damage associated with flowing liquids is 'cavitation' [13]. Damage to materials when solid particles are carried by a gas stream is called 'dry erosion' [14-19].

Dry erosion.

Dry erosion, or in other words solid-particle erosion, implies the removal of material from component surfaces due to successive impacts of hard particles entrained in a gaseous carrier fluid. Material removal due to solid-particle erosion is a consequence of a series of impacts, which result in very intense contact between the hard particles and the component surface [14-19].

Many researchers [7,20-21] have suggested factors that influence the dry erosion processes and their combination suggests the following:

- Particle movement- impact velocity, impact angle, kinetic energy of the particles, interference between incoming and rebounding particles.
- Erosive particle - hardness, size, shape, concentration and density.
- Target material - hardness, tensile strength, ductility and metallurgical structure.

Erosion of metals usually involves plastic flow, whereas more brittle materials may wear predominantly by fracture [17-18]. The contrasting behaviour of ductile and brittle materials under dry erosion is described with respect to impact angle [15,17,19]. The relationship shown in Figure 2.18. has become widely recognised as a guide for the prediction of the behaviour of materials in dry erosion conditions when the angle of impingement is defined.

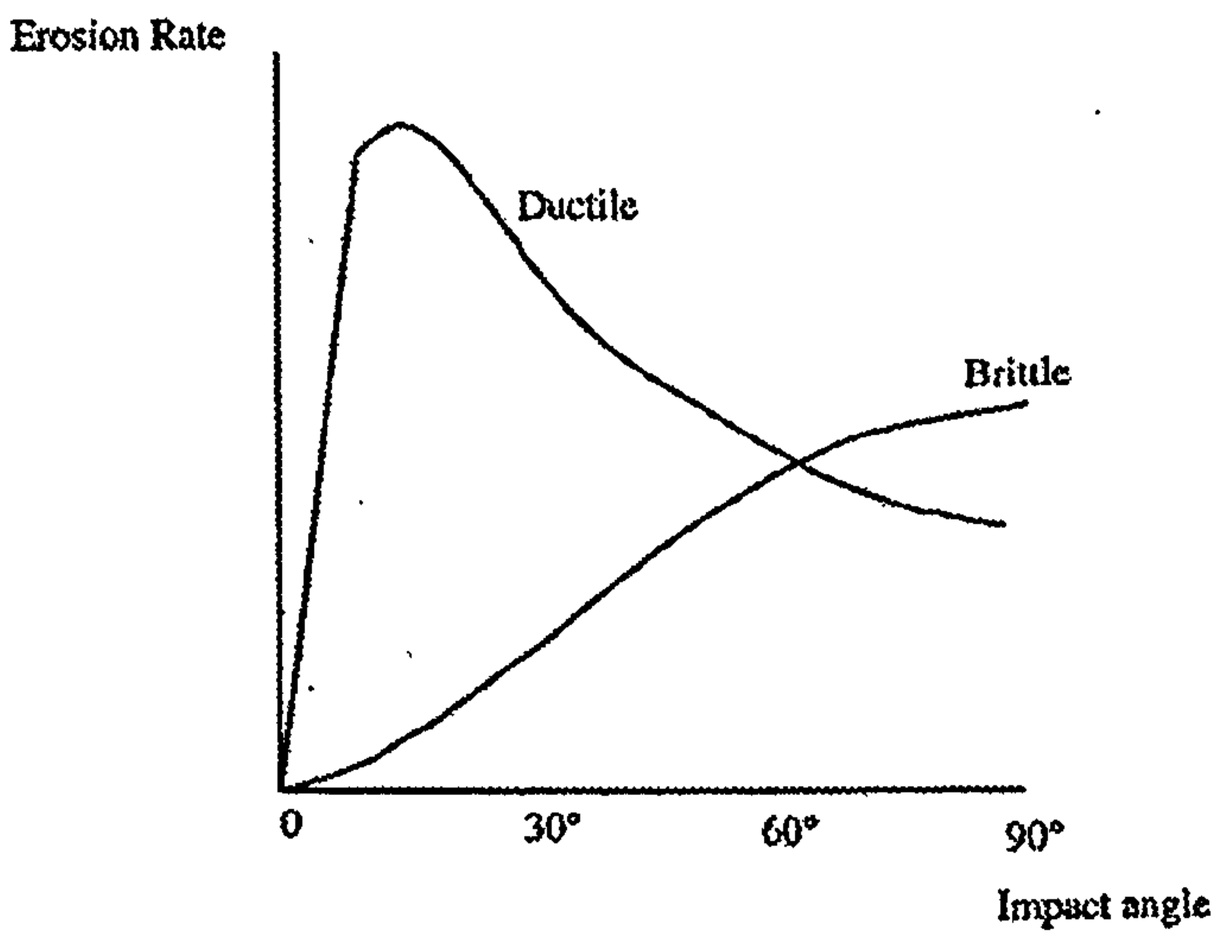

Figure 2.18. Dry solid particle impingement relationship with impact angle for ductile and brittle materials.

Liquid erosion-corrosion.

Liquid erosion-corrosion (i.e. in the absence of solids) can occur in a number of aqueous flow regimes, e.g. pump impellers, steam-turbine blades, in pipes, especially in regions where local turbulence occurs such as in presence of deposits, entrance of a liquid into a tube, at valves, bends. Fluid dynamics is of major importance to the above problem as is also the corrosivity of the fluid in many fluid-material combinations [22-29].

A particularly severe situation is that arising from a liquid impinging at high velocity directly upon a component surface. This is the scenario which is studied in the present research; hence the hydrodynamics associated with a submerged impinging jet are summarised below.

A free turbulent jet usually possesses four flow regimes (see Figure 2.19.) [25]:

1. A regime of flow development, where the flow extends up to 6.4 nozzle diameters i.e. $0 < z < 6.4d$, where 'd' is the nozzle diameter. The constant velocity core or potential core within the flow development regime is the region of the impinging jet in which the velocity profile of the jet changes from pipe flow to a free jet flow. As

the flow discharges from the submerged nozzle, the stream of jet starts to mix with the surrounding fluid. The mixing zone grows in width along the downstream direction of the jet. This leaves a conical potential core wherein the fluid property and the velocity are relatively constant [25-26].

2. A transition region between 6.4d and 8d.
3. A region of developed flow, extending out to about 100d.
4. A terminal region where the centreline velocity decreases steeply towards zero.

In addition to the above, a free turbulent jet spreads out through a cone of half-angle about 10° [25], entraining a considerable amount of surrounding fluid in the outer part of the jet.

When a submerged jet collides perpendicularly with a flat plate in a stationary solution, there forms three distinct flow regimes along the surface of the plate. The extent of these can be discussed in terms of the radial distance 'r' from the stagnation point (the point of the flat plate directly under the jet) and the jet diameter, 'd' (see Figure 2.19.):

1. The stagnation (also called impingement and laminar) region: this is a layer of fluid on the flat plate in which the jet is deflected from the axial direction to a radial flow. The flow in this region is laminar [26,30-35]. According to Esteban et al [32], the radial velocity increases from zero at the stagnation point to a maximum at r/d~1, and then decreases.
2. The wall jet region: this is a region adjacent to the flat plate which commences at some distance from the stagnation point where the radial velocity starts to decay and the thickness of the boundary layer increases with extending radial positions [26]. Furthermore, in the wall jet region, where fully developed turbulent flow exists [33,36], the turbulent intensity starts to decay with increasing r [26,36-37].
3. The transition zone: this is a highly turbulent region [33,37], located between the stagnation and the wall jet regions. It is probably a reasonable proposition that, in the

case when the submerged liquid jet strikes a flat metallic component, the maximum corrosion rate occurs at the transition phase of the two regions mentioned above [37].

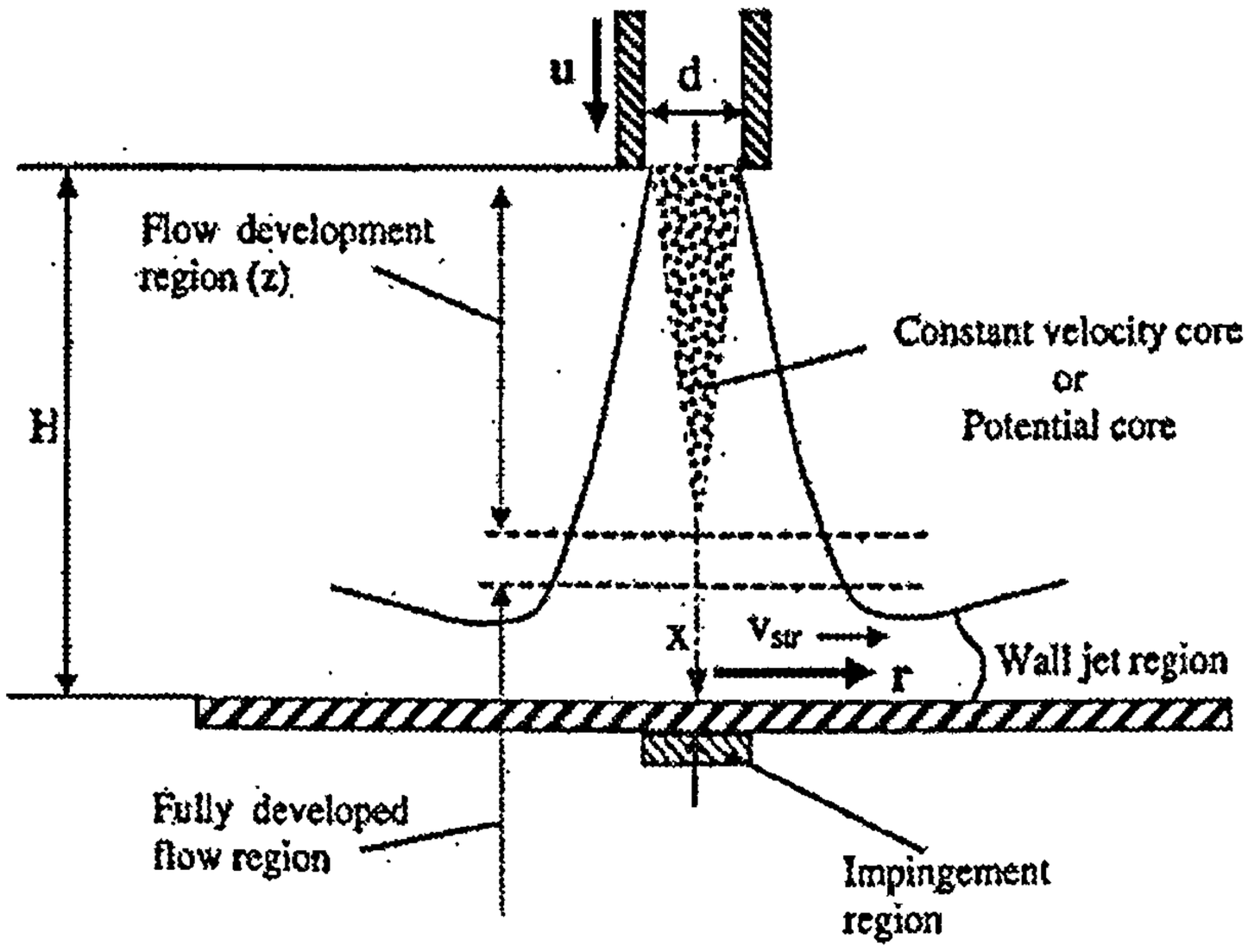

Figure 2.19. Submerged jet also called as free turbulent jet impinging onto a horizontal solid plate, showing typical velocity profiles in the main stream and the radial wall jet region [25-27].

Table 2.2. gives an indication of the radial extent the stagnation and wall jet regions, suggested by various authors [26,28,30-37], (note that the size of the transition zone equals the difference between the stagnation and the wall jet regions). It is clear that there is no universal agreement in these respects; the varying zone sizes quoted in Table 2.2. are very likely to be at least partly caused by the influence of the specific hydrodynamic conditions. For instance, it has been suggested [37] that the various regions increase in size as jet velocity increases.

Stagnation region	Wall jet region	Reference
r~1.0d		[30]
	r>2.0d	[31]
r~0.5d		[32]
r~1.1d		[33]
r=0.6-1.4d	r>4.0d	[26]
r=1.0d	r>2.0d	[34]
r=0.6-1.4d	r>3.0-5.0d	[35]
r=2.0d	r>4.0d	[37]
r=0.5d	r>1.25d	[36]
r=2.35d	r>3.0d	[28]

Table 2.2. Extent of the stagnation and wall jet regions, suggested by various authors [26,28,30-37]

Erosion-corrosion damage on a flat metallic component due to the action of a single-phase submerged impinging jet is associated with two possible mechanistic processes: mass transfer [26,30,32,33,36,37] and/or shear stress [22,28,32,33,37-40].

Mass transfer.

It is widely accepted [26,30,32,33,36,37] that the hydrodynamic parameter controlling erosion-corrosion for a number of systems is mass transfer. For instance it is quite clear that corrosion rates are influenced by mass transfer, when this factor controls the corrosion rate (e.g. carbon steel in seawater), on account of the role of the oxygen reduction cathodic reaction. In the stagnation zone, the mass transfer rate is most usually considered to be independent of radial positions, i.e. is uniform to the surface [32,36] and mass transfer is at its minimum in the stagnation region in relation to the transition and wall jet regions [32,37]. Maximum mass transfer is said to occur in the transition region where the turbulent intensity increases rapidly and high local shear stress and velocity gradually develop [33,37]. A contrasting scenario has been presented by Chin et al [26] according to which, maximum mass transfer develops at r<0.1d; between r=0.1d and

1.0d the local mass transfer rate is constant and beyond r=1.0d the mass transfer rate decreases with increasing radial distance.

It has been suggested by some [30,33], that maximum mass transfer is highly depended on the H/d parameter, and can have one or two peaks on the target surface. It has been described by Chia et al [30] that for H/d=1.2, the maximum mass transfer has two peaks; one at r=0.6d and the other at r=1.95d. For H/d=8, mass transfer is maximum at stagnation point whereas in the more complicated case of H/d=5 there are several zones of different magnitude of mass transfer.

Shear stress.

Shear stresses on a flat component under a submerged vertical impinging jet results from velocity gradients near the exposed surface [39]. The maximum velocity corresponds approximately to maximum shear stress [28], and as pointed by Dauson [33], the maximum shear stress coincides with the position of maximum mass transfer. At the stagnation point, where the vertical and horizontal components are at their smallest [22], average shear stress is zero [28] and any significant erosion at it may be attributed to the surface roughness effects or to a non-shear dominant erosion mechanism, i.e. impact forces [28]. As the radial distance from the stagnation point increases, the water velocity and shear stress increase linearly up to a maximum value occurring at the edge of the stagnation zone [32] (which in the case of [32] is r=0.5d).

On the other hand, R.C.Woolam et al [37], claim that the highest local shear stresses take place in the turbulent transition region (which according to Woolam et al [37] extends from r=2d to r=4d).

Silverman [23] has reviewed the impinging jet geometry. In cases where the corrosion is mass transfer limited, the corrosion rate is considered to be a function of the wall shear stress. Girald and Trass [22,28] have proposed that, in the wall jet region

(Figure 2.19.) away from stagnation point, the shear stress 'τ_w' follows the equation for ratio r/d > 2-3 with Reynolds number 'R_e' ranging from 2500 to 125000:

$$\tau_w = 0.0447 \rho u^2 R_e^{-0.182} \left(\frac{r}{d}\right)^{-2}$$

where 'u' is the nozzle exit velocity (m/s),

'd' is nozzle diameter (m),

'r' is the distance from the stagnation point (m),

'ρ' is the liquid density (kg/m^3),

'τ_w' is the shear stress (N/m^2).

Rajaratnam [27] has reported that the wall shear stress increases linearly with 'r' to a maximum value at $r/H \approx 0.14$ and then decreases as 'r' increases further. The maximum shear stress 'τ_m' is given by the expression below and is valid only for large impingement heights, i.e. H/d > 8.

$$\tau_m = \frac{0.16 \rho u^2}{(H/d)^2}$$

where 'τ_m' is the maximum shear stress (N/m^2) and

'ρ' is the liquid density (kg/m^3),

Some workers have claimed that shear stresses are important in developing erosion damage. As suggested by some [28], in the wall-jet region pure erosion results from shear stresses only. It was also pointed out by Giralt and Trass [28] that if shear stress is not the only factor governing erosion in the wall-jet region, at least it is the dominant one.

In contrast, others [38,40] suggest that shear stress is not a useful parameter to predict erosion-corrosion rate. Shear stresses in single-phase flow are in the order of ~0.05 MPa, (as opposed to the tensile strength of metallic materials which are in the order of several hundreds MPa, e.g. 320 MPa for Cu-10%Ni and 924-955 MPa for Marinel), thus [40] it is hard to imagine that these can cause erosion damage to metallic surfaces. However, the relation between shear stress and flow rates is the matter of interest to the critical shear stress necessary for the breakdown of protective surface layers on metals [27], which can be the cause of the onset of erosion-corrosion

Another possible mode of erosion damage under liquid impingement is the impact pressures that can result in plastic deformation of metallic targets, evident through slip and mechanical twinning [24,29]. Liquid impact produces a region where circumferential cracks can occur depending on the target material properties and the impact velocity. After impact, the flow moves radially and once it collides with a surface asperity, the force of impact can create a crack perpendicular to the surface. Subsequent impacts on existing cracks, pits or depressions can produce accelerated damage with large pieces of surface detached.

Cavitation.

This phenomenon exists when pressure variations (resulting from large velocity changes, e.g. in pipe bends) cause the formation of vapour bubbles in regions of the liquid where the pressure is lower than the vapour pressure of the liquid. This is followed by collapse of these bubbles as the fluid encounters a higher pressure zone resulting in release of immense energy of the order of 1000 - 2000 MPa [12], which subsequently leads to the damage of the surface e.g. mechanical 'cavitation' damage or to a combined 'cavitation corrosion' attack in corrosive environments. Bubble collapse in a cavitating system results in pressure transients at a surface and also micro-jets of liquid which impinge at velocities between 100 - 500 m/s [24,41]. The latter can, for instance, involve protective surface films being disrupted locally, exposing small anodic areas of bare

metal surrounded by large surrounding undamaged cathodic areas [12]. The surface roughening provides better nucleation sites for new bubble formation and the corrosion process is intensified. Propellers, impellers and hydraulic turbine gear, bends and protrusions (flanges, tees and elbows) are the most common places to encounter corrosion by cavitation. Cavitation depends upon the fluid characteristic, material and fluid velocity. Vapour pressure, air content, surface tension, and fluid viscosity are parameters that influence cavitation wear [42].

Solid-liquid erosion-corrosion.

Erosion of metals associated with impingement of solid particles entrained in a liquid stream is quite common in process industry, oil and gas refinery industry and many other multiphase flow industrial devices [20,43,44]. Other examples of erosive wear are in applications such as pipelines carrying sand/water slurries in mining operations. Particles may also be contaminants such as fine airborne grit particles mixing into lubricating oil. Metal components in pipelines, in nozzles, valves, tees and bends are subjected to severe erosive wear resulting in premature failure of these components [45].

It seems very feasible that the hydrodynamic aspects described in the previous section are greatly overcome by the dominant effect of solid particles entrained in the impinging jet [28]. This emphasises the high contribution of mechanical erosion to the overall damage in solid/liquid erosion-corrosion conditions. However, there is clear evidence in literature [46-48] of the role of corrosion and further modes of attack involving complex interactions between corrosion and erosion in contributing to the total material loss.

Erosion-corrosion mechanisms.

Aqueous erosion-corrosion has in the past been studied by weight, (or volume), loss comparisons to provide a ranking of resistance to material loss through erosion-corrosion processes. Although this quantitative information is important from a practical

viewpoint in determining the rate of material loss, it does not indicate how the individual processes of erosion and corrosion interact. Only recently [21,46-47,49-56] it has been recognised that, material loss by erosion-corrosion in aqueous systems is often governed by complex mechanisms, which include electrochemical corrosion and mechanical wear interactions. These separate constituents of the damage process can be unravelled and indeed quantified by experimental methodology that comprises determination of weight (or volume) losses together with electrochemical monitoring undertaken during the erosion-corrosion experiments. The actual material loss in a corrosive aqueous environment is often much higher than the sum of the losses attributed by pure corrosion and pure erosion mechanisms in isolation, and is recognised as the synergistic contribution.

There have been essentially two ways employed to analytically describe this complex interactive phenomenon. One approach, following the definition by ASTM [57] where the total weight loss is defined by:

$$T = W_o + C_o + S_T$$

where W_o = material loss under pure erosion conditions, in the absence of corrosion,

C_o = the corrosion rate in the absence of erosion,

$S_T = S' + S''$,

S' = the increase of mechanical wear due to corrosion, and

S'' = the increase of corrosion rate due to mechanical wear.

The components can be determined by a set of experiments. The total material loss, T, is found by weighing the test specimen before and after an erosion-corrosion test. W_o is also determined by weighing the test specimen before and after an erosion-corrosion test but when the specimen is cathodically protected i.e. corrosion processes are stopped. C_o is determined from electrochemical tests when no mechanical wear is acting on the specimen. $S'' = C_w - C_o$, where C_w is the corrosion rate determined from

electrochemical tests during an erosion-corrosion test. The value of S' is then calculated from $S' = T - (W_o + C_o + S'')$.

The other approach is:

$$T.W.L. = E + C + S$$

where E is W_o above and C is the contribution from electrochemical deterioration under erosion-corrosion conditions (C_w above) and all the parameters can be directly obtained during an impingement experiment. The synergistic component, S, which is equivalent to S' in the above representation, can be calculated from the formula:

$$S = T.W.L. - E - C$$

i.e. where S in the increase in erosion due to corrosion. This equation is incorporated in work by Neville et al [46], Hodgkiess et al [47] and Bjordal et al [48].

The detailed separate mechanisms of attack, i.e. pure erosion (E), pure corrosion (C) and synergy (S) are dependent upon the specific materials and environmental conditions. In recent years there is a world-wide development of a study in the performance and especially the mechanisms of erosion-corrosion on a range of materials, from which reasonably good or very good erosion corrosion resistance might be expected; i.e. Stainless steel, Titanium alloys, etc.

As an example, at perpendicular impact the pure erosive constituent appears in many materials to involve microdrilling mechanisms, especially at solid-liquid erosion-corrosion conditions. One practical consequence of the quantification of the erosion-corrosion components is that it demonstrates the possibility of securing significant reductions in damage rates by the elimination of the 'corrosion + synergy' contributions – achievable by the application of cathodic protection.

Madsen [58] in 1988 identified a synergism on 316 stainless steel, (16-18% chromium, 2-3% molybdenum, 10-14% nickel, 0.03% maximum carbon), and other materials, in a slurry pot test with tap water, 0.06M Na_2SO_4 and 2% silica sand at velocities of 5.8m/s and 15.6m/s at 26°C and 60°C. The synergistic effect accounted for

between 23% and 33% of the overall material degradation and up to 62% on stainless steel at low velocities.

Studies carried out by Zhou at al [59], involved a modified rotating cylinder electrode (RCE) system. Tests were carried out on mild steel in a solution of 0.5M $NaHCO_3$ + 0.5M Na_2CO_3 containing 300g/l of 100μm Al_2O_3 particles. The peripheral velocity of the RCE ranged from 2m/s to 8m/s. Corrosion and erosion rates were measured over this range of velocities and potentials of –0.67 V_{sce} to +0.2V_{sce}. The enhancement of erosion by corrosion was only seen in the same potential range where integranular stress corrosion cracking occurs. The mechanism proposed for the synergy was that the impacting particles induced tensile stresses and hence corrosion cracks leading to material removal. The contribution from corrosion increased with velocity but decreased significantly with the introduction of the passive film.

The corrosion component of the erosion-corrosion damage is likely to, at least partly, involve mass transfer phenomena of the types that are relevant to liquid erosion. Materials whose resistance depends upon a protective film are prone to erosion-corrosion attack due to constant removal of the protective film, (which may range from thick visible film of corrosion products to the thin invisible passivating films), from the metal surface [12]. In consequence, for both passive and active corrosion materials, corrosion rates are likely to increase by mass transfer effects.

Passive films on stainless steels are well known for providing protection against active dissolution in static conditions. However, when they are introduced to an erosive media the passive film can break down and the addition of corrosive and mechanical wear accelerates material degradation [60] namely synergism.

Synergy has been quantified by Hodgkiess et al [47] on UNS S31603 stainless steel to be 30% under an impinging jet of 800 mg/l solids at 17m/s and 25°C, and 17% in similar conditions with 1000 mg/l solids at 25m/s and 50°C, with erosion contributions at 67.6% and 80.7% respectively. In the presence of solids, the passive film is penetrated causing dissolution of the substrate and wear by the erosive particles [62].

Erosion-corrosion mechanisms were studied on other alloys: W-alloy white cast iron [63] and grey cast iron [64]. The white cast iron deteriorates by corrosion weakening the carbide/matrix bond, cavitation holes forming and aggravating the wear and the carbides, subjected to repeated impact eventually fall off. Hence by increasing the chromium and tungsten content, the corrosion resistance and hardness of the alloy increases, reducing the erosion-corrosion rate. Corrosion, both direct and indirect, had a large effect on the erosion-corrosion of the grey cast iron. It contributed up to 55% of the overall weight loss when subjected to an impinging jet of 500mg/l solids at 50°C. The matrix was mechanically eroded by a ploughing action as well as electrochemically corroded which was accentuated near the graphite flakes.

As illustrated in the previous paragraphs, the corrosion resistance of alloys plays a large role in determining the extent to which they deteriorate in erosion-corrosion conditions. The synergistic effect becomes apparent when the mechanisms, either breakdown of passive films or the weakening of matrix/hard phase bonds, are identified.

HVOF thermal spray coatings have showed [47-48] to possess increased erosion-corrosion resistance in zone-conditions compared with that of conventional alloys, namely stainless steel. In conditions of an impinging jet at 17m/s containing 800 mg/l solids, a Ni-Cr-Si-B coating had about 50% reduction in weight loss compared with the stainless steel in a three hour test period. The synergistic effect (23% of the overall weight loss), on the coating, was attributed to the roughening of the surface on a micro scale and the corrosion of the matrix leading to the faster removal of protruding hard particles by the impacting sand.

Although there is a clear evidence in the literature of the study of the complex interactions between corrosion and erosion and their contribution to the total material loss on a range of materials which are known to posses reasonably good or very good erosion corrosion resistance, there is not such work for metallic system of Cu/Ni alloys, in which good general corrosion resistance but rather limited erosion-corrosion resistance is generally found.

Chapter 3

Historical notes and use of copper nickel alloys.

The development of the copper-nickel alloys began in response to a requirement by the British Navy for an improved condenser material.

Condenser tubes are among the critical components of marine steam powered plants, in particular since sea water is the commonly used coolant; moreover the relatively severe conditions of operation, (flow of water, heat transfer with occasional hot spots, occasional contamination of the water etc), increase the susceptibility to corrosion attack. As a result, the selection of pure copper limits the service life of condenser tubes and increases the frequency of inspection and replacement of more advanced condensers, operating at higher flow and heat exchange rates.

The corrosion of condenser tubes was first extensively studied by the investigators working under the Corrosion Research Committee of the Institute of Metals set up in 1910. In 1930 the work of this committee was taken over by the British Non-Ferrous Metals Research Association [66,79], (BNFMRA), and has since continued without intermission.

At the beginning of the century, Admiralty brass, an alpha phase brass, (containing about 70% copper, 1% tin, balance zinc) was in general use as the condenser tube material. Dezincification of that brass was a major problem, but that was solved by the addition of small amounts of arsenic. However, the arsenical 70:30 and 70:29:1 brasses proved insufficiently resistant to impingement attack and severe erosion-corrosion problems were observed when the seawater flow velocity was higher than about 1.5m/sec.

The need for higher velocities, in order to achieve higher cooling rates and more compact designs, led the marine condenser designers to the development of new condenser alloys. By the beginning of the Second World War (1939), however, the position had been reached by the development of two important groups of such alloys.

The first is Aluminium brass (an alpha phase brass with 20% zinc, 2% aluminium, balance copper – with small amounts of arsenic to prevent dezincification). The second is the 70% copper-30% nickel alloy (70-30 cupronickel). Although the limiting flow velocity for seawater in contact with Aluminium brass is about 2.5m/sec, the advantage of that alloy is its relatively low cost.

Even with the condenser-tube alloys that were resistant to impingement attack, rapid pitting, particularly with aluminium brass, was occasionally encountered and appears to be caused by localised turbulence or partial blocking of flow inside the tube. This was confirmed by the war-time experience, which showed that "the condenser tube problem may be considered as virtually solved", but that "severe corrosion was liable to occur in other parts of the cooling systems in the ships" [67].

Hence, notwithstanding the cost advantages of the material, Aluminium brass tubes have found very limited use in naval condensers (where reliability and long service life are of primary importance), but have been widely used in the past in the brine heater of MSF plants because of its often good resistance to high temperature brine [68].

The use of 70-30 cupronickel encountered some problems mainly because of its susceptibility to accelerated attack in high-velocity seawater.

Based on observations that the properties of 70-30 copper-nickel tended to vary with iron and manganese levels, a composition was sought to optimise resistance to velocity effects, deposit attack and pitting corrosion. In 1939, tests made by the BNFRMA[79] showed that small amounts of iron and manganese, could influence the corrosion behaviour of Cu-30%Ni. Typical levels of 0.6% iron and 1.0% manganese were finally chosen. According to the BNFMRA work a jet impingement test at a velocity of 3m/sec, was used to evaluate the effect of flow velocity on the corrosion rate of copper-nickel alloys.

Once successful service experience was achieved, interest was transferred to lower nickel compositions, initially as a replacement for copper seawater pipe-work in naval applications.

For the first set of experiments, alloys with variable Cu,Ni, Fe and Mn ratios, were tested, and the outstanding observation was the excellent resistance to sea-water

corrosion, under both stagnant and impingement conditions, of the alloys containing 5-10% nickel and 1-2% iron, the behaviour of which was comparable with that of alloys of high nickel and lower iron contents. Increasing the iron content markedly improved the resistance to impingement attack, while increasing the nickel content resulted in the formation of a thinner and strongly protective film.

A higher degree of corrosion resistance appeared to be offered by the alloy containing 10% nickel, 1.5% iron, and 0.8% manganese, (higher iron content and lower manganese level than the 70-30 cupronickel), which suggested the potential value of the 90-10 cupronickel as a condenser tube, and research on this alloy was extended.

Since the 1950s, the 90-10 alloy has become accepted for condenser service as well as for sea water pipe work in merchant and naval service.

As a result of the excellent corrosion resistance characteristics of the copper-10 % nickel alloy, it has become the standard condenser tube material for service on board British and US Navy vessels and finds wide application in water boxes, salt water conduits, desalination plant tubing, ship hull and offshore structures, cladding, fish farming enclosures, and other applications that required contact with seawater over extended periods of time [69].

Chapter 4

The Erosion-Corrosion behaviour of Cu and Cu-base materials. – Detailed review of the Erosion-Corrosion behaviour of Copper Nickel Alloys.

The discovery of the art of copper extraction and of simple copper-alloy manufacturing, dates back far in the history of mankind. In fact this discovery is one of the basic milestones along the road of human evolution and is generally referred to as the 'Bronze Age'.

Copper is a very versatile material and its properties both with regard to erosion-corrosion and mechanical strength can be easily improved by alloying [66]. Most copper base alloys show a reasonable corrosion resistance towards seawater at moderate flow rates. Copper nickel alloys were developed to withstand high water velocities. Improvement in the corrosion properties of the cupro-nickels was achieved by additions of iron, manganese, chromium and niobium. However, they can undergo serious damage under conditions of high flow velocities and polluted seawater, particularly by sulphides and ammonia. There are hundreds of copper alloys with different properties and these are grouped in a limited number of families [65,68] and the most important of these are discussed below.

4.1. Copper.

Materials which have a designated minimum copper content equal to or higher than 99.3%, are described by the term "copper". These materials occupy a moderately noble position in the seawater galvanic series and in many marine environments, including total immersion. Their corrosion resistance is good as they are attacked evenly and slowly provided the velocity of water does not exceed 1 m/sec. The corrosion rate seriously increases in waters with speeds above this value.

Because of the high thermal conductivity of copper, it is used in condensers and heat exchanger tube, in evaporators, in distiller tubing, and in air conditioning and

refrigeration units. On the other hand, because of its excellent electrical conductivity, a large number of coppers, find applications as bus bars and bus conductors, coaxial cables and tubes, wave guides, in windings and switches, in motors and transistors bases etc [65].

A major use for "copper" is for pipework in domestic and industrial plumbing systems.

Copper usually performs satisfactory but, over several recent decades, leaks in copper piping systems due to pitting corrosion, have been experienced in many countries all over the world, e.g. Scotland, Finland, New Zealand [70].

Such problems are often associated with specific water composition and many aspects of this matter have been discussed in relevant investigations [71-73].

4.2. The brasses.

Brasses are basically binary alloys of copper and zinc. Small amounts of other elements might be included to enhance some special properties.

According to their crystallographic structure, brasses are generally divided into the following categories:

a) Single phase (alpha) brasses with up to 37 % Zn.

b) Two phase (alpha + beta) brasses which start to form at about 37.5 % Zn.

c) Single phase (beta) brasses which contain about 46 % Zn.

d) Two phases (beta + gamma) brasses containing above 59 % Zn.

The *alpha brasses* are very similar to copper, but in general they possess better corrosion resistance. They are tough, ductile materials and their strength improves with the increase of the zinc content. Alpha brasses suffer considerably from the selective dissolution of zinc and the phenomenon is known as dezincification. The loss of zinc reduces the mechanical properties of the material since the dezincified portions are weak, permeable and porous. Nowadays, the use of alpha brasses must be limited to the inhibited types (containing arsenic). Inhibited alpha brasses are successfully used in small seawater cooled condensers, provided the flow speeds are low and the water is clean.

The *alpha-beta* brasses are two-phases alloys whose zinc content lies within the limit 37.5 to 45.0 %. Alpha-beta brasses suffer severely from dezincification when in contact with seawater even if the dezincification of the alpha-beta alloys is not as obvious as with the alpha-phase materials. To date no reliable method of inhibiting the dezincification of the two phase brasses has been discovered [74]. Despite this fact, some two-phase brasses are used in desalination plants and in ship building. The alpha-beta alloys must be continually inspected and remedied by patching and painting. As a rule alpha-beta brasses should not be used in contact with seawater.

The *beta* brasses, containing 50 % of each of copper and zinc, should not be used in contact with seawater. They suffer rapid dezincification, which is manifested in the form of intercrystalline cracking [74]. The corrosion resistance of beta brasses towards seawater is considerably inferior to that of the alpha-beta brasses.

The *gamma brasses*, with less than 45 % Cu, possess neither the mechanical nor the corrosion properties necessary for the construction of plants operating with seawater.

4.3. The bronzes.

Bronzes are basically copper-tin alloys, containing up to 8 % tin. The higher the tin content of these alloys the more resistant they are to corrosion by seawater. Care must, therefore, be paid that the heat treatment of the high-tin alloys does not produce tin-reach segregates since that will lower the corrosion resistance in seawater.

Alloys of copper containing up to 10 % aluminium, referred to as aluminium bronzes, have proved to be very useful in seawater, as their corrosion resistance is very high. This type of copper alloy owes its good corrosion characteristics to the presence of a very thin transparent film on its surface, which heals very rapidly when damaged. They also exhibit good resistance to erosion and wear. However, dealloying of aluminium bronze has repeatedly shown to be a problem [75-76]. Although small additions of nickel has found to improve its character, severe selective phase corrosion can occur near the heat affected zone of welded cast of nickel-aluminium bronze during exposure to seawater environment.

4.4. The Copper-Nickel alloys.

Copper-nickel alloys are another important range of copper-base engineering materials with erosion-corrosion resistance, especially in marine conditions, usually superior to brasses and bronzes [77-78]. Since copper-nickel alloys form the basis of this research, their erosion-corrosion behaviour is described in more detail. Much valuable and detailed work on erosion-corrosion behaviour of copper-nickel alloys in seawater was done in 1970's and 1980's and during this period a number of review papers appeared, the main features of which are now summarised.

4.4.1. Effect of iron and nickel on the corrosion behaviour of copper-nickel alloys.

The beneficial effect of incorporating iron in the copper-nickel alloys has long been known and this addition is essential to obtain adequate corrosion resistance by assisting in protective film formation [68,79]. It has been established [80-81] that the main component of the protective film forming, in the early stages of growth, on these alloys in seawater consists essentially of cuprous oxide (Cu_2O), with the protective value enhanced by the incorporation of nickel and iron causing decrease in both ionic and electronic conductivity.

Small additions of iron to copper-nickel alloys are also known to improve their resistance to erosion-corrosion [82], because iron is necessary for the occurrence of nickel enrichment in the corrosion product layer [83].

Figure 4.1. shows the effect of iron content on the impingement attack on 90-10 copper-nickel from 30-day tests obtained at 3m/s water velocity. Although the experimental data were obtained at different laboratories, using different tests under different conditions, there is fairly good agreement between the data. A distinct minimum is apparent between 1.5 and 2.5% iron. Optimum iron levels are a result of solid solubility. The corrosion resistance improves with increased iron so long as it remains in solid solution [79].

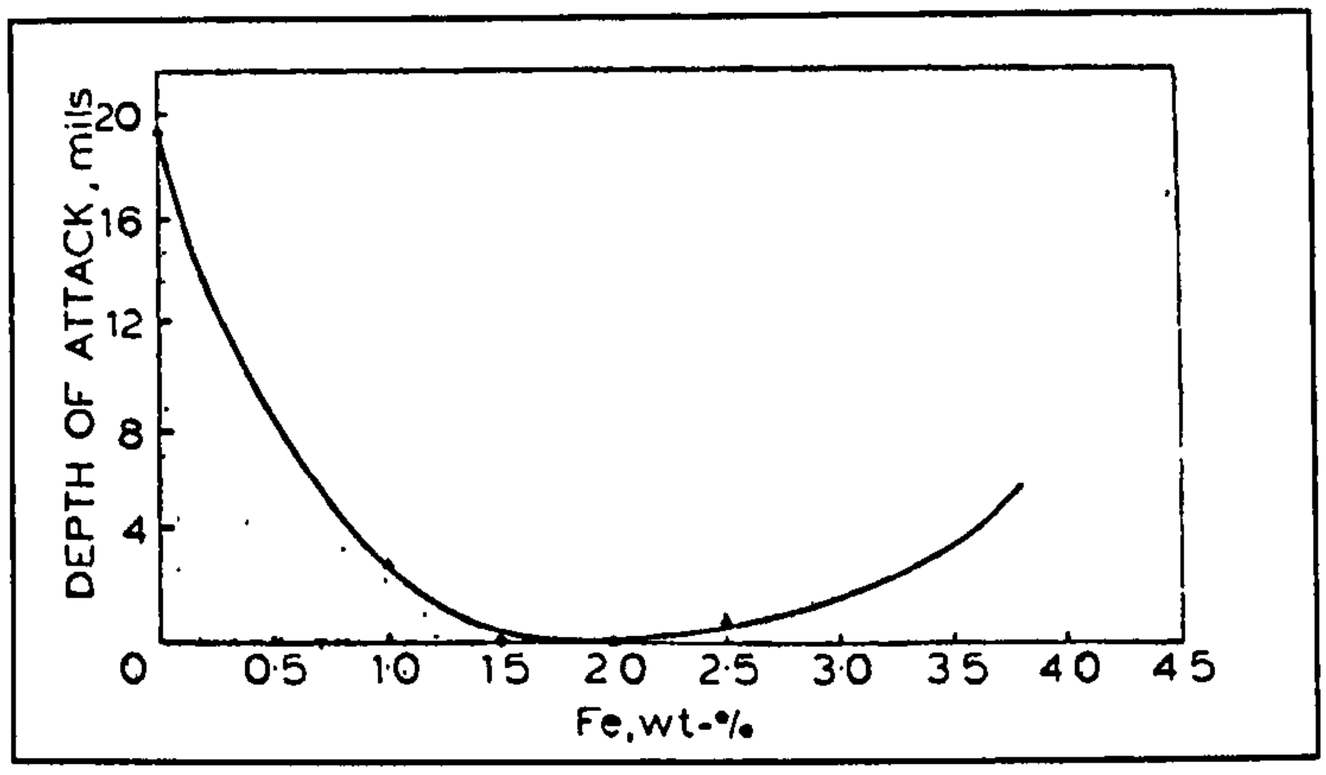

Figure 4.1. Effect of impingement attack on Cu-10%Ni in seawater; all data from 30-day tests, curve is best fit for data obtained at 3m/s [79].

According to Efird [83], nickel has a beneficial effect in improving the corrosion resistance of copper alloys in quiet and flowing seawater, with iron acting to lower the nickel level required for good corrosion resistance. The best resistance to impingement at 7.5 m/s is obtained with iron levels of 0.8 to 1.4% with nickel ≥10%. This is true for resistance under conditions of accelerated attack only and does not necessarily hold for resistance to the initiation of accelerated attack.

In general the iron level required for nickel enrichment stimulation is apparently dependent on the amount of nickel in the alloy. The required iron level increases with decreasing nickel content.

4.4.2. Effect of other components on the corrosion behaviour of copper-nickel alloys.

Manganese is necessary as a deoxidant during the melting process, but its effect on corrosion resistance is less well defined than that of iron [79]. Before the development of Cu-10%Ni there were indications that variations in the corrosion resistance of Cu-30%Ni tubes could be due to variations in the manganese content. This was investigated [79] and it was found that, at low iron contents, the addition of manganese improved the impingement resistance but, at iron contents above 0.3 %, manganese had no effect.

Anderson and Efird [84] reported that the addition of chromium (up to 3%) increased the hardness of Cu-10%Ni and allowed its use in contact with flowing seawater at velocities higher than those permitted for the chromium free alloy.

Although it should be emphasised that the impurity levels must be tightly controlled because elements such as lead, sulphur, carbon and phosphorus, while having minimal effect on corrosion resistance, can influence hot ductility and, therefore, influence weldability and hot workability [79].

4.4.3. Nature of the protective film.

The good corrosion resistance of Cu-10%Ni in seawater is related to the formation of a protective film of corrosion products in the early period after initial exposure. The behaviour thus depends on the composition and structure of that film, as well as on some other parameters, such as its adherence, strength, catalytic properties, etc. All those properties may vary, depending on the conditions and mode of initial exposure. Hence, much attention has been given to studies of the effect of environmental variables on the formation and properties of the protective film [85-86].

It is generally considered [86] that the inner part of the film is cuprous oxide (Cu_2O) with cupric oxide (CuO) appearing in the outer parts of the film, and that the films contain other metallic ions together with chlorides, hydroxides and carbonates. An indication of the detailed complexity of the films on Cu/Ni alloys in marine conditions was provided by Kato at al [87-88]. Their work concluded, from exposing Cu-10%Ni samples to air-saturated 3.4% NaCl solution and analysing the corrosion product layers by SEM and X-ray diffraction, that the protective films formed under open-circuit corrosion conditions had the following features:

1. The films were comprised of a relatively thick outer layer, mainly cuprous hydroxy-chloride [$Cu_2(OH)_3Cl$], and an inner layer containing appreciable amounts of chloride, oxygen and copper, and some nickel;

2. Were rich in chloride throughout the film with a maximum concentration along a plane located within the inner layer near the inner layer/outer layer interface;
3. Were relatively poor in Ni and Fe in the inner layer, compared to levels in the outer layer, and
4. Had, in early stages of growth, outer surfaces consisting of a cuprous, (probably Cu_2O) compound which, with time, gave way to carbonate and finally to cuprous hydroxy-chloride [$Cu_2(OH)_3Cl$] compounds.

The inner film is normally reddish. The outer film may be greenish, brown or yellow brown. Although $Cu_2(OH)_3Cl$ and Cu_2O oxides are the principal components of the film, the lattice usually includes other metallic ions, iron, nickel, aluminium, calcium, sometimes silicon and sometimes other species. Principal anions include chlorides, hydroxides and carbonates, bicarbonates and oxides [85].

It has been reported that the greater corrosion resistance of the copper-nickel alloys, Cu-10%Ni and Cu-30%Ni, appears to be due to the outer, loosely adherent corrosion product layers, since the corrosion rate increases when these layers are removed [99]. The same research showed that the Cu-30%Ni has slightly better corrosion resistance than Cu-10%Ni, but in general the vulnerability of attack is not of great difference.

According to Popplewell [90], the appearance of the corrosion film depends on the iron content of the alloy; the film on samples with 0.3 % iron or less was bright green, that on samples with 1.5 % iron (in solution in the alloy) was dark green, and that on samples with 1.5 % iron, heat treated to precipitate an iron rich phase, was nearly black.

The colour of the film depends on the water flow velocities [92]. Cu-10%Ni tubes were exposed to flowing natural seawater with a flow velocity of 1m/s and 2m/s. After the exposure with these different applied flow velocities a significant difference in colour of the protective film was observed (gold-brown with 2m/s and greenish-grey with 1m/s).

Moreover, Ijsseling [93] showed that the appearance, thickness and adherence of the film depends also on the temperature of formation. In tests in flowing (at 1.5 m/s)

seawater, a dark brown, adherent layer was formed at 10° C, a less adherent dark brown one at 20-30° C, and very thin, adherent, gold-brown film was formed at 40-50° C.

The rate of film formation, Figure 4.2., was portrayed by Tuthill et al[86] from measurements of the copper content of condenser sea water effluent over a 3-month period after start up. Copper content was found to decrease by 10% in 10 minutes and by 1% in an hour. After 3 months, the copper in the effluent was at virtually the same level as that in the intake water. This indirectly shows that the maturity of the protective film reduced the corrosion rate of the condenser tube surfaces.

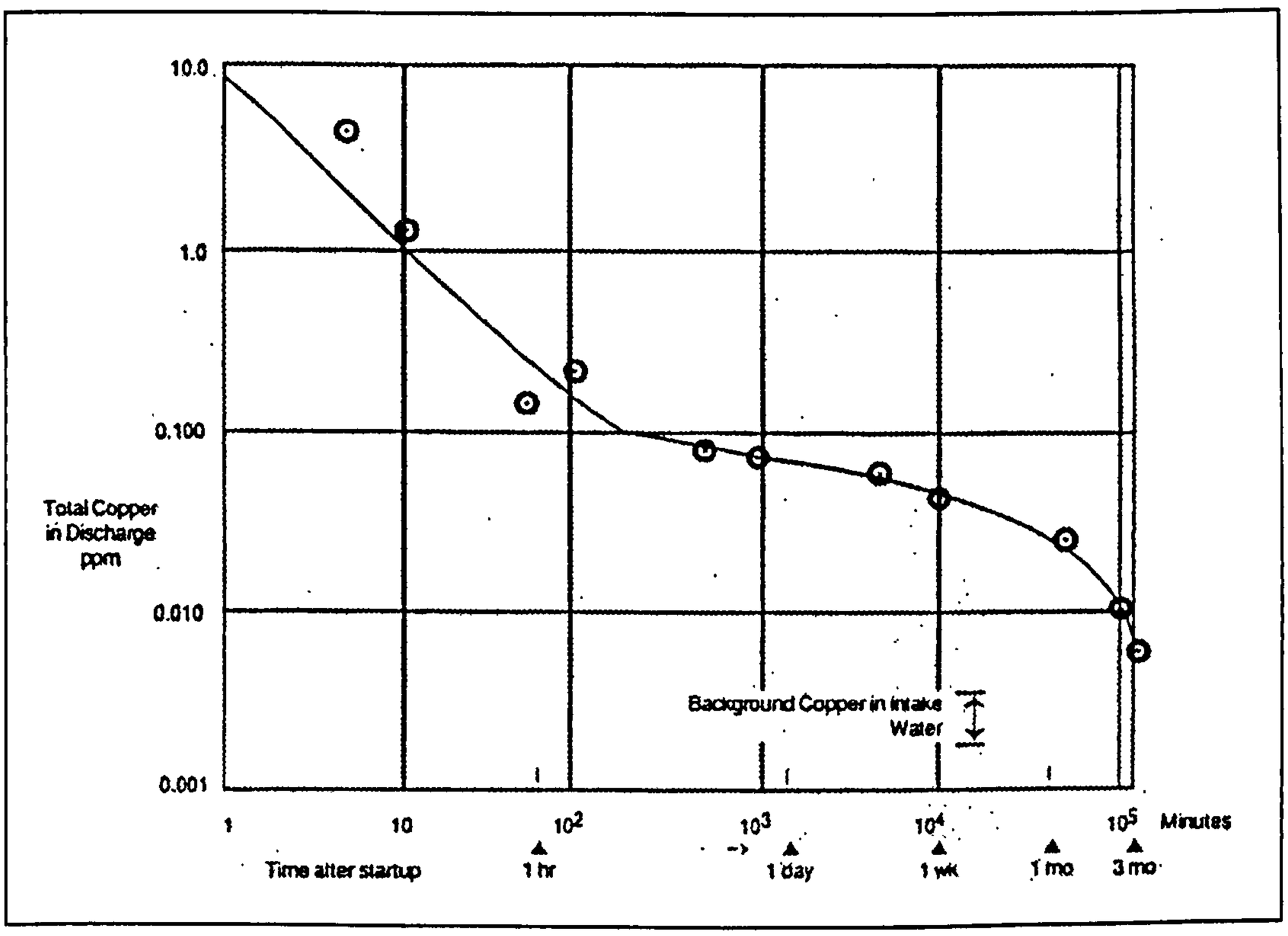

Figure 4.2. Formation rate of corrosion product film on Cu-10%Ni in seawater [86].

The flow velocity has a distinct influence on the corrosion behaviour, mainly on account of the transport of reactant and/or corrosion products. Moreover, at low flow velocities there is the possibility of the deposit of sand, debris, mud, etc., increasing the chance of the formation of macro corrosion cells (differential aeration and concentration cells). When under impingement conditions the flow is interrupted long enough, the possibility exists for the damaged zone to repassivate and so the ultimate effect will be

lower than with continuous flow. The repassivation rate will depend on factors such as oxygen content, temperature, flow velocity, alloy composition and chloride content [95-96].

The film, however, continues to become even more protective with time, as indicated by corrosion rate measurements made over several years. Studies in quiet seawater show that the time span approaches 4 years before the decrease in corrosion rate becomes negligible. In flowing water, the corrosion rate, as shown in Figure 4.3., was found to decrease continually over at least a 14-year period [86]. However, it is clear from Figure 4.3. that all the rates shown at 1 year or greater exposure time, are extremely low.

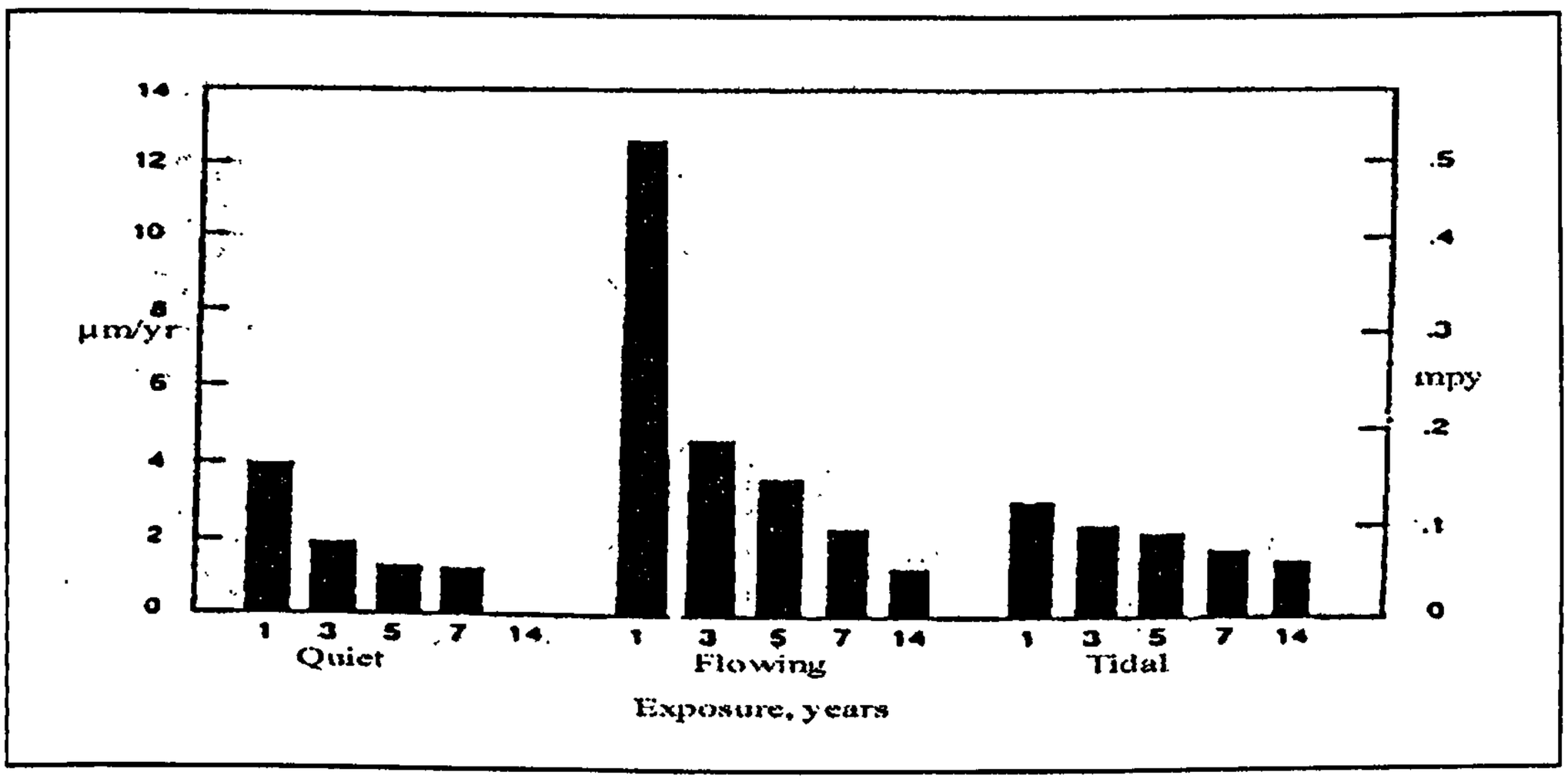

Figure 4.3. Corrosion rates for Cu-10%Ni for long-term seawater exposures [86].

In general the composition and properties of the film depend on the alloy composition and the condition of seawater at the time of initial exposure. In polluted seawater, any sulphides present can interfere with film formation, producing a black film containing cuprous oxide and sulphide [85]. This film is not as protective and adherent as films formed in unpolluted water. However, if an established cuprous oxide film is present, then periodic exposure to polluted water can be tolerated without damage to the film.

4.4.4. Effect of temperature.

The main uses of Cu-10%Ni are as tubing for condensers, and heat exchangers using seawater as the coolant, and in desalination plants. Hence, the range of temperatures of interest would be from subzero (for arctic conditions) to about +150° C.

A rise in temperature would, as a rule, increase the rate of chemical reactions and is thus likely to increase the corrosion rate if a chemical reaction is the rate-controlling step. This is, however, rarely the case in most corrosion processes; such processes are frequently controlled by diffusion phenomena, solubility effects, structure and degree of perfection of the protective films, and many other factors for which the effect of temperature is not an accelerating one [85].

Generally the corrosion of copper base alloys in deaerated seawater flowing from 0.9 to 2.7 m/s increases as the seawater is heated to 63°C. Maximum corrosion occurs at the intermediate temperatures 54 to 71°C. As the seawater increases to high temperatures (~107°C), a significant decrease in corrosion is noted [97].

The main effect at higher temperatures is the very fast formation of an efficient protective corrosion product layer. According to Ijsseling et al [93], in aerated seawater, as the temperature is increased from 10 to 40°C, the protective layer of corrosion products is more readily formed.

Moreover, the protective quality also seems to increase with increasing temperature. At a temperature of 40°C an efficient protective corrosion product film is formed within a few days of exposure. On the contrary, at lower temperatures increasingly more time is needed to obtain a corrosion product layer, which, moreover, is less protective than that formed at 40°C, and that means higher corrosion rates.

As an example Tuthill, Todd and Oldfield [86] reported that at 16°C it took slightly over one hour for a thin film to cover the surface and three months before a reasonable mature film covered the specimens of Cu-10%Ni. At even lower temperatures of 2°C it took a week before a thin visible film covered the surface of the same specimens.

Also, Fink [99] reported that in tests of 156 days in seawater the corrosion rate, (quoted as mils per year), of Cu-10%Ni showed a continuous decrease as the temperature was increased between 55 to 120°C, and Syrett [121] studied the results from previous investigations and finally considered that an increase in temperature causes either little change or reduces the corrosion rates for Cu-10%Ni.

4.4.5. Effect of velocity.

The development of iron containing Cu-10%Ni was initially prompted by the need for better materials on ship condenser alloys, exposed to relatively high seawater velocities. Although higher coolant flow velocities improve the efficiency of condensers and heat exchangers, the velocity can not be increased to the limit of materials endurance; the maximum design flow velocities for such equipment are usually limited by the increase in cost of power to overcome pressure drops at high velocities.

One theory, based on work carried out by Efird [101], is that seawater moving over a surface creates a shear stress between that surface and the layer of seawater closest to the metal surface. As velocity increases the corrosion rate will at first increase slowly, as a result of increased oxygen supply, (cathodic depolarisation), and also by removing corrosion products from the component surface. Eventually the degree of turbulence and the shear stress will be such that the protective film is locally removed and the active underlying metal will be exposed; at this "breakdown" velocity the rate of attack will increase dramatically [80].

Efird [101] studied and estimated the critical shear stress for various Cu-base alloys. His research suggested that shear stresses depended on velocity and geometry. As pipe diameters increased, copper-based alloys tolerated higher nominal velocities. Taking the Cu-10%Ni alloy as an example, the critical velocity for a 0.03m diameter pipe was 4.4.m/s, while the critical velocity for a 3m diameter pipe was 6m/s. The critical shear stress in seawater for the tested copper-base alloys were:

Alloy	Critical Velocity	Temperature °C	Critical Shear Stress (MPa)
Aluminium brass	2.2	12	0.000019
Cu-10%Ni	4.5	27	0.000043
Cu-30%Ni	4.1	12	0.000048
84-16 Cu-Ni + 0.5 Cr	12.0	27	0.000297

Table 4.1. Critical velocity and Shear stress of Cu-base alloys in seawater [101].

Sato and Nagata [102], showed that the shear stress at the inlet end of a condenser tube is about double that further down the tube. This explains why inlet-end erosion-corrosion is such a common occurrence and also explains the preference for the copper nickel alloys that have been developed because of their greater velocity tolerance.

As noted above, the velocity range of interest for sea water flow in Cu-10%Ni tubes in not unlimited; because of power cost considerations. The maximum design flow rates for condensers and heat exchanger tubing in normal service usually lie between 1.8 and 2.4 m/s and most measurements have been made in that range [103-104]. General experience is that Cu-10%Ni, with iron content about 1.5 %, is the optimum choice of a material for seawater cooling systems, with water velocities up to about 2.5 m/s [81,105].

The data of Syrett and Wing [106] were obtained in a recirculating flow loop, with aerated water, deaerated water, and water containing sulphide (0.2 g/m^3), at 20-28.4°C and pH 8.2. Under most of the experimental conditions examined, corrosion occurred fairly uniformly across the exposed surfaces of the specimens. However, in aerated seawater the copper nickel alloy suffered localised corrosion at 3 m/s and higher velocities. The rate of localised corrosion, measured by the linear polarisation method, was high and became more intense as the velocity was increased from 3 to 5 m/s. The authors emphasised that turbulent conditions existed at all flow velocities, (Reynolds numbers from 7400~(0.5m/s) to 74000~(5m/s)), and that it would be more appropriate to relate the corrosion data to Reynolds values rather than to the flow velocities.

At even lower velocities, the corrosion process depends on the time needed for the formation of a protective film on the surface of the specimens. Cu-10%Ni tubes were

exposed to flowing seawater [107] with a flow velocity of 1.5 m/s. Average weight loss tests showed a decrease with increasing time, indicating a decrease of the corrosion rate. According to Ijsseling's [107] opinion this is due to the slow formation of a protective layer. The applied flow velocity was 1.5 m/s and it can be clearly seen that the flow velocity of the seawater is an important factor regarding the time necessary to build up a protective layer, i.e. the corrosion rate was decreased by a factor of 60 times, at a 100 days compared to 15 days exposure.

Ross and Anderson [103] reported, that at a fixed velocity of 2.4 m/s, the weight loss after 4 months, (deaerated water, 32°C), decreased from 30 to 10 mg/cm^2 with increasing pH between 3 and 8. There were effects of temperature, oxygen content, and pre-treatment, in addition to those of the flow velocity and the pH. The main conclusion was that the corrosion behaviour of copper-nickel alloys is dependent upon the initial film which is influenced by the specific environmental conditions at exposure; and that of all alloys studied (Admiralty and aluminium brass, 90-10 and 70-30 cupronickels), the 90-10 Cu-Ni alloy is the most logical material choice for hot sea water environments under the investigated conditions.

Ijsseling [92] measured the corrosion rate of Cu-10%Ni samples by the polarisation resistance method. The corrosion resistance at a flow velocity of 1-3 m/s was found to be better than that at 0.1 m/s. This suggests that excessively low water velocities can be undesirable for copper nickel alloys. At water velocities less than about 1 m/s, solid deposits in the water streams tend to settle on the metal surface. Some deposits can cause crevice or deposit attack. In addition, deposits may stimulate impingement attack, e.g. where a lodged shell fragment in small diameter tubing diverts flow against the tube wall. Maximum seawater velocity for Cu-10%Ni to avoid impingement attack and pitting [108] is given at about 2.6 m/s.

According to Anderson and Efird, polarisation resistance measurements indicated a film formation on Cu-10%Ni, with no significant difference in film-forming tendencies between the normal seawater and the double salt concentration, (19.4 parts per thousand – ppt – chloride ion, to 39.7 ppt chloride ion), at 54.5°C [119].

Cohen and Rice [110-112] tested Cu-10%Ni alloy tubes in seawater at 130°C for 3 months with an inlet oxygen concentration of 72 ppb. According to their total weight loss results, uniform corrosion was observed. No erosion or cavitation corrosion took place on either the inlet or outlet ends of the tubes, even at the highest velocity of 5m/s, and the corrosion rates increased with velocity; at 1.2, 2.4 and 4.8m/s the average corrosion rate was 13.208μm/y, 20.06μm/y and 47.75μm/y respectively.

Nahman and Duffy [113] measured the corrosion rates of Cu-10%Ni in sea water at ambient temperature by weighing each specimen before and after the test; they found that the corrosion rate at ambient temperature first decreased from 7.6μm/y to 2.54μm/y, then increased to over 101.6μm/y (=4mil/y), when the flow velocity was gradually increased from 0 to 2.1-2.4 to 4.6 m/s, respectively.

Mifflin and Bird [114], reported a similar phenomenon of decreasing corrosion over a range of increasing flow velocity from 0.8-12 m/s in cooling water which varied from 50 mg/l to 12000 mg/l of chloride. . They tested Cu-10%Ni specimens at 1.2m/s brackish (up to 12000 ppm chloride) cooling water velocity, where it suffered both general plus pitting corrosion. Pitting attack was identified as denickelification. As the velocity was decreased further to 1.2m/s, more severe denickelification resulted. According to the observations made by Yandushkin and Kuris [115], a cupronickel (of 6% Ni content) in sea water was successively subjected to active dissolution, then passivity, then corrosion-erosion as the flow velocity was gradually increased from 0 to 3.6 to over 6 m/s.

At high velocities, pitting corrosion appeared on Cu-10%Ni specimens according to the BNF Metals Technology Centre [116]. Jet impingement tests were carried out for 28 days, at velocities of 9.2 m/sec with sea water obtained from Portland Harbour and containing 3% added air. The results showed that Cu-10%Ni was subject to pitting with pit depths about 10μm, (at temperatures from –1 to 15°C).

At very high flow velocities above the breakdown of the protective film, (i.e. above 9m/s for 30 days at 27°C), the surface of the samples of 90-10 can be extremely smooth [101]. That means that where the material is used in these flow regions, such as

ship hull applications, the surface would become smoother with time. This could create definite advantages in the reduction of friction factor and energy required to move the vessels as operating service increased; although it has to be emphasised that the material loss is greater.

L.E. Eiselstein [117] at al, using the linear polarisation method, reported that after 16 days of exposure to filtered Pacific Ocean water at a flow rate of 3 m/s, (pH=8.1 and 23.2°C), the corrosion rate of Cu-10%Ni was 17μg/m^{2}sec but increased sharply to 538 μg/m^{2}sec, when the water was polluted with sulphide.

Lee at al [118] showed that for the copper alloys, increasing seawater velocity generally results in slightly active corrosion potentials. Especially the corrosion potential of Cu-10%Ni exposed to seawater at 10-25° C, showed a general shift in the negative direction between –0.2V to –0.3V (SCE), as the velocity increased from 3 to 15m/s.

Some of the published data on the corrosion rate of Cu-10%Ni in flowing sea water are summarised in Figure 4.4., as a function of flow velocity [85]. Although the data indicate a general trend of increasing corrosion rates with velocity, Figure 4.4. needs to be considered with caution since the data cover a wide range of conditions. For instance, the a-line relates to desalination plant brine heater simulation tests, (120°C, deaerated brine), the b-line on the left-hand side has been substantially mis-plotted, and the c-line relates to 230 hours exposure tests to aerated seawater at 20-28.4°C.

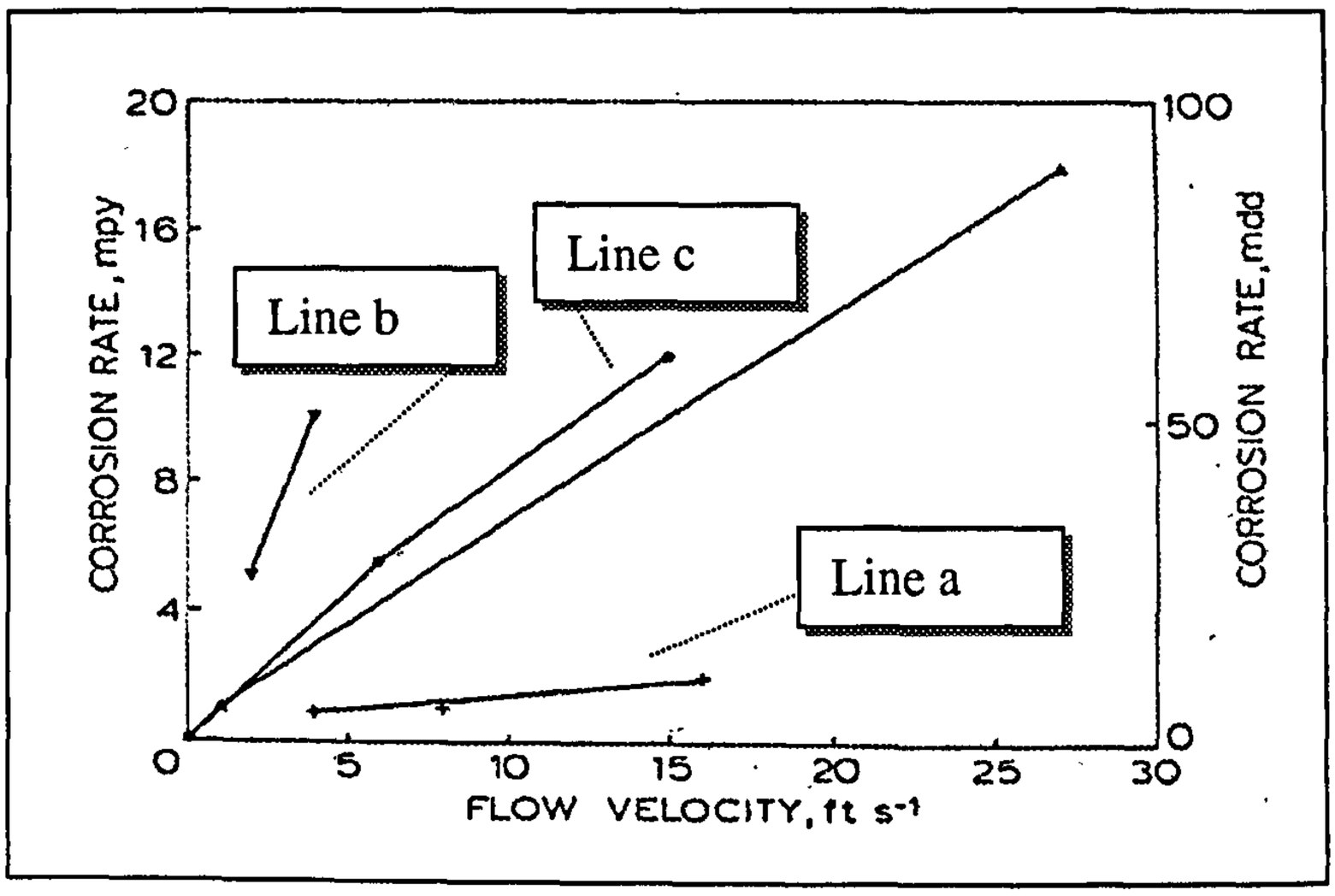

Figure 4.4. Effect of seawater flow velocity on corrosion of Cu-10%Ni at various temperatures; 1ft/sec ≈ 0.3 m/sec, 1mil=0.001in=25.4μm [85].

4.4.6. Effect of pH.

As pH decreases the corrosion rate increases. Low pH levels prevent copper-base alloys in general from developing or maintaining protective films, (which consist of corrosion products at the metal surface), and thus high corrosion rates are sustained.

It has been reported by Tuthill and co-workers [86] that there was no film formation on Cu-10%Ni in seawater below pH 6, even though there was adequate oxygen, 5.5-7.5 mg/l, present. The unfilmed corrosion rates were high since high oxygen levels in combination with low pH further accelerate corrosion [97].

At higher pH's, where some oxygen was present, corrosion rates were low and normal [86].

Furthermore, lowering the pH of either fresh water or seawater, increases the rate of erosion-corrosion. It was shown [120] that at 65°C the erosion-corrosion attack is much more extensive and appeared at lower velocities when the pH was decreased from 8 to 6.5. If the pH of warm (35°C) seawater flowing at about 2.7 m/s is adjusted to 3.6, no protective film forms on the surface of Cu-10%Ni [121].

4.4.7. Effect of oxygen content of water on corrosion rate.

Corrosion of copper alloys is either eliminated or greatly reduced when the seawater has been deaerated, because the anodic dissolution of the metal cannot take place without the concomitant reduction of oxygen [121]. According to Tuthill, Todd and Oldfield [86] the corrosion rates of Cu-10%Ni remain low in the 20 to 200 ppb oxygen range, (say in comparison to aluminium brass). Moreover higher dissolved oxygen (200 to 600 ppb) content does not significantly reduce the corrosion resistance of copper-nickel alloys at high temperatures (>77°C) [97]. This explains the preference of Cu-10%Ni alloy in desalination applications [121]. Furthermore it has been reported [104] that at a test temperature of 110°C (simulated desalination plant conditions), and flow velocities up to 3m/s, the erosion-corrosion resistance of Cu-10%Ni was significantly increased when the oxygen content of the water was reduced from about 75ppb O_2 to 5 ppb O_2. At the lowest oxygen concentration, the Cu-10%Ni alloy corroded at 63.5 μm/y at velocities up to 3m/s, but on the other hand, when the oxygen content was about 75 ppb, the corrosion rate ranged from about 406.4μm/y at 3.7 m/s to about 279.4μm/y at 1.7 m/s.

Under conditions duplicating those in a desalination plant, at 107°C, a flow velocity about 2m/s and pH=7.2-7.5, the corrosion rate of Cu-10%Ni increased from 38.1 to 45.72 μm/y when the oxygen content of the water was increased from 5 to 85ppb [122].

Bates and Popplewell [123] conducted tests on Cu-10%Ni in sulphide contaminated synthetic water, (total sulphide content was 10 ppm), at a flow velocity of 1.4m/s. The attack after 30 days in aerated and deaerated water was 14 and 3mg/cm^2, respectively, but increased to 12mg/cm^2 in the deaerated water after 90 days; it remained unchanged in the aerated water.

4.4.8. Corrosion in polluted seawater.

Copper-nickel alloys corrode at increased rates in polluted waters, particularly when sulphides or other sulphur compounds are present [80,86,108]. Sulphides form a black corrosion product, which is less adherent and protective than the normal oxide film. Under susceptible conditions, unwanted pitting or accelerated general corrosion may occur.

In the complete absence of oxygen, a sulphide film can show an acceptable degree of protection. Syrett found [94] that corrosion rates still remain low in sulphide concentrations as high as 55 g/m^3 and velocities up to 5 m/s. However the sulphides become detrimental if dissolved oxygen is also present in the seawater, or if exposure to oxygen-free sulphide polluted waters is followed by exposure to aerated, unpolluted water [80,81,94,105,124]. Generally the corrosion rate of Cu-10%Ni increases with increasing concentrations of dissolved sulphide in both stirred and stagnant conditions [125]. It has been indicated that copper nickel alloys with a more stable passive film formation, (like Cu-30%Ni), are less severely attacked after exposure to sulphide-polluted seawater. Gudas and Hack [126] reported that even 0.01 ppm sulphide for one day caused some accelerated attack on the Cu-10%Ni alloy, but with Cu-30%Ni, 0.05 ppm sulphide or more was necessary to cause increased corrosion.

This comes into agreement with the work [109] where it is noted that sulphide is very corrosive towards the alloys with low nickel content. In addition to that it is concluded that the higher the nickel content the more severe the susceptibility to pitting attack. However increasing the sulphide pollutant in the seawater, reduces the severity of pitting tendency. For alloys with lower nickel content (like Cu-10%Ni), the extent of localised attack seems to be slight.

Besides it was concluded that the Cu-10%Ni with a small addition of Cr, about 0.7%, performs as well as Cu-30%Ni [85]. This contradicts the conclusion of Anderson and Badia [127], where it was reported that Cu-10%Ni alloy performed much better than

Cu-30%Ni alloy when the impingement velocity is greater than 6m/s and a chromium(+0.7%) modified Cu-10%Ni performed much better than Cu-10%Ni and Cu-30%Ni, in polluted and unpolluted seawater.

MacDonald, Syrett and Wing [128-129] investigated the corrosion of Cu-Ni alloys, in flowing (1.6 m/s) seawater containing sulphide, polysulphides, or sulphur. Under these conditions, cuprous sulphide forms as the principal corrosion product causing damage to the protective film on the metal surface and hence lack of passivity.

The importance of proper protective film formation on tubes and pipes must be emphasised. It is stated that if during the early life of condenser tubes clean seawater passes through, good protective films will form which are likely to withstand most adverse conditions. The ideal situation, whether in a ship or power plant, is to recirculate aerated, clean seawater at initial start up for sufficient time to form a good protective film. If, however, polluted waters are encountered during the early life, the films formed on the condenser tubes will likely not be fully protective and the risk of premature failure will be considerably increased [108].

It is also reported [85] that all copper-nickel alloys are liable to deep attack in jet impingement tests with contaminated seawater, particularly when the water contains hydrogen sulphide. Under these conditions the Cu-10%Ni alloy gave the best results because it suffered less severe localised attack than other copper alloys, like Cu-30%Ni. The severity of attack increased as the level of sulphide increased [130].

In some contrast to the above-described general deterioration effect of sulphides, two studies have reported different findings in water of relatively high flow rates. At high impingement velocity – above the 'breakdown' of the protective film -, (>5.5m/s), corrosion of copper-nickel alloys decreases with increasing sulphide concentration. This is due to the formation of a copper sulphide layer, which thickens with time; that acts as a physical barrier to further corrosion [131].

According to other work [132] the corrosion susceptibilities, (as measured by polarisation resistance), of copper-nickel alloys, (even with +0.7% chromium), in sulphide polluted seawater, whether aerated or deaerated under a jet impingement

velocity of 6.1 m/s, were found to be lower than those in unpolluted seawater under the same conditions.

4.4.9. Effect of sea organisms.

Gilbert and LaQue [133] showed that even plankton is a variable in the corrosion behaviour of copper-nickel alloys, because these organisms could exert both chemical and mechanical effects, the latter through abrasive action of the animals or their hard skeletons, e.g. the silicious material in diatoms.

4.4.10. Biofouling.

Copper and copper alloys are more resistant to the attachment of biofouling organisms than steel and most of the other common materials of construction. They are also resistant to the microfouling that occurs within condenser and heat exchanger tubing [105]. The resistance to biofouling is an inherent characteristic of copper alloy and appears to be associated with copper ion formation within the corrosion product film. Efird concluded [134] that copper-base alloys possess fouling resistance due to the formation of an adherent cuprous oxide corrosion product, which is toxic to the organisms. Coupling to steel or less noble materials or cathodic protection, which suppresses copper ion formation, allows biofouling to occur on copper alloys as readily as on other materials [94].

It has been reported that, at velocities below 0.9 m/s, sediment settles out readily in horizontal runs of pipe and tubing [86]. Unless removed periodically, under-sediment corrosion in the form of general pitting attack may occur. Slime layers also build up at low velocities providing a good habitat for biofouling organisms to attach to the slime layer and grow. At normal heat exchanger tube velocities, much of the biofouling is

swept away because it is so lightly attached to the slime layer, which is one factor tending to keep the tubes clean and heat transfer capability in an acceptable range.

4.4.11. Dealloying.

The nickel content determines the corrosion behaviour over a wide range of nickel concentration. Increasing the nickel content reduces dissolution of the Cu-rich matrix, and even a small percentage of nickel significantly decreases the corrosion rate of Cu-Ni alloys. For nickel contents <50% there is simultaneous dissolution of both components with eventual redeposition of copper. For nickel contents ≥50% selective dissolution of copper takes place, as has been shown by electrochemical and X-ray diffraction examinations [135].

Mansfeld et al [136] reported that de-alloying of all copper alloys only occurred in natural seawater (long term exposure > 30 days), and no evidence of dealloying was noted in artificial seawater., which suggested that it was due to the action of micro-organisms. According to his research, intergranular corrosion is usually explained by the more reactive nature of the grain boundaries, due to the differences in their chemical composition, from that of the grains producing a galvanic couple with a very small anode coupled to a large cathode; bacteria may locally change the interfacial chemistry resulting in preferential grain boundary attack and intergranular corrosion. This implicit necessary involvement of micro-organisms in dealloying does not seem to have been suggested by others.

4.4.12. Effect of seawater treatments.

Ferrous sulphate

The possibility of being able to control corrosion behaviour of copper alloy condenser tubes more precisely than by relying on adventitious iron corrosion products in

the system was first recognised by Bostwick [137]. He has shown how small regular additions of ferrous sulphate to the cooling water can have dramatic effects on limiting the deterioration of copper-base condenser tubes, on which proper protective films have evidently previously not formed.

The points of interest concerning ferrous sulphate treatment to prevent corrosion of copper base condenser tubes can be summarised as follows [138]:

a) It is most important to inject a fresh ferrous sulphate solution directly into the condenser water box, or at a point in the cooling water intake pipe close to the condenser. Experience suggests that the further from the condenser the point of injection is, the less effective the treatment will be.

b) There is some evidence that chlorination can cause an increased risk of corrosion at higher than normal levels and that ferrous sulphate can prevent these damaging effects.

c) With copper-nickel alloy tubes, ferrous sulphate treatment is normally unnecessary. However, there have been instances where corrosion has developed in abnormal circumstances and the treatment has proved beneficial with such cubes.

d) Although ferrous sulphate treatment is normally used in seawater situations, beneficial effects have also observed in fresh water.

e) Studies of the films formed as a result of ferrous sulphate treatment, indicate that lepidocrocite FeO.OH is sometimes present. North and Pryor [139] showed that this film provides corrosion resistance to copper surfaces.

Chlorination.

Coastal power and process industry plants have used chlorine to control biofouling and slime formation for many years. General experience indicates that Cl_2 concentrations in the range of 0.2-0.5 ppm will control biofouling with no effect on the corrosion of copper-nickel alloys [140]. Excessive chlorination, however, can damage copper alloy tubing.

On the other hand there is some evidence that at high velocities, chlorination has the effect of increasing the impingement rate in the Cu-10%Ni alloy [141]. For an impingement jet velocity of 9m/s, the depth of impingement attack was increased from 0-0.2 to 0.6-0.8 mm as the free chlorine concentration was increased from 0 to 4ppm [142]. It should be noted however that 9m/s velocity is not normally encountered or recommended for copper-nickel alloys, in cooling water systems.

4.4.13. Effect of suspended particles.

Suspended fine solid particles as a rule, increase the erosion-corrosion rate of many materials, including Cu/Ni alloys, in flowing seawater.

Sand is common in seawater from open channels in shallow waters. High sand loading can be detrimental to copper alloy tubing and can damage the protective film, exposing bare metal to high unfilmed corrosion rates. In general for any given sand loading, damage to Cu-Ni alloys increases with the size and the sharpness of the sand present and the impact angle [143]. The presence of suspended solids will clearly represent a factor that will further damage protection corrosion product layers [143-144].

The general order of copper nickel alloy resistance to liquid/solid 2-phase flow, follows [145]:

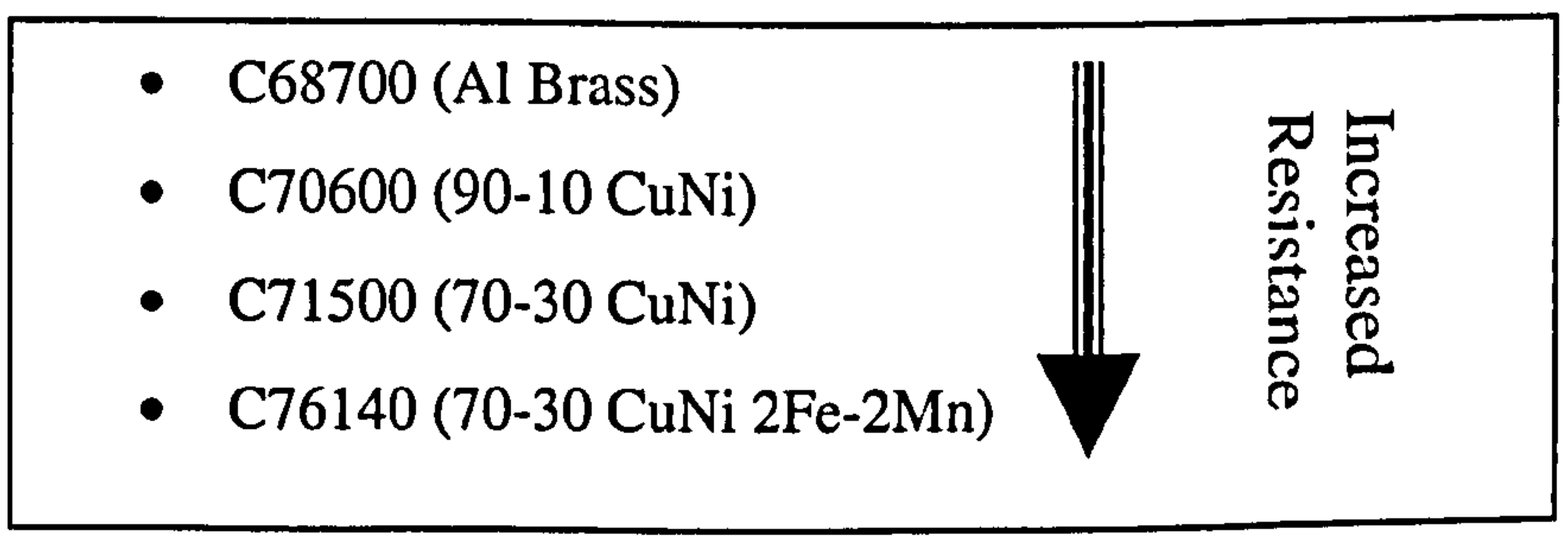

4.4.14. Effect of silt.

Silt or mud has no abrasive effect on the corrosion film, but can be very damaging for Cu/Ni alloys, if allowed to deposit in tubing and remain in place over substantial periods of time. Silt tends to be swept through the tubing when the units are operated near normal velocities of 2m/s. At lower velocities, the amount of silt that may be deposited is a function of the settling rate, the actual velocity and the length of the tube. At velocities below 1 m/s, experience [146] has shown that corrosion failures can be expected within 6-12 months unless frequent cleaning is successful in removing deposits before under-deposit corrosion initiates.

What is believed to happen in a silt type deposit is, first, oxygen depletion in the lower part of the deposit next to the tube surface. The upper layer of the deposit remains aerobic with active bacteria. Second, and after the lower layer is depleted in oxygen, sulphate reducing bacteria become increasingly active, generating sulphides. As the sulphide concentration increases, the protective film, already weakened by the absence of oxygen begins to break down and a general pitting type of attack follows. This is generally referred to as microbiologically influenced corrosion (MIC).

If the deposits are removed and the surface is cleaned before pitting has penetrated the tube wall, the film is easily reformed when clean seawater is reintroduced and the tubing is returned to service. Even if the tube is not clean after silt removal, the film will reform, but it takes a longer time.

One of the great strengths of the copper nickel alloys is their ability to recover from abuse, reform good films and give good continued service.

4.5. Modified high strength Cu/Ni alloys – Marinel.

Although many traditional seawater corrosion problems have been countered by the use of Cu-10%Ni and Cu-30%Ni, other environment-induced effects have been identified, notable among them strength degradation and hydrogen embrittlement. Marinel alloy was developed in response to the oil and gas industry's requirements, for a material for use in the most severe engineering duties in marine environments.

Not a great deal of attention in the literature appears to devote to the corrosion and particular to the erosion-corrosion behaviour of this alloy. This is probably because Marinel was developed primarily to produce a high strength material with good resistance to hydrogen embrittlement, for applications for instance as a bolting material offshore [147-148]. However a small number of corrosion studies on modified Cu/Ni alloys with some similar compositional features as Marinel provide an indication that this alloy may possess some useful enhanced durability characteristics in comparison with conventional Cu-10%Ni.

For example as has already been reported in this chapter, Anderson and Efird [84] showed that the addition of chromium (up to 3%) increased the hardness of Cu-10%Ni and allowed its use in contact with flowing seawater at greater velocities than those permitted for the chromium free alloy.

Also Efird [101] suggests that a small addition of chromium (about 0.5%) to cupronickels, greatly increases the adherence to the protective film, thereby significantly extending the seawater velocity limits for the alloy. The critical velocity for a Cu-10%Ni pipe, (0.03m diameter) is 4.4 m/s, while the critical velocity for a (Cu-16%Ni-0.5%Cr) pipe with same dimensions is 12m/s.. The calculated critical shear stress for Cu-10%Ni in seawater was 43.1 N/m^2, when for the same conditions the critical shear stress for (Cu-16%Ni-0.5%Cr) was 296.9 N/m^2. Similar results were also reported from Alhajji et al [109], where a chromium modified copper-nickel alloy, (Cu-16%Ni-0.7%Cr), performed better than Cu-10%Ni under impingement conditions in both sulphide polluted and unpolluted seawater.

Generally, the corrosion susceptibilities, (as measured by polarisation resistance), of copper-nickel alloys, (even with +0.7% chromium), in sulphide polluted seawater, whether aerated or deaerated under a jet impingement velocity of 6.1 m/s, were found [132] to be lower than those in unpolluted seawater under the same conditions. However, the presence of sulphide in the seawater caused an increase in corrosion under impingement conditions compared to that in clean water conditions.

C.Clark and P.Guha [149] showed that Hiduron 191, (15%Ni, 5% Mn, 1% Fe, 1.4% Al, Bal. Cu), possesses superior jet impingement resistance and general corrosion resistance in sea water compared with both Cu-30%Ni and Cu-10%Ni., probably because of the beneficial effect of the aluminium additions in increasing hardness and promoting formation of a passive surface layer. It was therefore expected that, because of its higher aluminium content, Marinel should be at least as good as Hiduron 191, and in practice cavitation erosion tests in 'high', (but unspecified), velocity sea water carried out at the UK Admialty Research Establishment, Holton Heath, give the highest ranking to Marinel for various cupronickel alloys [147] (Table 4.2.).

Alloy	Typical hardness, HB	Volume erosion rate, $mm^3 h^{-1}$
Marinel (wrought)	280	1·0
Hiduron 191 (wrought)	210	1·8
70Cu–30Ni cupronickel (wrought)	110	1·9
Hiduron 501 (cast)*	170	3·3

*Cast cupronickel containing approximately 15%Ni, 10%Mn, 1%Fe, and 1·4%Al.

Table 4.2. Cavitation erosion tests in high velocity sea water [147].

Studies by Alexander [150], suggested that the solubility of chromium in the Marinel alloy is very low and that the chromium is dispersed as a fine precipitate. Microprobe analysis indicated that niobium was present as nickel-niobium rich particles which may acted as inhibitors to grain grown and thus promote improved ductility.

4.6. Summary.

This research was set against the background of much activity in recent years studying the performance and especially the mechanisms of erosion-corrosion on a range of materials from which reasonably good or very good erosion corrosion resistance might be expected; such materials as stainless steel, titanium alloys, HVOF thermal sprayed coatings.

It was found that against this background it would be of interest to study the metallic system of Cu/Ni alloys, in which good general corrosion resistance but rather limited erosion-corrosion resistance is generally found.

Hence the focus of this study is to concentrate on:

- One Cu/Ni alloy, Cu-10%Ni, in order to conduct an in-depth study, designed to extend the knowledge of the basic mechanisms of deterioration in an aqueous erosion-corrosion environment in the light of recent advances in the general area of erosion-corrosion.
- The more-recently-developed, high-strength alloy (Marinel), to assess and understand in detail any changes in erosion-corrosion behaviour associated with the specific alloying elements present in this alloy.

In particular, this study defines the complex mechanistic aspects of the interactions of erosion-corrosion and quantifies each contribution in different environmental parameters.

Chapter 5

Materials and Methods

5.1. Specimen preparation

The materials investigated in this project comprised two copper-nickel alloys. The work has been focused on a standard Cu-10Ni-Fe-Mn alloy, which is used extensively in a variety of marine industries, and on MARINEL alloy, which is a high strength precipitation-hardened copper-nickel alloy.

5.1.1. *Cu-10%Ni.*

This alloy was in fact a Cu-10Ni-Fe-Mn alloy specified by BS:CN102, UNS:C70600, but is hereafter referred to as Cu-10%Ni.

The Cu-10%Ni alloy was provided in the form of plate, the size of which was 200mmx200mm. The specified chemical composition of Cu-10%Ni and some mechanical properties are shown in Table 5.1. and Table 5.2. respectively [151].

After polishing and etching in acid ferric chloride solution, the microstructure was observed to consist of equiaxed grain structure, typical of Cu/Ni alloys, as presented to Figure 5.1.

	Copper	Nickel	Iron	Manganese	Tin	Carbon	Lead	Sulphur	Zinc
Min	Rem.	9	1.2	0.5	0.0	0.05	0.03	0.05	0.5
Max	Rem.	11	2	1	0.02	0.05	0.03	0.05	0.5

Table 5.1. Chemical composition of Cu-10%Ni [151].

Mechanical Property	
Proof Stress (N/mm^2)	140
Tensile Strength (N/mm^2)	320
Elongation %	40

Table 5.2. Typical mechanical properties of Cu-10%Ni. [151].

SEM Analysis done on an as-received and polished specimen showed the typical and expected chemical analysis for Cu-10%Ni alloy. The analysis demonstrating this more clearly was:

Cu - %	**Ni - %**
86.8	11.8

Table 5.3. Typical chemical analysis of a polished as-received specimen.

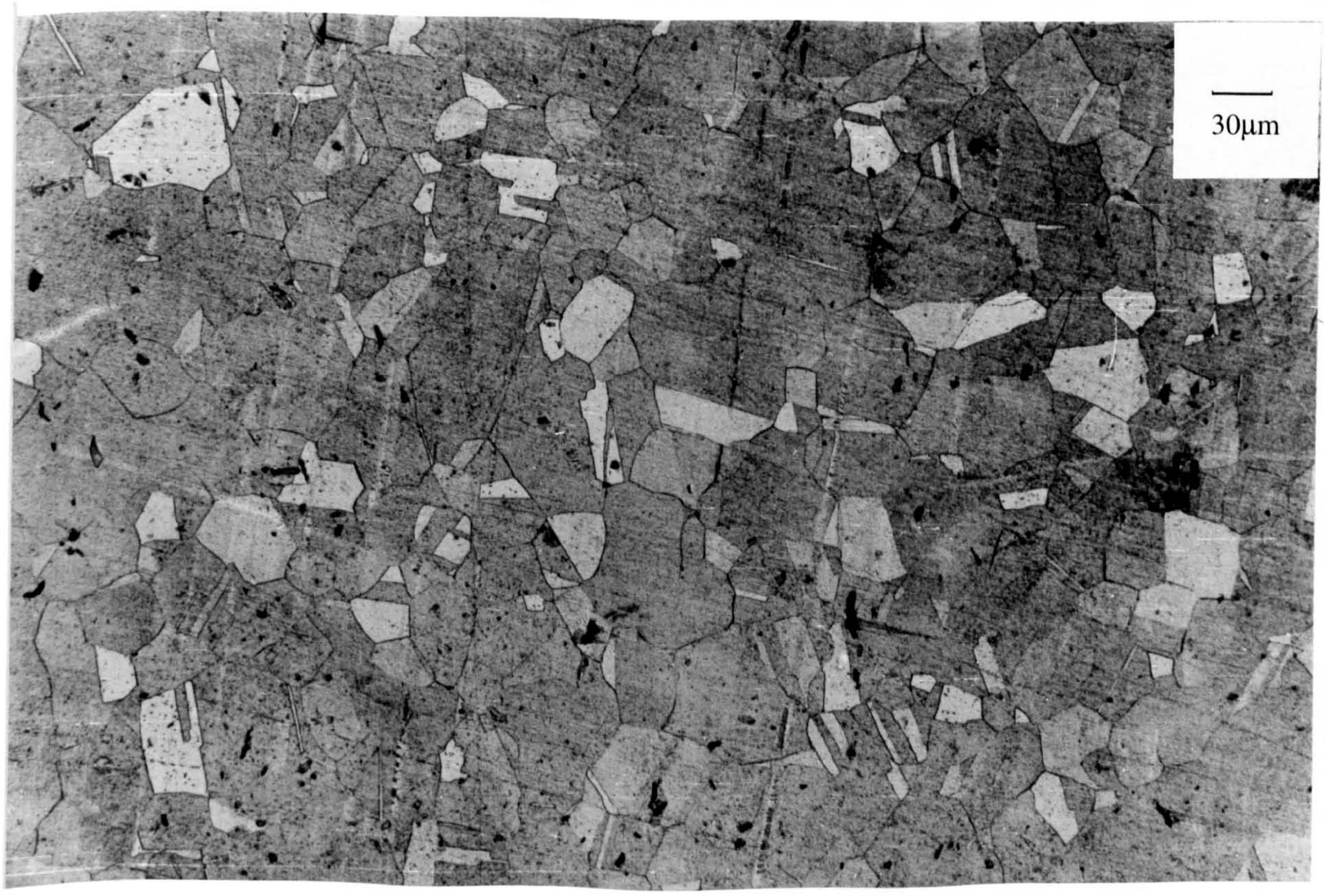

Figure 5.1. Etched structure of Cu-10%Ni alloy.

5.1.2. *Marinel.*

Marinel alloy is a patented high strength precipitation-hardened copper-nickel alloy developed by Langley Alloys, containing about 19% nickel and 4% manganese and strengthened by additions of aluminium, chromium, iron and niobium. According to the company, the Marinel is manufactured by "Induction Melting and Forging", and it is heat treated by "Hot Worked and Aged Condition". The alloy was developed in response to the oil and gas industry's requirement for a corrosion resistant material, for use in the most severe engineering duties in marine environments. It is of particular benefit when cathodic protection is being applied to a subsea structure, as the alloy is highly resistant to hydrogen embrittlement. The chemical analyses of the batches of Marinel supplied by the manufacture are summarised in Table 5.4.

Copper	**Nickel**	**Iron**	**Manganese**	**Niobium**	**Chromium**	**Aluminium**	**Sulphu**
BAL.	18.69-19.47	0.92-1.05	4.04-4.40	0.68-0.97	0.31-0.56	1.78-1.88	0.001-0.(

Table 5.4. Chemical composition of Marinel.

Typical mechanical properties of the Marinel are given in Table 5.5.

Mechanical Property	
Yield Stress ($N/mm^{2)}$	705 – 719
Tensile Strength (N/mm^2)	924 – 955
Elongation %	16 – 18

Table 5.5. Mechanical properties of Marinel.

The Marinel alloy was provided in the form of bars, with diameters 15mm, 25mm and 50mm.

The etched structure of Marinel, obtained by a similar process like for Cu-10%Ni, is presented in Figures 5.2a-b.

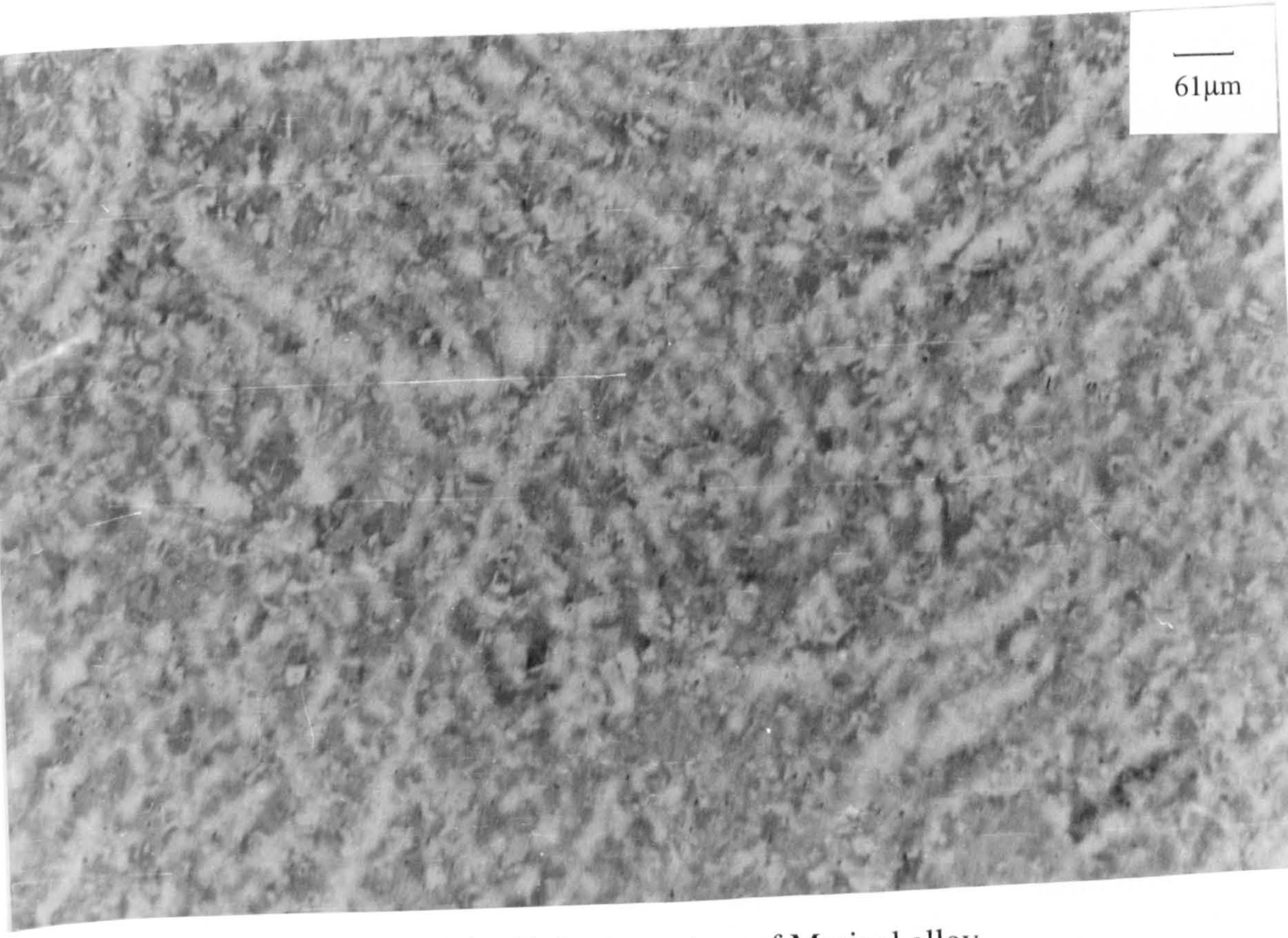

Figure 5.2a. Etched structure of Marinel alloy.

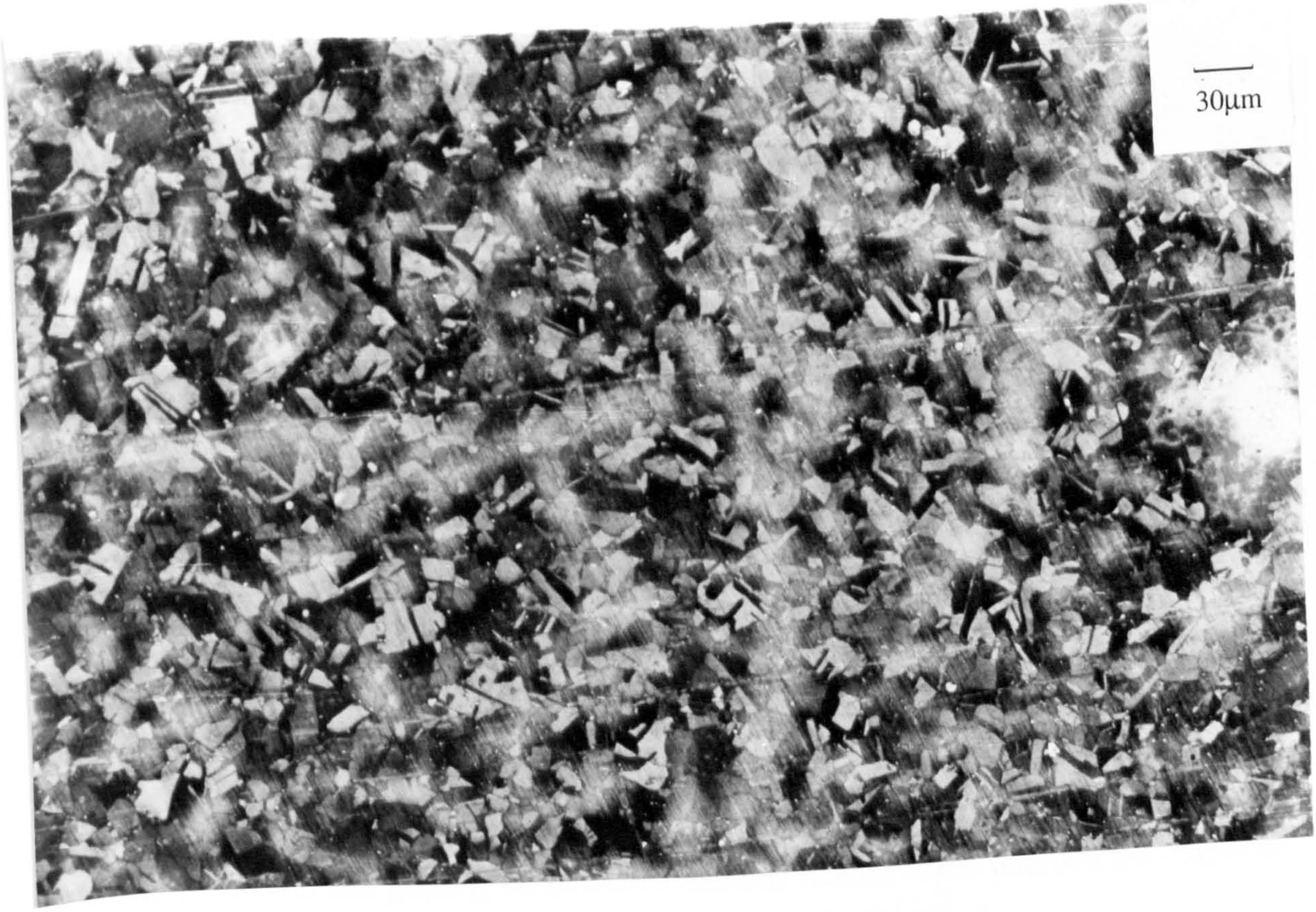

Figure 5.2b. Etched structure of Marinel alloy.

SEM Analysis done on an as-received and polished specimen showed the typical and expected chemical analysis for Cu-10%Ni alloy. The analysis demonstrating this more clearly was:

Copper	Nickel	Niobium	Chromium
72.10	20.90	0.61	0.64

Table 5.6. Typical chemical analysis of an as-received and polished specimen.

Some light particles were evident in the polished as-received specimens as shown in Figure 5.3., and further SEM analysis done on several particles, showed significant enrichment in Ni and Nb, depletion in Cu and similar concentration of Cr, compared to the average analysis. This feature agrees with previously work on Marinel [147] and the analysis demonstrating this more clearly was:

Copper	Nickel	Niobium	Chromium
20.50	54.50	19.70	0.71

Table 5.7. Typical chemical analysis on a light particle of a polished as-received specimen.

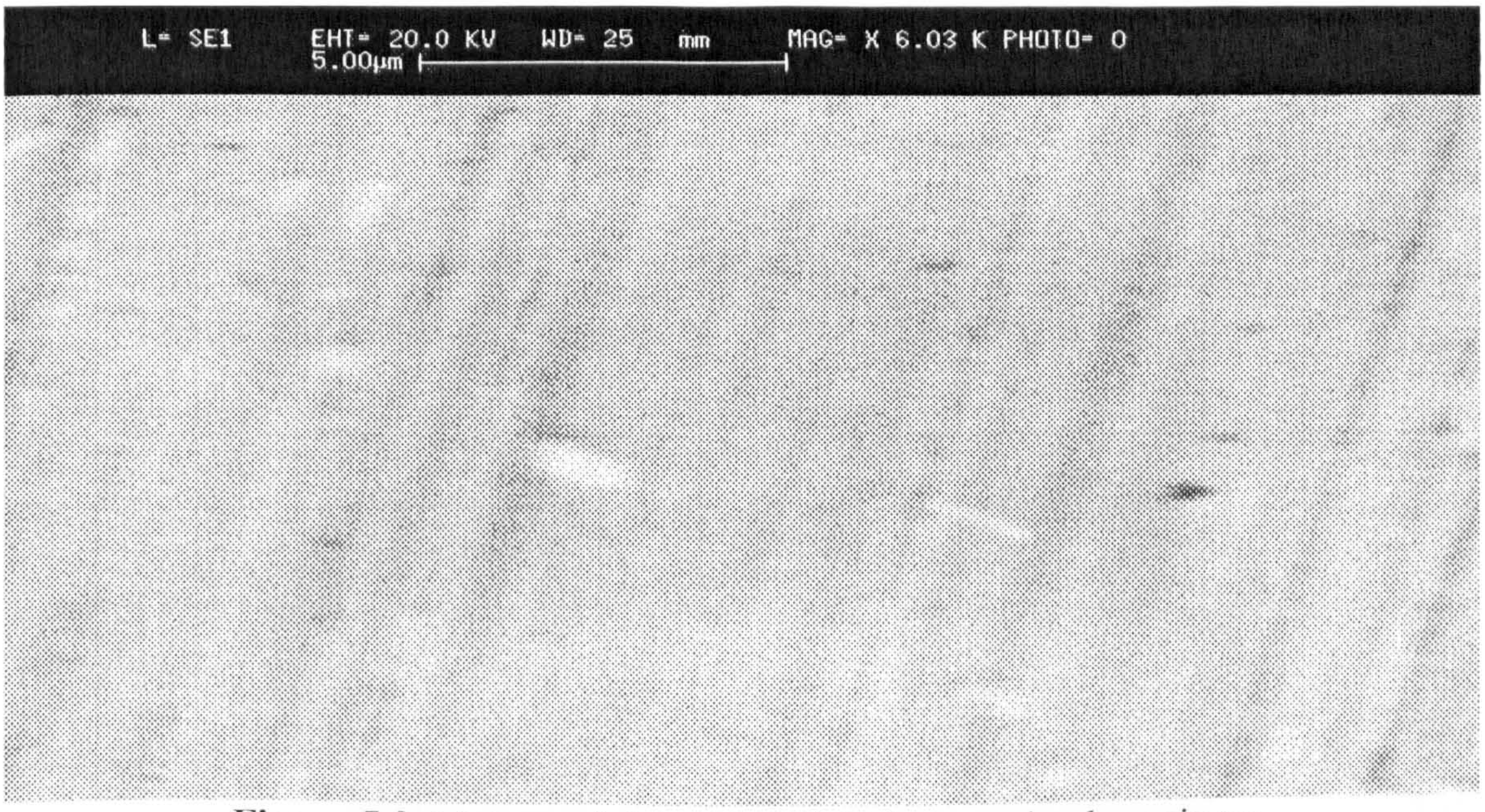

Figure 5.3. Light particles on a polished as-received specimen.

Evidently from the chemical analysis, the Cr is distributed throughout the entire microstructure and this gives good evidence that this feature could improve the corrosion resistance of Marinel.

5.2. Mounting and polishing techniques.

Most of the experimental work utilised specimens of either plates of 20x20mm size for the Cu-10%Ni alloy, or discs with diameter of 25mm for the Marinel alloy, which were mounted in a non-conducting epoxy resin type Metset FT with an electrical connection wire soldered to the rear side of the specimen. Some experiments were conducted on concentric specimens which comprised small, (4mm diameter for Cu-10%Ni and 6mm for Marinel), specimens encapsulated in the same overall mount as a larger specimen with a central hole, (of 6mm diameter for Cu-10%Ni and 8mm diameter for Marinel), the two samples separated by a resin layer of 2mm thickness.

Schematic representations of specimens encapsulated in a cold mount epoxy are shown in Figure 5.4a. for Cu-10%Ni and Figure 5.4b. for Marinel.

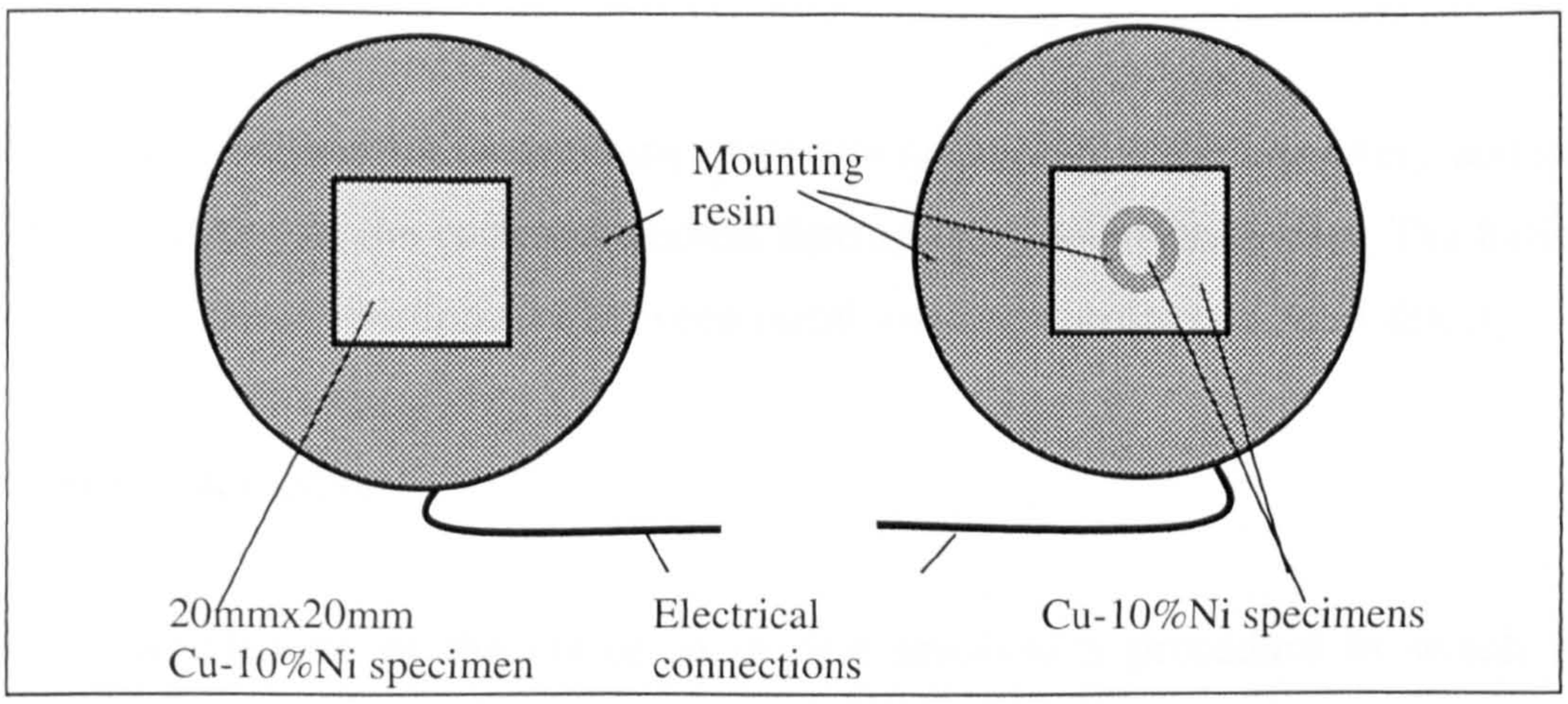

Figure 5.4a. Schematic diagram of a working Cu-10%Ni electrode.

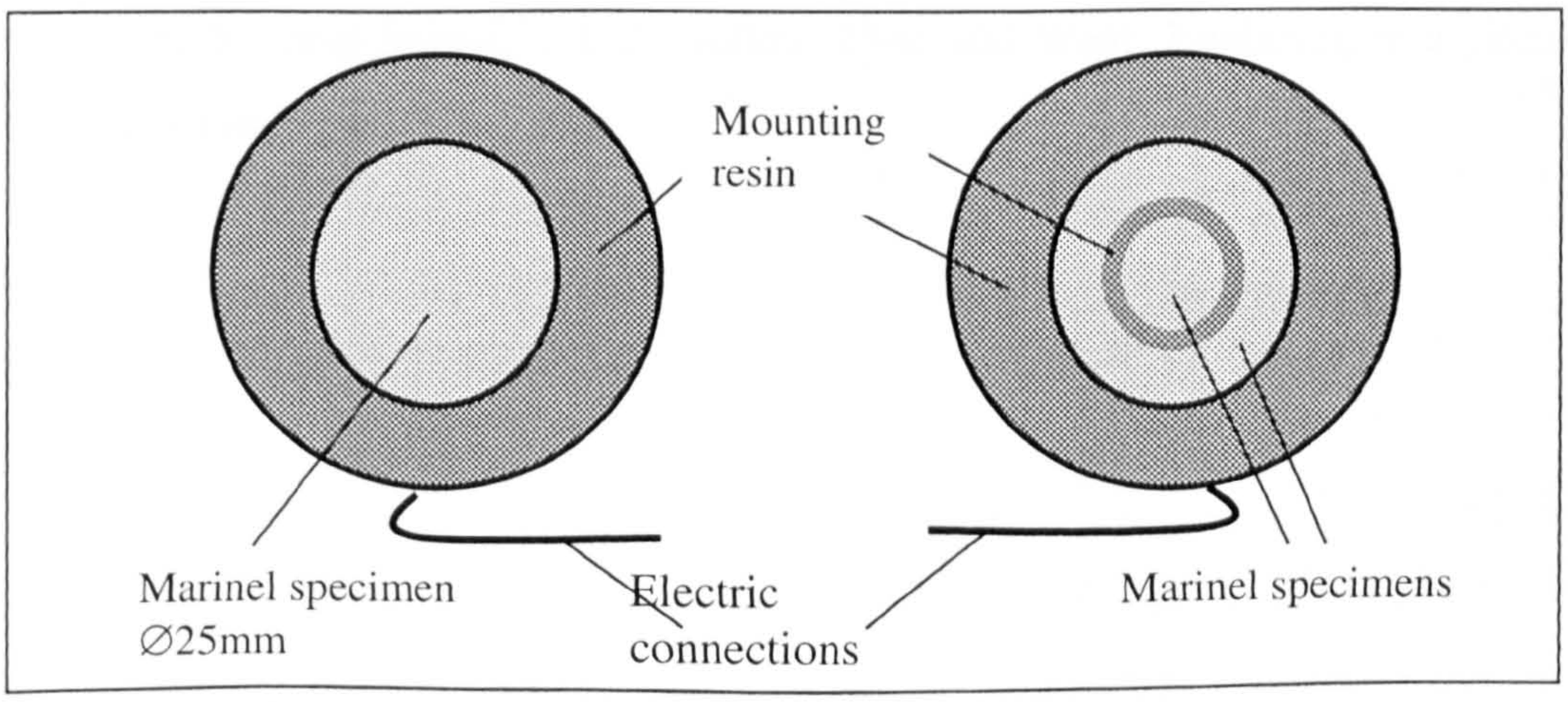

Figure 5.4b. Schematic diagram of a working Marinel electrode.

5.2.1. *Polishing.*

All specimens were investigated in the "as-polished" condition. The polishing process comprised successive grinding on 240,400,800,1200 SiC grit papers and finally 6-micron diamond polishing. The equipment used was a polishing disc type Metaserv Universal Polisher and the specimen was polished on a polishing cloth (Microcloth®) using a diamond abrasive type Meta-D from Buehler Ltd. The polished surface was first washed with methanol and air-dried.

5.3. Corrosion measurement

A powerful method for determining corrosion rates, both in the laboratory and in plant, is the evaluation of the corrosion current density from polarisation data. The basis of this approach is the proportionality between metal loss and corrosion current density.

5.3.1. *Tafel Extrapolation.*

The determination of the corrosion current involves a procedure in which a sample is polarised from its free-corrosion potential, E_{corr}, by means of a computer-controlled potentiostat. In this research the equipment used was a "Multistat", (manufactured by Sycopel Scientific Ltd, Bolton, Tyne and Wear, England), in a circuit like the one shown in Figure 5.5.

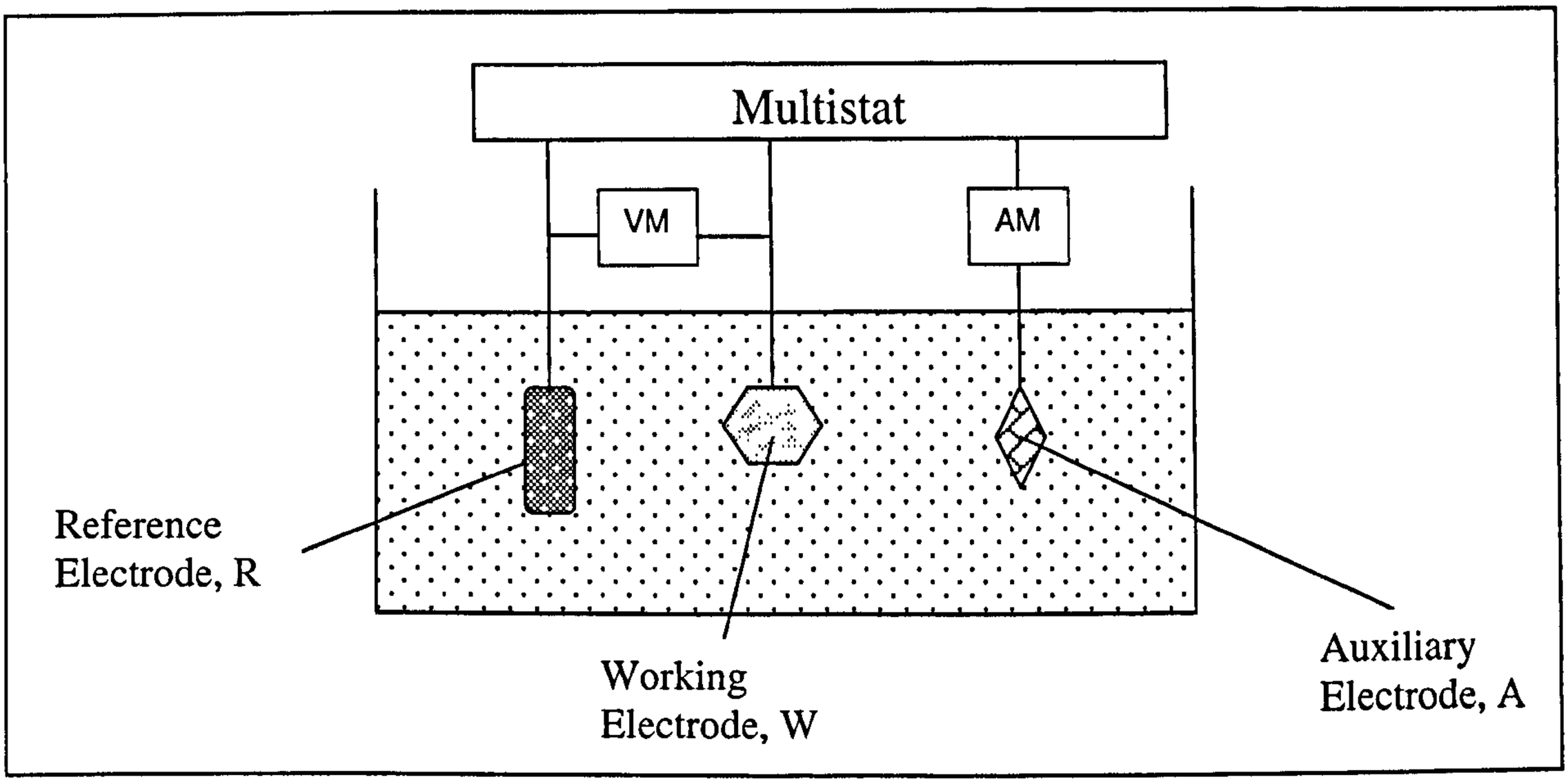

Figure 5.5. A schematic diagram of a corrosion-rate monitoring system comprising a three-electrode cell.

The computer-controlled potentiostat is essentially, a sophisticated DC generator, constructed so as to provide a carefully controlled output voltage. In the present application, the multistat drives a current through a circuit consisting of a working electrode, (which consists of the material whose corrosion rate is desired), and an auxiliary electrode. Experiments were carried out in 3.5% NaCl solution (made from Analar NaCl dissolved in distilled water). The pH of the solution was about 6.3, and all electrochemical measurements were done during in-situ impingement.

With the multistat disconnected, the specimen under investigation is corroding naturally with anodic current, $I_a = I_c = I_{corr}$, (cathodic current), no current flows in the external circuit and the potential recorded on the voltmeter is the free-corrosion potential, E_{corr}. The specimens were immersed for 30 minutes prior to the polarisation, so as to settle the free corrosion potential.

The multistat can be used to drive the specimen electrode potential at controlled rates, (in this work 8mV/min), in either the positive or negative direction from E_{corr}. For the anodic scan the sample potential was shifted from E_{corr} (free corrosion potential) in the positive direction until a current density of 500$\mu A/cm^2$, measured in the external circuit between the working and auxiliary electrodes, was reached. Cathodic scans were carried out by shifting the potential, from E_{corr}, in the negative direction again until a

current density of 500μA/cm^2 was reached. The potential was measured using the saturated calomel reference electrode (SCE).

Considering the latter alternative, namely the supply of a current of electrons to W, (note that this is equivalent to cathodic protection). This causes the specimen potential to move in the negative direction and this supply of electrons to W will stimulate the cathodic reaction and suppress the anodic reaction. Thus, $I_c > I_a$ and, for moderate shifts in potential from E_{corr},

$$I_c - I_a = I_m \quad \text{(the current measured in the ammeter, AM)}$$

Or in terms of current density, $i = \frac{I}{A}$ and

$$i_c - i_a = i_m \quad \text{(assuming general corrosion over entire surface area A)}$$

As the multistat output is continuously adjusted to increase i_m, the corresponding i_m/E relationship will follow a plot like the one represented by ABC in Figure 5.6. When E is sufficiently remote from E_{corr}, (usually 50mV or more), $i_c >> i_a$ and indeed i_a will be so small that i_m essentially equals i_c. The linear plot of E versus $\log_{10}i$ follows from the Tafel relationship, $E_c - E_{corr} = b_c \log \frac{i_c}{i_{corr}}$, (assuming general corosion over entire specimen), when the cathodic reaction rate is controlled by activation polarisation phenomena.

Extrapolation of the linear plot back to E_{corr} will yield the value of the corrosion current i, and further extrapolation, will represent the cathodic polarisation curve, back to the equilibrium electrode potential for the cathodic reaction.

If next the multistat polarity is reversed so as to cause the potential of W to move in the positive direction, plot ADE, (Figure 5.6.), will be recorded, for which initially i_a-i_c=i_m and at sufficient displacement of potential from E_{corr}, i_m=i_a.. Extrapolation of the linear plot back to E_{corr} also provides a value of i_{corr}. In this thesis the results are plotted in

terms of current density, to facilitate comparisons between different sizes of specimens which have been used.

In most electrochemical monitoring exercises, a linear portion of the measured, say anodic, polarisation plot can be identified with reasonable certainty. However, in this project and also in other erosion-corrosion research [5], it has been found that this procedure is considerably facilitated by "correcting" the measured current density, i_m, in an anodic polarisation scan by taking into account the residual cathodic current density via,

$$i_a = i_m + i_c$$

This procedure was extremely useful in defining more precisely the linear anodic polarisation plot and was used extensively in this project. Hence an example of this approach is given below.

Figure 5.7. shows in semi-logarithmic scale the anodic and the cathodic curves generated for a Cu-10%Ni specimen after exposure for 30 minutes under a 1mm impinging jet at 17m/s. For both cases, in order to facilitate comparison, the actual E_{corr} values have been adjusted to zero on the y-axis.

For a step of +25mV, we read the "measured" current density i_m from the anodic curve and the residual "cathodic" current density from the cathodic curve.

For the first +25mV, $i_m=10\mu A/cm^2$ and $i_c=3.8\mu A/cm^2$, so according to the formula

$$i_a=i_m+i_c \Leftrightarrow i_a=13.8\mu A/cm^2.$$

Similar for +50mV, $i_m=33\mu A/cm^2$ and the $i_c=2.4\mu A/cm^2$, $i_a=35.4\mu A/cm^2$,

and for +75mV, $i_m=83\mu A/cm^2$ and the $i_c=1.6\mu A/cm^2$, $i_a=84.6\mu A/cm^2$,

Taking these values for the real anodic current density, a new genuine anodic curve is plotted, (i.e. based on values of i_a rather than i_m). As stated earlier extrapolation back to E_{corr} yields the value of the corrosion current density i_{corr}.

In this case the value of the corrosion current density is i_{corr}=4.5 μA/cm^2 .

It has to be noted that this value of corrosion density is the instantaneous corrosion rate at the time where the polarisation scan took place.

The corrosion current density can be transformed to Weight Loss by using Faraday's Law.

According to Faraday's Law, 1 Faraday of charge, (=96487 Coulomb, but in the following calculations this number is rounded off to 96500 Coulomb), associates with

$\frac{A_m}{n}$ grams of metal dissolution,

Where "A_m" is the Atomic mass of metal

And "n" is the number of electrons involved in the reaction $M \rightarrow M^{n+} + ne^-$

So from Faraday's Law: Weight Loss = $\frac{i_{corr} * 10^{-6} * A_m}{n * 96500}$ g/cm^2/s

Multiplying by the surface area, A :

Weight Loss = $\frac{i_{corr} * 10^{-6} * A_m * A}{n * 96500}$ g/s =

$$\frac{i_{corr} * 10^{-6} * A_m * A * 10^3 * 3600}{n * 96500} \text{ mg/h}$$

Calculation of the atomic mass, A_m, of an alloy, e.g. Cu-10%Ni is as follows,

The Average Atomic Mass = (0.9*63.55 + 0.1*58.56) = 63.051 grams ,

Where 63.55 and 58.56 are the atomic masses of copper and nickel respectively.

For a specimen surface area = 4 cm^2 , and taking the valencies for Cu and Ni as 2,

$$\text{the Weight Loss} = \frac{i_{corr} * 10^{-6} * 63.051 * 4 * 10^{3} * 3600}{2 * 96500} = i_{corr} * 4.7 * 10^{-3} \text{ mg/h}$$

For the case where the value of the corrosion current density is $i_{corr} = 4.5\ \mu A/cm^2$,

the weight loss = $4.5 * 4.7 * 10^{-3} = 0.021$ mg/h

By a similar averaging procedure, a value of Atomic mass for the Marinel alloy was obtained; Average Atomic Mass =(0.77*63.55 + 0.19*58.69 +0.04*54.94) =

=62.245 grams,

where 54.94 is the atomic mass of manganese.

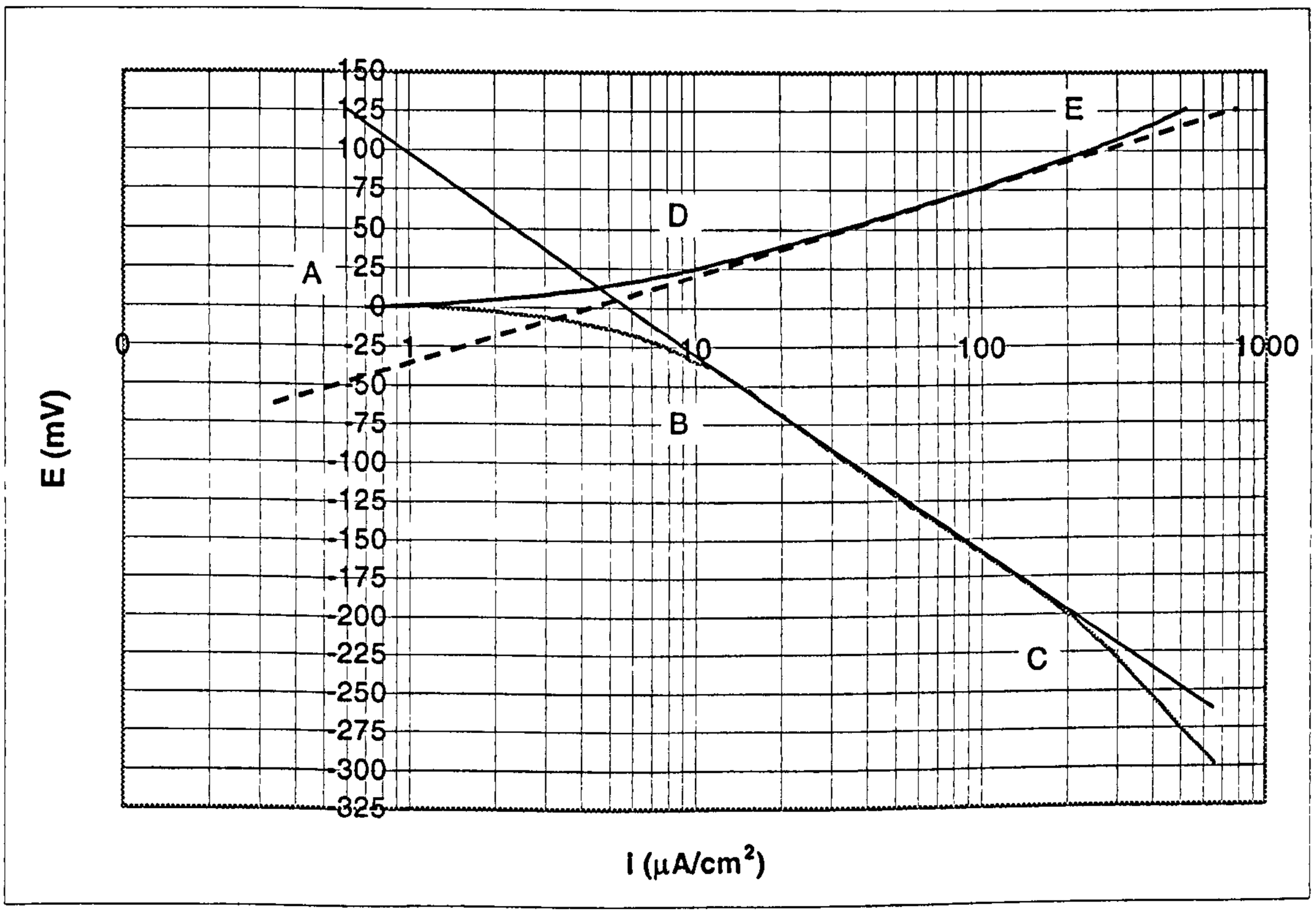

Figure 5.6. Anodic and Cathodic polarisation tests.

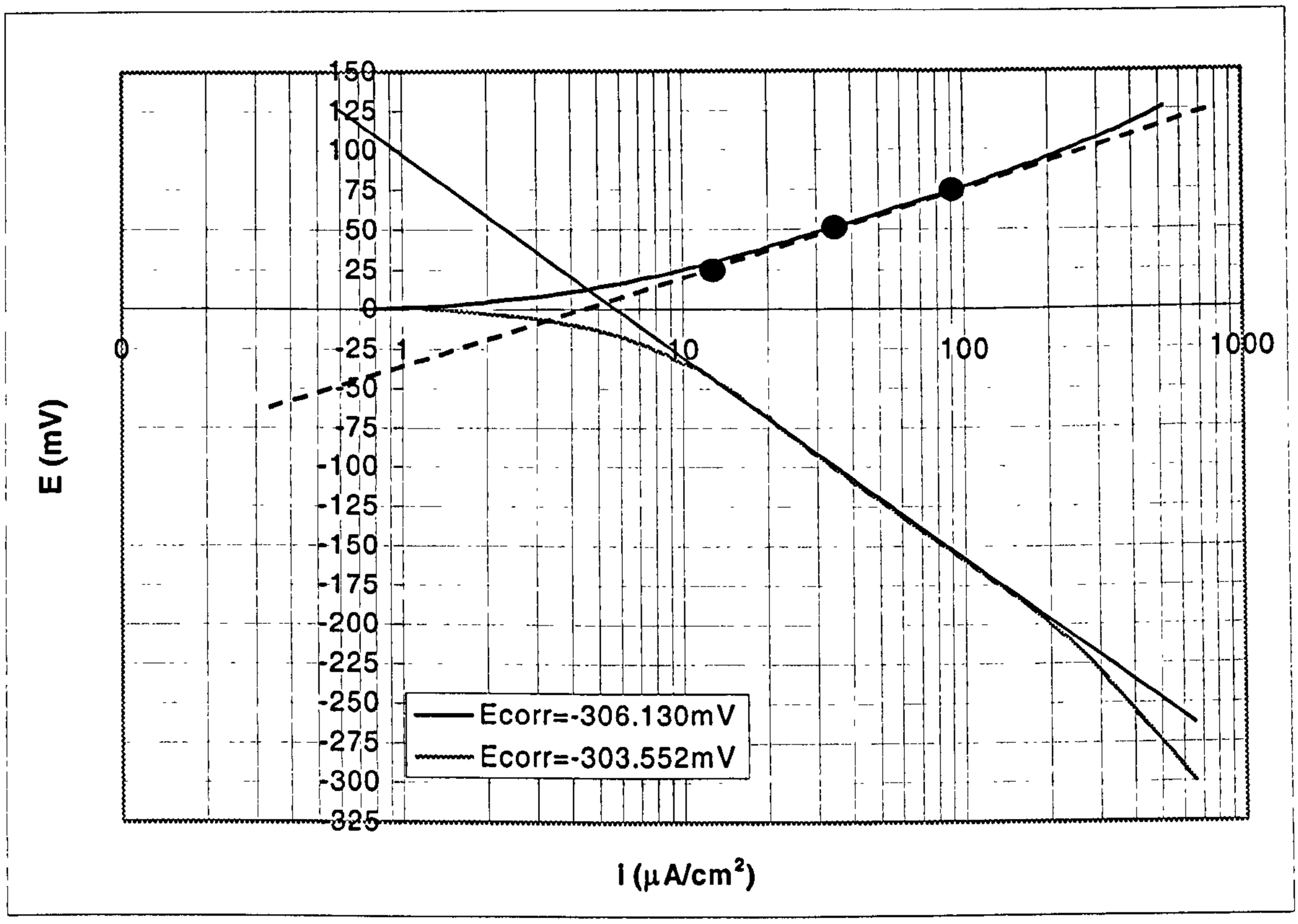

Figure 5.7. Anodic and Cathodic polarisation plots of Cu-10%Ni after exposure of 30 minutes under an 1mm impinging jet at 17m/s.

As it has already been mentioned, these values of corrosion current density are the instantaneous corrosion rates at the time where the polarisation scan took place. In order to obtain the total amount of material loss due to corrosion for the whole time period, the following approach was used.

The examined time period, say 48 hours, was divided into a group of time periods, say 4, 8, 16, 24 and 48 hours. For these periods of time a set of full anodic and cathodic polarisation scans was performed as separate experiments and the instantaneous direct corrosion rates were calculated using the above Tafel-extrapolation method. A graph of instantaneous direct corrosion rate vs. time was plotted and the area under the graph is the total material loss by corrosion.

5.3.2. *Polarisation Resistance.*

The measurement of full anodic polarisation curves for use in determining i_{corr} by Tafel extrapolation requires separate experiments; i.e. only one full procedure can be carried out on one specimen because of concern about changes in the specimen surface after a full anodic polarisation test.

In order to obtain frequent indications of the trends in corrosion rate as a function of time on one specimen, polarisation resistance, (alternatively called "linear polarisation"), monitoring was carried out. In this technique, the polarisation shift from E_{corr} is limited so as not to disturb the surface significantly.

In this project, the method employed undertaking a short (22mV) anodic polarisation scan after say 4, 8, 16, 24, and 48 hours, and calculating the gradient of the potential/current density plots using Excel by Microsoft, to yield in each case a value which is termed $R_p^{'}$. Then the values of $1/R_p^{'}$ for the various exposure times are calculated, on the reasonable basis of a direct relation between $1/R_p^{'}$ and corrosion rate. The plot of $1/R_p^{'}$ against time provides an indication of changes in the corrosion rate.

It is recognised that this procedure represents a variation on the polarisation resistance method as described in ASTM standard G 59-97, 2000, (Standard Test method for Conducting Potentiodynamic Polarisation Resistance Measurements) - hence the use of symbol $R_p^{'}$ rather than R_p. It should be emphasised that no attempt was made to quantitatively convert the calculated values of $R_p^{'}$ to corrosion rates. The $R_p^{'}$ values were used simply to provide indications of trends in corrosion rate with time.

5.3.3. *Direct measurement of Weight Loss of specimens after exposed to static water.*

Static corrosion tests were also performed, by simply immersing the specimens in the electrolyte in a beaker under free corrosion conditions, and monitoring the weight losses after certain intervals of time.

The conductivity of the electrolyte, 3.5% NaCl solution, was measured using water analyser type JENWAY, to be 53000μS/cm at 19°C. The conductivity was maintained by regularly checking the solution and diluting with distilled water to avoid solution changes due to evaporation.

5.4. Erosion-corrosion measurements

5.4.1. *Liquid erosion-corrosion measurement.*

The liquid erosion-corrosion test apparatus comprised an electrochemical monitoring (three-electrode cell) attached to an impinging jet rig where recirculating saline water was directed at a chosen angle to the working electrode surface 'W' at a range of velocities (2.38 to 69 m/s). Most of the experiments in this work were conducted at 90° impinging angle but some tests at 30°, 45°, 60°, 90° angles were also carried out.

Figure 5.8a. and Figure 5.8b. show the liquid impingement rig of closed circulating loop comprising a low-pressure centrifugal pump, which feeds saline water from the reservoir to a higher-pressure pump. The rig contains two nozzles, but only one is shown in Figure 5.8a for simplification reasons.

The circulating water was constantly filtered to provide a liquid-jet free from suspended solids. The system comprised stainless steel pipes with the exit nozzle diameters of 1mm and 4mm.

The velocity of the system was varied, by changing the pressure of the high-pressure pump, in combination with the diameter of the nozzle. The distance between the

nozzle and the specimen was kept constant for all impingement tests at H=5mm in order to maintain the flow development region.

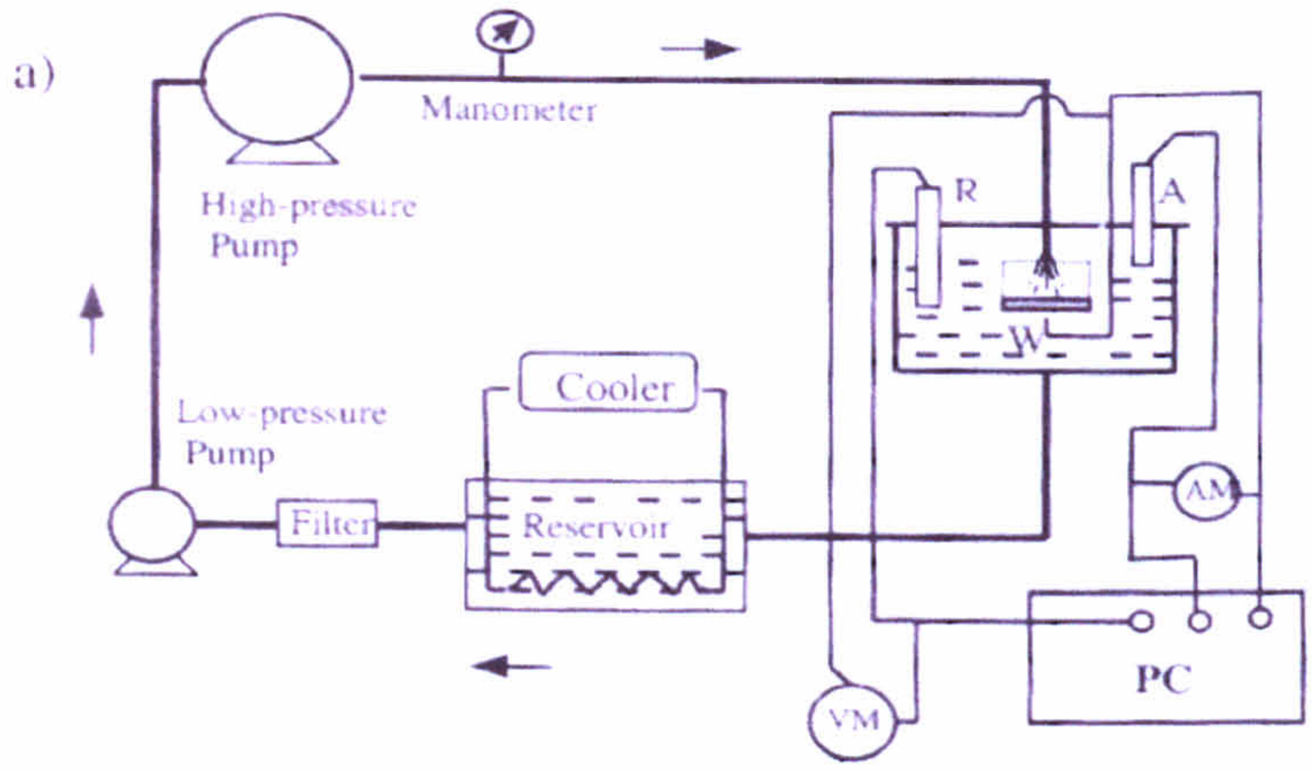

Figure 5.8a. A schematic diagram of a liquid jet impingement rig comprising a three-electrode cell: where, R-reference electrode; A-auxiliary electrode, W-working electrode; VM-voltmeter, AM-ammeter.

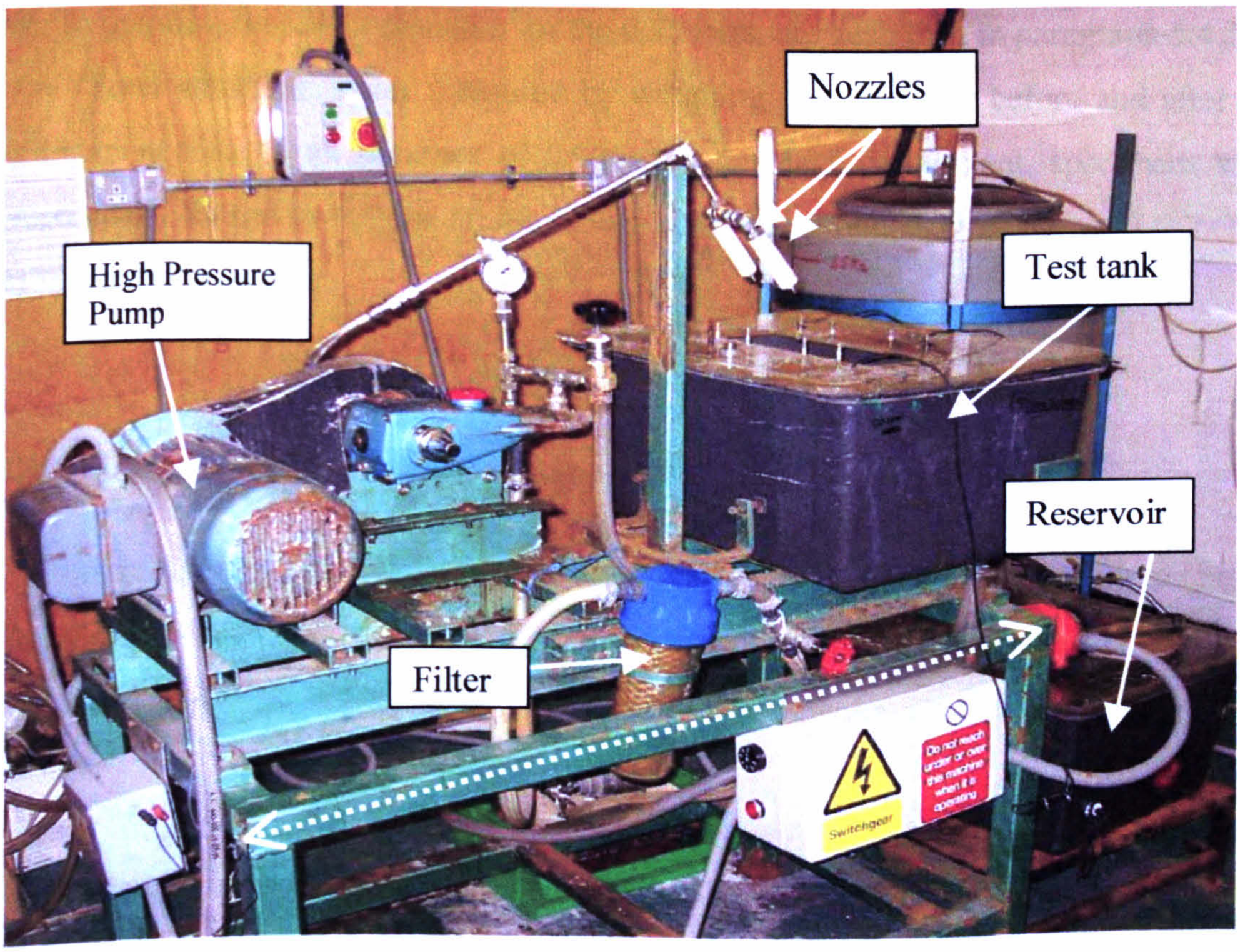

Figure 5.8b. Double nozzle liquid jet impingement rig, for erosion-corrosion experiments. Length of doted line = 1.2m.

Experiments were carried out at 19±2°C and 35±1°C in 3.5% NaCl solution (made from distilled water). The temperature of the system was maintained by using a commercially available thermostat-controlled heating device for experiments performed at high temperature (35°C). For experiments at an ambient temperature (19°C), a water-cooling coil of stainless steel was used. Anodic and cathodic scans were conducted for different velocities and different temperatures. The auxiliary electrode was a platinum spade electrode and the reference electrode was a saturated calomel electrode (SCE).

Weight loss tests were carried out under liquid impingement both at the free corrosion potential and also under cathodic protection (C.P.) to suppress the corrosion component and hence quantify the synergism (S) using the formula T.W.L = C + E + S

For cathodic protection the electrode potential of the specimen was maintained at a negative potential at a value of 75 mV more electronegative than E_{corr} for Cu-10%Ni, and at a value of 85 mV more electronegative than E_{corr} for Marinel. The procedures in order to optimise the target potential for the C.P. tests, are described in paragraph 5.4.2.

Total weight loss was measured by weighing the specimen before and after the impingement tests to an accuracy of 0.0001g. After each experiment, specimens were ultrasonically bathed to remove all remaining corrosion products from the surface before air drying and weighing.

5.4.2. *Cathodic Protection of Cu/Ni alloys.*

In order to find the effective target potential for the Cu-10%Ni, at which the direct corrosion component is suppressed, three different approaches were followed.
By similar procedures, a value for the target electrode potential for the Marinel alloy was obtained.

5.4.2a. *Calculations based to Nernst equation.*

The value of the equilibrium electrode potential E_o, (which is the conventional target potential for C.P.), can be calculated using the 'Nernst' equation.

$$E_o = E_o^o + \frac{RT}{nF} \ln \frac{C_{M^{n+}}}{C_M}$$

where E_o^o : The 'standard equilibrium electrode potential', which represents a particular value of the equilibrium electrode potential when the activities of the constituents are all unity. Lists of 'Standard Electrode Potentials', of a wide range of electrode reactions are readily available in the electrochemical literature.

R : General gas constant

T : Absolute temperature

$C_{M^{n+}}$: Concentration of metal ion in the aqueous solution

C_M : Concentration of metal in the solid metal

For the reaction $Cu^{2+} + 2e^- = Cu$,

the 'Nernst' equation is

$$E_o = E_o^o + \frac{RT}{nF} \ln \frac{C_{Cu^{2+}}}{C_{Cu}} \quad ,$$

where $T = 19^oC + 273 = 292$ K, and $n = 2$.

For 90/10 Cu/Ni, we take the concentration of metal ion in the solid metal, $C_{Cu} = 0.9$, and we assume that the concentration of Cu ion in the aqueous solution is,

$$C_{Cu^{2+}} = 10\text{mg/l} = \frac{10*10^{-3}}{63.5} = 0.157 * 10^{-3} = 1.57 * 10^{-4} \text{ mole/l.}$$

resulting to the 'Nernst' equation:

$$E_o = +0.34 + \frac{8.314*292}{2*96500} \ln \frac{1.57*10^{-4}}{0.9}$$

$= +0.34 + 0.0126 * \ln(1.744*10^{-4}) = +0.34 - (0.0126 * 8.654) = +0.34 - 0.109 =$

$= +0.231$ SHE.

But SCE = 0.214 Volts more negative than SHE, so the value of E_o for the Cu in the Cu-10%Ni alloy is almost zero volts in SCE, E_o= 0Volts.

Even if we assume that the concentration of Cu ion in the aqueous solution is lower, say 0.1mg/l, then

$$C_{Cu^{2+}} = 0.1\text{mg/l} = \frac{0.1*10^{-3}}{63.5} = 0.157 * 10^{-3} = 1.57 * 10^{-6},$$

and the 'Nernst' equation is:

$$E_o = +0.34 + \frac{8.314*292}{2*96500}\ln\frac{1.57*10^{-6}}{0.9}$$

$= +0.34 - (0.0126 * 13.26) = +0.34 - 0.167$

$= +0.173$ (SHE) =

$= +0.173 - 0.214 = -0.05$ V (SCE).

Following the same procedure the value of the equilibrium electrode potential E_o for the $Ni^{2+} + 2e^- = Ni$ can be found, assuming that the concentration of Ni ion in the solid metal, $C_{Ni} = 0.1$, and the concentration of Ni ion in the aqueous solution is,

$$C_{Ni^{2+}} = 1\text{mg/l} = \frac{1*10^{-3}}{58.71} = 0.0170 * 10^{-3} = 1.70 * 10^{-5} \text{ mole/l.}$$

So, the 'Nernst' equation in that case is:

$$E_o = -0.25 + \frac{8.314*292}{2*96500}\ln\frac{1*10^{-5}}{0.1}$$

$= -0.25 + 0.0126 * \ln(10^{-4}) = -0.25 - (0.0126 * 6.907) = -0.25 - 0.087$

$= -0.337$ (SHE) =

$= -0.337 - 0.214 = -0.55$ V (SCE).

5.4.2b. *Calculations based on Weight Change Tests.*

A series of cathodically protected erosion-corrosion tests at impinging velocity of V=17m/s and exposure period of 1 hour took place, in order to find experimentally the most appropriate electrode potential for C.P. of Cu-10%Ni in this work. The free corrosion potential, E_{corr}, was measured as E_{corr} = –0.3Volts (SCE), for these impinging conditions. After each experiment, specimens were ultrasonically bathed to remove all remaining corrosion products from the surface before air drying and weighing. Table 5.8. shows the different values for electrode potential for the series of C.P. tests and the weight difference of the specimen after each experiment.

Electrode Potential (V)	Weight difference after each experiment
-0.8	+0.7
-0.6	+0.4
-0.4	+0.1
-0.37	±0
-0.35	-0.1

Table 5.8. The different electrode potential for the series of C.P. tests and the weight difference of the specimen after each experiment.

The above data shows that applying C.P. tests at a potential related to nickel corrosion, leads to weight gains which presumably are associated with re-deposition of copper.

Microscopically examination of the cathodically protected specimen at E_o = -0.35 Volts SCE, showed some evidence of corrosion attack. So, the above experimental results, indicate (for a value of E_{corr} = -0.3 V), the target electrode potential of (E_{corr} – 0.07) = -0.37 Volts (SCE).

5.4.2c. *Calculations based to Tafel back extrapolation.*

Figure 5.9. shows in semi-logarithmic scale the anodic and the cathodic curves generated for a Cu-10%Ni specimen after exposure for 30 minutes under an 1mm impinging jet at 17m/s. For both cases, in order to facilitate comparison, the actual E_{corr} values have been adjusted to zero on the y-axis.

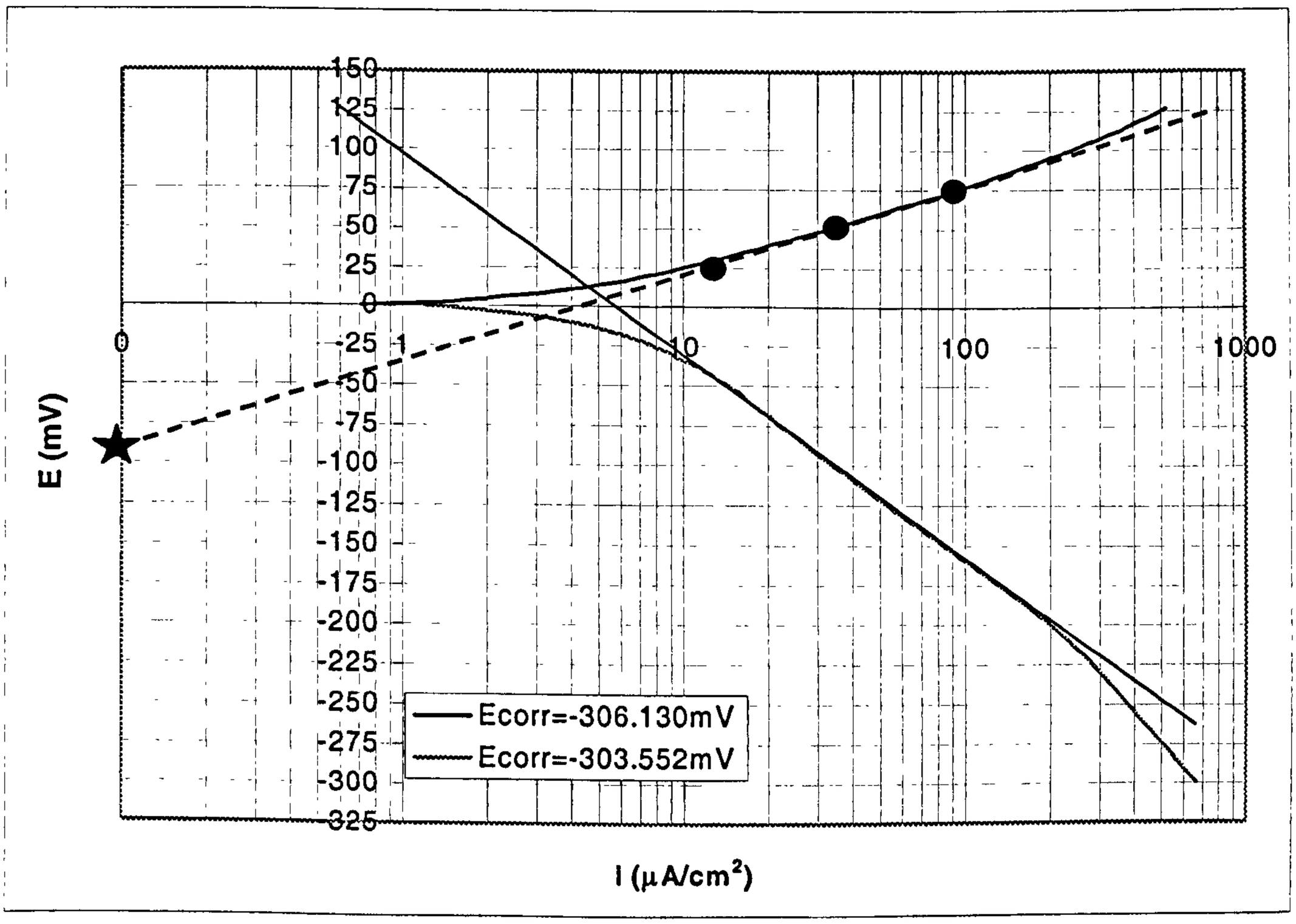

Figure 5.9. Anodic and Cathodic polarisation plots of Cu-10%Ni after exposure of 30 minutes under an 1mm impinging jet at 17m/s.

The effect of a negative shift in potential of 75 mV from E_{corr} can be estimated from Figure 5.9. as follows:

The i_{corr} is about 4.5 $\mu A/cm^2$ and the residual anodic current density, i_a, is about 0.18 $\mu A/cm^2$ at (E_{corr} -75mV).

Thus i_a is about $^{0.18}/_{4.5} * i_{corr} = {}^{1}/_{25} * i_{corr}$

5.4.2d. *Concluding remarks on optimum potential for Cathodic Protection.*

It is clear from the foregoing that the choice of potential for the cathodic polarisation tests represented a balance between the likelihood of weight gains at more negative potentials and residual corrosion at less negative potentials. Consideration of the data in 5.4.2b. and 5.4.2c. led to the decision to adopt as the target potential for the cathodic polarisation tests for Cu-10%Ni, a value of 75 mV more electronegative than E_{corr}.

Following similar procedures, a value of 85 mV more electronegative than E_{corr}, was adopted as the target potential for the cathodic polarisation tests for the Marinel.

5.5. Examination techniques.

Different modes of attack and damage mechanisms of the materials were assessed using a light microscope, a scanning electron microscope (SEM) type Leica Cambridge Stereoscan 360 and a Taylor Hobson Talysurf.

5.5.1 *Scanning electron microscopy (SEM).*

The samples to be examined under the SEM should be handled very carefully after the experiment, since the evidence of damage mechanism can be destroyed during transportation from the place of experiment to the SEM laboratory. The samples were dried and carbon coated in an evaporative coater to make the surface conductive. The coating is very thin (approximately 20nm), so that it does not hinder the identification of the underlying material.

5.5.2 *Talysurf.*

A Talysurf instrument manufactured by Taylor Hobson was used to measure the surface texture of the wear scars produced under erosion tests. The principle of the instrument is to move a stylus over a representative length of the surface under examination. For the current study we used a standard diamond stylus 112/2009 with a 2μm tip.

Figure 5.10a. shows a stylus moving over a surface with the result that the oscillatory movement causes the armature to tilt. The armature supports the pole pieces around, which are two coils I_1 and I_2, each carrying a high frequency current. The air gap between the armature and the pole pieces varies as the stylus traverses the surface under investigation. This results in a variation of the impedance of the coils and hence the magnitude of the high frequency current that actuates the pen recorder and the surface texture is obtained in the form of a trace. A profilometric trace of a surface as obtained with a Talyserf is schematically shown in Figure 5.10b.

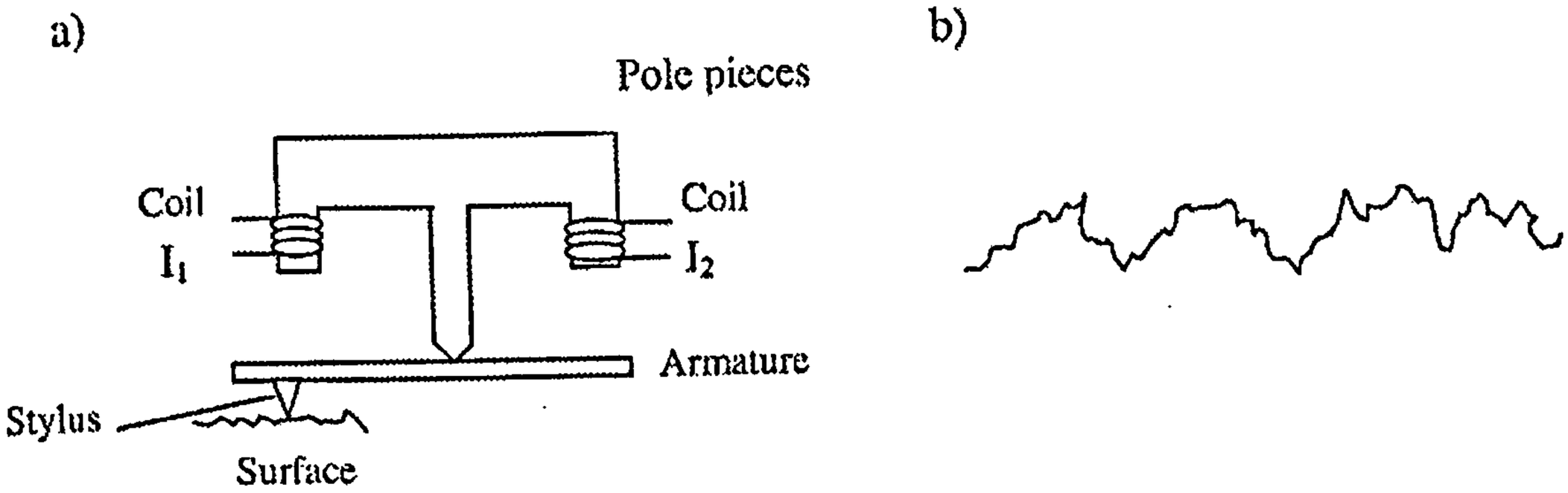

Figure 5.10. a) Principles of a Talyserf; b) profilometric trace of a surface where the peaks and spacing between them are distorted, due to difference in horizontal and vertical magnifications.

Chapter 6

Results related to the effect of velocity and time on erosion-corrosion of Cu-10%Ni and Marinel.

6.1. Effect of time on the total weight loss of Cu-10%Ni and Marinel, upon static exposures in 3.5% NaCl solution.

As a preliminary task prior to the work on erosion-corrosion, a small amount of experimentation was undertaken in the material loss of the alloys in static conditions at 19±2°C for periods up to 5040 hours, (210 days). Table 6.1. shows that the rate of weight loss for the Cu-10%Ni and for the Marinel is gradually reduced by time. Obviously the total weight loss after the first 4 hours is always higher for the Marinel.

		Cu-10%Ni		Marinel	
Condition	**Time (hours)**	**Actual Weight Loss (mg)**	**Average rate of weight loss (mg/h)**	**Actual Weight Loss (mg)**	**Average rate of weight loss (mg/h)**
Static	4	0.01 , 0.01	0.0025	0.01 , 0.01	0.0025
Static	1680	3.0 , 3.1	0.0018	4.5 , 4.5	0.0027
Static	3360	4.0 , 4.1	0.0012	5.7 , 6.3	0.0018
Static	5040	4.3 , 4.6	0.0009	5.9 ,6.2	0.0012

Table 6.1. Total weight loss values of Cu-10%Ni and Marinel upon static exposures of 4 hours, 1680 hours (70 days), 3360 hours (140 days) and 5040 hours (210 days).

6.1.1. Microscopical examination.

Cu-10%Ni : For exposure periods of 70 days and longer, the surface of the specimens under the microscope displayed an almost amorphous appearance, typical of the formation of a film on the surface which clearly obliterated any visible appearance of the underlying metal structure, Figure 6.1..

Marinel : After 70 days and longer periods, some areas were like the Cu-10%Ni in which an amorphous film covered the surface; some other areas indicated a thinner film with interference blue-green colours and evidence of the metallurgical structure, seen in the as received material, Figure 6.2. and Figure 6.3..

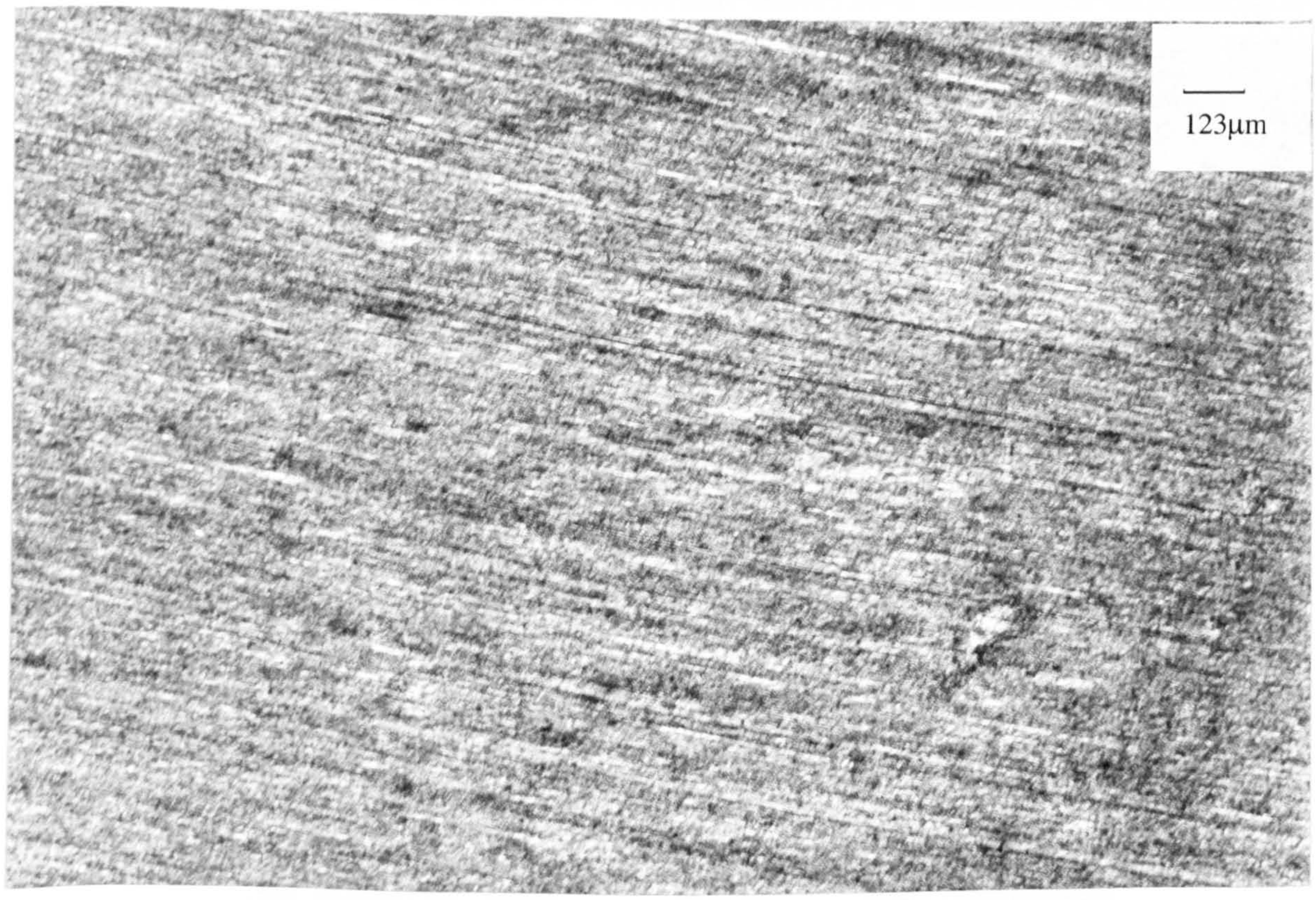

Figure 6.1. Almost amorphous appearance on Cu-10%Ni specimen after static exposure of 70 days.

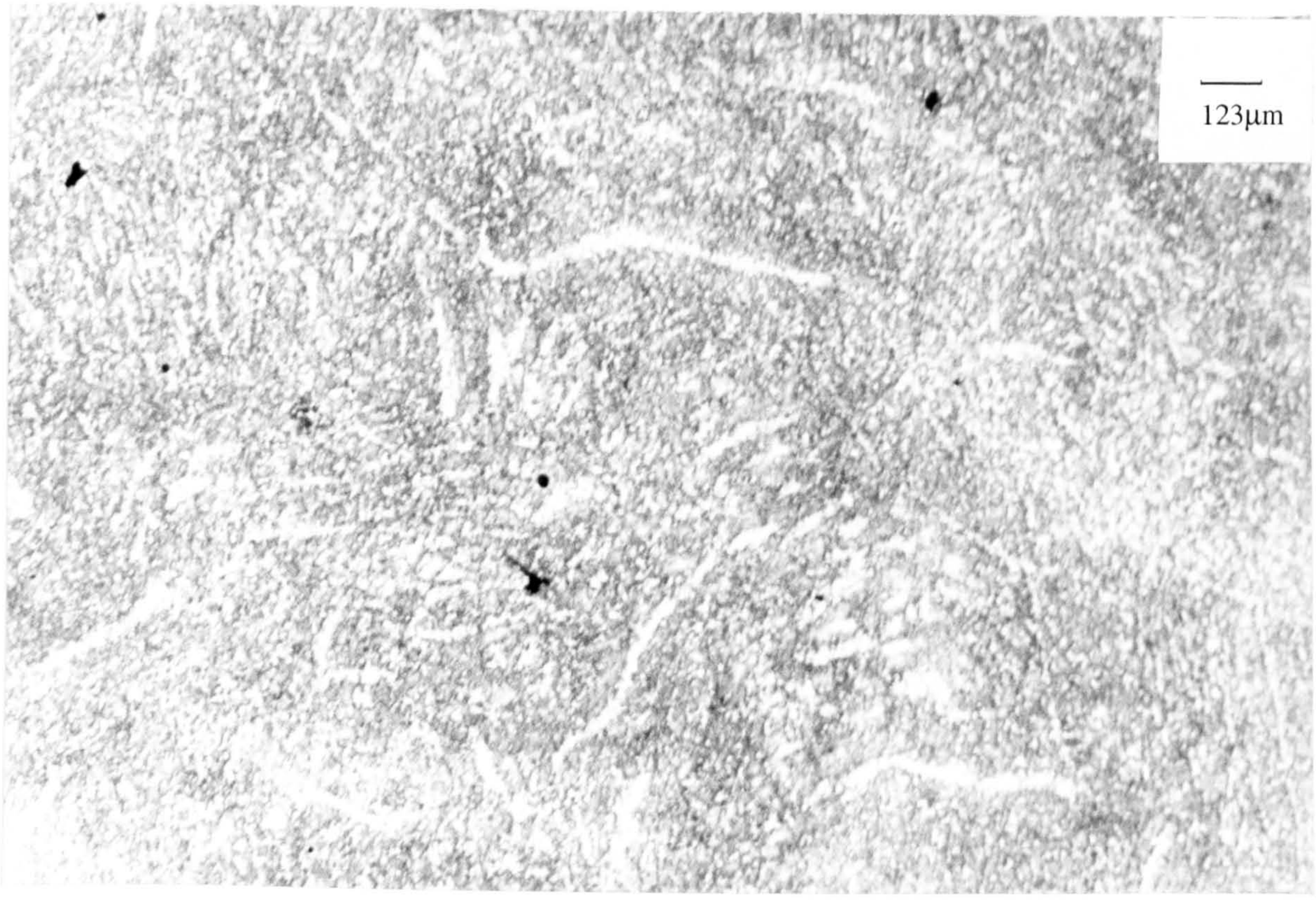

Figure 6.2. Amorphous appearance on Marinel specimen after static exposure of 70 days.

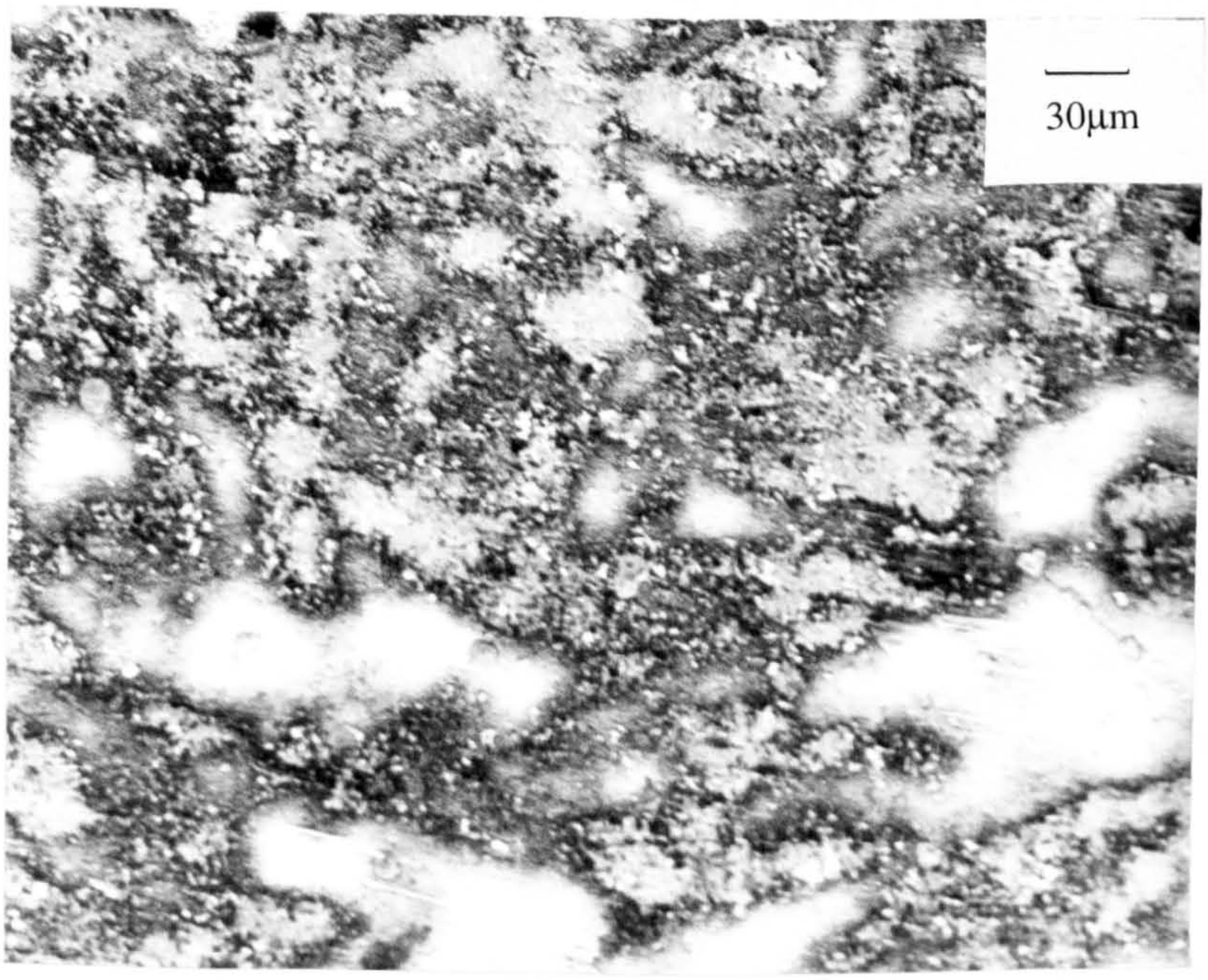

Figure 6.3. Some evidence of metallurgical structure on Marinel specimen after static exposure of 70 days.

6.2. Effect of velocity on corrosion rate after 30 minutes under liquid impingement.

As a preliminary activity to the main effort on the investigation of the overall features of erosion corrosion, some experiments were undertaken simply to study the effect of impingement velocity upon the pure, electrochemical corrosion process. These tests involved exposure of the specimens for 30 minutes under impingement conditions followed by anodic or cathodic polarisations. Each test includes at least one replication. The results of this part of the work are described in the following sections, 6.2.1 (for Cu-10%Ni), and 6.2.2 (for Marinel).

6.2.1. Cu-10%Ni.

6.2.1.1. *Impinging nozzle diameter 1mm.*

Figure 6.4a. and Figure 6.4b. show in linear and semi-logarithmic scales respectively, the typical anodic polarisation curves generated from tests after 30 minutes in 3.5% NaCl solution. Evidently a substantial negative shift in E_{corr}, (to between –299 to –310mV), appeared at all impingement velocities compared to static conditions. It is quite clear that Cu-10%Ni is very active after this short immersion in this saline water. The current passing through the specimens reached high values while the shift in the potential from E_{corr} was still low. The polarisation curves for all velocities are general together implying similar corrosion behaviour.

Figure 6.5a. and Figure 6.5b. show in linear and semi-logarithmic scales respectively, the typical cathodic polarisation curves generated from tests after 30 minutes in 3.5% NaCl solution. The (not unexpected) substantial depolarisation, of the cathodic reaction under impingement compared to static conditions, is clearly evident.

Figure 6.6a-b. show in semi-logarithmic scale, the anodic and cathodic polarisation curves for duplicate specimens of Cu-10%Ni generated from tests after 30 minutes in 3.5% NaCl solution at an impinging velocity of 4.5m/s; and Figure 6.7a-b-c. show the anodic and cathodic polarisation curves after 30 minutes at 17m/s. The Full Lines are the raw polarisation data, the Dashed Lines are the linear Tafel

plots and the Dots are the Anodic polarisation data corrected from the residual cathodic current, (by the method described in Chapter 5).

The obtained i_{corr} values for the impinging velocities of 4.5m/s and 17m/s, together with the i_{corr} values for the 59m/s and the 86m/s, (found according to the "Tafel extrapolation" procedure, as described in Chapter 5), are presented in table 6.2. This table also includes the converted i_{corr} values to weight losses via Faraday's Law.

As it can be seen from Table 6.2. and Figure 6.8. the corrosion rates increase with velocity. It is quite clear that the corrosion rate increased dramatically as expected from 0 to 4.5m/s, is similar at 17m/s as at 4.5m/s, and exhibits large increase at higher velocities.

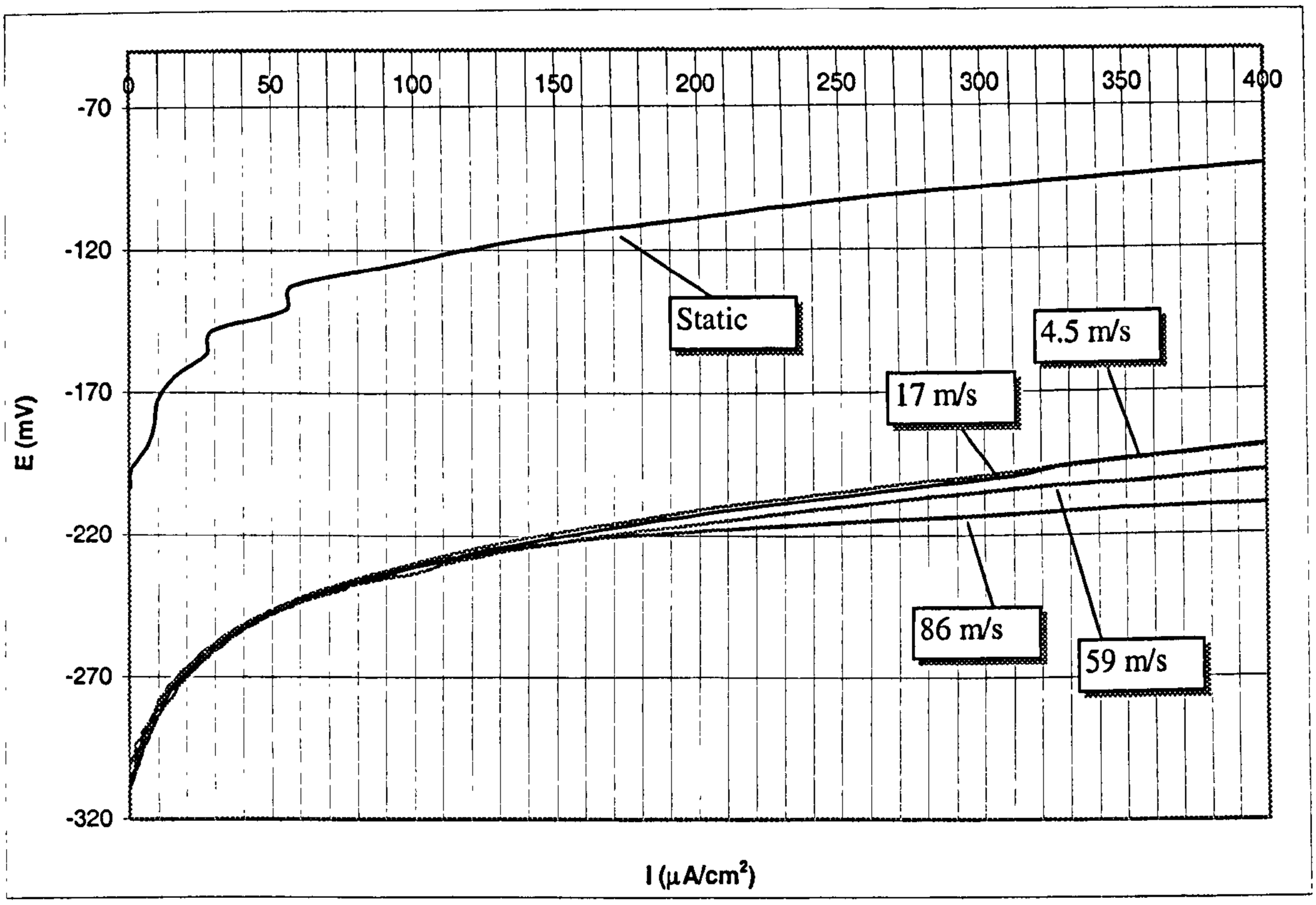

Figure 6.4a. Anodic polarisation tests of Cu-10%Ni upon an initial exposure of 30 minutes under the impinging jet. The nozzle diameter is 1mm.

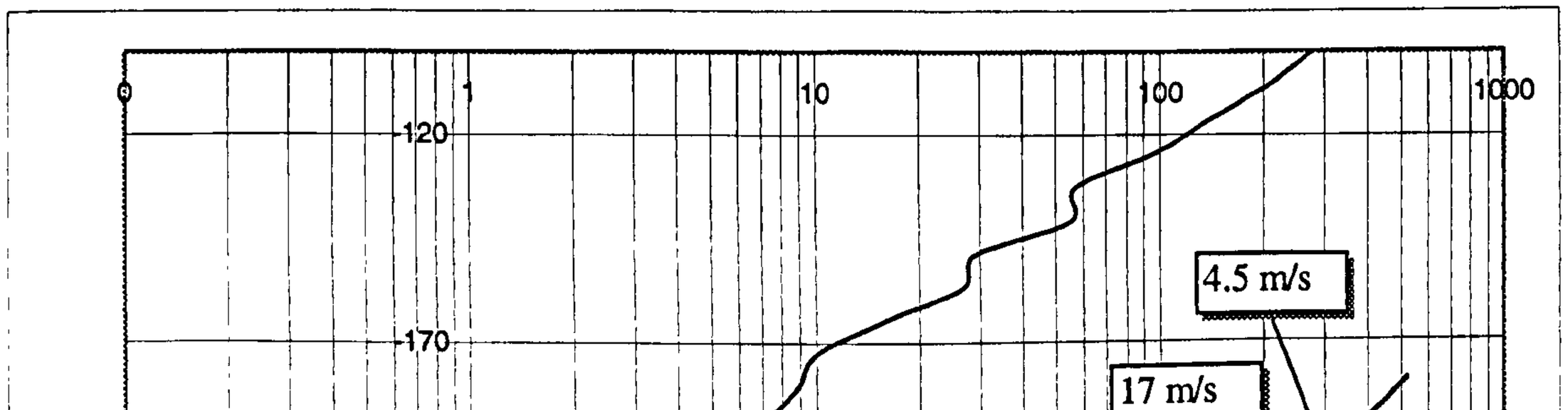

Figure 6.4b. Anodic polarisation tests of Cu-10%Ni upon an initial exposure of 30 minutes under the impinging jet. The nozzle diameter is 1mm.

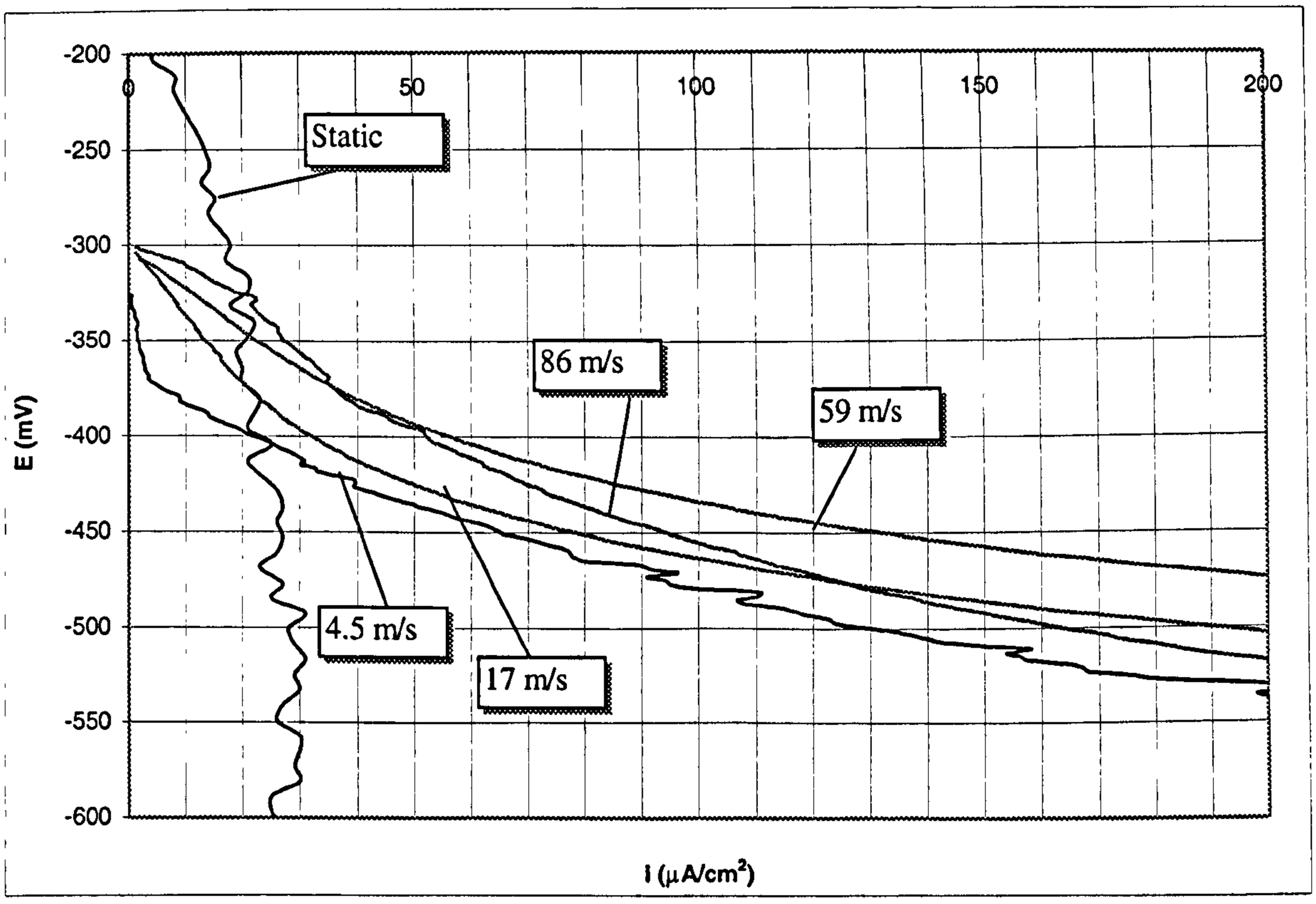

Figure 6.5a. Cathodic polarisation tests of Cu-10%Ni upon an initial exposure of 30 minutes under the impinging jet. The nozzle diameter is 1mm.

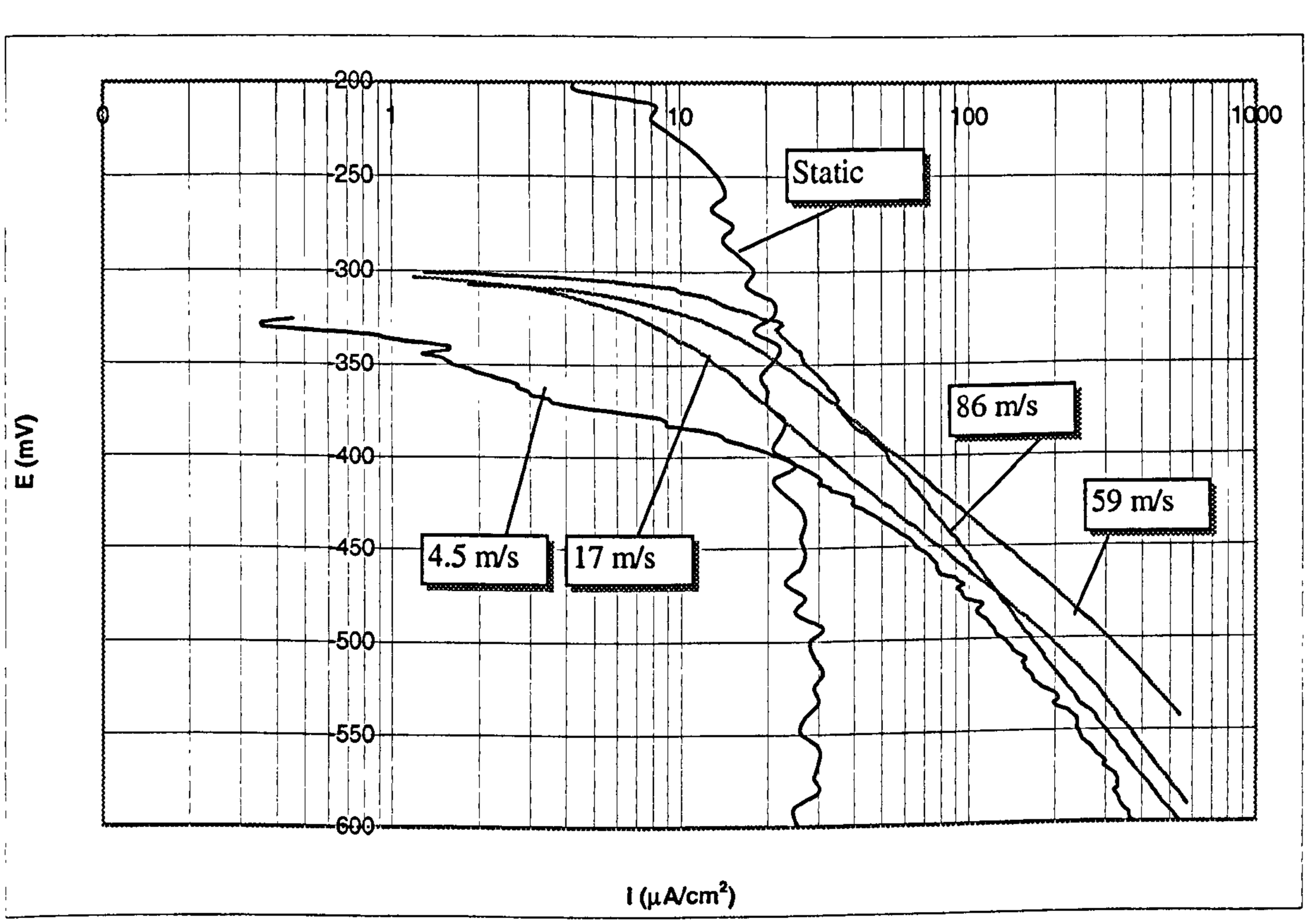

Figure 6.5b. Cathodic polarisation tests of Cu-10%Ni upon an initial exposure of 30 minutes under the impinging jet. The nozzle diameter is 1mm.

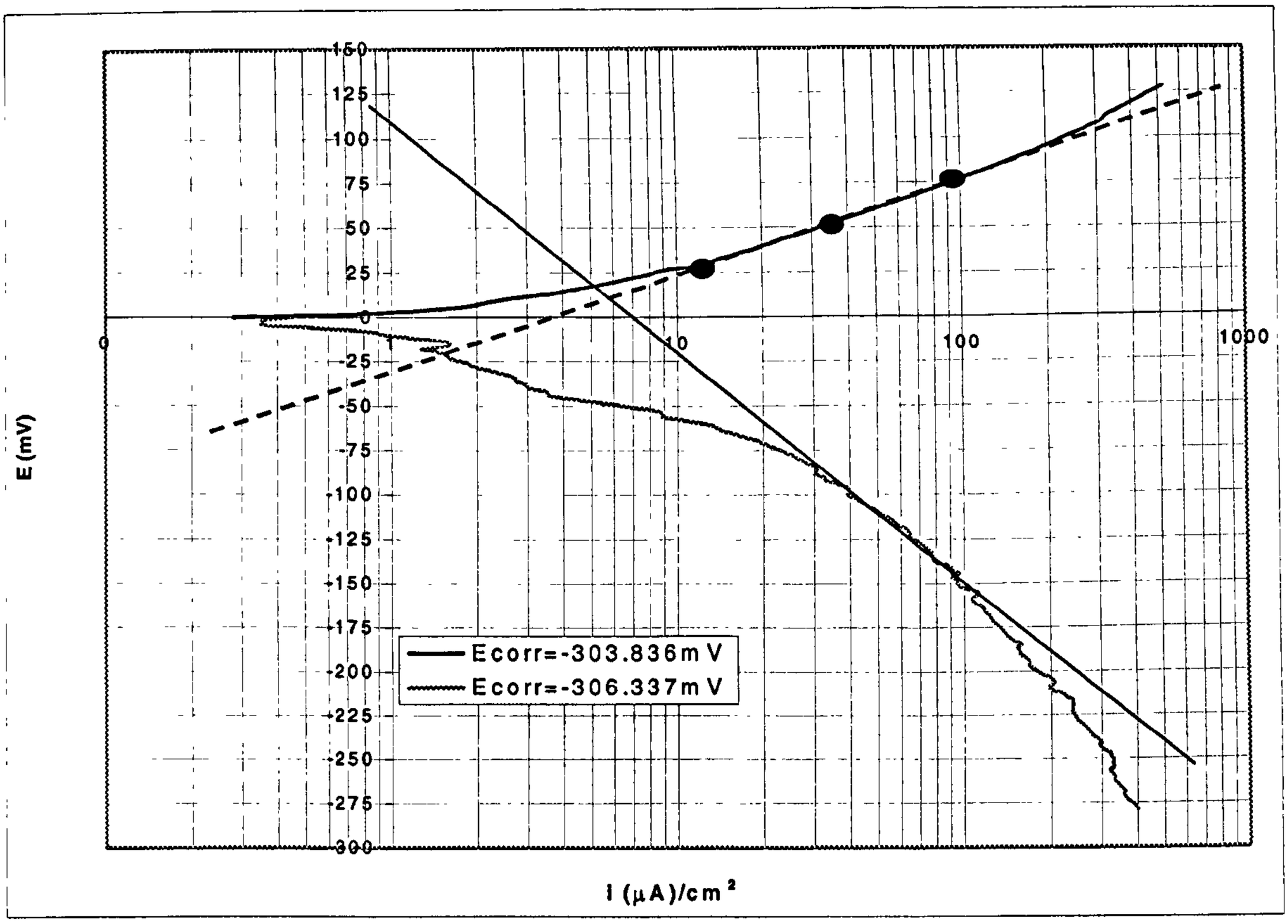

Figure 6.6a. Anodic+Cathodic polarisation tests of Cu-10%Ni upon an initial exposure of 30 minutes under the impinging jet. The nozzle diameter is 1mm and the impinging velocity V=4.5m/s.

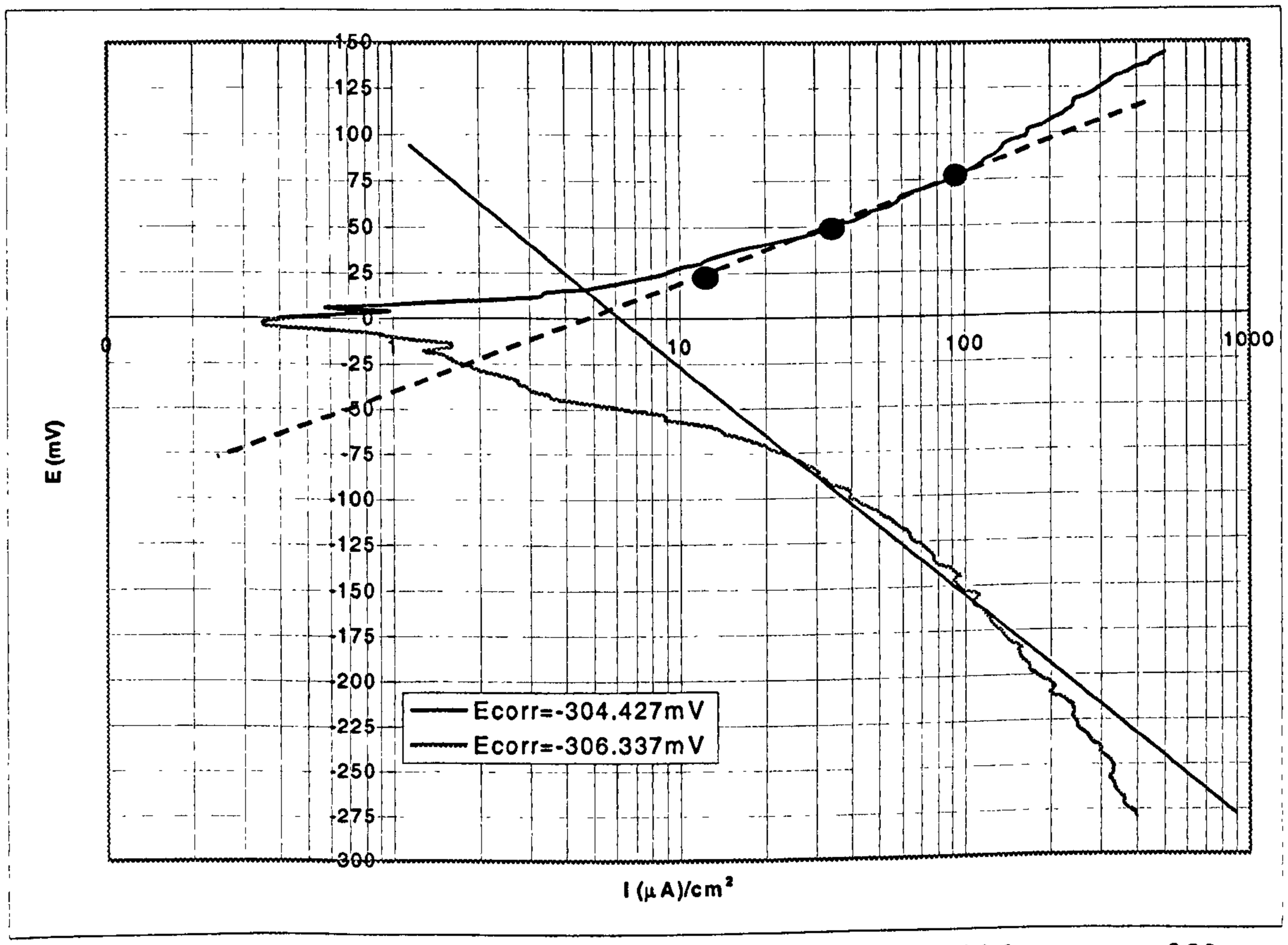

Figure 6.6b. Anodic+Cathodic polarisation tests of Cu-10%Ni upon an initial exposure of 30 minutes under the impinging jet. The nozzle diameter is 1mm and the impinging velocity V=4.5m/s.

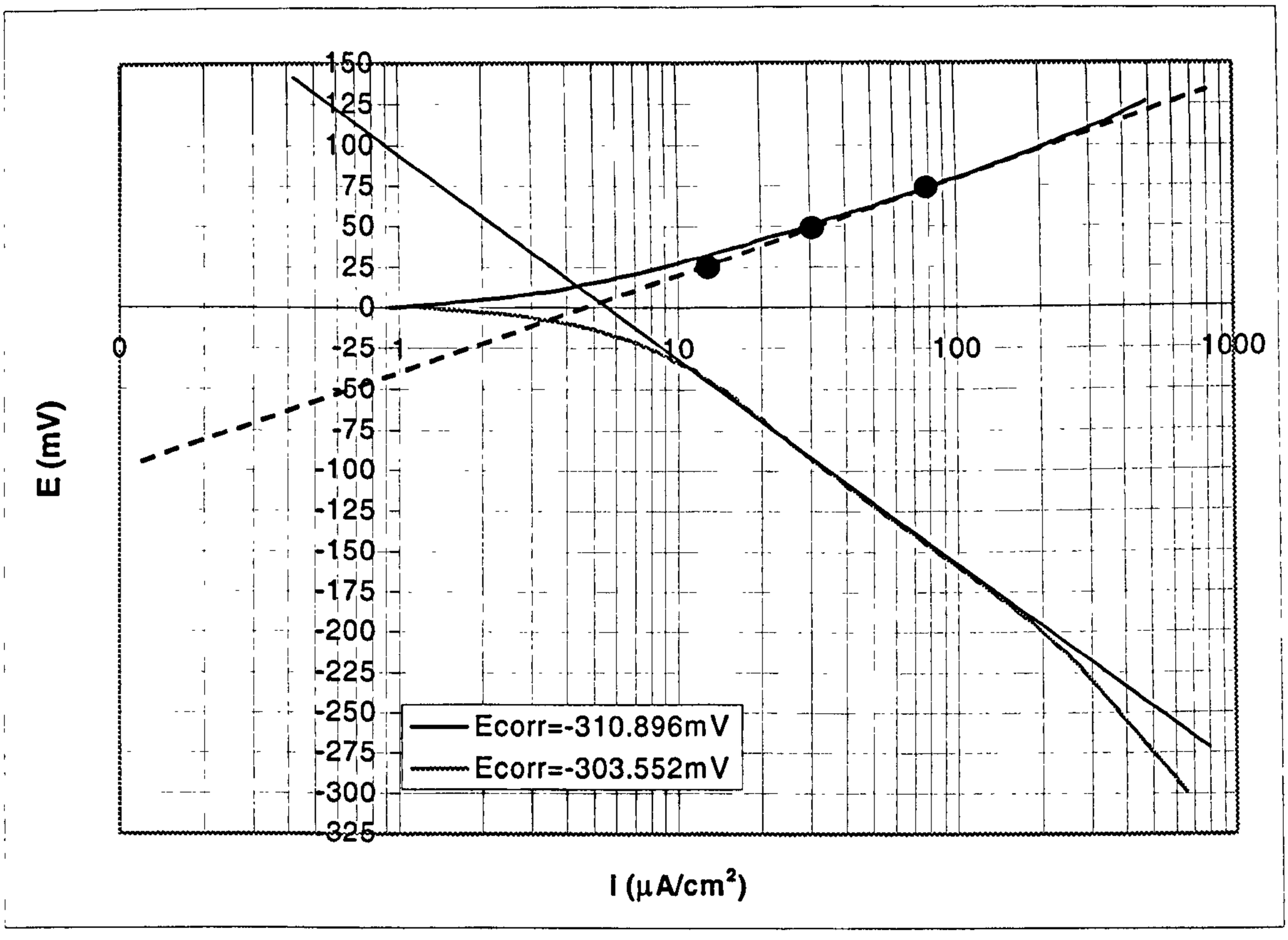

Figure 6.7a. Anodic+Cathodic polarisation tests of Cu-10%Ni upon an initial exposure of 30 minutes under the impinging jet. The nozzle diameter is 1mm and the impinging velocity V=17m/s.

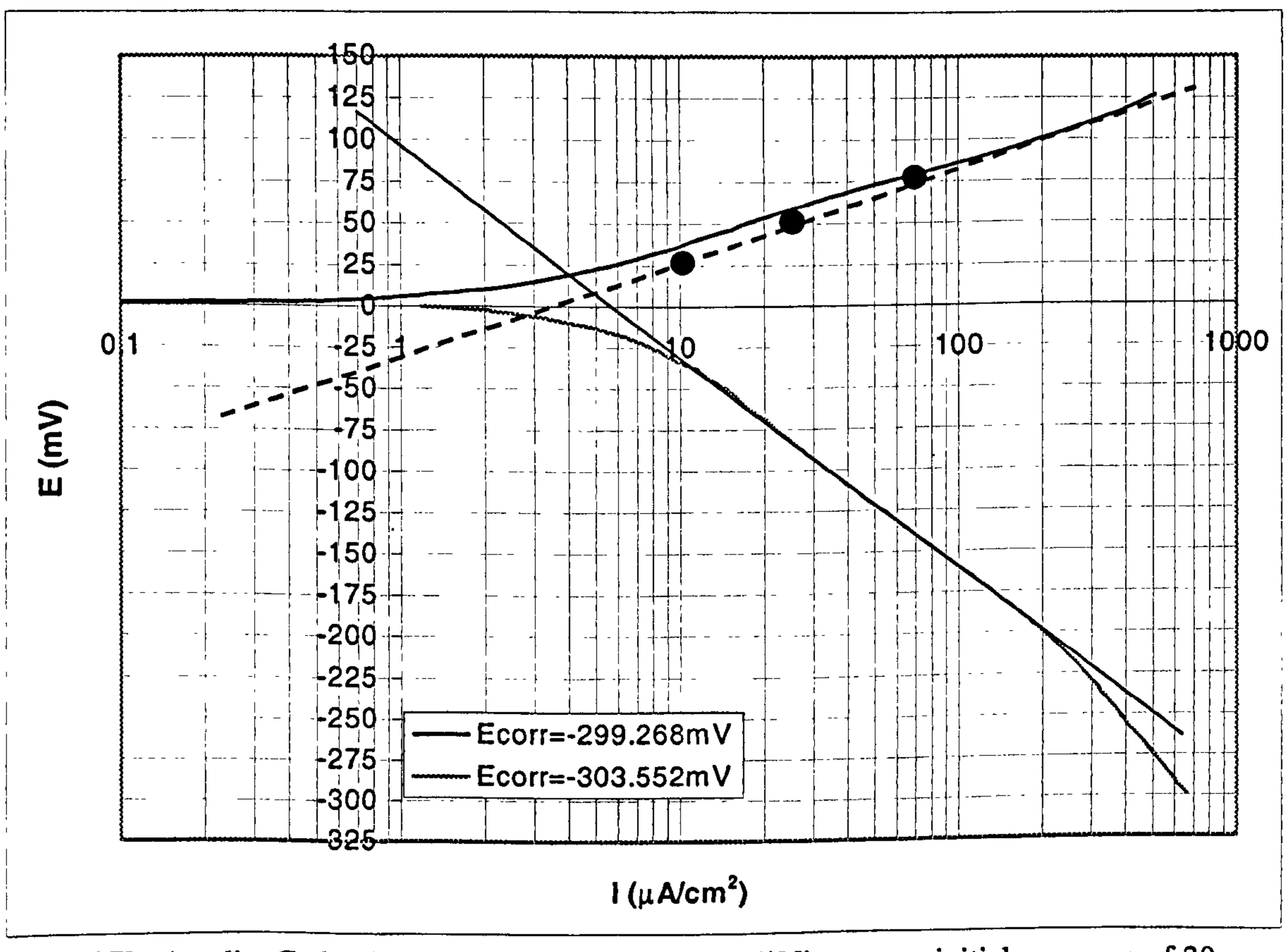

Figure 6.7b. Anodic+Cathodic polarisation tests of Cu-10%Ni upon an initial exposure of 30 minutes under the impinging jet. The nozzle diameter is 1mm and the impinging velocity V=17m/s.

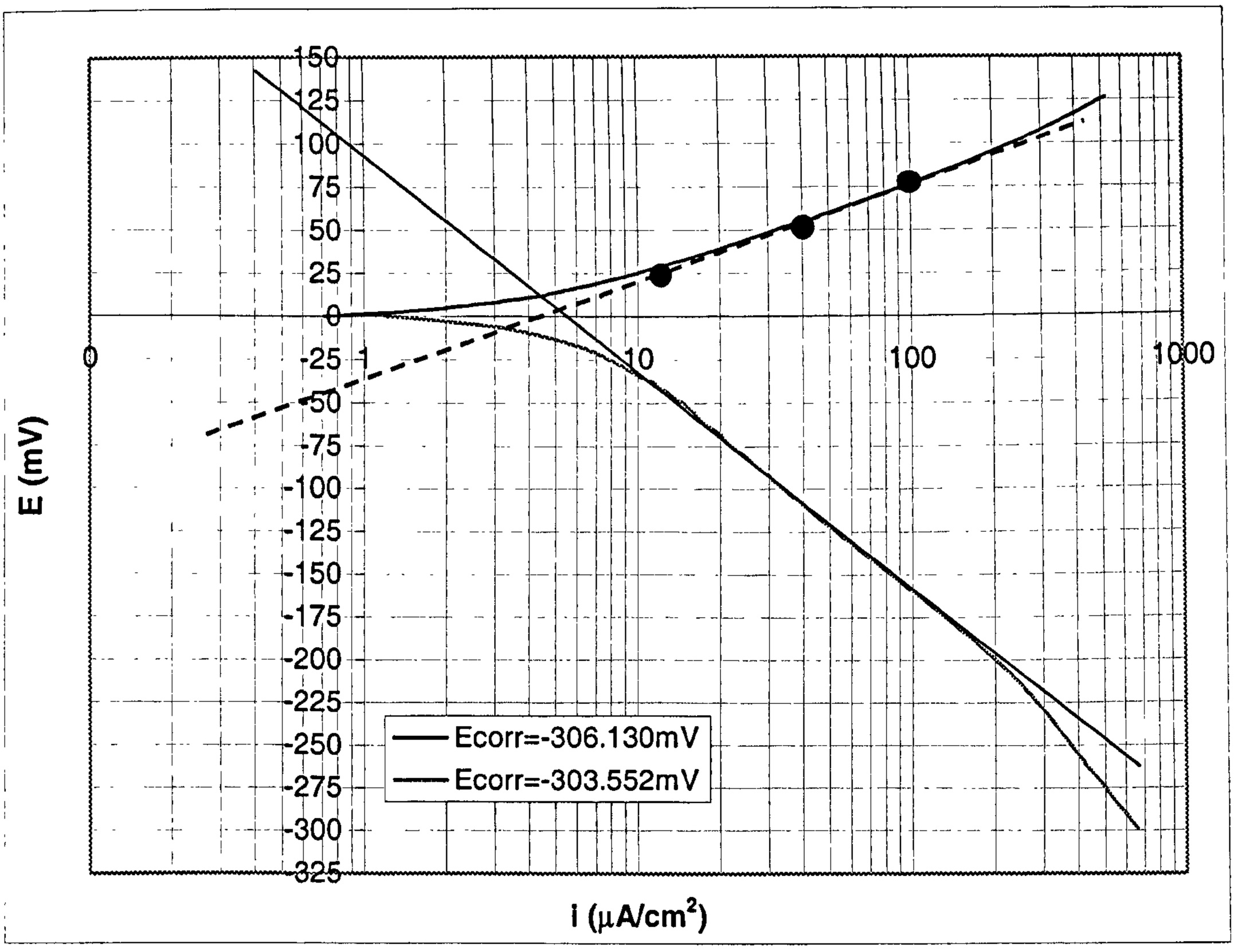

Figure 6.7c. Anodic+Cathodic polarisation tests of Cu-10%Ni upon an initial exposure of 30 minutes under the impinging jet. The nozzle diameter is 1mm and the impinging velocity V=17m/s.

Velocity (m/s)	Direct Corrosion current density ($\mu A/cm^2$)	Direct Corrosion current density ($\mu A/cm^2$) – average	Weight Losses (mg/h) – average
0	0.5 , 0.5 , 0.5	0.50	0.002
4.5	3.6 , 4.3	3.95	0.018
17	4.5 , 3.4 , 4.5	4.13	0.019
59	6.2 , 8.3 , 9.5	8.00	0.038
86	11.0 , 11.0	11.00	0.052

Table 6.2. Dependence of corrosion rate on impingement velocities with 1mm nozzle.

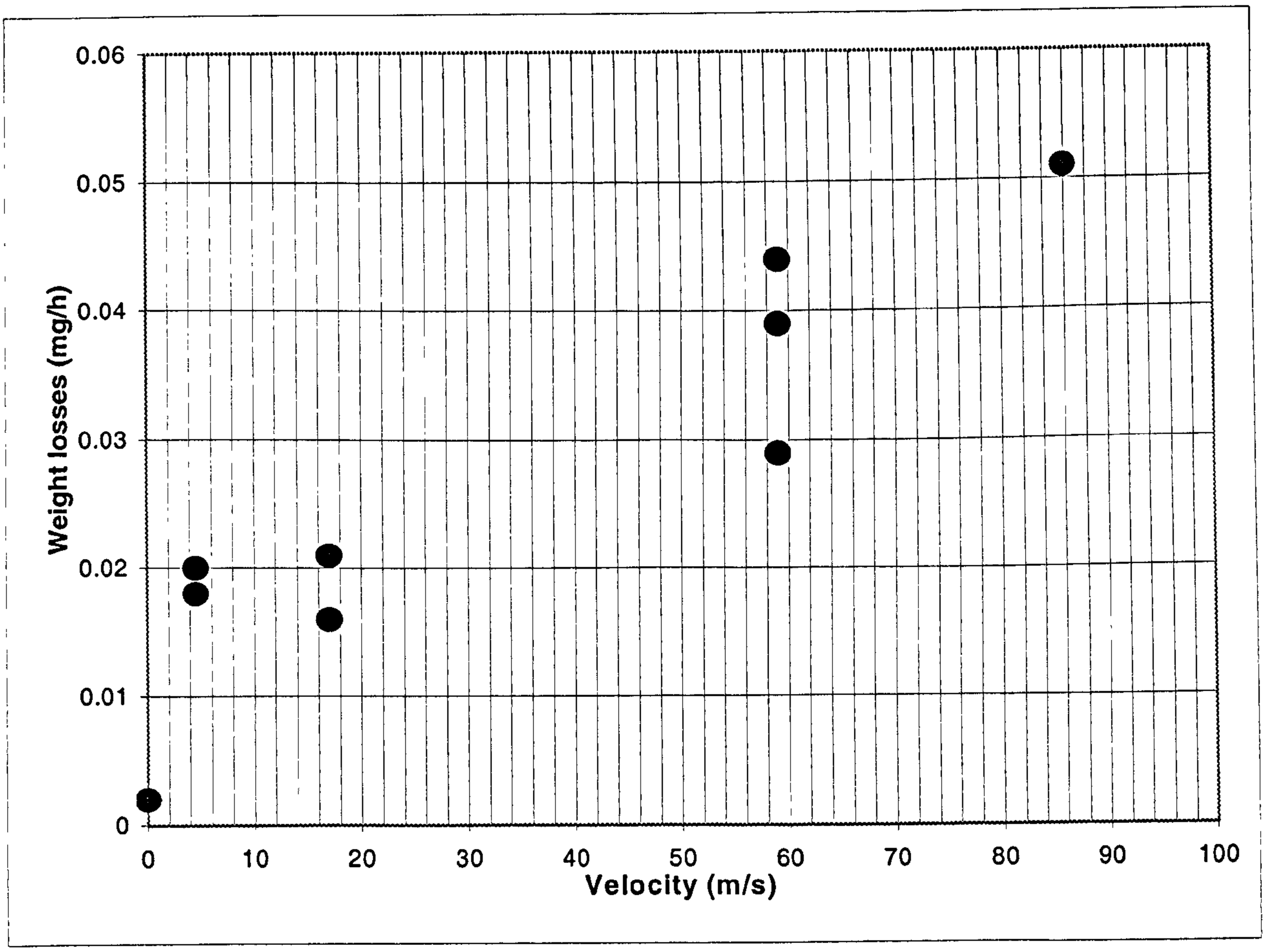

Figure 6.8. Corrosion rate of Cu-10%Ni after 30 minutes exposure time, as a function of impinging velocity at 1mm nozzle diameter.

6.2.1.2. *Impinging nozzle diameter 4mm.*

Figure 6.9a. and Figure 6.9b. show similar effects on the values of E_{corr}, (which were between –313 and –317mV under impingement), and the general shape of the anodic polarisation curves after 30 minutes impingement, as are demonstrated for the 1 mm nozzle in Figures 6.4a-b.

Figure 6.10a-b. show the typical cathodic polarisation plots. For each impinging velocity, using the same method displayed on Figure 6.6a. for a 1mm nozzle, a value of i_{corr} was obtained. Figure 6.11. and Table 6.3. present the data, (i_{corr} and weight loss values), showing the steadily increasing corrosion rate with increase in velocity.

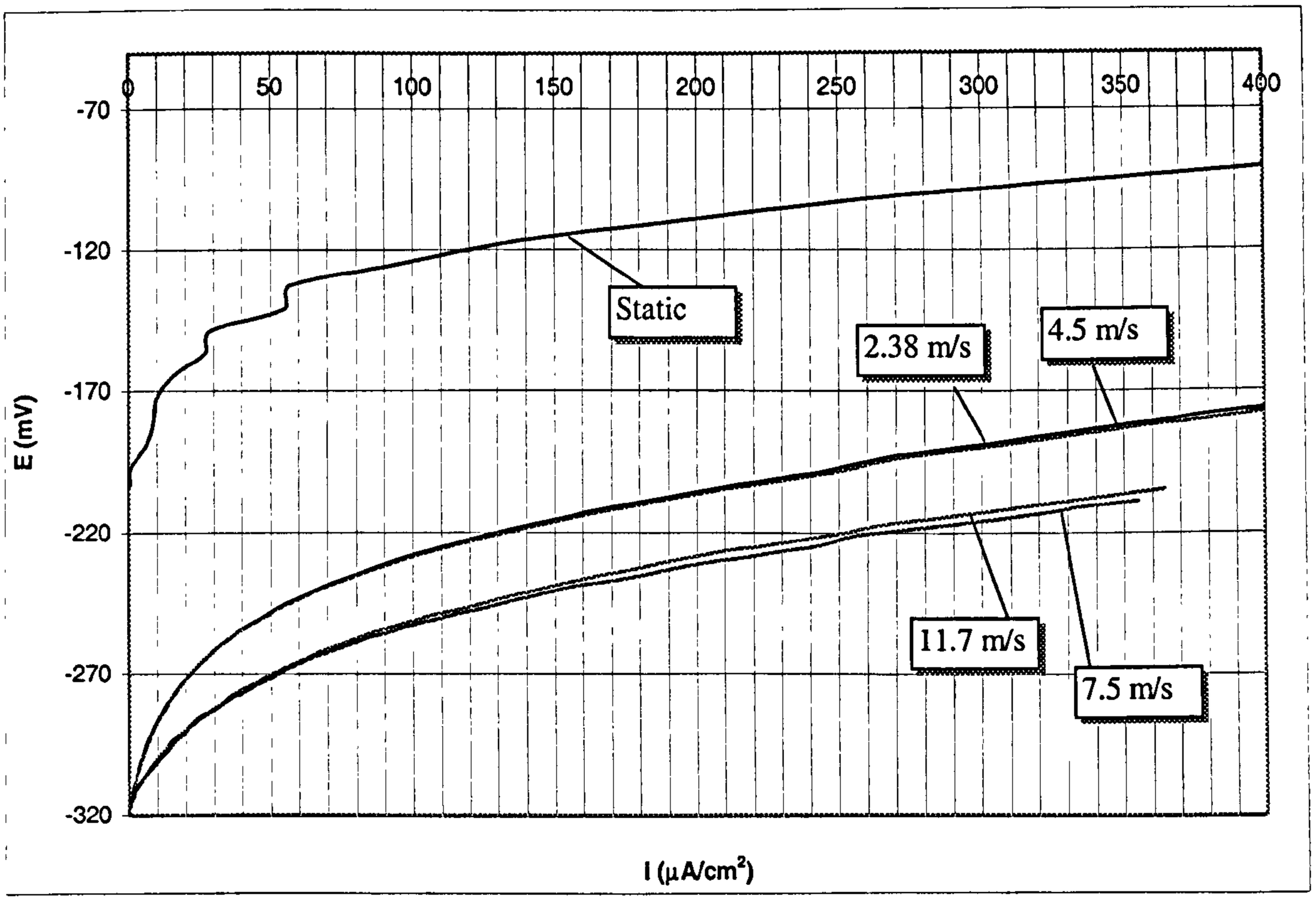

Figure 6.9a. Anodic polarisation tests of Cu-10%Ni upon an initial exposure of 30 minutes under the impinging jet. The nozzle diameter is 4mm.

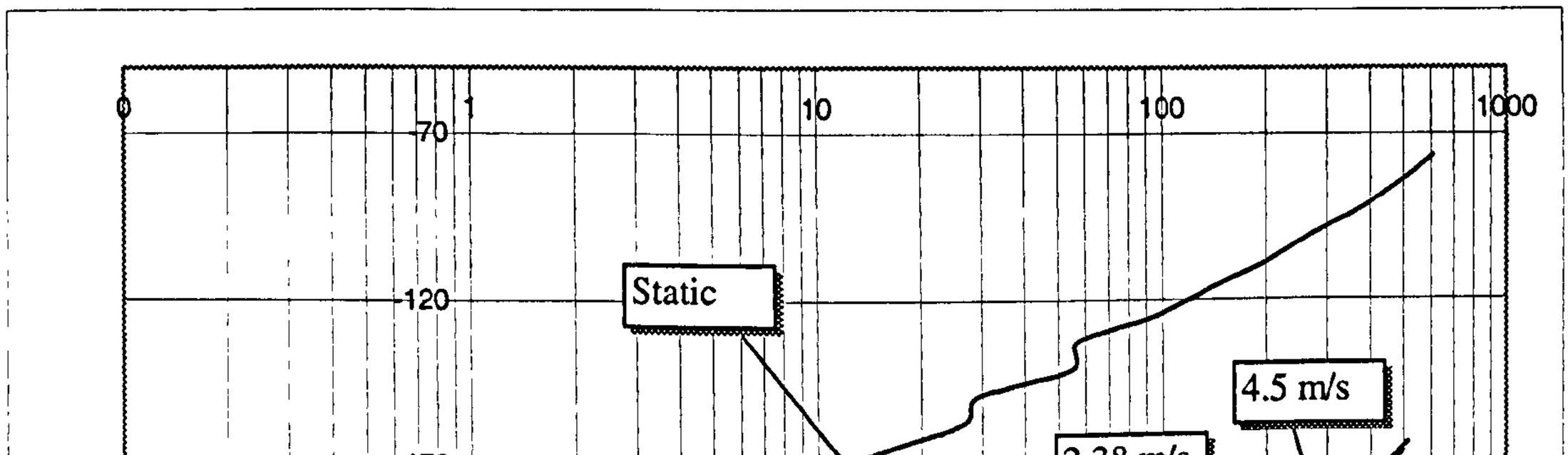

Figure 6.9b. Anodic polarisation tests of Cu-10%Ni upon an initial exposure of 30 minutes under the impinging jet. The nozzle diameter is 4mm.

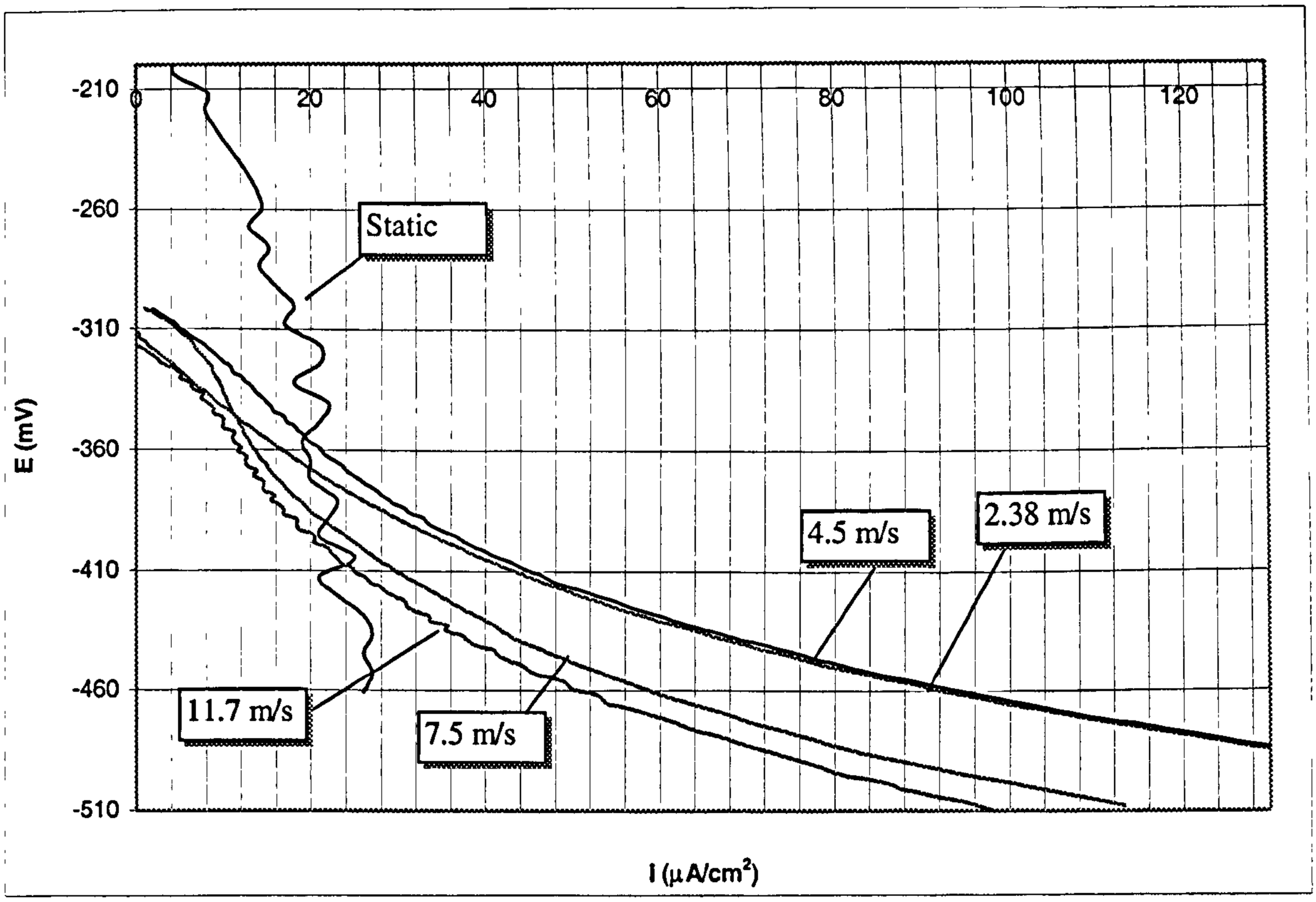

Figure 6.10a. Cathodic polarisation tests of Cu-10%Ni upon an initial exposure of 30 minutes under the impinging jet. The nozzle diameter is 4mm.

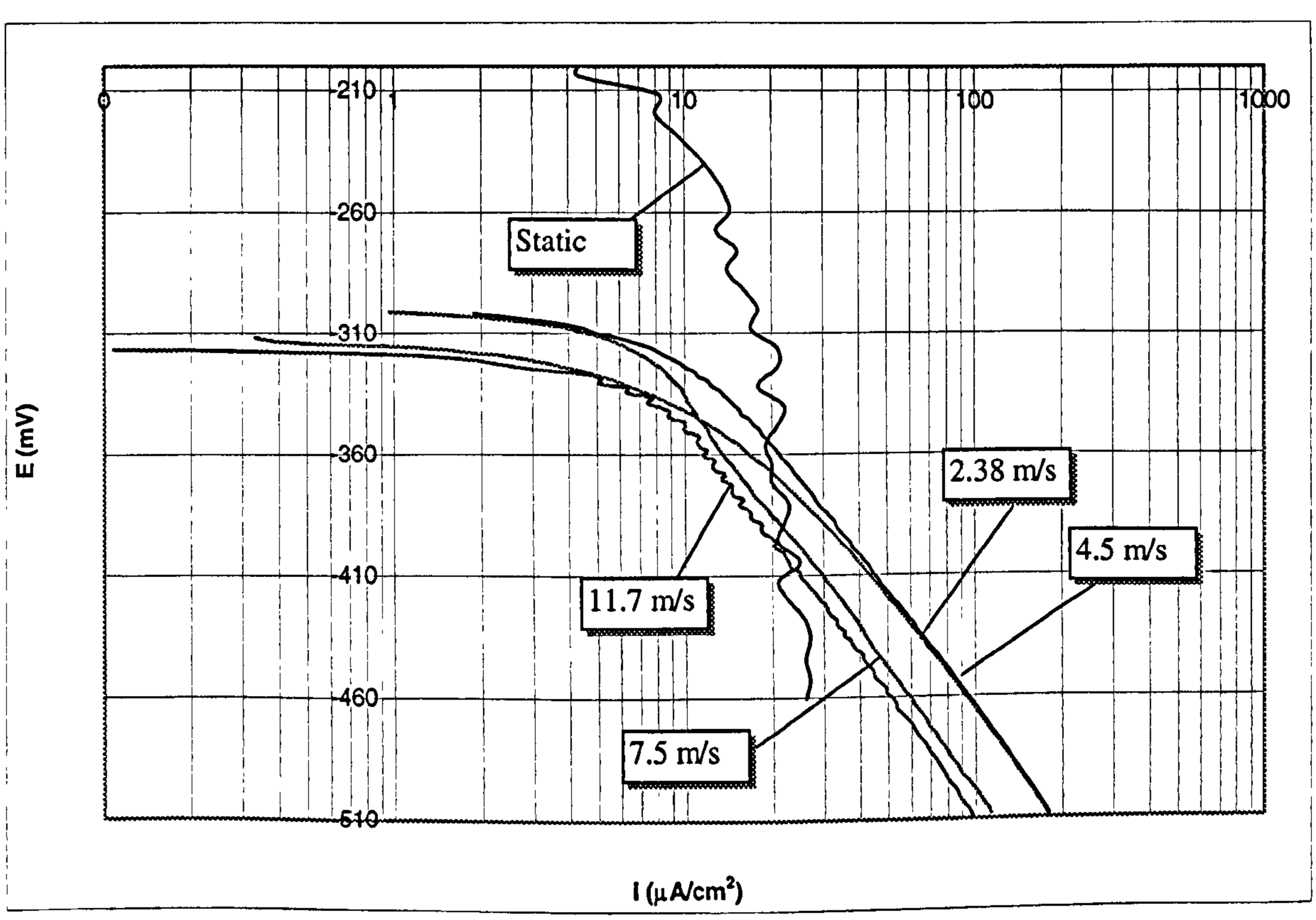

Figure 6.10b. Cathodic polarisation tests of Cu-10%Ni upon an initial exposure of 30 minutes under the impinging jet. The nozzle diameter is 4mm.

Velocity (m/s)	Direct Corrosion Current density ($\mu A/cm^2$)	Direct Corrosion current density ($\mu A/cm^2$) – average	Weight Losses (mg/h)
0	0.5 , 0.5 , 0.5	0.50	0.002
2.38	5.5 , 5.6	5.55	0.026
4.5	6.0 , 6.2	6.10	0.028
7.5	10.0 , 10.0	10.00	0.047
11.7	11.5 , 11.5	11.50	0.054

Table 6.3. Dependence of corrosion rate on impingement velocities with 4mm nozzle.

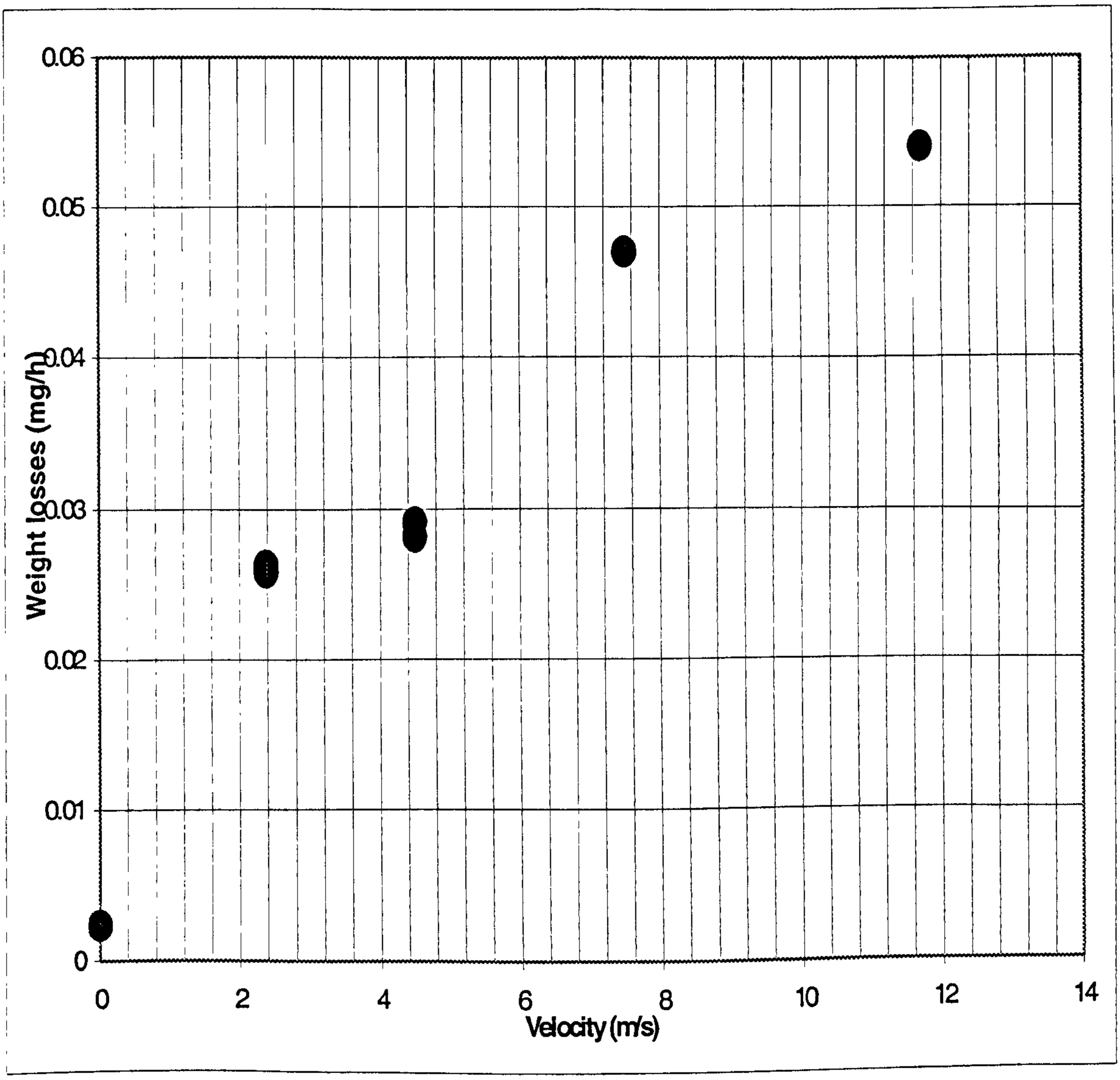

Figure 6.11. Corrosion rate of Cu-10%Ni after 30 minutes exposure time, as a function of impinging velocity at 4mm nozzle diameter.

6.2.1.3. *Concluding remarks on the effect of velocity on corrosion rate after 30 minutes under liquid impingement for Cu-10%Ni.*

The average corrosion rate/impingement velocity data at the two nozzle diameters are compared directly in Figure 6.12. and Table 6.4.

Although there is the expected general trend of increasing corrosion rate with impinging velocities, two other features of the results are:

a) For low impinging velocities the measured direct corrosion rate of the Cu-10%Ni specimens is lower when the nozzle diameter of the impinging jet is 1mm, rather than 4mm.

b) There is a step or inflection in the graphs near 4 m/s.

These features are discussed in Chapter 9.

Velocity (m/s)	Weight Losses (mg/h) - average	Direct Corrosion current density (μA/cm2) – average	Diameter of the nozzle (mm)
0	0.002	0.50	None
2.38	0.026	5.55	4
4.5	0.028	6.10	4
4.5	0.018	3.95	1
7.5	0.047	10.0	4
11.7	0.054	11.5	4
17	0.019	4.13	1
59	0.038	8.00	1
86	0.052	11.00	1

Table 6.4. Dependence of corrosion rate on impingement velocities with 1mm and 4mm nozzle.

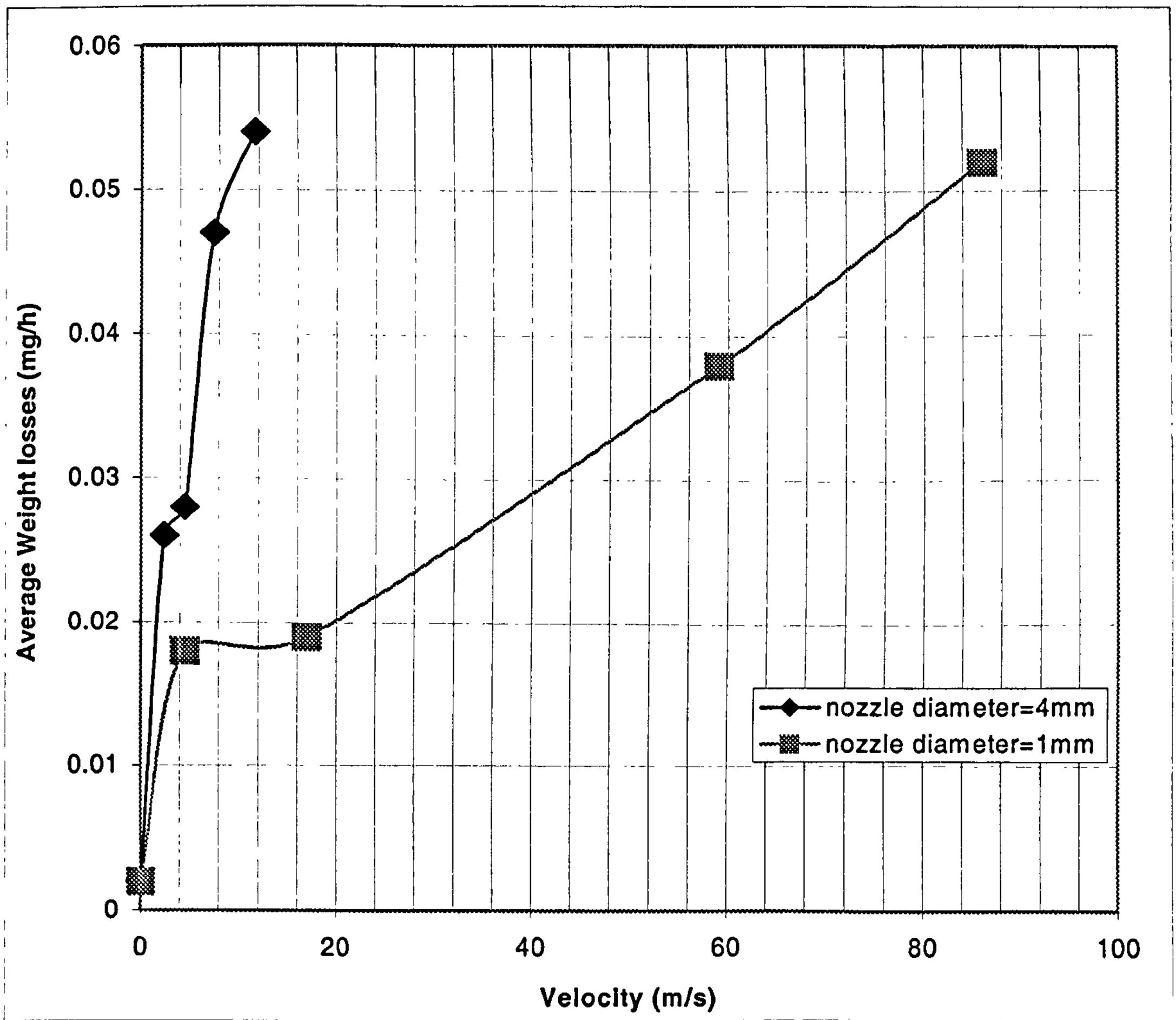

Figure 6.12. Corrosion rate of Cu-10%Ni as a function of impinging velocity at 1mm and 4mm nozzle.

6.2.2. Marinel.

6.2.2.1. *Impinging nozzle diameter 1mm.*

Figure 6.13a-b. and Figure 6.14a-b. show the typical anodic and cathodic polarisation curves generated from tests after 30 minutes in 3.5% NaCl solution. The same kind of behaviour promoted by impingement as that for the Cu-10%Ni alloy is displayed; i.e. a substantial negative shift in E_{corr}, (to –294 to –307mV), and to more-active anodic polarisation behaviour together with substantial cathodic depolarisation.

Figure 6.15a. and Figure 6.15b. show the anodic and cathodic polarisation curves for Marinel generated from duplicate tests after 30 minutes in 3.5% NaCl solution at an impinging velocity of 17m/s.

The obtained i_{corr} value for the impinging velocity of 17m/s, together with the i_{corr} values for the 4.5, 59 and 86m/s, (found according to the "Tafel extrapolation" procedure, as described in Chapter 5), are presented to Table 6.5. This table also presents the converted i_{corr} values to weight losses via Faraday's Law.

As it can be seen from Table 6.5. and Figure 6.16. the corrosion rates increase with velocity with the most dramatic rise occurring between 0 and 4.5 m/s.

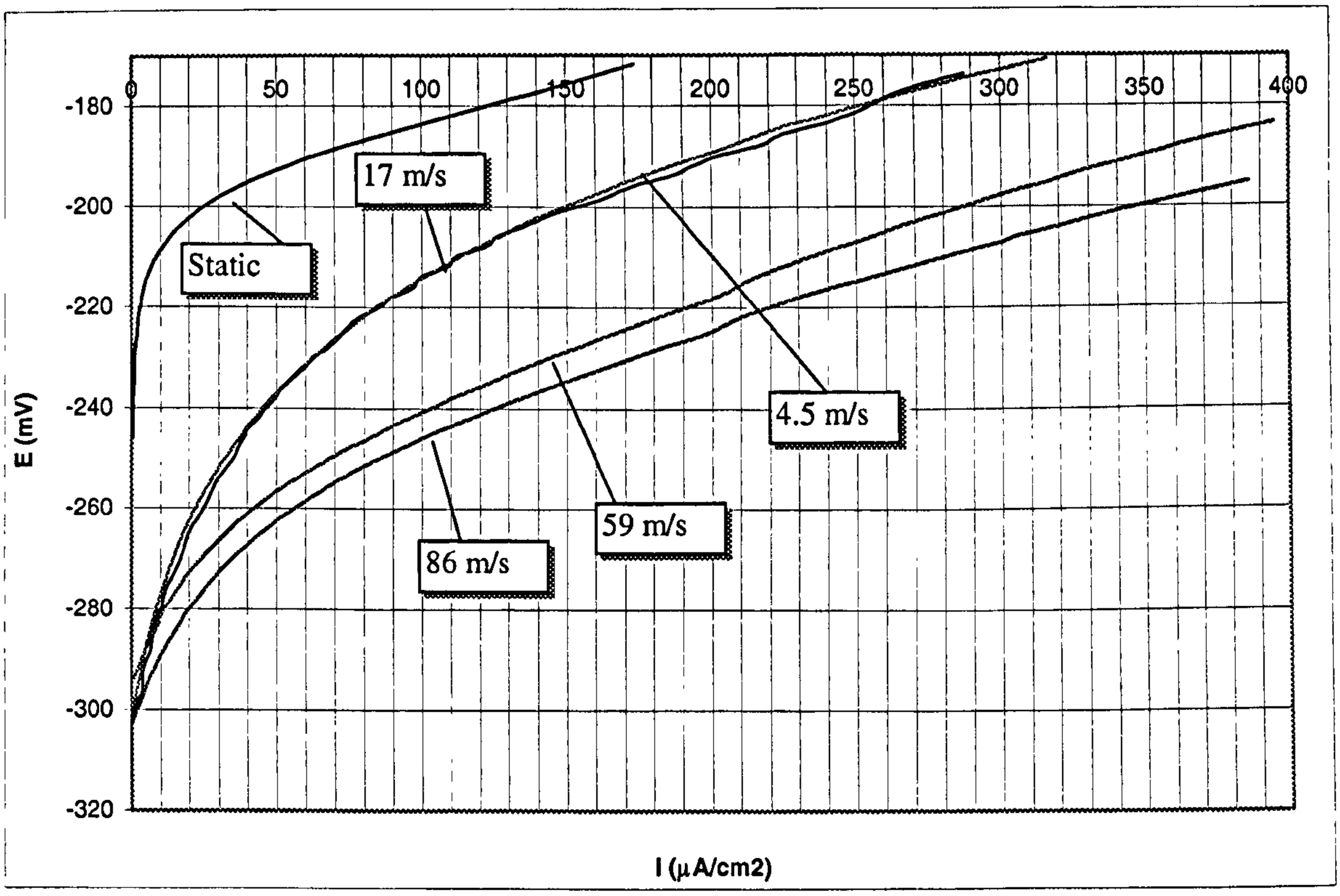

Figure 6.13a. Anodic polarisation tests of MARINEL upon an initial exposure of 30 minutes under the impinging jet. The nozzle diameter is 1mm.

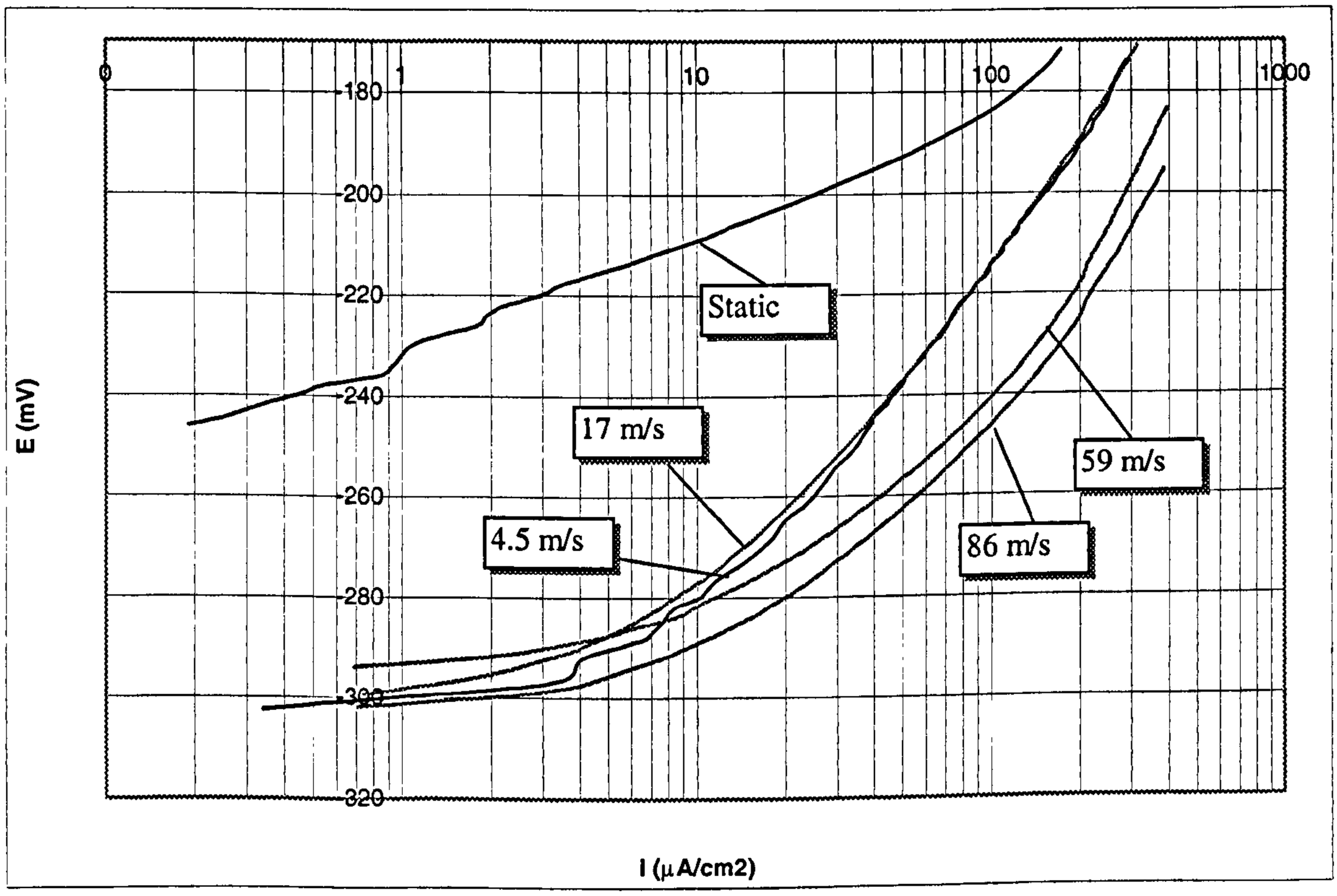

Figure 6.13b. Anodic polarisation tests of MARINEL upon an initial exposure of 30 minutes under the impinging jet. The nozzle diameter is 1mm.

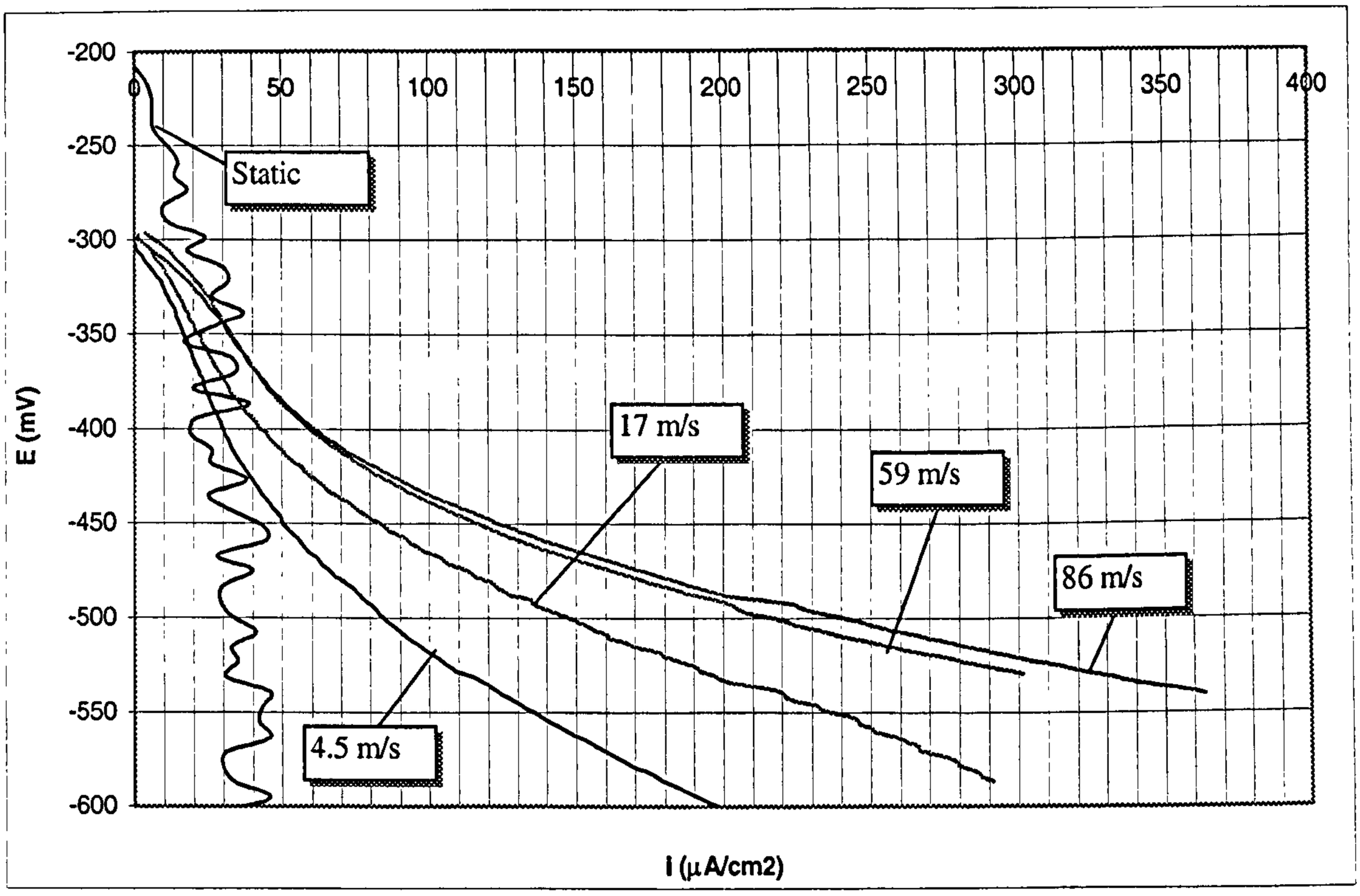

Figure 6.14a. Cathodic polarisation tests of MARINEL upon an initial exposure of 30 minutes under the impinging jet. The nozzle diameter is 1mm.

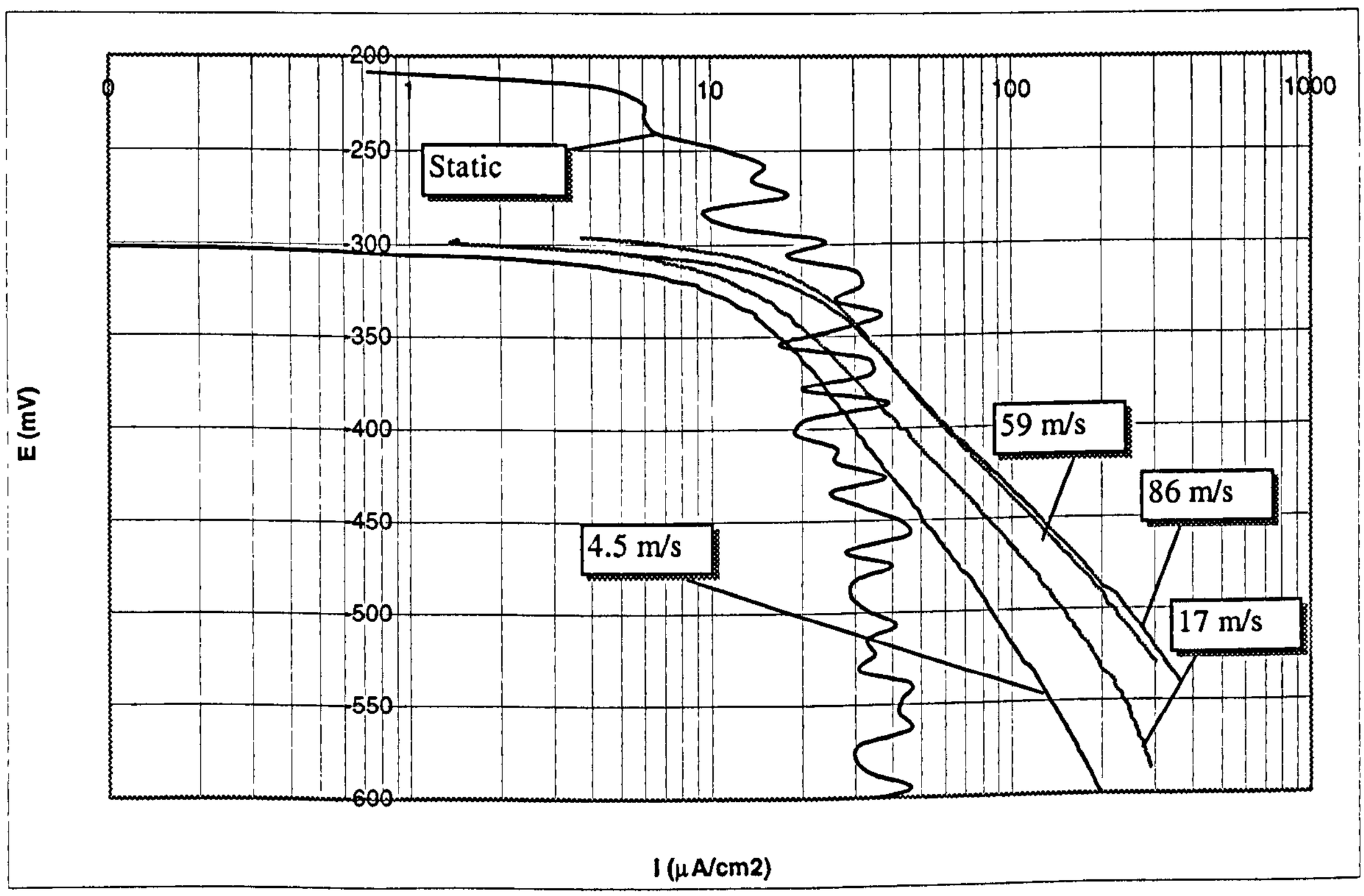

Figure 6.14b. Cathodic polarisation tests of MARINEL upon an initial exposure of 30 minutes under the impinging jet. The nozzle diameter is 1mm.

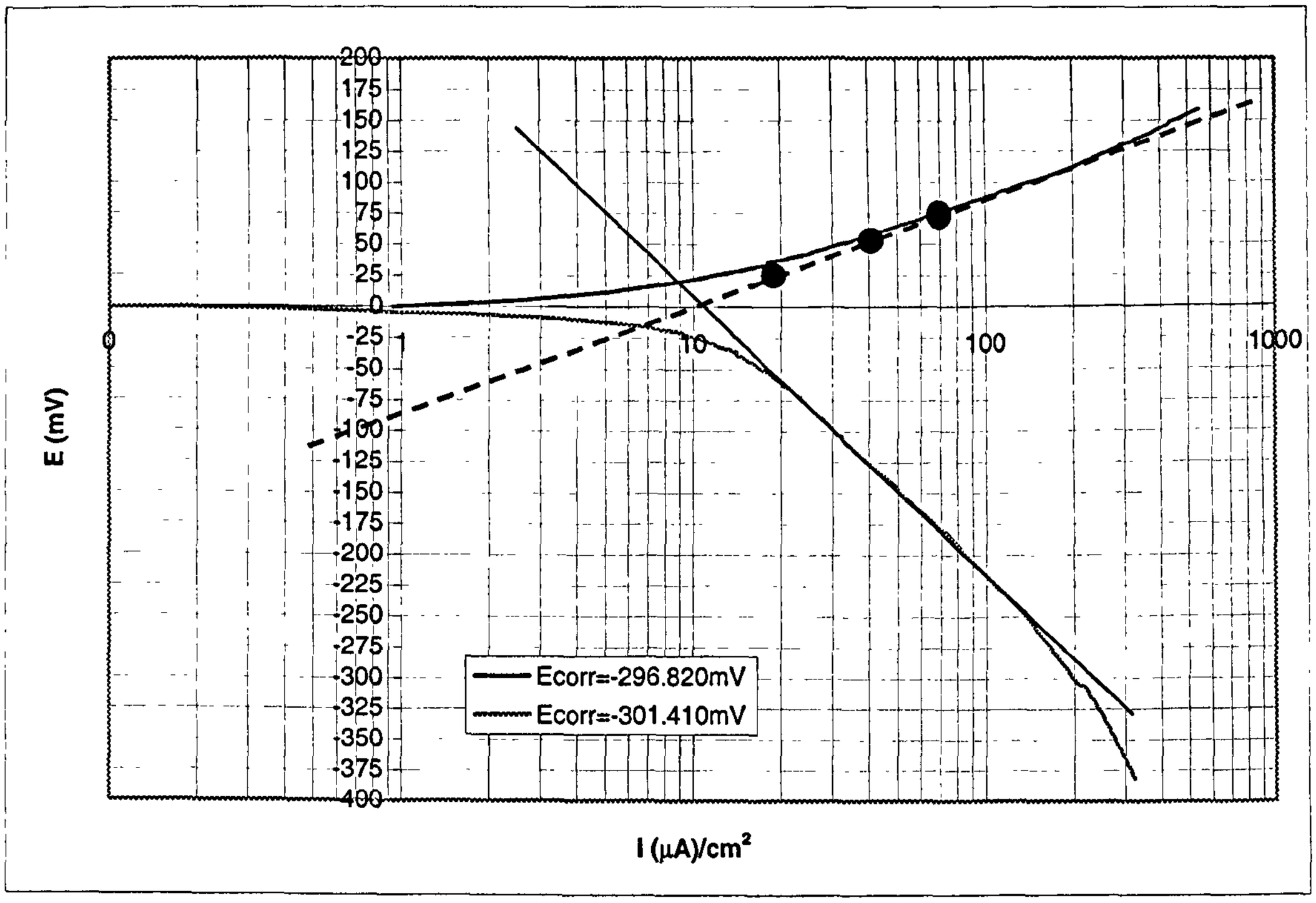

Figure 6.15a. Anodic+Cathodic polarisation tests of MARINEL upon an initial exposure of 30 minutes under the impinging jet. The nozzle diameter is 1mm and the impinging velocity V=17m/s.

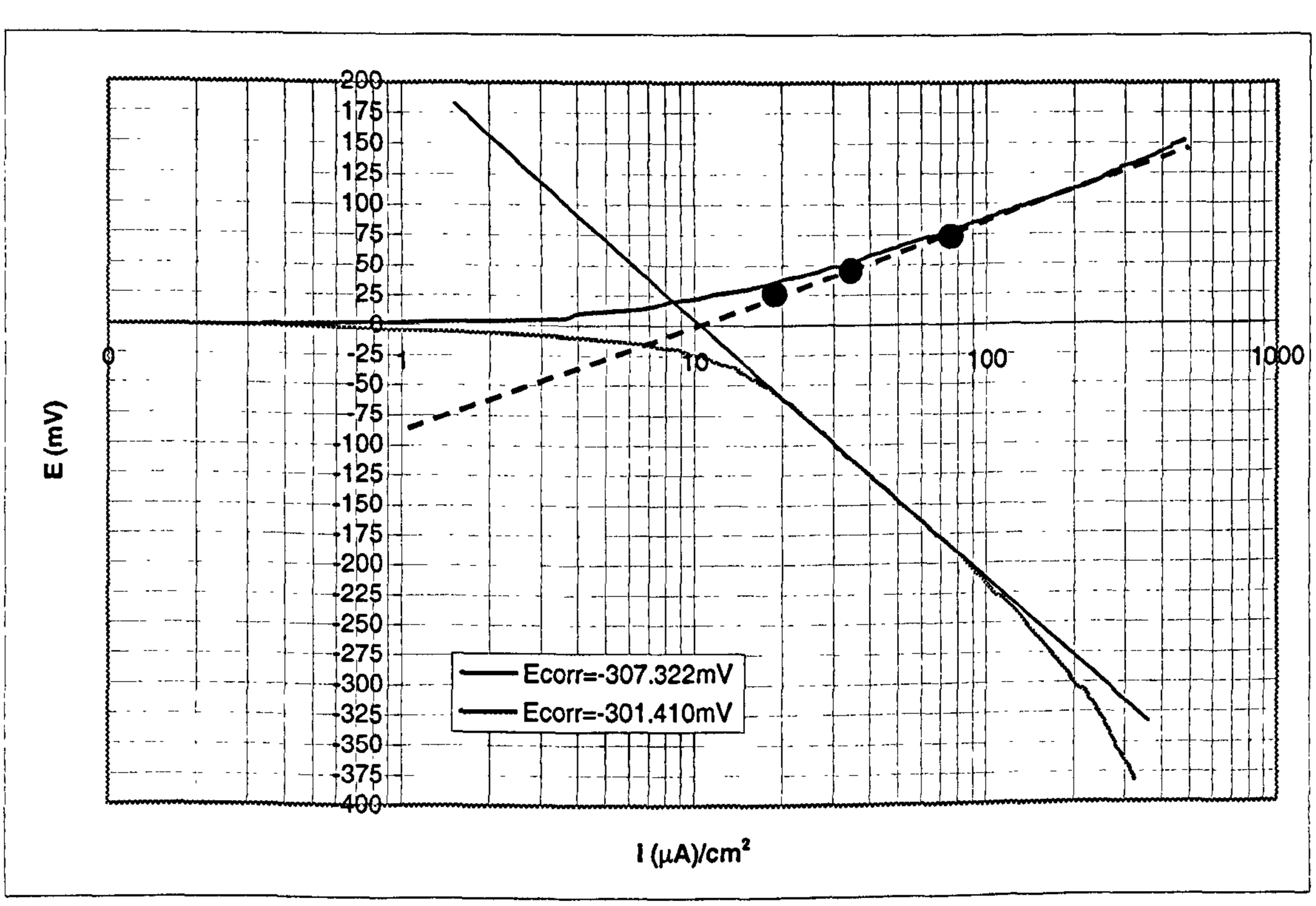

Figure 6.15b. Anodic+Cathodic polarisation tests of MARINEL upon an initial exposure of 30 minutes under the impinging jet. The nozzle diameter is 1mm and the impinging velocity V=17m/s.

Velocity (m/s)	Direct Corrosion Current density ($\mu A/cm^2$)	Direct Corrosion current density ($\mu A/cm^2$) – average	Weight Losses (mg/h) – average
0	0.4 , 0.5 , 0.6	0.5	0.003
4.5	9.0 , 9.0	9.0	0.050
17	10.0 , 10.0	10.0	0.055
59	17.0 , 17.0	17.0	0.094
86	18.0 , 18.0	18.0	0.100

Table 6.5. Dependence of corrosion rate on impingement velocities with 1mm nozzle.

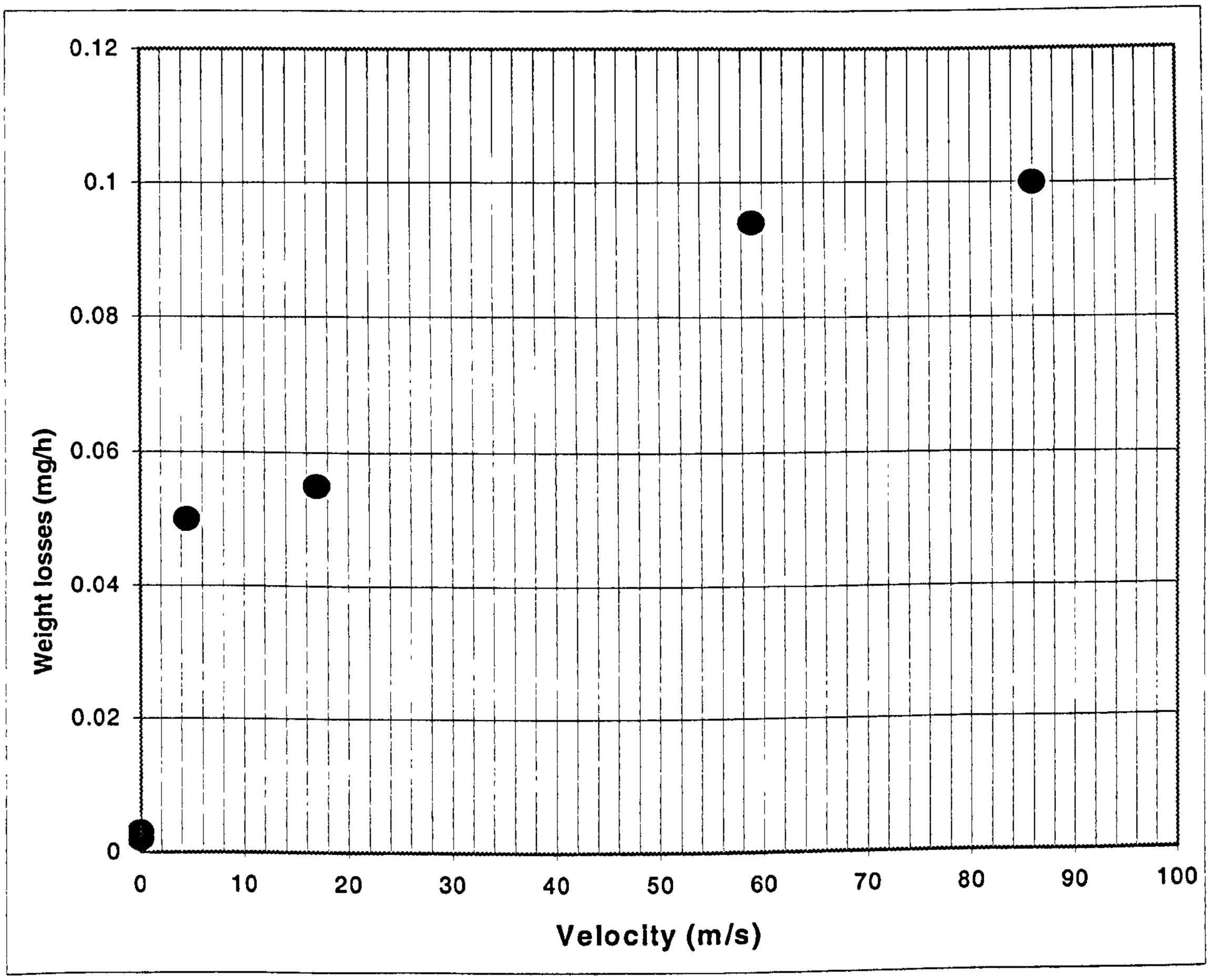

Figure 6.16. Corrosion rate of Marinel after 30 minutes, as a function of impinging velocities at 1mm nozzle diameter.

6.2.2.2. *Impinging nozzle diameter 4mm.*

Figure 6.17a. and Figure 6.17b. show similar effects on the values of E_{corr}, (which were between –297 and –319mV under impingement), and the general shape of the anodic polarisation curves after 30 minutes impingement, as are demonstrated for the 1 mm nozzle in Figures 6.13a and Figure 6.13b.

Figure 6.18a. and Figure 6.18b. show the typical cathodic polarisation plots. For each impinging velocity, by plotting the anodic and the cathodic plot in one graph and following the Tafel extrapolation procedure, a value of i_{corr} was obtained. Figure 6.19. and Table 6.6. present the data, (i_{corr} and weight loss values), of the effect of increasing velocity on corrosion rate.

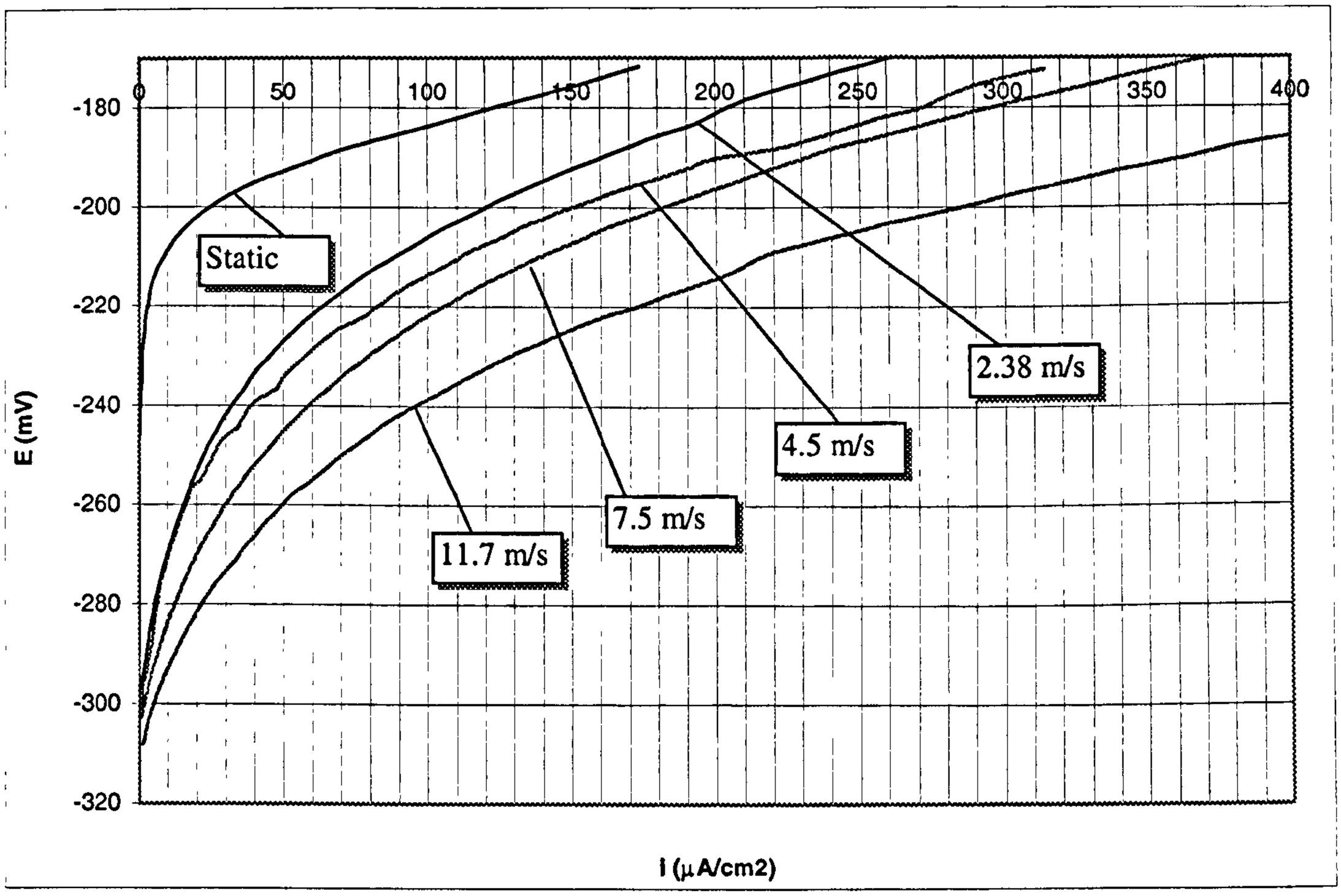

Figure 6.17a. Anodic polarisation tests of MARINEL upon an initial exposure of 30 minutes under the impinging jet. The nozzle diameter is 4mm.

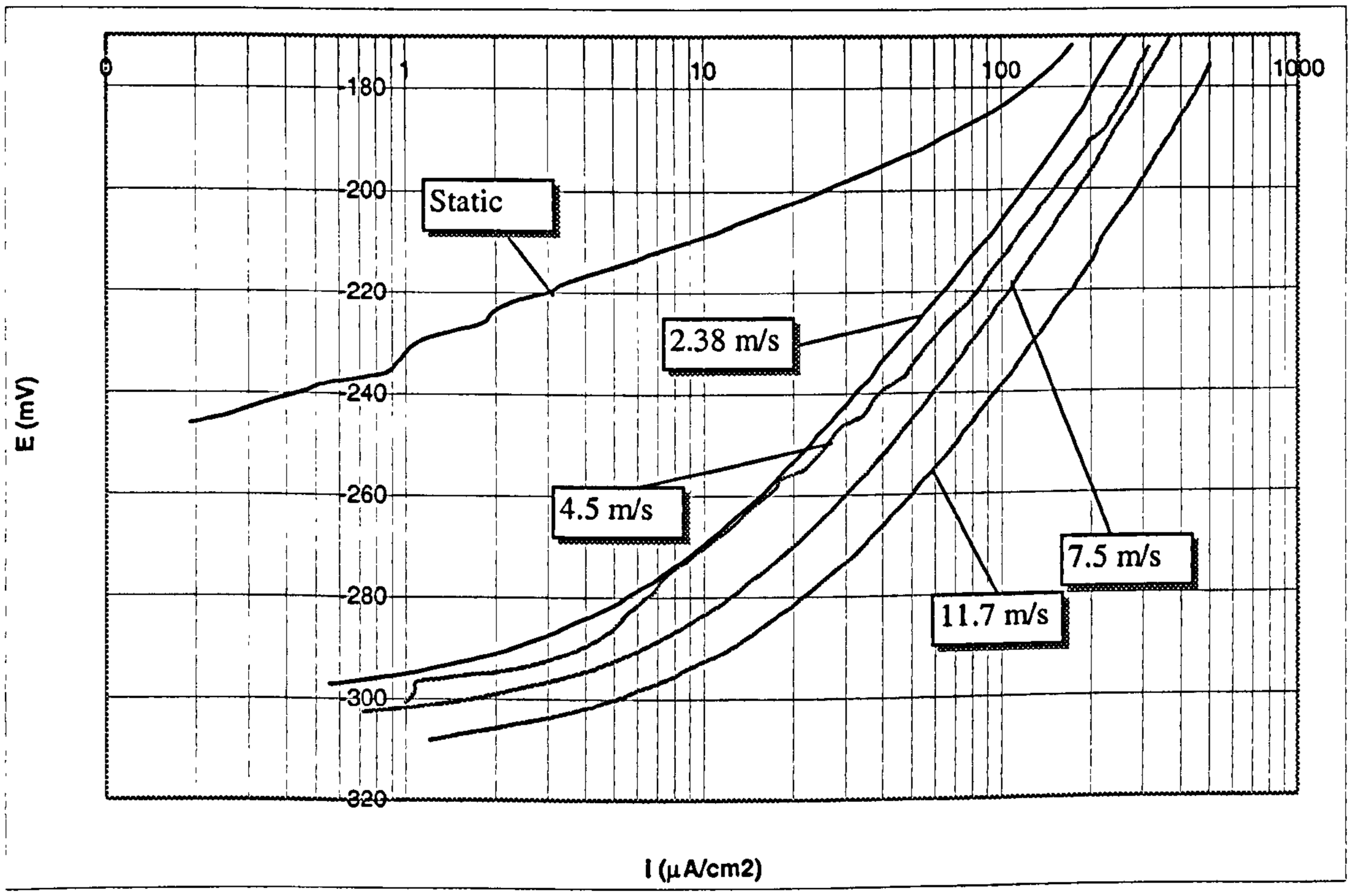

Figure 6.17b. Anodic polarisation tests of MARINEL upon an initial exposure of 30 minutes under the impinging jet. The nozzle diameter is 4mm.

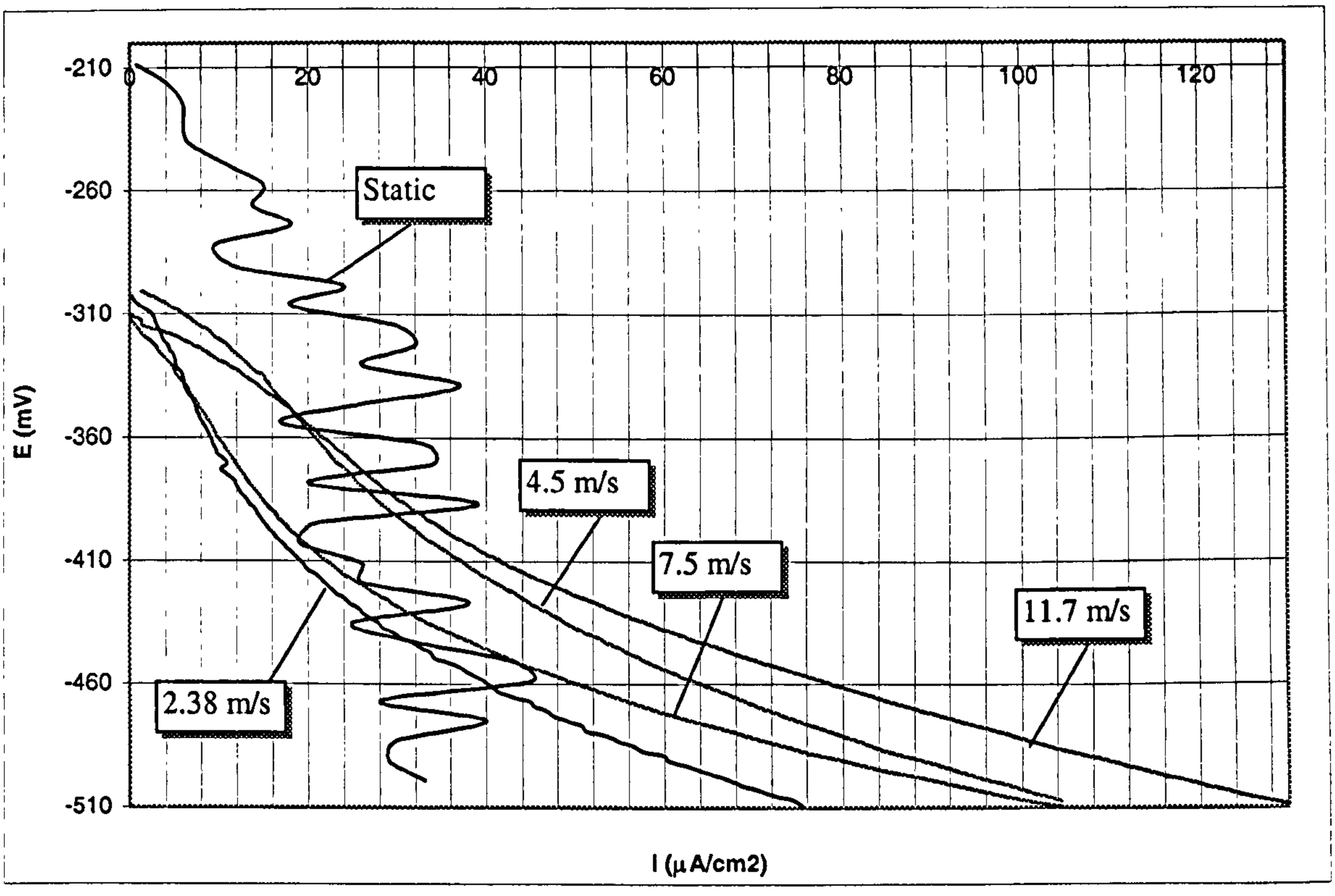

Figure 6.18a. Cathodic polarisation tests of MARINEL upon an initial exposure of 30 minutes under the impinging jet. The nozzle diameter is 4mm.

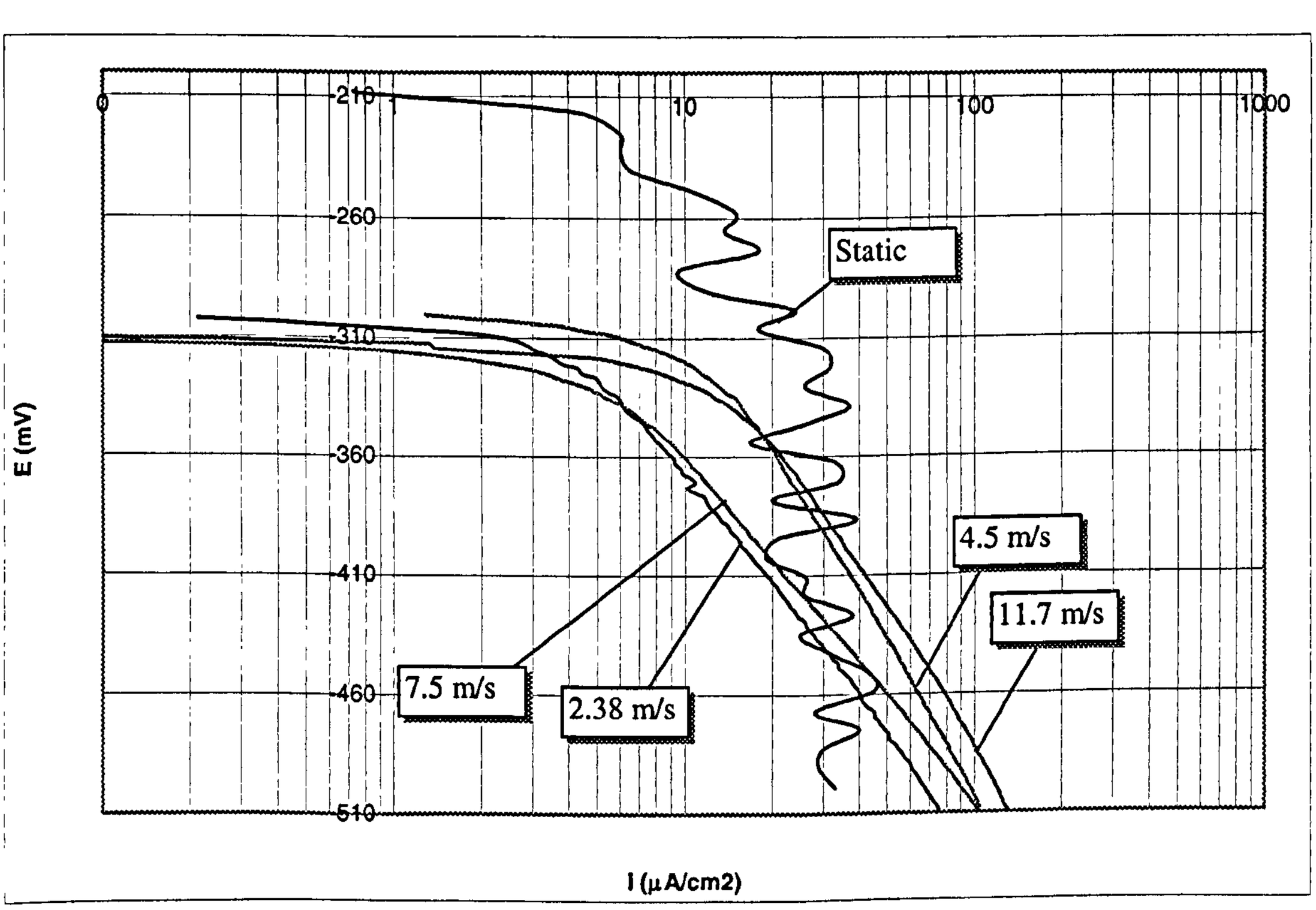

Figure 6.18b. Cathodic polarisation tests of MARINEL upon an initial exposure of 30 minutes under the impinging jet. The nozzle diameter is 4mm.

Velocity (m/s)	Direct Corrosion current density ($\mu A/cm^2$)	Direct Corrosion Current density ($\mu A/cm^2$) – average	Weight Losses (mg/h) - Average
0	0.4 , 0.5 , 0.6	0.50	0.003
2.38	4.5 , 4.6	4.55	0.025
4.5	6.5 , 6.5	6.50	0.036
7.5	6.5 , 7.0	6.75	0.037
11.7	13.0 , 13.0	13.00	0.072

Table 6.6. Dependence of corrosion rate on impingement velocities with 4mm nozzle.

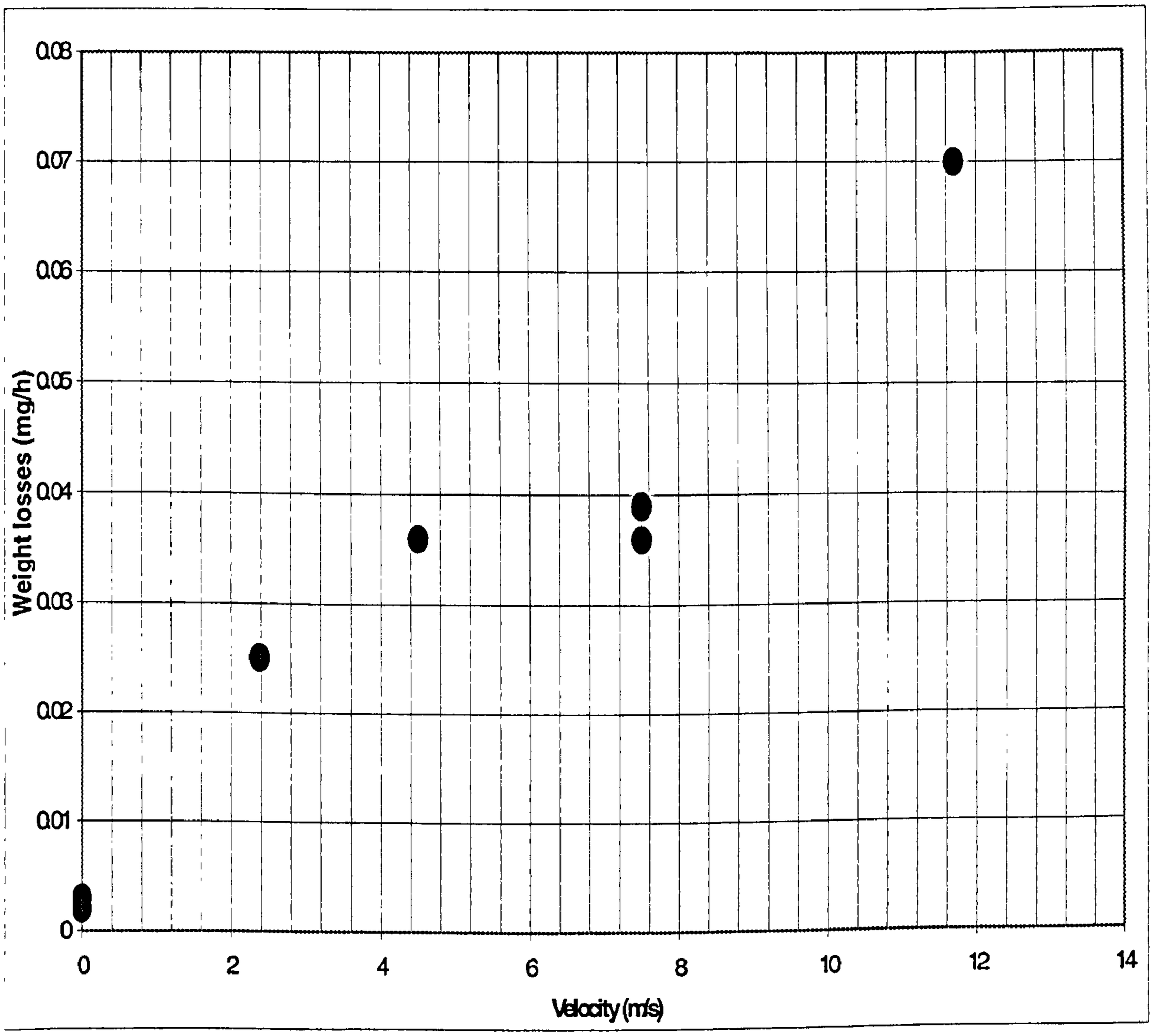

Figure 6.19. Corrosion rate of Marinel after exposure time of 30 minutes, as a function of impinging velocities at 4mm nozzle diameter.

6.2.2.3. *Concluding remarks on the effect of velocity on corrosion rate after 30 minutes under liquid impingement for Marinel.*

The average corrosion rate/impingement velocity data at the two nozzle diameters are compared directly in Figure 6.20. and Table 6.7. and, as for Cu-10%Ni (Figure 6.12.) exhibit a general trend of increasing corrosion rate with impinging velocities.

Also similar to Cu-10%Ni, there is a step in the corrosion rate/velocity curve. On the other hand, the corrosion rates for Marinel are substantially higher than for Cu-10%Ni.

Although different corrosion rates at similar velocities are shown for Marinel, there is not a systematic difference as for Cu-10%Ni and indeed the differences at the two nozzle sizes are proportionately much less for Marinel than for Cu-10%Ni.

Velocity (m/s)	**Weight Losses (mg/h) – average**	**Direct Corrosion current density ($\mu A/cm^2$) – average**	**Diameter of the nozzle (mm)**
0	0.003	0.50	None
2.38	0.025	4.55	4
4.5	0.036	6.50	4
4.5	0.050	9.00	1
7.5	0.037	6.75	4
11.7	0.072	13.00	4
17	0.055	10.00	1
59	0.094	17.00	1
86	0.100	18.00	1

Table 6.7. Dependence of corrosion rate on impingement velocities with 1mm and 4mm nozzle.

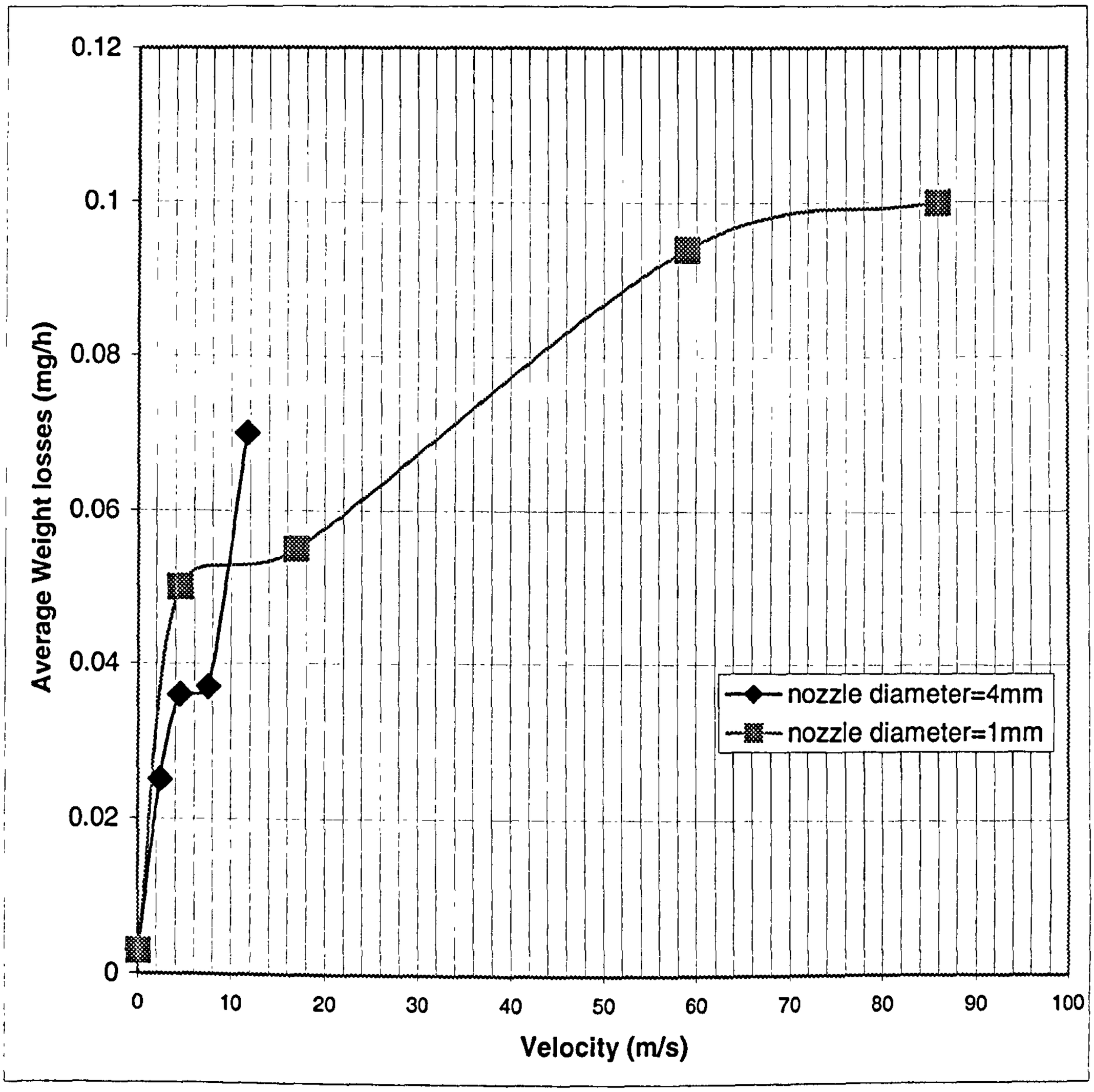

Figure 6.20. Corrosion rate of Marinel as a function of impinging velocity at 1mm and 4mm nozzle.

6.3. Overall Erosion Corrosion Processes.

The previous section (6.2.), presented results focused on the influence of short-term impingement upon the electrochemical corrosion processes. The remainder of this chapter and the following chapter are concerned with the overall erosion corrosion processes and involve much longer time scales. The results of this part of the work are described in the following sections, 6.3.1 (for Cu10%Ni), and 6.3.2 (for Marinel).

6.3.1. General erosion-corrosion of Cu-10%Ni.

6.3.1.1. *Effect of velocity on erosion-corrosion for 4 hours.*

These tests involved exposure of the specimens for 4 hours under impingement conditions. Each test, (anodic and cathodic polarisation, total weight loss and cathodic protection), includes at least one replication.

6.3.1.1.1. *Total Weight Loss.*

The total weight loss/impingement velocity data for the two nozzle diameters are compared directly in Table 6.8. Consideration of the static and 1mm nozzle results demonstrates a clear trend of increasing weight loss with impingement velocity. Comparison of the low velocity (2.38m/s – 4.5m/s) weight losses is difficult on account of the accuracy of the balance 0.0001g.

Nozzle Diam.(mm)	Velocity (m/s)	Total Weight Loss (mg)	Average Total Weight Loss (mg)
Static	0	0.01 , 0.01 , 0.01	0.01
4	2.38	0.6 , 0.7	0.65
4	4.5	0.6 , 0.6	0.60
1	4.5	0.5 , 0.5	0.50
1	17	0.9 , 1.1	1.00
1	86	2.0 , 2.4	2.20

Table 6.8. Total weight loss/impingement velocity data at the two nozzle diameters after 4 hours exposure time.

6.3.1.1.2. *Weight Loss due to the Pure Erosion component.*

Experiments, in which the specimen was cathodically protected, and the weight loss of the material after the test was measured, obtained the contribution of the pure erosive component to the total damage. These results are presented in Table 6.9. Once again comparison of the low-velocity results is compromised by the small recorded weight losses relative to the accuracy of the balance, 0.0001g. However, the 86m/s result provides the expected indication of higher erosive losses at higher impinging velocities.

Nozzle Diam.(mm)	Velocity (m/s)	Pure Erosion Weight Loss (mg)	Average Pure Erosion Weight Loss (mg)
4	2.38	0.3 , 0.3	0.30
4	4.5	0.3 , 0.4	0.35
1	4.5	0.3 , 0.3	0.30
1	17	0.2 , 0.2	0.20
1	86	0.5 , 0.5	0.50

Table 6.9. Weight loss values due to the erosion component after 4 hours exposure time.

6.3.1.1.3. *Weight Loss due to the Direct Corrosion component.*

Figure 6.21a. and Figure 6.21b. show the typical anodic polarisation curves generated from tests after 4 hours in 3.5% NaCl solution. Evidently a substantial negative shift in E_{corr}, (to between -278 to –303mV), appeared at all impingement velocities compared to static conditions. There is a much greater difference clearly visible between the anodic polarisation curves at the various velocities than is apparent in the 30 minutes exposure tests, (Figure 6.4a. and Figure 6.4b.).

Table 6.10. gives the corrosion rates after 4 hours as calculated by the Tafel extrapolations, following the correction procedure of plotting in one graph the anodic and cathodic polarisations for each condition, as described in Chapter 5. Although these are quoted as mg/h it has to be recognised that they are instantaneous corrosion rates measured after 4 hours. In order to obtain the total amount of material loss due to direct corrosion for the whole time period of the 4 hours for each velocity, a graph of instantaneous direct corrosion rates vs. time was plotted, for time periods of 30 minutes (from Table 6.12.) and 4 hours (from Table 6.10.), and the area under the graph was the total material loss by corrosion. This approach is described in Chapter 5 as well. Figure 6.22. shows as an example such a graph for 17m/s and the calculated total weight loss by direct corrosion is the sum of the areas A_1, A_2, and A_3.

$$\text{Direct Corrosion Weight Loss} = A_1 + A_2 + A_3 = 0.0047 + 0.0665 + 0.0367 =$$

$$= 0.108 \text{ mg}$$

These results are expressed in mg and they are also included in Table 6.10.

It is quite clear that, as was the case for the 30 minutes results (Table 6.12.), there is a general trend of increasing instantaneous corrosion rate with velocity and for low impinging velocities the direct corrosion rate of Cu-10%Ni is higher when the nozzle diameter of the impinging jet is 4mm than with a 1mm nozzle.

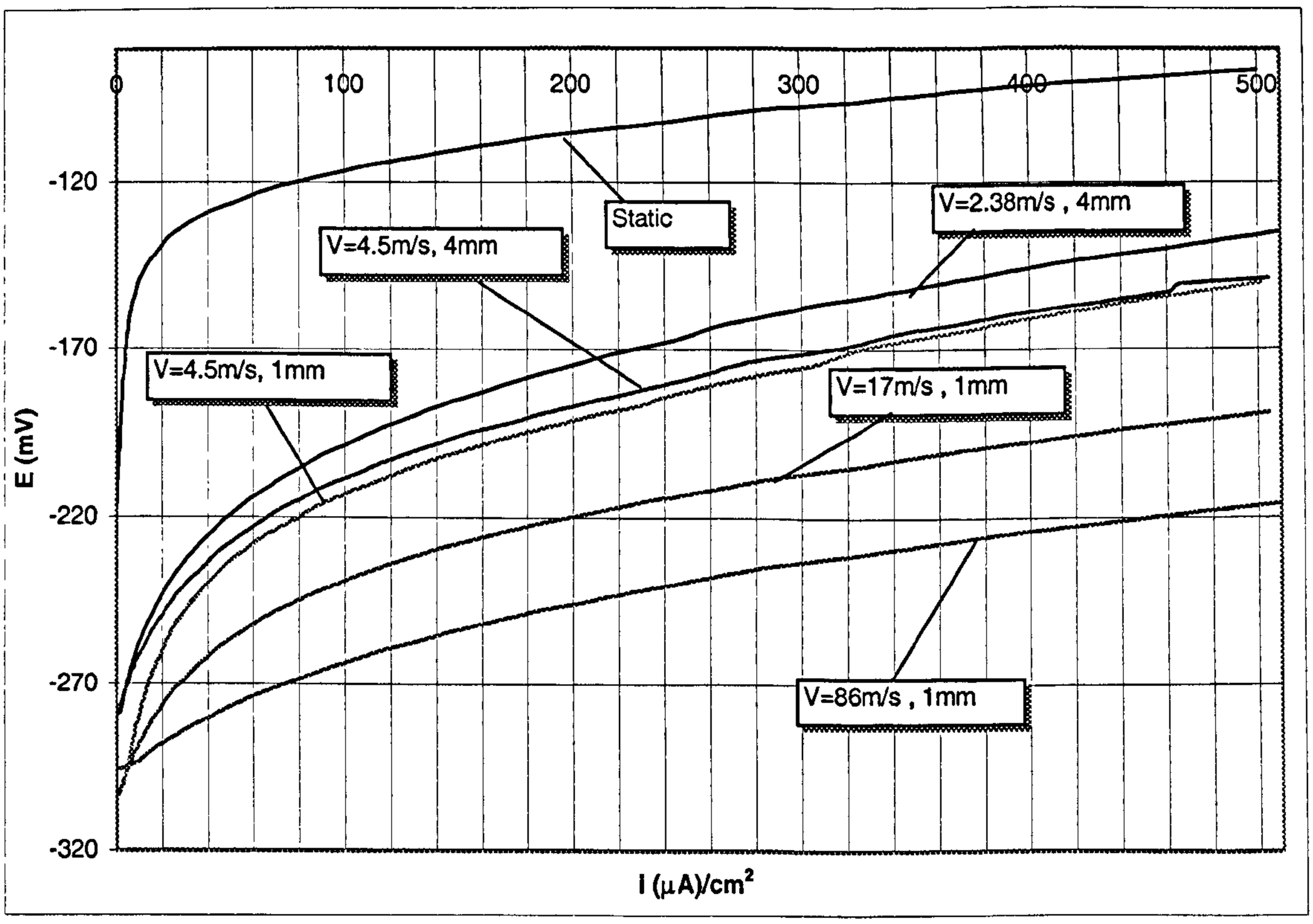

Figure 6.21a. Anodic polarisation tests of Cu-10%Ni upon an initial exposure of 4 hours under the impinging jet.

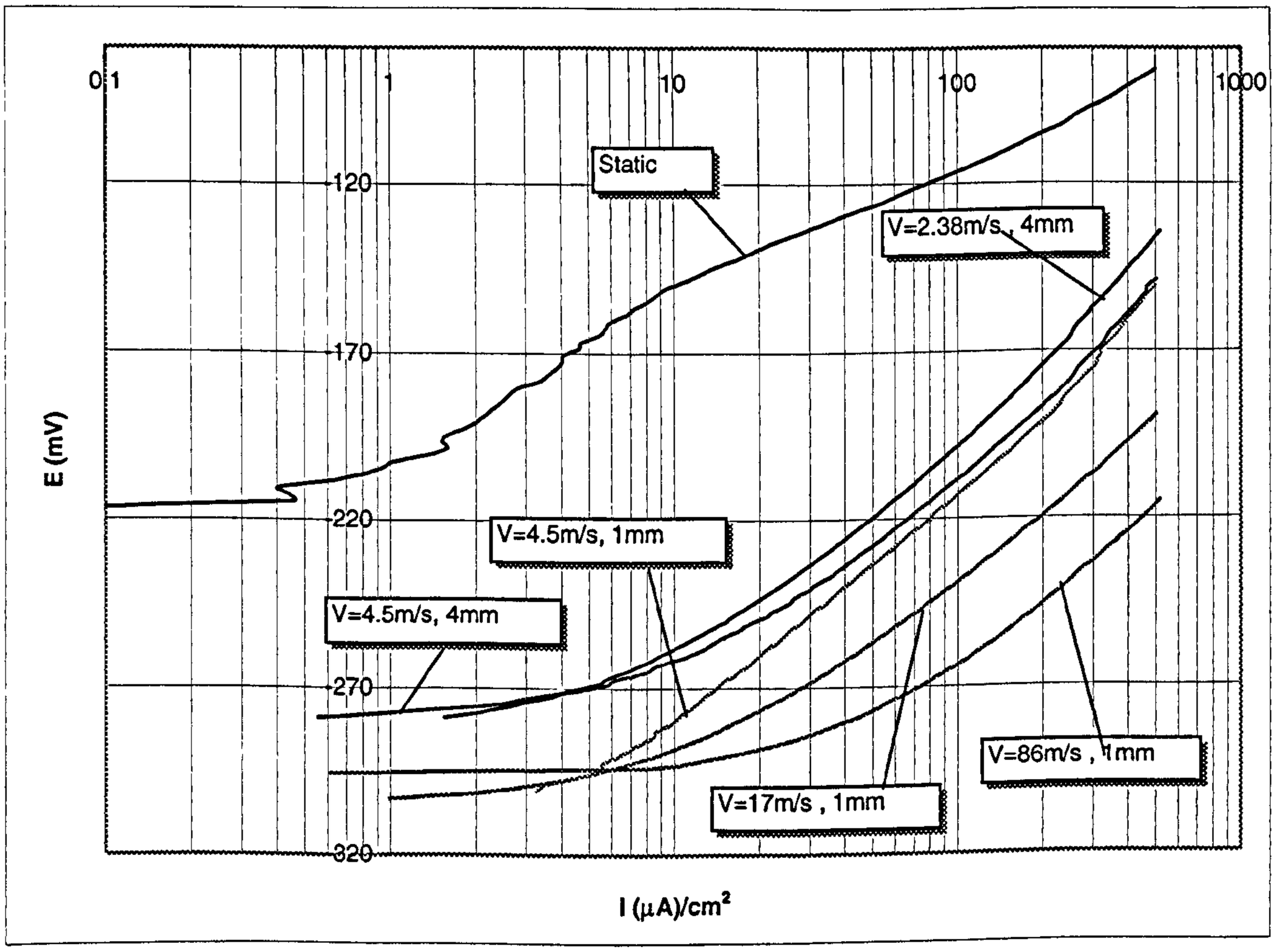

Figure 6.21b. Anodic polarisation tests of Cu-10%Ni upon an initial exposure of 4 hours under the impinging jet.

Nozzle Diam.(mm)	Velocity (m/s)	Direct Corrosion current density ($\mu A/cm^2$)	Direct Corrosion current density ($\mu A/cm^2$) – Average	Instantaneous Direct Corrosion Weight Loss (mg/h)	Direct Corrosion Weight Loss (mg)
Static	0	0.5 , 0.6	0.55	0.003	0.009
4	2.38	9.0 , 8.0	8.50	0.039	0.122
4	4.5	8.5 , 8.5	8.50	0.039	0.126
1	4.5	6.3 , 6.0	6.15	0.029	0.087
1	17	8.0 , 9.5	8.75	0.041	0.108
1	86	33.0 , 34.0	33.50	0.157	0.280

Table 6.10. Weight loss values due to the direct corrosion component after 4 hours erosion corrosion.

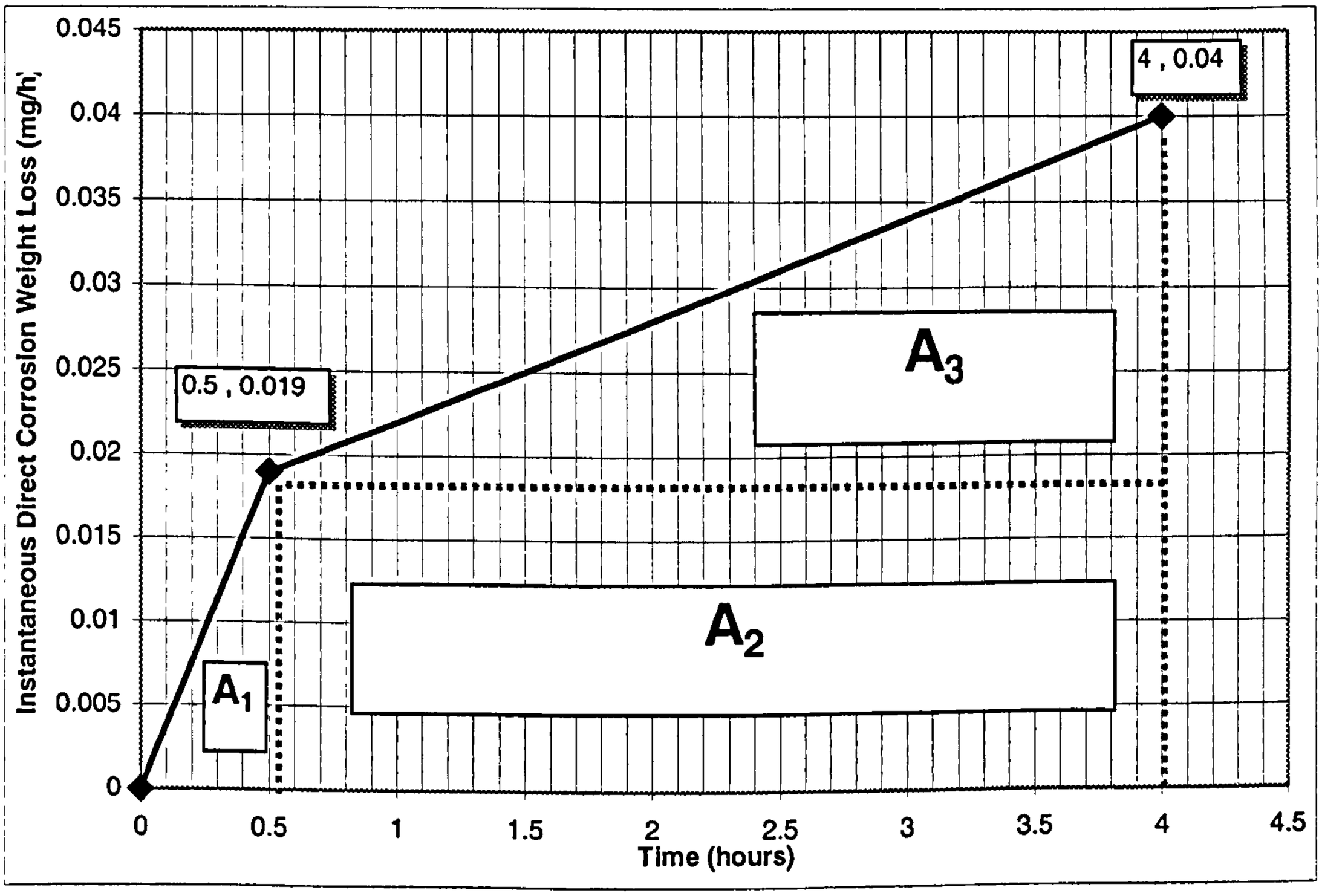

Figure 6.22. Demonstration of the "area under the graph" procedure for an impinging velocity of V=17m/s.

6.3.1.1.4. Remarks on the effect of velocity on erosion corrosion for 4 hours.

Table 6.11. shows the average weight loss values due to erosion, corrosion and indirect corrosion (synergy).

Nozzle Diam.(mm)	Velocity (m/s)	Average Total Weight Loss (mg)	Average Pure Erosion Weight Loss (mg)	Average Pure Corrosion Weight Loss (mg)	Average Synergy (mg)
Static	0	0.01	~	0.01	~
	%		~	100	~
4	2.38	0.65	0.30	0.12	0.23
	%		46	19	35
4	4.5	0.60	0.35	0.13	0.12
	%		58	22	20
1	4.5	0.50	0.30	0.09	0.11
	%		60	18	22
1	17	1.00	0.20	0.11	0.69
	%		20	11	69
1	86	2.20	0.50	0.28	1.42
	%		23	13	64

Table 6.11. Weight loss values due to erosion, corrosion and indirect corrosion (synergy) effect, after 4 hours exposure time.

As mentioned earlier, some of the weight losses are rather near to the weighing sensitivity. However, what is quite evident is the complexity of the erosion corrosion process on this alloy in that the material loss involves significant contributions from pure erosion, pure corrosion and synergy. A particular interesting feature is that, at the higher velocities of 17m/s and 86m/s, it is not the pure erosive component that increases substantially but rather the combined corrosion-induced erosion (i.e. synergy).

6.3.1.2. *Effect of time on erosion corrosion.*

The effect of time was studied mainly by focusing on the velocity of 17m/s, (with the 1mm nozzle) and undertaking experiments for 4, 8, 48 and 72 hours. Additionally a limited study, involving experiments for 4 and 8 hours, was carried out at a velocity of 86 m/s, (with the 1mm nozzle).

6.3.1.2.1. Total Weight Loss.

Table 6.12. shows the total weight loss/exposure time data. It is quite clear that for exposure time periods of 4 and 8 hours, the measured total weight loss of the Cu-10%Ni specimens is lower when the impinging velocity is 17m/s, rather than 86m/s.

Obviously the results state that at both velocities, an increased exposure time period resulted in an increased total weight loss. The rate of material loss appears to be at a constant up to 8 hours but falls somewhat thereafter.

Time (hours)	Velocity (m/s)	Total Weight Loss (mg)	Average Total Weight Loss (mg)
4	17	0.9 , 1.1	1.00
8	17	2.0 , 2.2	2.10
48	17	8.5 , 9.1	8.80
4	86	2.0 , 2.4	2.20
8	86	4.4 , 4.8	4.60

Table 6.12. Total weight loss/exposure time data.

6.3.1.2.2. Weight Loss due to the Pure Erosion component.

Experiments, in which the specimen was subject to cathodic protection, obtained the contribution of the pure erosive component to the total damage. These results are presented in Table 6.13. Again the weight loss is greater at the higher velocities.

Time (hours)	Velocity (m/s)	Pure Erosion Weight Loss (mg)	Average Pure Erosion Weight Loss (mg)
4	17	0.2 , 0.2	0.20
8	17	0.4 , 0.4	0.40
48	17	0.7 , 0.8	0.75
4	86	0.5 , 0.5	0.50
8	86	0.7 , 0.8	0.75

Table 6.13. Weight loss values due to the erosion component.

6.3.1.2.3. Weight Loss due to the Direct Corrosion component.

Figure 6.23a-b. and Figure 6.24a-b. show typical anodic and cathodic polarisation curves respectively after the various time periods. The detailed trends in the polarisation curves will be discussed in Chapter 9; for the moment their use is to facilitate determination of corrosion rates via the Tafel extrapolation method. The instantaneous corrosion rates expressed in mg/h as calculated by the Tafel extrapolation method, and the direct corrosion weight losses expressed in mg as obtained by the "area under the graph" method, are shown in Table 6.14. The direct corrosion rate clearly increases with velocity. The time dependence of the instant corrosion rate in not completely evident. This matter is considered further in section 6.3.1.2.5.

Time (hours)	Velocity (m/s)	Direct Corrosion current density ($\mu A/cm^2$)	Direct Corrosion current density ($\mu A/cm^2$) – Average	Instantaneous Direct Corrosion Weight Loss (mg/h)	Direct Corrosion Weight Loss (mg)
4	17	8.0 , 9.5	8.75	0.041	0.11
8	17	8.5 , 7.8	8.15	0.038	0.27
48	17	16.0 , 19.0	17.5	0.082	2.71
72	17	14.5 , 13.5	14.0	0.066	4.49
4	86	33.0 , 34.0	33.5	0.157	0.28
8	86	53.0 , 54.0	53.5	0.251	1.09

Table 6.14. Weight loss values due to the direct corrosion component.

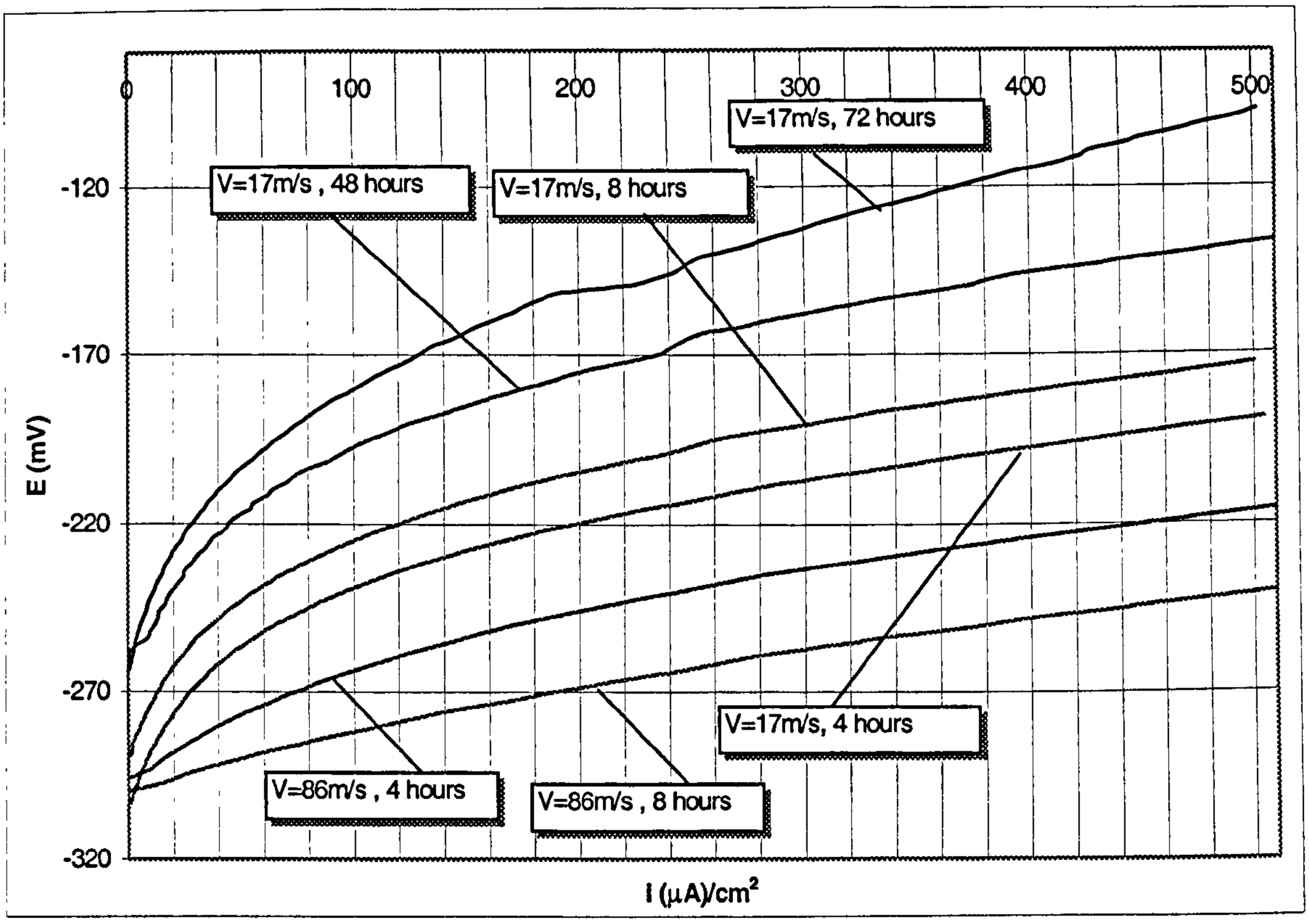

Figure 6.23a. Anodic polarisation curves of Cu-10%Ni upon exposures of 4, 8, 48 and 72 hours under impinging velocities of 17m/s and 86m/s.

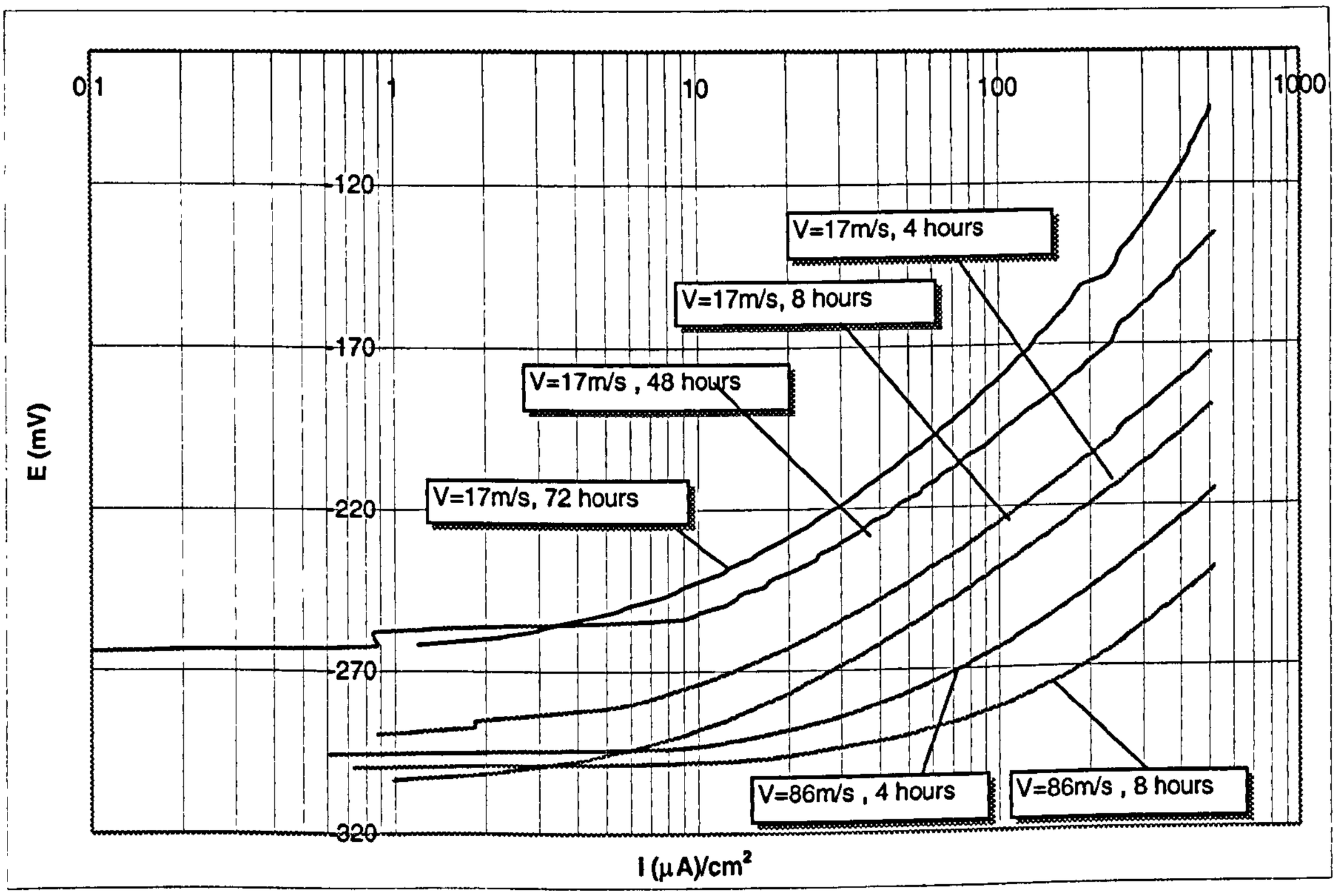

Figure 6.23b. Anodic polarisation curves of Cu-10%Ni upon exposures of 4, 8, 48 and 72 hours under impinging velocities of 17m/s and 86m/s.

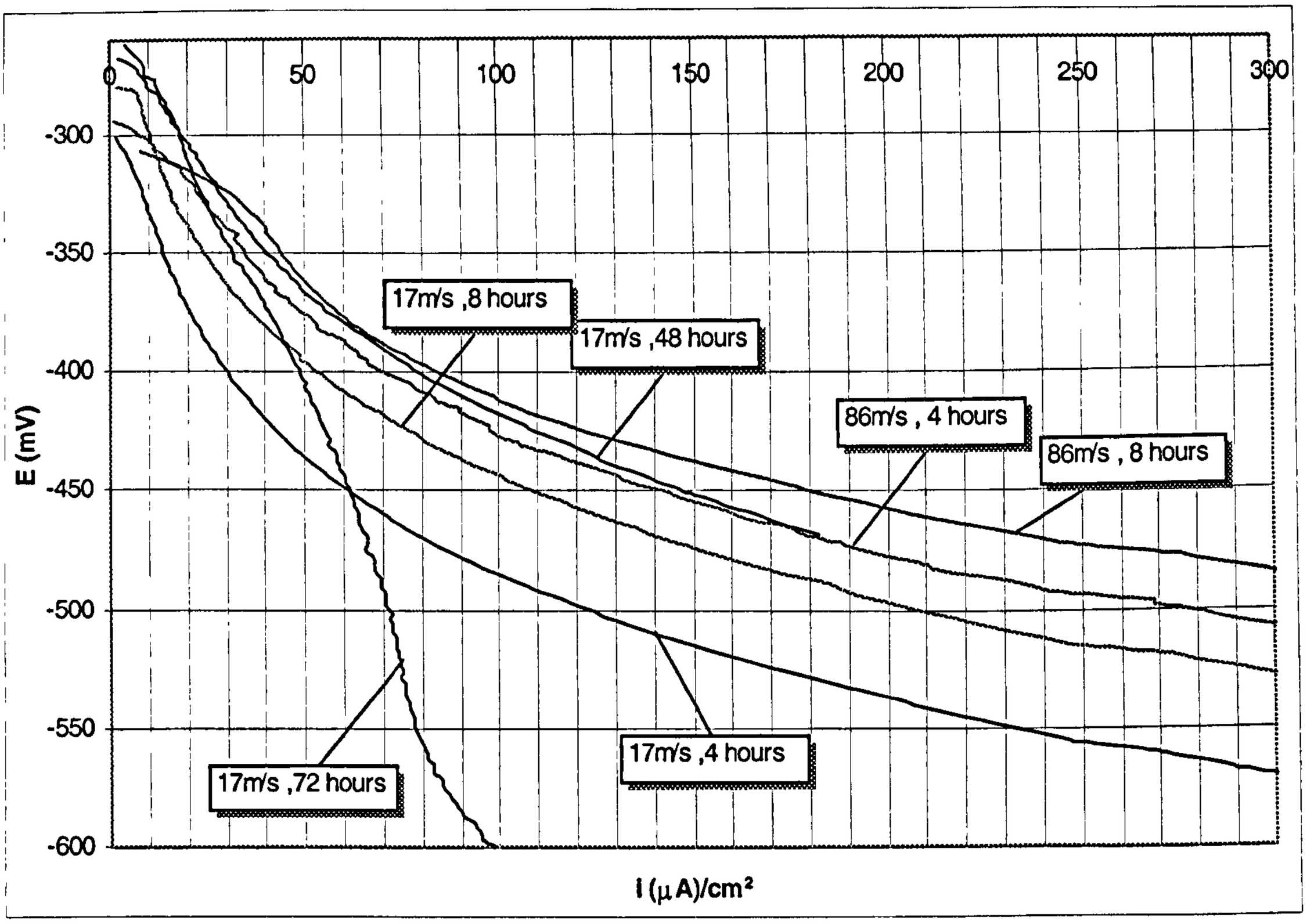

Figure 6.24a. Cathodic polarisation curves of Cu-10%Ni upon exposures of 4, 8, 48 and 72 hours under impinging velocities of 17m/s and 86m/s.

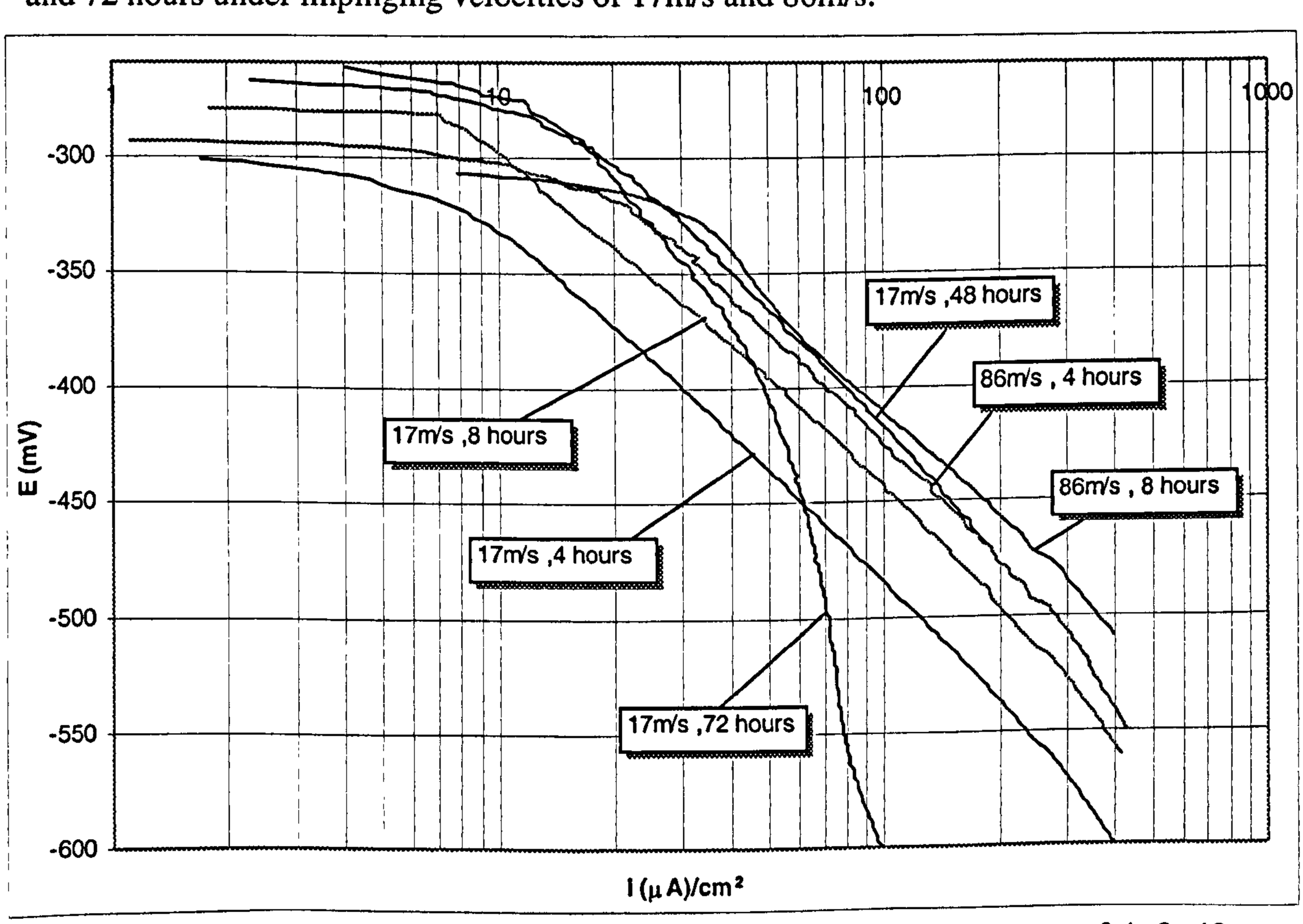

Figure 6.24b. Cathodic polarisation curves of Cu-10%Ni upon exposures of 4, 8, 48 and 72 hours under impinging velocities of 17m/s and 86m/s.

6.3.1.2.4. Remarks on the effect of time on erosion-corrosion process.

Table 6.15. shows the weight loss values due to erosion, corrosion and indirect corrosion (synergy).

Time (hours)	Velocity (m/s)	Average Total Weight Loss (mg)	Average Pure Erosion Weight Loss (mg)	Average Direct Corrosion Weight Loss (mg)	Average Synergy (mg)
4	17	1.00	0.20	0.11	0.69
	%		20	11	69
8	17	2.10	0.40	0.27	1.43
	%		19	13	68
48	17	8.80	0.75	2.71	5.34
	%		9	31	60
4	86	2.20	0.50	0.28	1.42
	%		23	13	64
8	86	4.60	0.75	1.09	2.76
	%		16	24	60

Table 6.15. Weight loss values due to erosion, corrosion and indirect corrosion (synergy) effect.

Perhaps the most interesting feature is that, for both velocities and all times, the dominant contributor to overall erosion-corrosion material loss is the synergy whose values are remarkably similar in the range 60-69%. There is also a noticeable decrease in the percentage contribution from pure erosion with increasing time.

6.3.1.2.5. Linear polarisation type tests.

In order to obtain more data to assist in the evaluation of trends in corrosion rate with time, one experiment was carried out at 17 m/s, in which a series of linear polarisation type monitoring exercises was undertaken at times of 30 min, 2, 4, 8, 16, 24, 32, 48, and 72 hours. This involved undertaking a short (22mV) anodic polarisation scan and calculating the gradient of the potential/current density plot, to yield a value for the polarisation resistance $R_p^{'}$. Figure 6.25a. and Figure 6.25b. show the duplicate resulting anodic polarisation curves.

Table 6.16. shows the average values of E_{corr}, $R_p^{'}$ and $1/R_p^{'}$ for Cu-10%Ni at different time exposures, for an increase by 22mV to the value of E_{corr}. According to the results the value of E_{corr} shifts continuously in the positive direction for Cu-10%Ni, whereas the time dependence of corrosion rate appears to be more complex.

Figure 6.26a. presents the $1/R_p^{'}$ values versus time plots, and Figure 6.26b. presents the $1/R_p^{'}$ average values versus time plots. It is interesting to note that the comparative values of $1/R_p^{'}$ follow the same relative trends with time as exhibited by the corrosion rates obtained by Tafel extrapolation from full anodic polarisation experiments, (Table 6.14.)

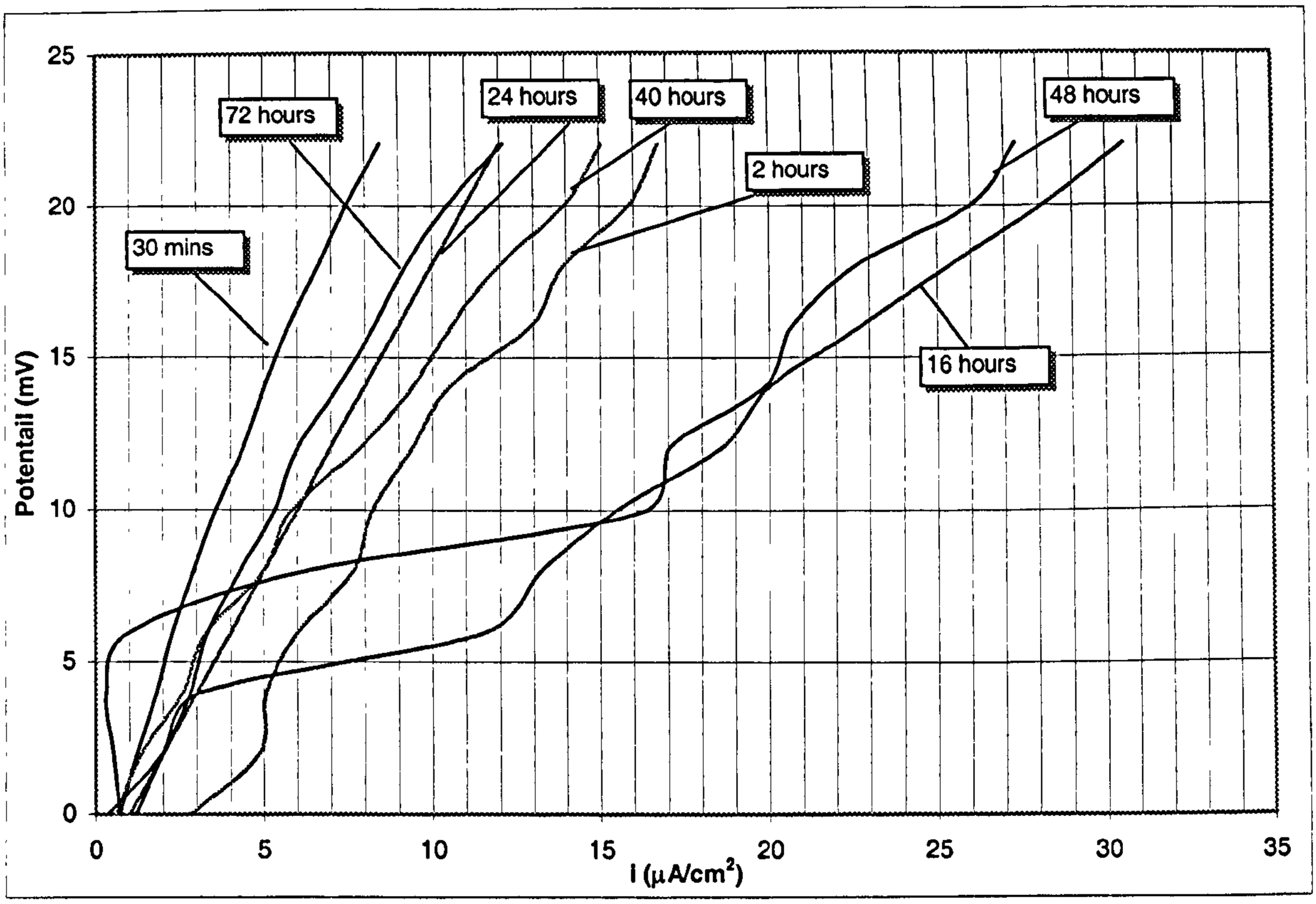

Figure 6.25a. Anodic polarisation curves of the specimen of Cu-10%Ni, for an increase by 22mV to the value of E_{corr}, upon exposures of 30mins, 2, 16, 24, 48 and 72 hours under impingement velocity of 17 m/s.

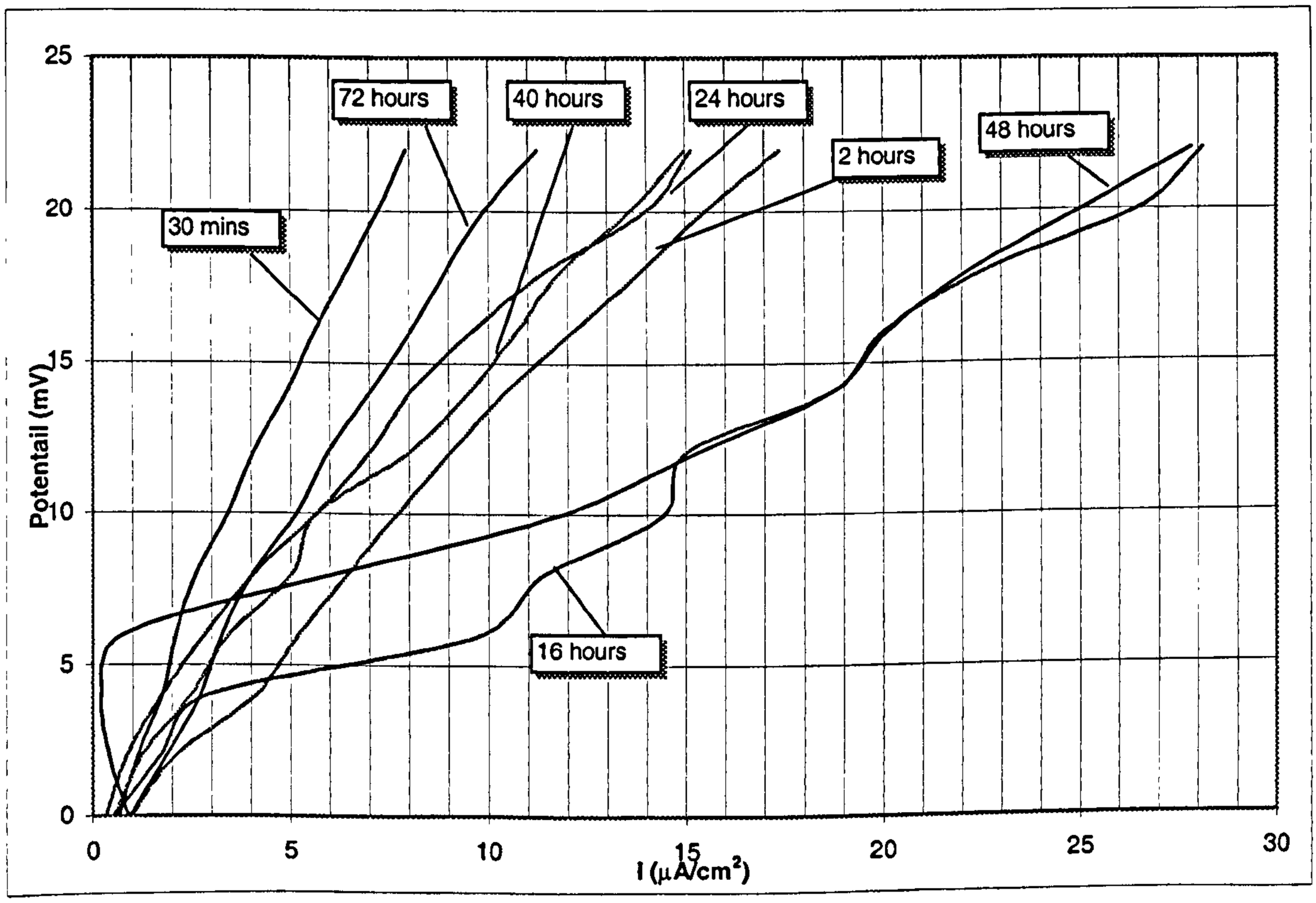

Figure 6.25b. Anodic polarisation curves of the specimen of Cu-10%Ni, for an increase by 22mV to the value of E_{corr}, upon exposures of 30mins, 2, 16, 24, 48 and 72 hours under impingement velocity of 17 m/s.

Time (hours)	Average E_{corr} (mV)	Average $R_p^{'}$ *(KOhm*cm²)*	Average $1/R_p^{'}$ *(1/(KOhm*cm²))*
½	-306.130	2.849	0.351
2	-304.921	1.576	0.634
4	-303.258	1.460	0.684
8	-289.127	1.410	0.709
16	-286.569	0.698	1.432
24	-284.470	1.563	0.639
40	-274.460	1.445	0.692
48	-264.733	0.652	1.533
72	-260.432	2.059	0.485

Table 6.16. The average values of E_{corr}, $R_p^{'}$, $1/R_p^{'}$ for Cu-10%Ni at different time exposures, for an increase by 22mV to the value of E_{corr}.

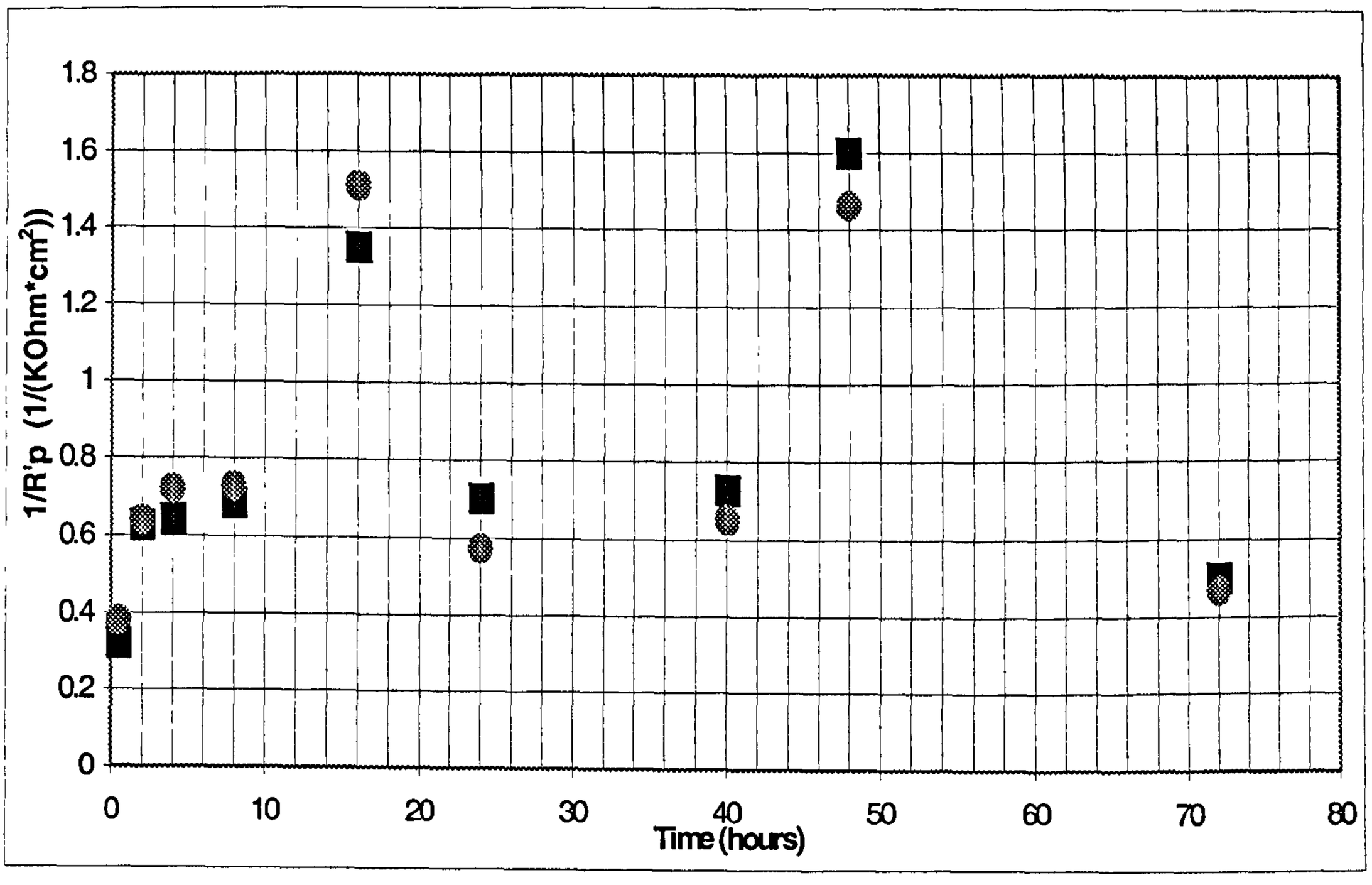

Figure 6.26a. $1/R_p'$ values vs. Time curve for the specimen of Cu-10%Ni under impingement velocity of 17 m/s.

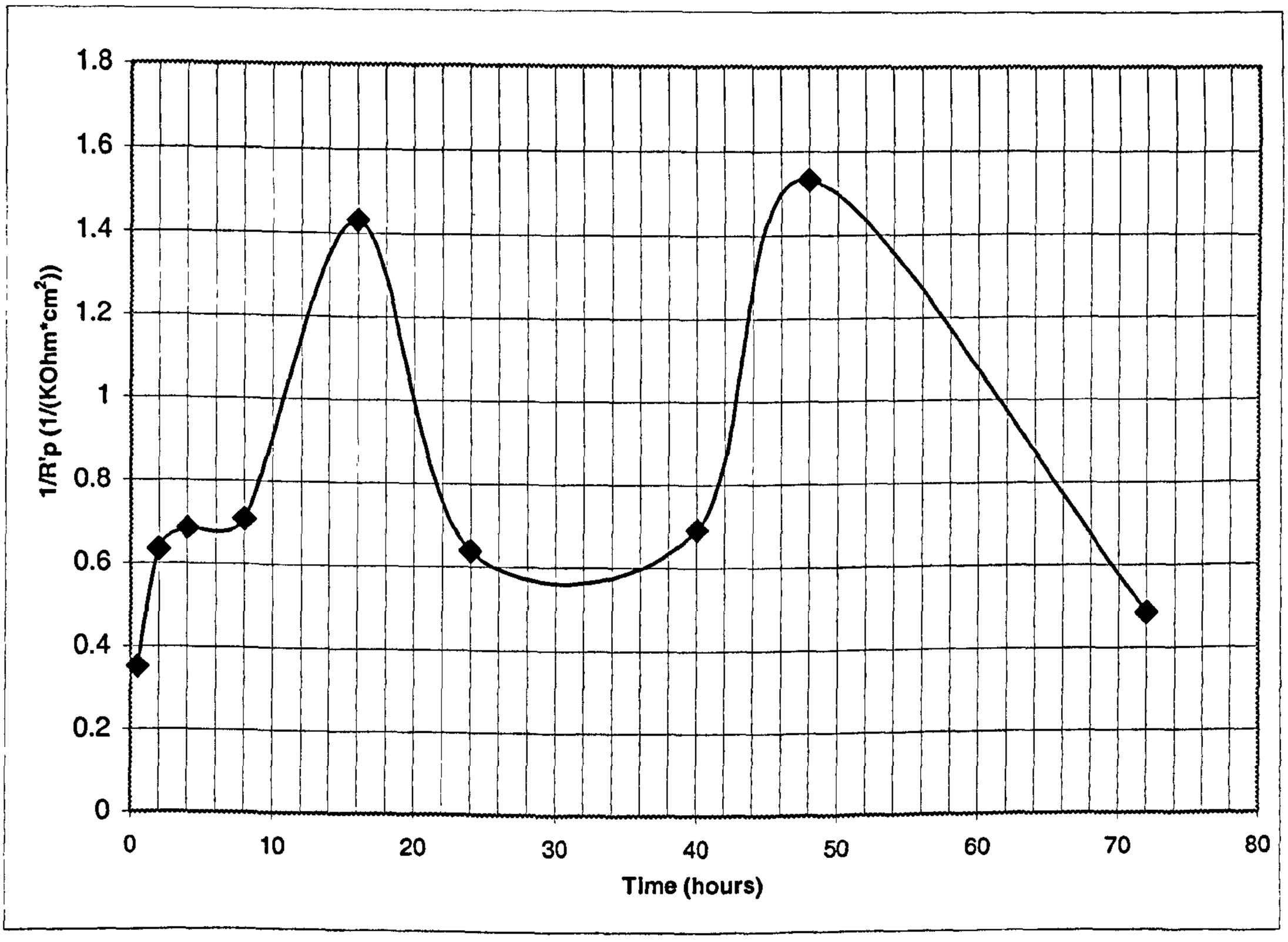

Figure 6.26b. $1/R_p'$ average values vs. Time curve specimen of Cu-10%Ni under impingement velocity of 17 m/sec.

6.3.1.3. *Microscopical examination.*

6.3.1.3.1. <u>As-received and polished specimen.</u>

Analysis done on an as-received and polished specimen showed the typical and expected chemical analysis for Cu-10%Ni alloy. The analysis demonstrating this more clearly was:

Cu - %	Ni - %
86.8	11.8

Table 6.17. Typical chemical analysis of an as-received and polished specimen.

6.3.1.3.2. <u>Low Impinging Velocities (2.38m/s, 4.5m/s).</u>

Specimens exposed to erosion-corrosion conditions without any electrochemical intervention, (relevant photographs labelled "T.W.L.").

For both these velocities there was no evidence to the unaided eye of different zones of attack on the specimen surfaces.

At the velocity of 2.38 m/s after a 4-hour exposure, the surface under the jet was covered with a patchy film with yellow-gold patches, Figure 6.27. In the outer regions the metal grain structure showed up, Figure 6.28., but only faintly – implying mild attack and similar features were barely visible in the directly impinged zone. Also there was evidence of shallow pitting over the entire surface. It has to be noted that the velocity of 2.38m/s is less than the critical velocity, (3-4m/s), normally quoted for Cu-10%Ni.

At 4.5 m/s with a 4mm nozzle, the entire surface was covered with a light yellow film. There was some evidence of some shallow pitting under the jet, Figure 6.29.

At 4.5 m/s with a 1mm nozzle, a bright yellow film covered the centre of the specimen and a brown yellow film covered the outside. Numerous shallow pits appeared

just under the jet, Figure 6.30, but otherwise there was no evidence of severe damage to the metal.

The photographic evidence gives evidence that a visible film forms, (even if it is discontinuous and pitted) in just 4 hours under impingement conditions.

Specimens subjected to continuous cathodic protection, (relevant photographs labelled "C.P.").

At 2.38 m/s, there is no evidence of any corrosion attack.

At 4.5m/s with a 4mm nozzle the very slight evidence of the grain structure confirmed some slight corrosion attack even when implying Cathodic Protection, but the duplicate specimens recorded small measurable weight losses, (Table 6.9).

At 4.5m/s with a 1mm nozzle a light yellow film covered the surface. At high magnification some pits were revealed under the jet, but not elsewhere.

Specimens subjected to erosion-corrosion with final anodic polarisation, (relevant photographs labelled "A.P.").

At 2.38m/s the whole surface was covered with a yellow-red film.

At 4.5m/s with a 4mm nozzle a light yellow film covered the surface, but no hydrodynamics effects were appeared.

At 4.5m/s with a 1mm nozzle the anodic polarisation revealed some zones of coloured film. The colour of the centre was red-black, the intermediate was green, and the outside zone was yellow. The centre and the intermediate zones were subjected to quite significant general attack, as demonstrated by Figure 6.31., but the corrosion attack was much less severe at the outside zone, Figure 6.32.

6.3.1.3.3. High Impinging Velocities (17m/s, 86m/s).

V = 17m/s, Exposure time = 4 hours.

Specimens exposed to erosion-corrosion conditions without any electrochemical intervention.

The surface under the microscope displayed some clear hydrodynamics zones. The central, (i.e. directly-impinged), region is shown at low and high magnification in Figures 6.33. and Figure 6.34., respectively. A red ring appeared at the outside zone, which can be seen better on Figure 6.35. The central region shows some large pits but no general corrosion, whereas the rest of the specimen shows general corrosion. Figure 6.36, shows the outside zone with a structure typical of an etched specimen which implies general corrosion with possible accentuation of attack at the grain boundaries. It seems that the damage is more severe in the outer region of the specimen except for the pits, which appear under the jet. The roughness value for the entire surface was R_a=0.06μm, while for an as-received polished specimen was R_a= 0.02μm.

Specimens subjected to continuous cathodic protection.

There is an evidence of a thin film on the specimen's surface, through which the bright metal surface can be seen when the film is scratched, Figure 6.37.

Specimens subjected to erosion-corrosion with final anodic polarisation.

The revealed structure, after the anodic polarisation, was not much different for the specimen after erosion-corrosion. In general the entire surface was etched and pits under the jet were also observed.

V = 17m/s, Exposure time = 8 hours.

Specimens exposed to erosion-corrosion conditions without any electrochemical intervention.

There was no evidence of any hydrodynamic effect. The etched structure with some pits was evident over the entire surface of the specimen, Figure 6.38.

Specimens subjected to continuous cathodic protection.

Figure 6.39. shows a thin red black film over the entire surface, with no evidence of corrosion attack.

Specimens subjected to erosion-corrosion with final anodic polarisation.

An etched structure covered the entire surface.

V = 17m/s, Exposure time = 48 hours.

Specimens exposed to erosion-corrosion conditions without any electrochemical intervention.

The etched appearance was obvious for the whole surface, Figure 6.40. and a surface profile showed a uniform condition of the entire surface as demonstrated in Figure 6.41. The roughness value for the entire surface was R_a=0.35 μm. Also the specimen was mounted in cross-section, but there was no evidence of intergranular attack revealed by this examination.

Specimens subjected to continuous cathodic protection.

There was no evidence of any corrosion attack. There was some minor pitting under the jet but the general appearance was similar to that of the 4-hour cathodic protection sample.

Specimens subjected to erosion-corrosion with final anodic polarisation.

An etched structure covered the entire surface.

V = 86m/s, Exposure time = 4 hours.

Specimens exposed to erosion-corrosion conditions without any electrochemical intervention.

The surface under the microscope displayed some clear hydrodynamics zones. Figure 6.42. shows extensive pitting under the jet and the etched structure, which showed up everywhere. Figure 6.43. confirms that similar grain structure with a few pits, was shown even at the outer region of the specimen. The surface profile (Figure 6.44) shows clear evidence of surface roughing in the 1mm nozzle directly under the 1mm jet, with R_a=0.25 μm, but also reveals that the pits at the outer region, (evident in Figure 6.42) do not penetrate to an appreciable depth, R_a=0.04 μm.

Specimens subjected to continuous cathodic protection.

No evidence of any corrosion attack appeared, only significant pitting under the jet, Figure 6.45. but the Talysurf profile, Figure 6.46, shows negligible roughening, with a Roughness value, R_a=0.03μm.

Specimens subjected to erosion-corrosion with final anodic polarisation.

These specimens showed rather similar structures to these after normal erosion-corrosion.

V = 86m/s, Exposure time = 8 hours.

Specimens exposed to erosion-corrosion conditions without any electrochemical intervention.

The surface under the microscope displayed more extensive pitting under the jet than for 4 hours, Figure 6.47., but the grain structure with a few pits, Figure 6.48., was revealed even at the outer region of the specimen. The surface profile exhibited, (Figure 6.49.), significantly rougher surface than after 4 hours with a roughness value in the central, (directly-impinged zone), of R_a=1.83μm. An interesting feature was the appearance of a second eroded zone, about 4.5mm from the centre, with a roughness value of R_a=0.67μm.

Specimens subjected to continuous cathodic protection.

Like for the 4-hour sample, there was no evidence of any corrosion attack. The surface under the microscope displayed some clear hydrodynamics zones, which can just be detected in the Talysurf profile in Figure 6.50. This trend is also evident on Figure 6.51., (which shows the directly-impinged zone) and Figure 6.52., (which reveals the extensive pitted directly-impinged zone on the right, R_a=0.07μm, then an unattacked band with a further ring of pits further out from the centre, R_a=0.05μm). Despite the apparently spectacular appearance of the pitted regions in the photographs, the surface profile, Figure 6.50., demonstrates that the pits were of negligible depths.

Specimens subjected to erosion-corrosion with anodic polarisation.

Figure 6.53. shows severe pitting under the jet and the etched structure, which showed up everywhere, even at the outer region of the specimen, Figure 6.54.

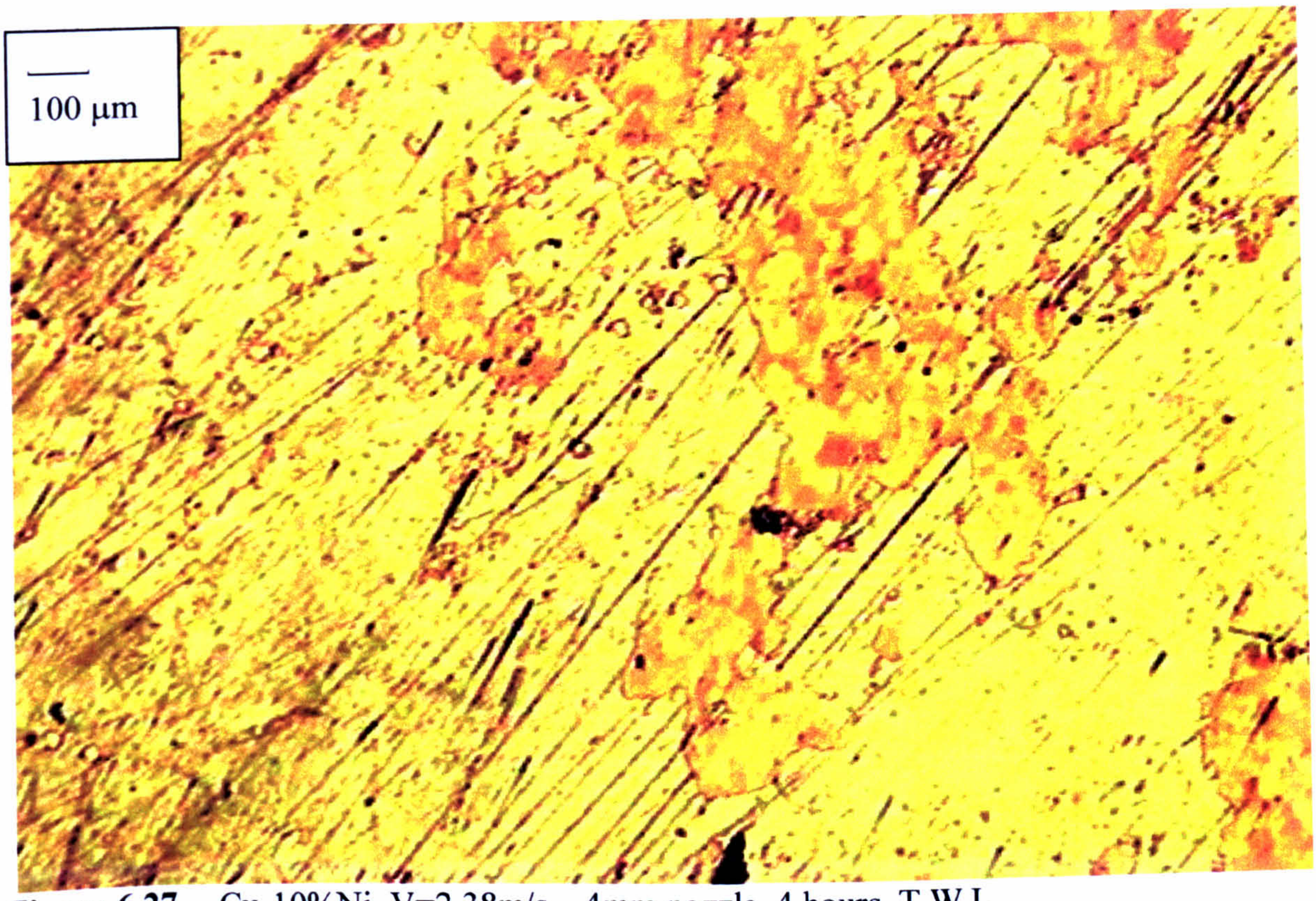

Figure 6.27. Cu-10%Ni, V=2.38m/s – 4mm nozzle, 4 hours, T.W.L.
A patchy film with yellow-gold patches direct under the jet.

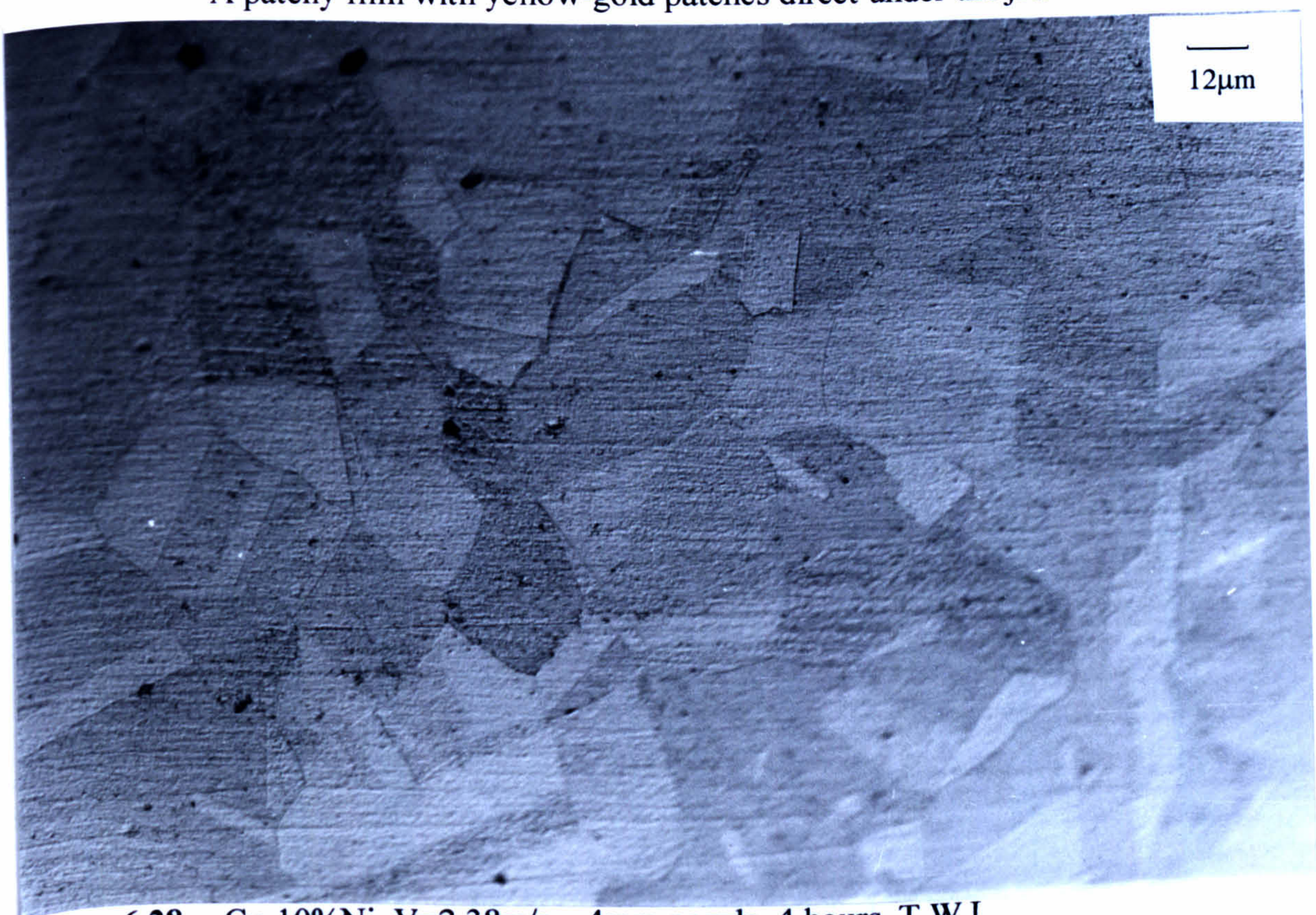

Figure 6.28. Cu-10%Ni, V=2.38m/s – 4mm nozzle, 4 hours, T.W.L.
The metal grain structure showed up faintly, in the outer regions.

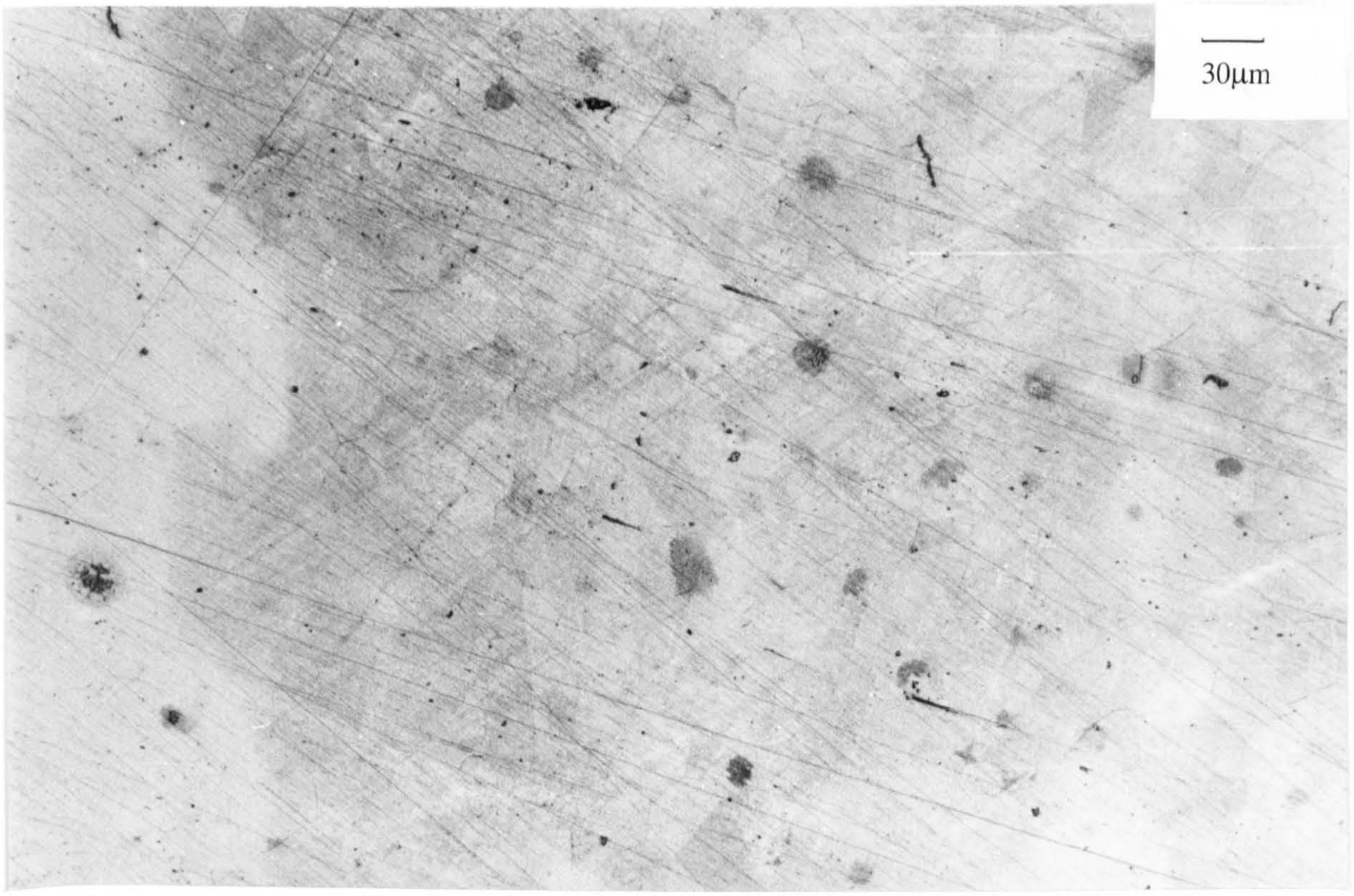

Figure 6.29. Cu-10%Ni, V=4.5m/s – 4mm nozzle, 4 hours, T.W.L.
The entire surface was covered with a light yellow film.

Figure 6.30. Cu-10%Ni, V=4.5m/s – 1mm nozzle, 4 hours, T.W.L.
Numerous shallow pits appeared just under the jet.

Figure 6.31. Cu-10%Ni, V=4.5m/s – 1mm nozzle, 4 hours, A.P.
General attack at the centre and the intermediate zone.

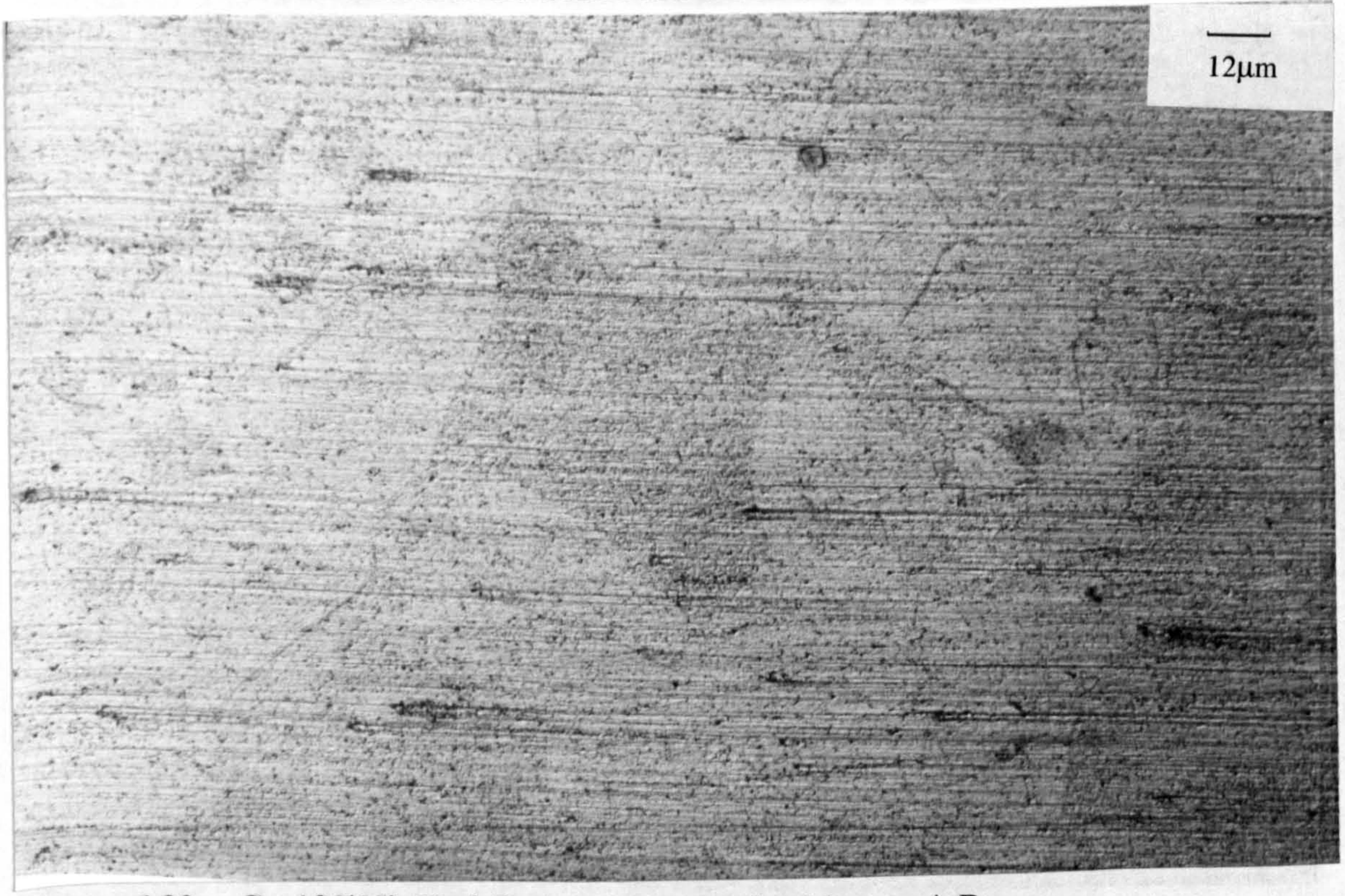

Figure 6.32. Cu-10%Ni, V=4.5m/s – 1mm nozzle, 4 hours, A.P.
Less severe corrosion at the outside region.

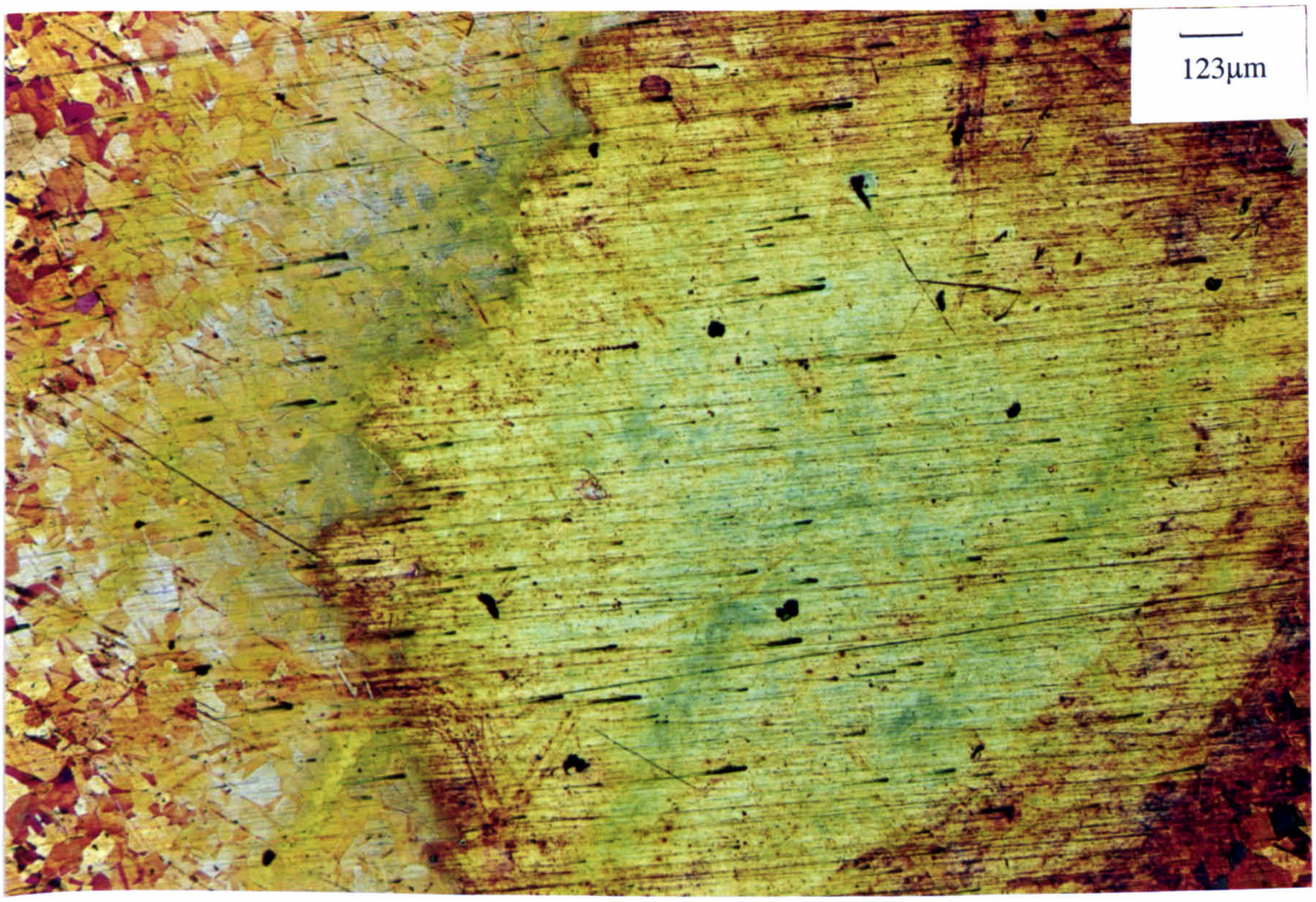

Figure 6.33. Cu-10%Ni, V=17m/s, 4 hours, T.W.L.
Low magnification of the directly-impinged region.

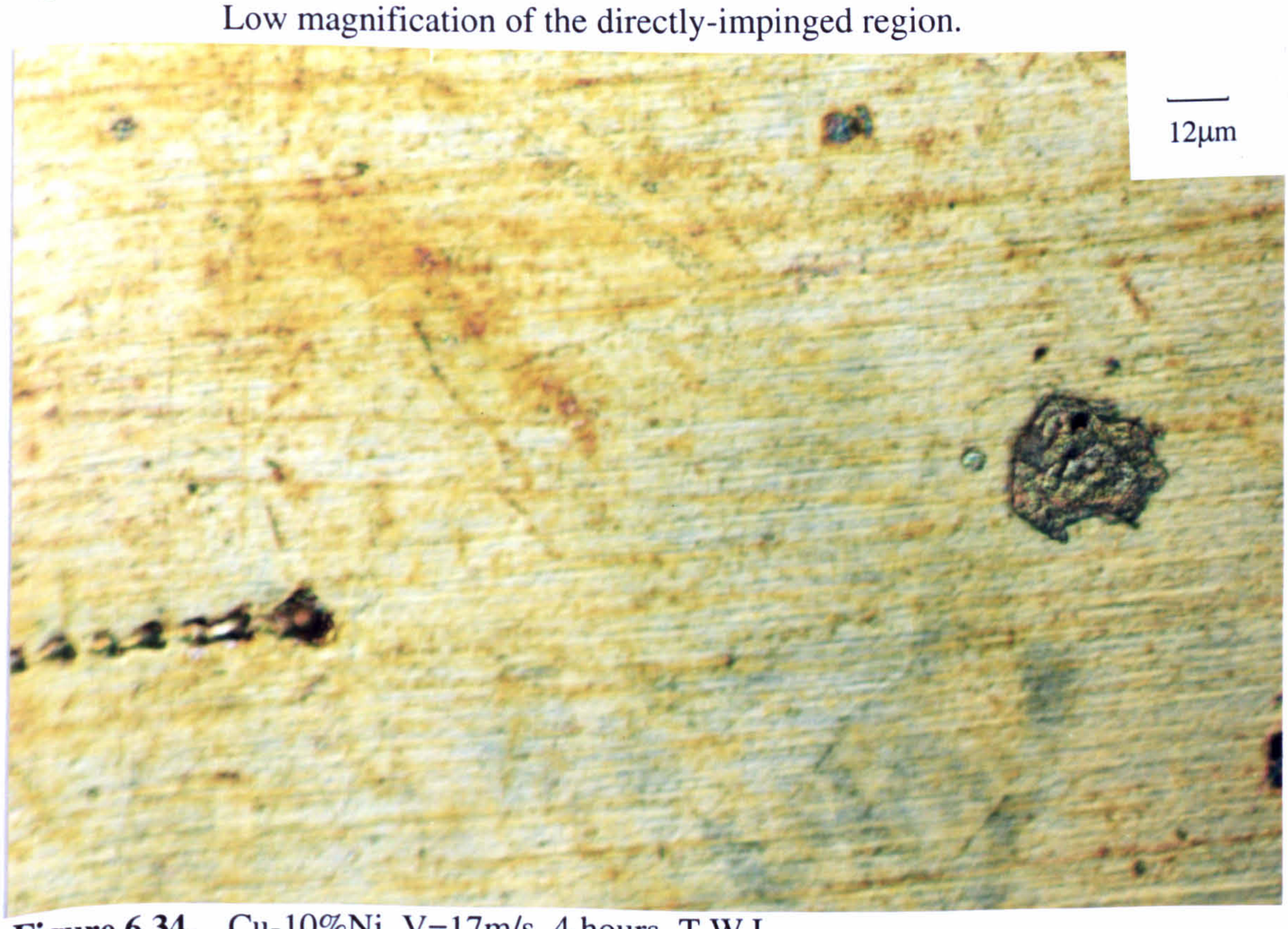

Figure 6.34. Cu-10%Ni, V=17m/s, 4 hours, T.W.L.
High magnification of the directly-impinged region.

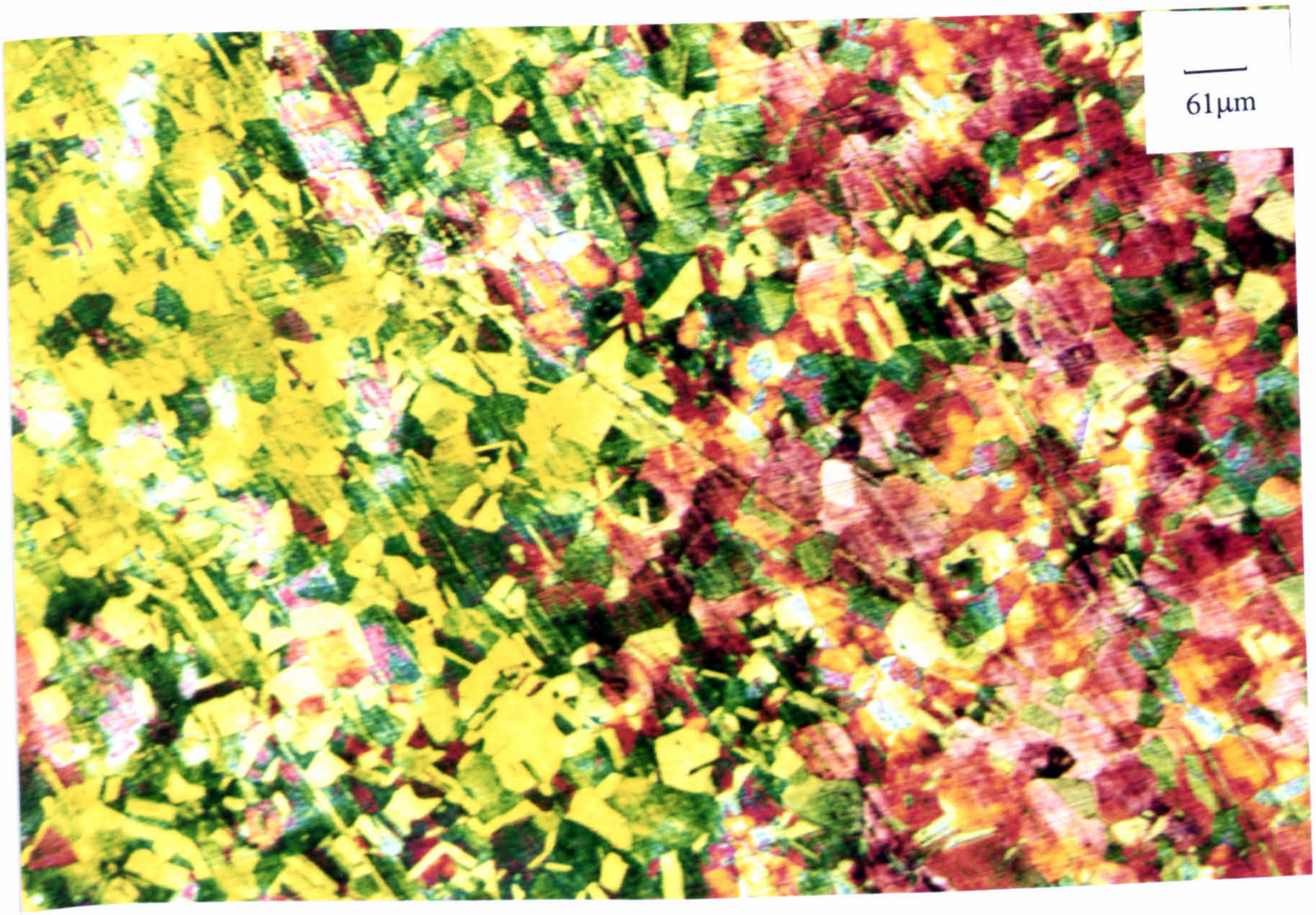

Figure 6.35. Cu-10%Ni, V=17m/s, 4 hours, T.W.L.
A red ring appeared at the outside zone.

Figure 6.36. Cu-10%Ni, V=17m/s, 4 hours, T.W.L.
The etched structure at the outside zone–(green colour at the above photo).

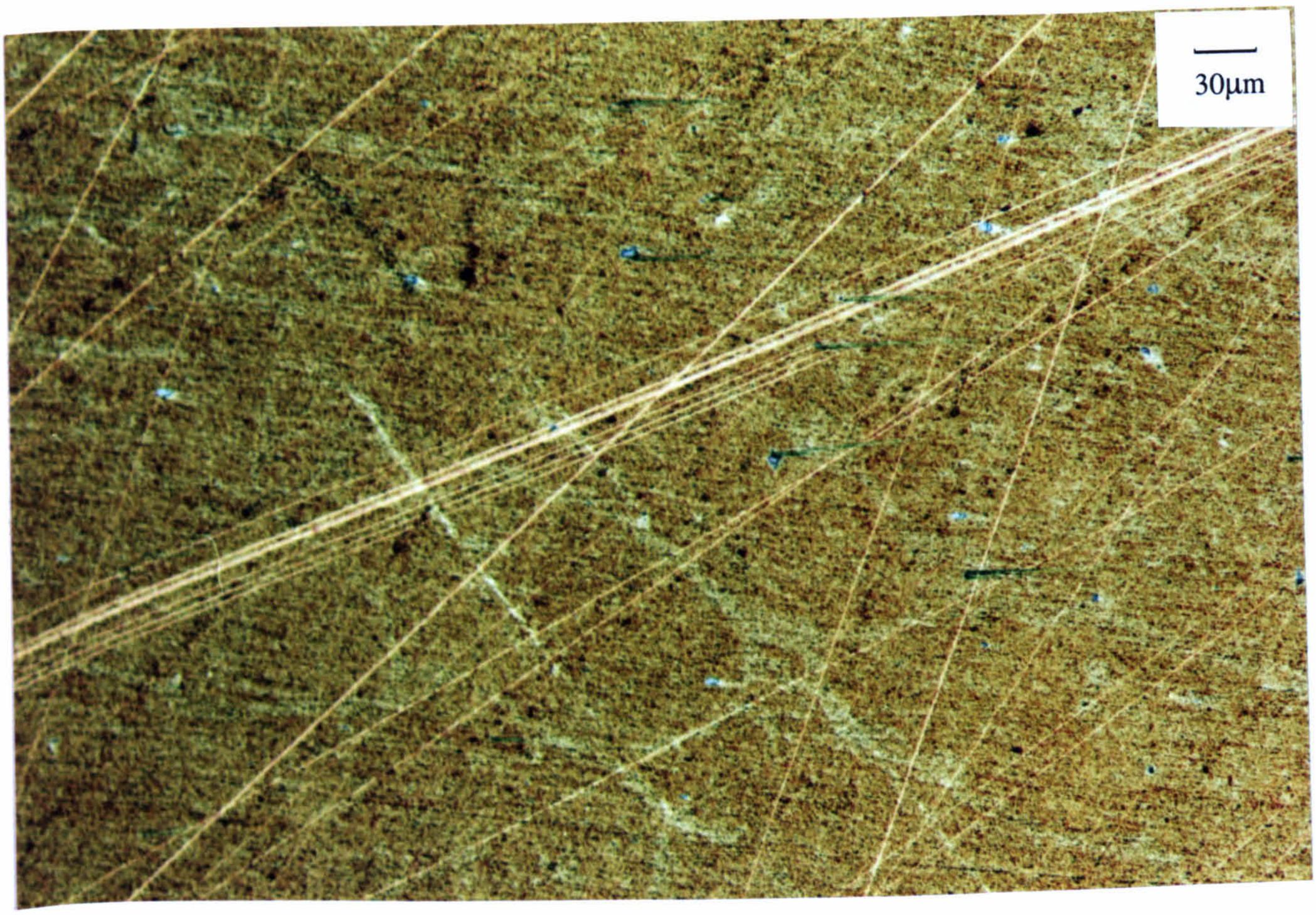

Figure 6.37. Cu-10%Ni, V=17m/s, 4 hours, C.P.
A thin film covered the whole surface.

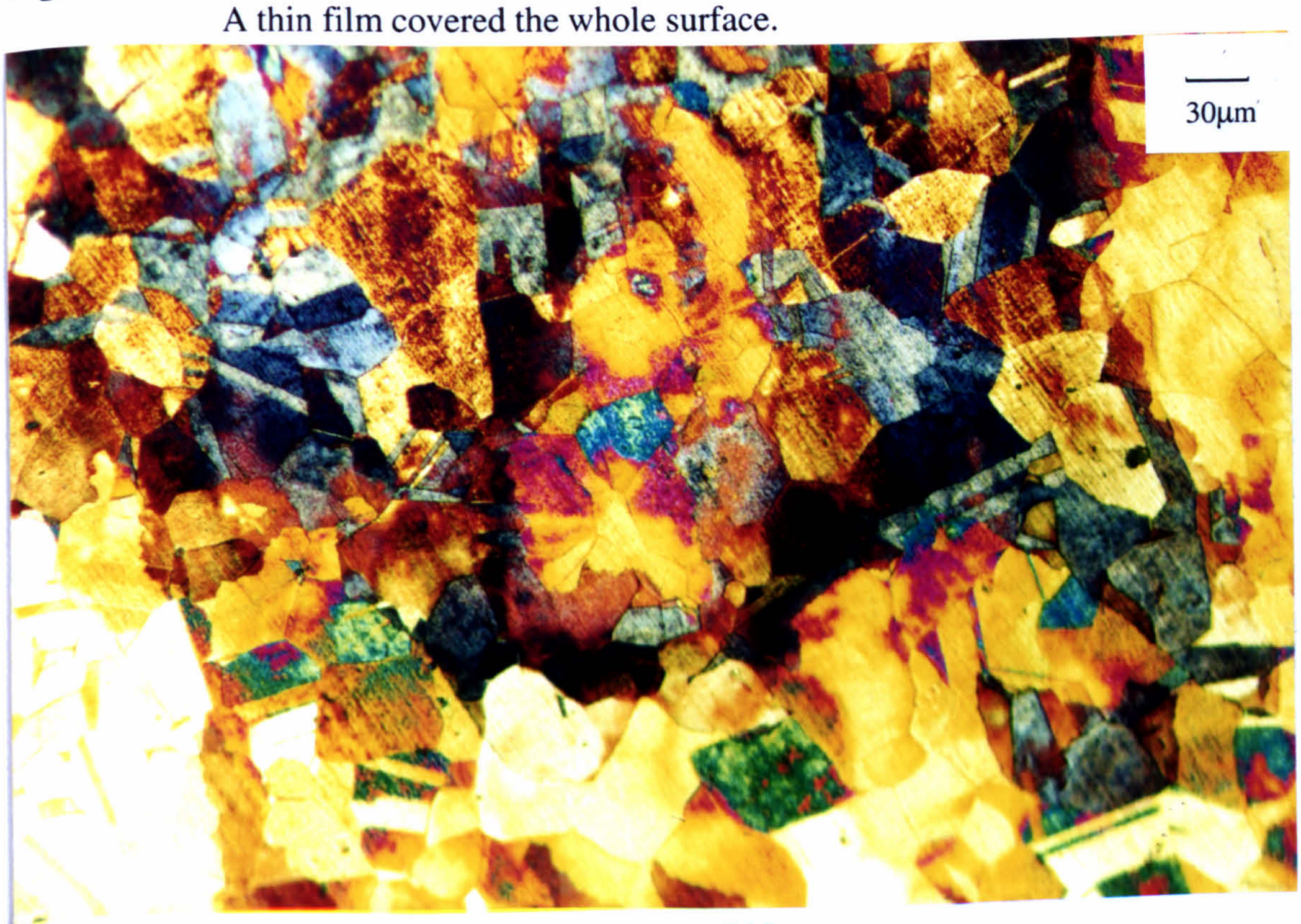

Figure 6.38. Cu-10%Ni, V=17m/s, 8 hours, T.W.L.
The etched structure with some pits covered the entire surface.

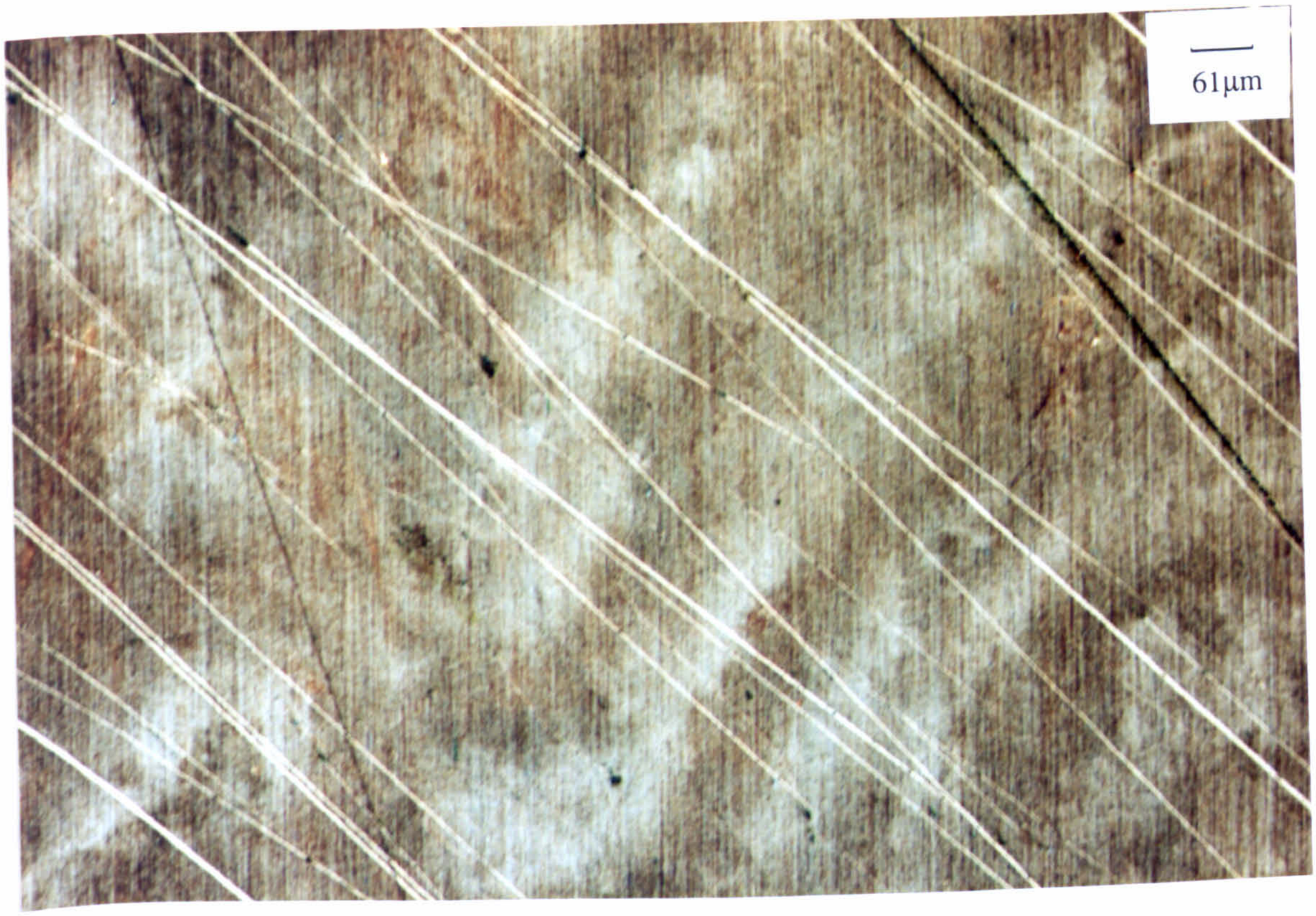

Figure 6.39. Cu-10%Ni, V=17m/s, 8 hours, C.P.
A thin red black film over the entire surface.

Figure 6.40. Cu-10%Ni, V=17m/s, 48 hours, T.W.L.
The etched appearance was obvious for the whole surface.

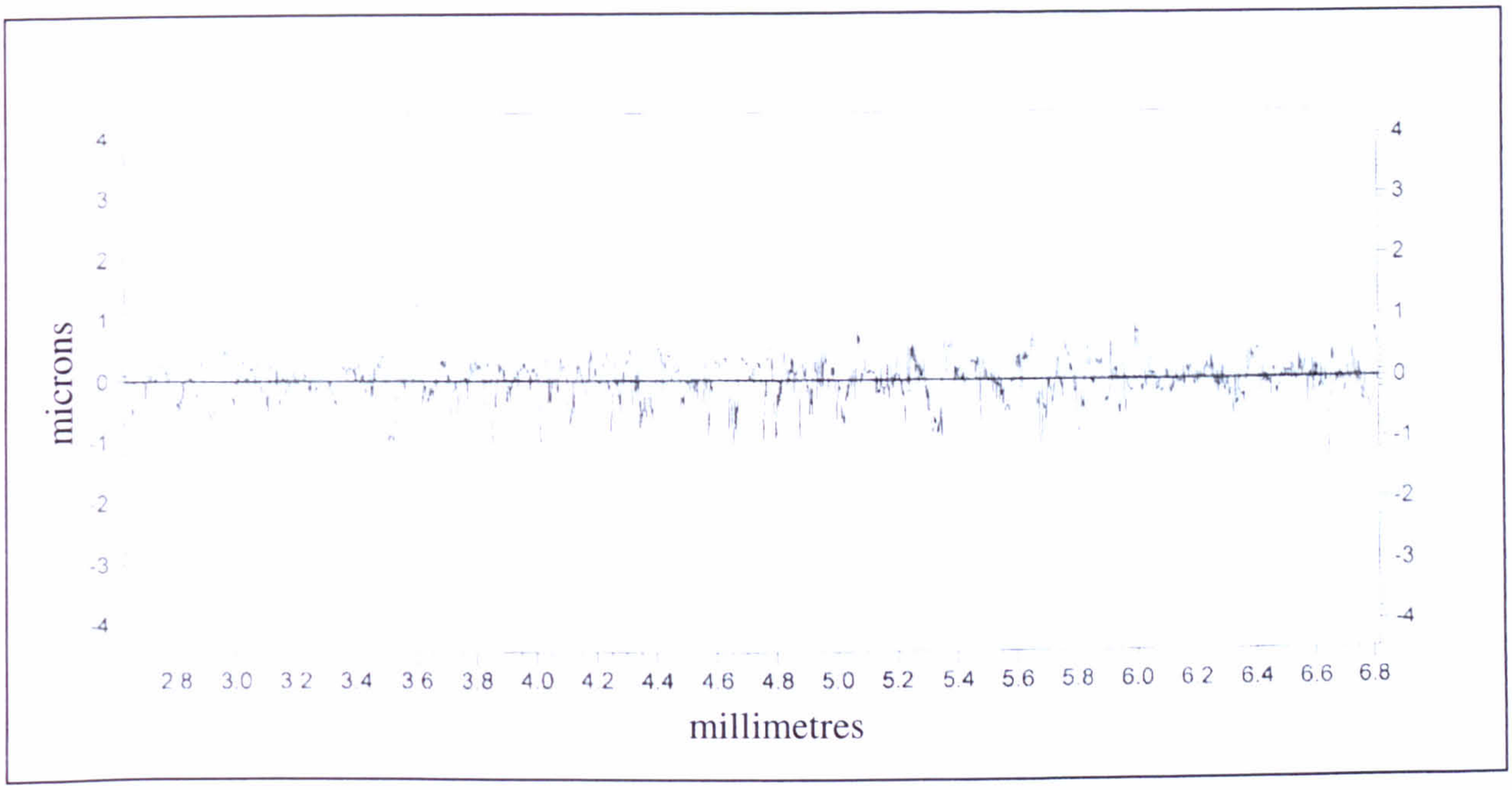

Figure 6.41. Cu-10%Ni, V=17m/s, 48 hours, T.W.L.
Surface profile with R_a=0.35μm for the entire surface.

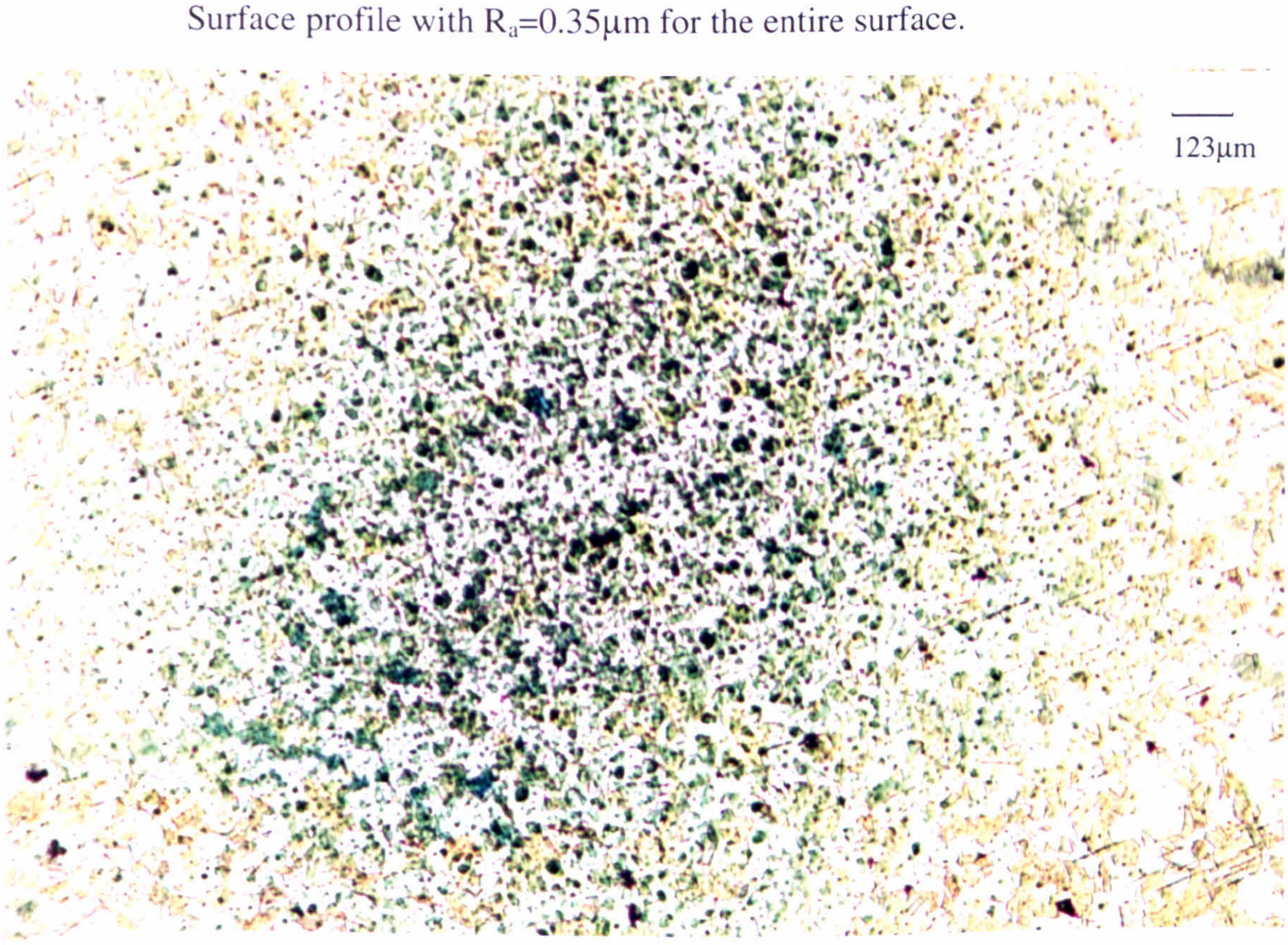

Figure 6.42. Cu-10%Ni, V=86m/s, 4 hours, T.W.L.
Clear hydrodynamic zones with extensive pitting under the jet.

Figure 6.43. Cu-10%Ni, V=86m/s, 4 hours, T.W.L.
The grain structure with a few pits at the outer regions.

Figure 6.44. Cu-10%Ni, V=86m/s, 4 hours, T.W.L.
Surface profile with R_a=0.25μm for the area under the jet.

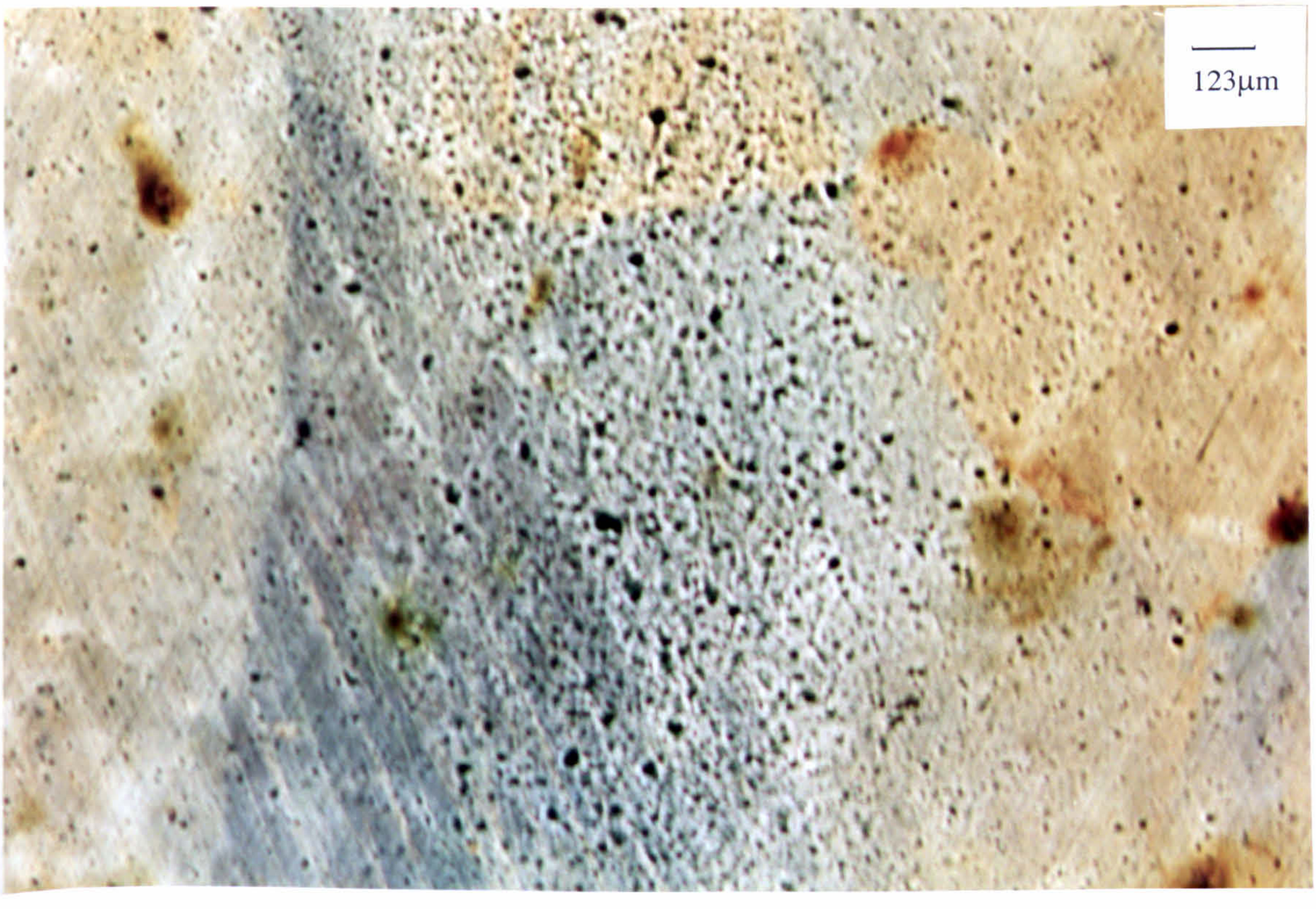

Figure 6.45. Cu-10%Ni, V=86m/s, 4 hours, C.P.
Significant pitting under the jet.

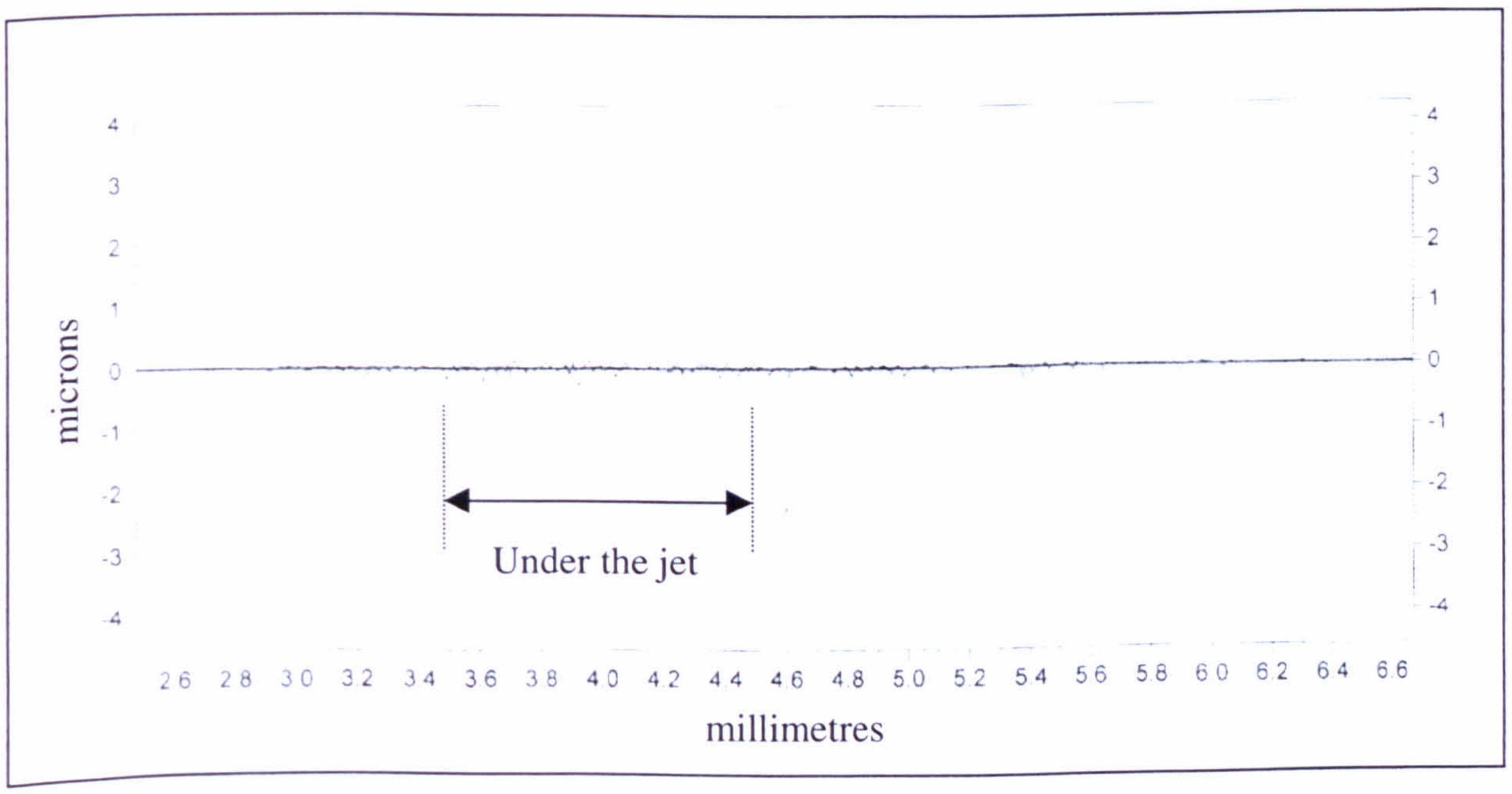

Figure 6.46. Cu-10%Ni, V=86m/s, 4 hours, C.P.
Surface profile with R_a=0.03μm for the area under the jet.

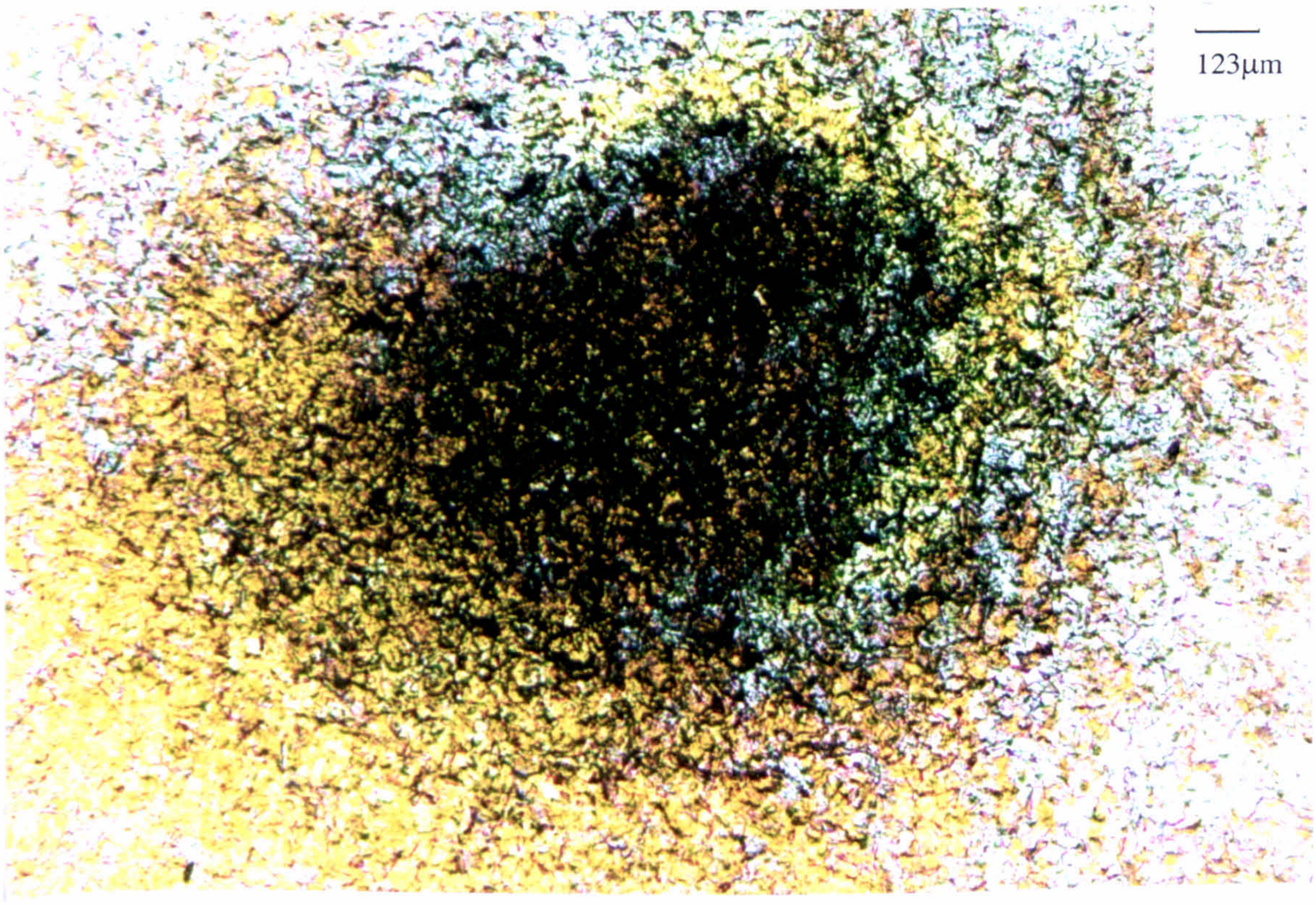

Figure 6.47. Cu-10%Ni, V=86m/s, 8 hours, T.W.L.
More extensive pitting under the jet.

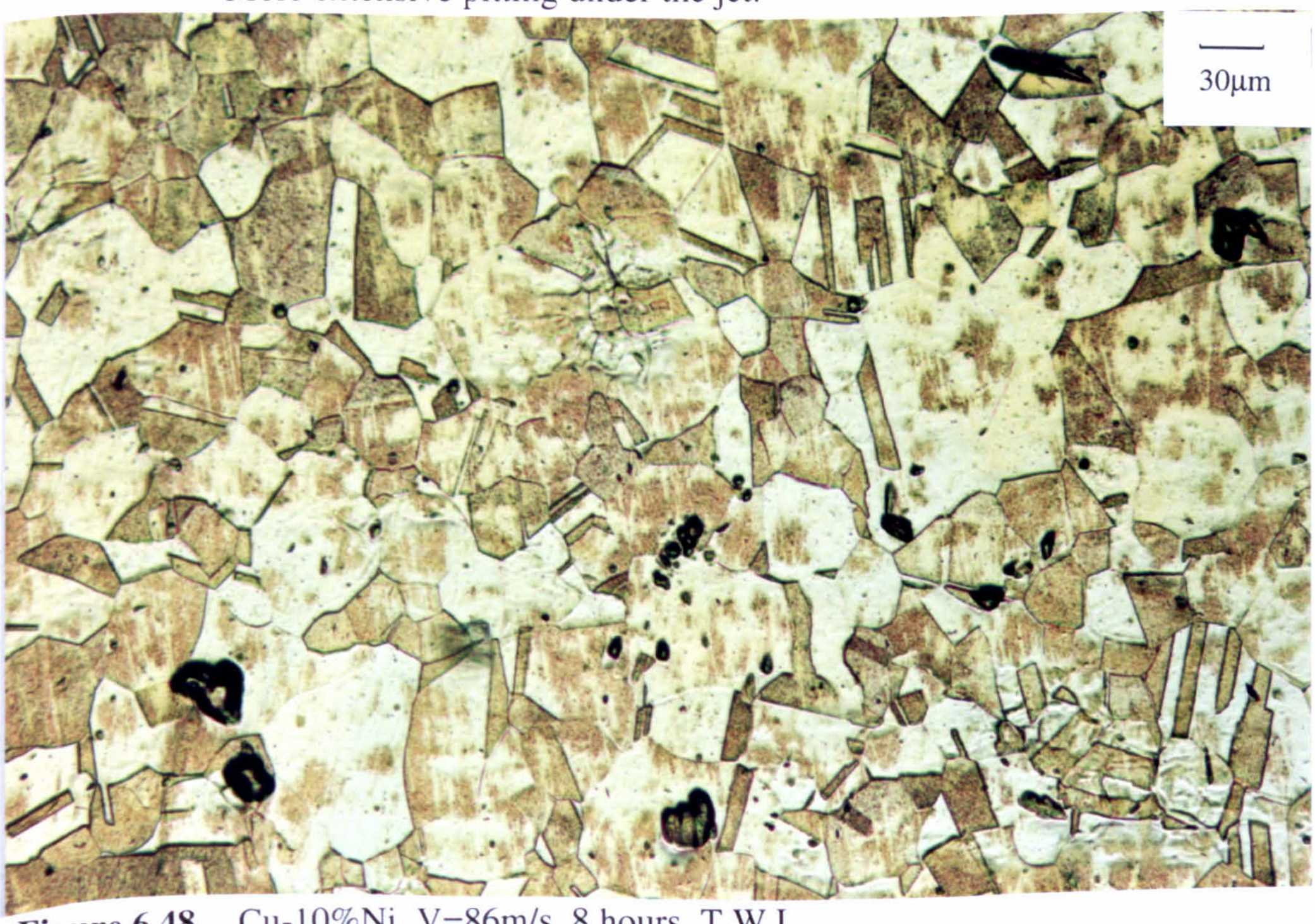

Figure 6.48. Cu-10%Ni, V=86m/s, 8 hours, T.W.L.
The grain structure with a few pits even at the outer regions.

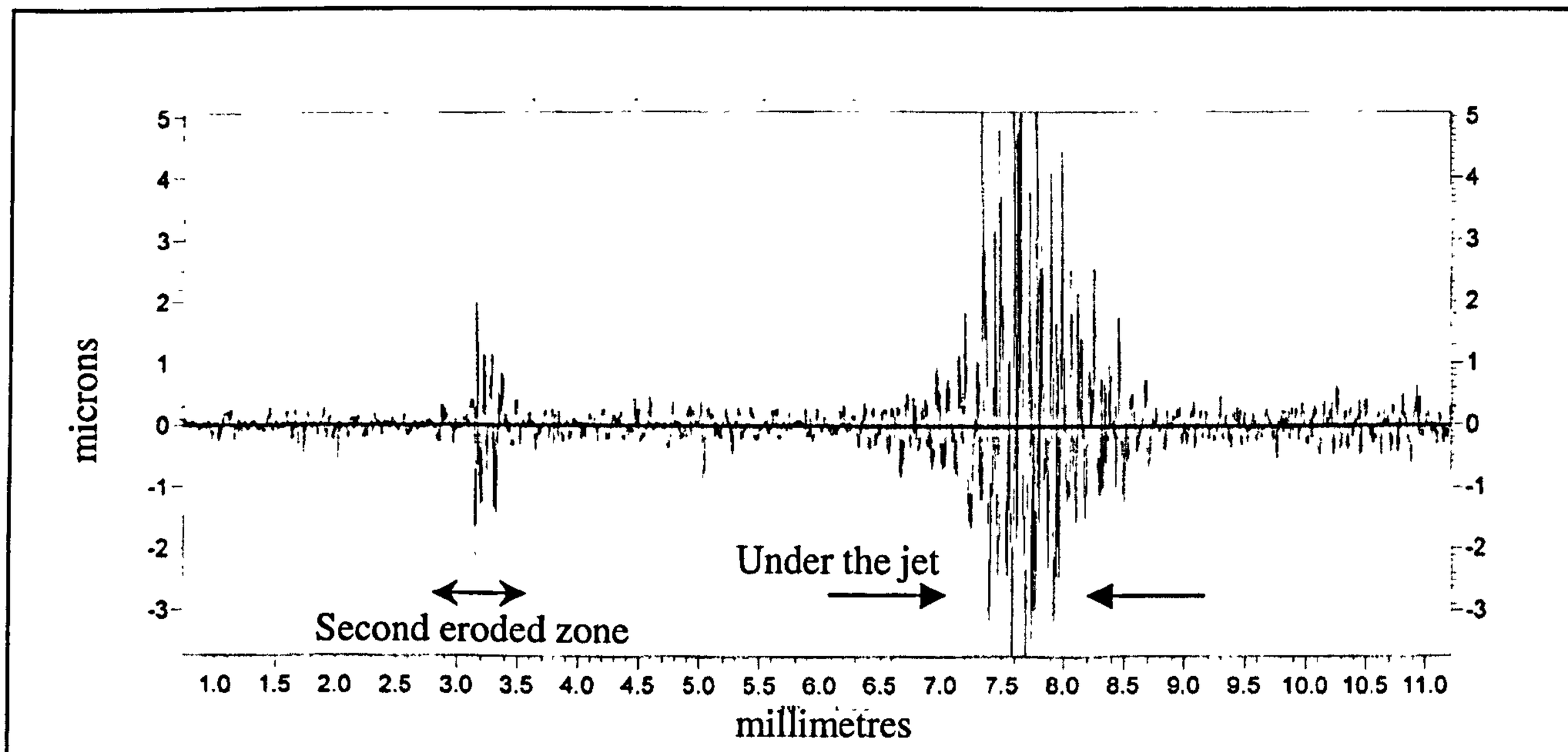

Figure 6.49. Cu-10%Ni, V=86m/s, 8 hours, T.W.L.
Surface profile with evidence of a rougher surface direct under the jet.

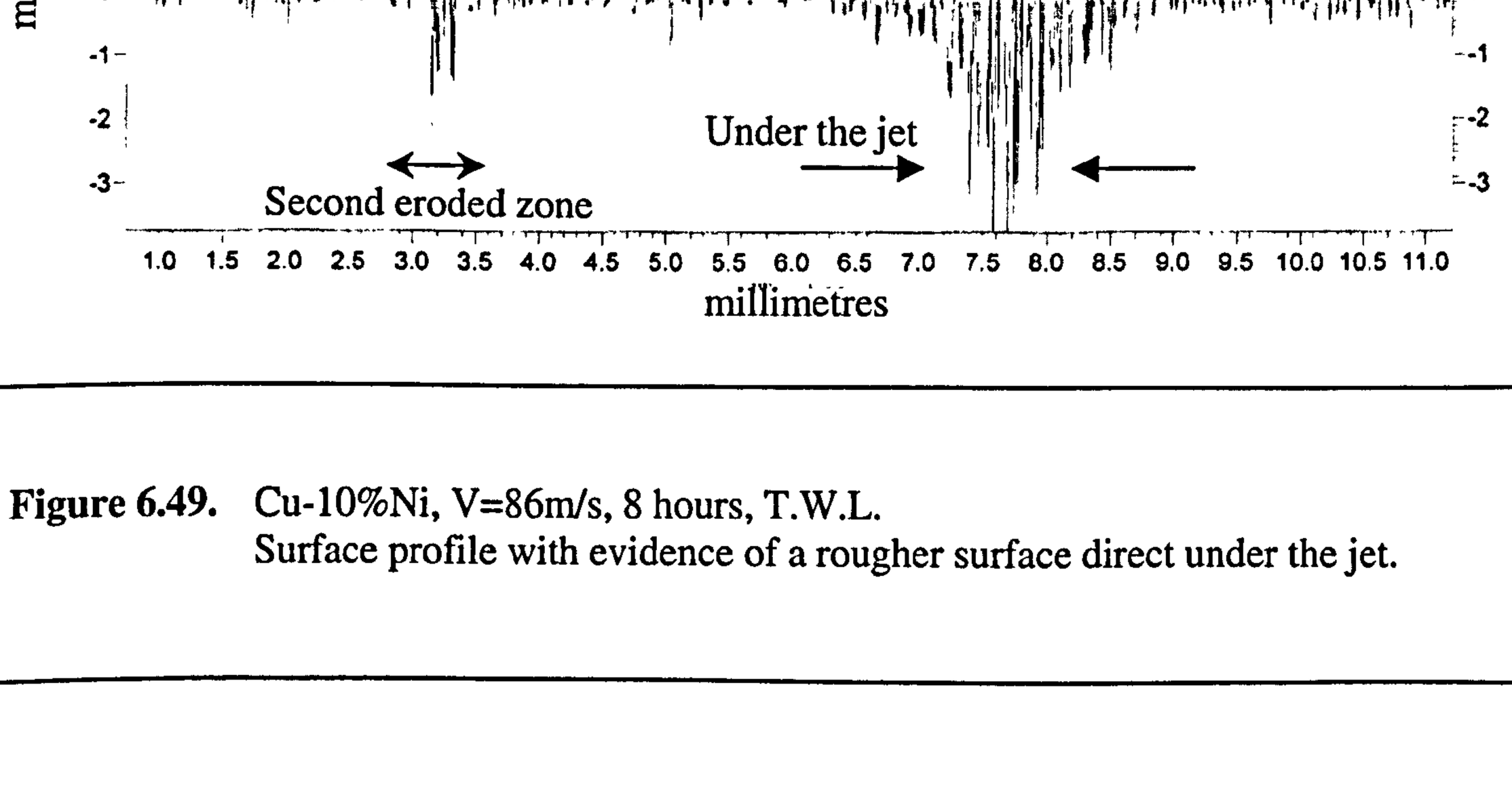

Figure 6.50. Cu-10%Ni, V=86m/s, 8 hours, C.P.
Surface profile with clear evidence of hydrodynamic zones.

Figure 6.51. Cu-10%Ni, V=86m/s, 8 hours, C.P.
The directly impinged zone.

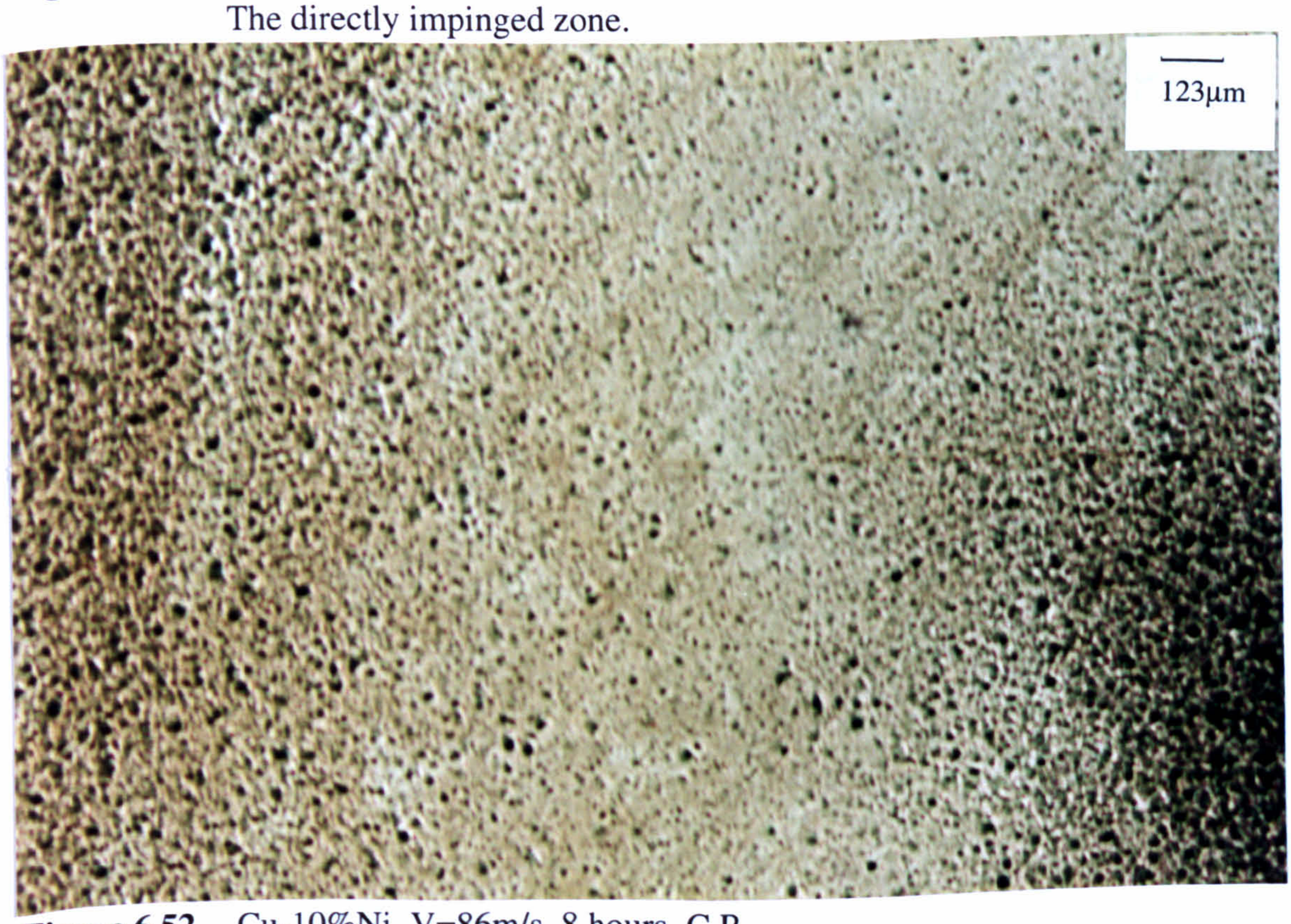

Figure 6.52. Cu-10%Ni, V=86m/s, 8 hours, C.P.
Microscopical evidence of clear hydrodynamic zones-Centre at the right.

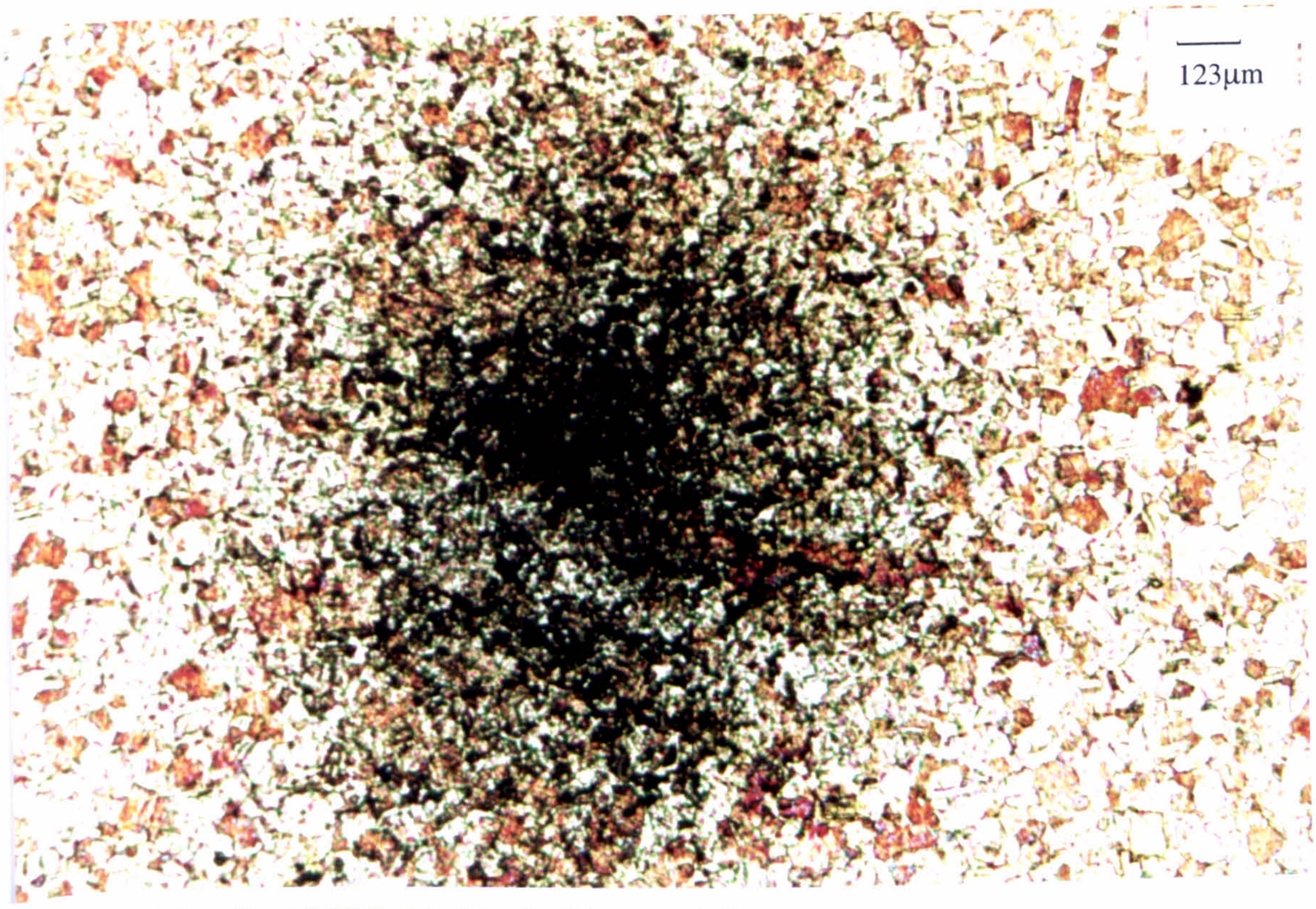

Figure 6.53. Cu-10%Ni, V=86m/s, 8 hours, A.P.
Severe pitting and etched structure under the jet.

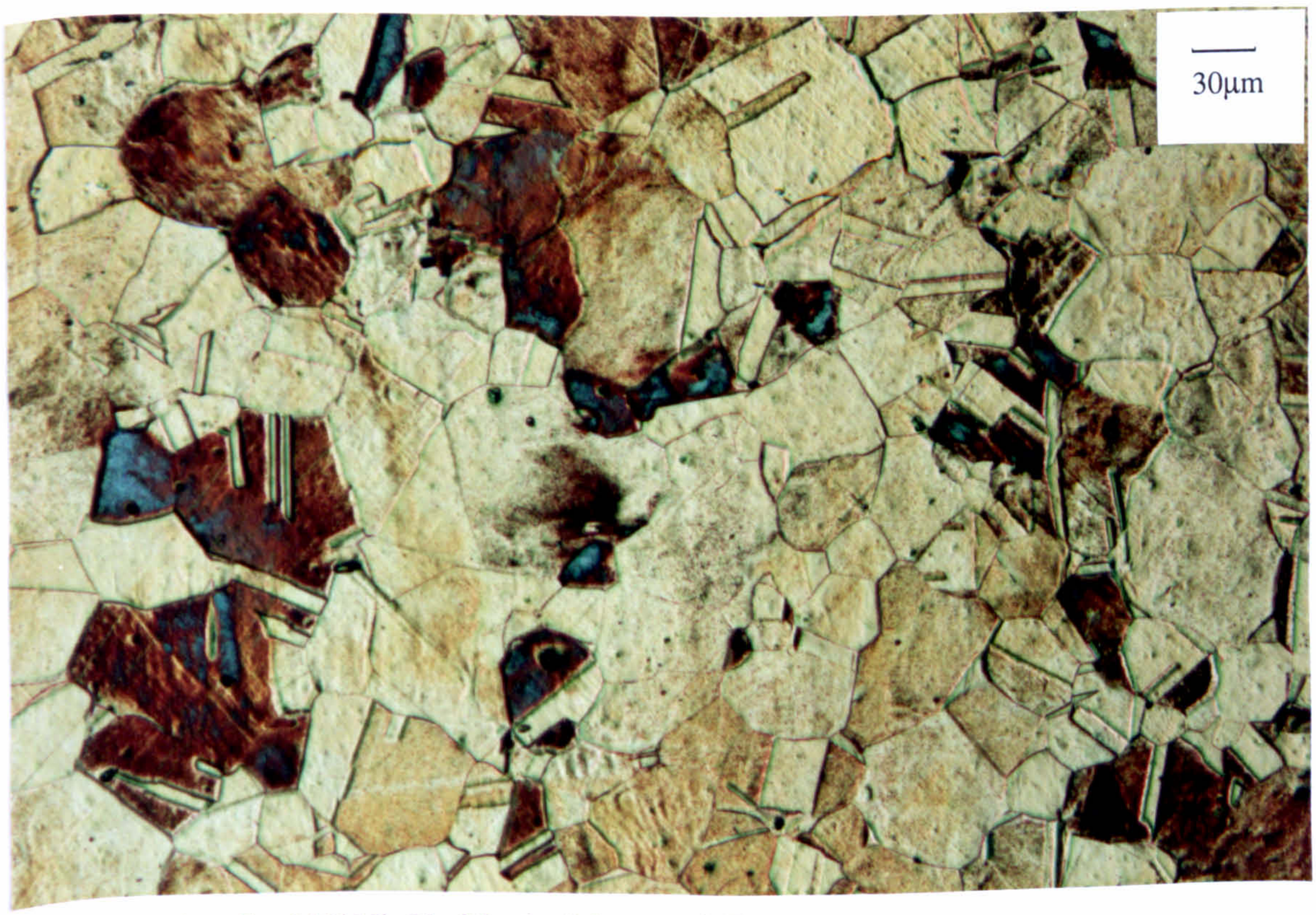

Figure 6.54. Cu-10%Ni, V=86m/s, 8 hours, A.P.
The etched structure at the outer regions of the specimen.

6.3.2. General erosion-corrosion of Marinel.

6.3.2.1. *Effect of velocity on erosion-corrosion for 4 hours.*

As was the case for the experiments on Cu-10%Ni these tests involved exposure of the specimens for 4 hours under impingement conditions, with at least one replication for each type of experiment.

6.3.2.1.1. *Total Weight Loss.*

The total weight loss/impingement velocity data for the two nozzle diameters are compared directly in Table 6.18. A general effect of increasing weight loss with velocity is clear. There is some evidence that for the 4mm diameter, the measured total weight loss of the Marinel specimens is higher, but the differences are small relative to the accuracy of the balance, 0.1mg.

Nozzle Diam.(mm)	Velocity (m/s)	Total Weight Loss (mg)	Average Total Weight Loss (mg)
Static	0	0.01 , 0.01 , 0.01	0.01
4	2.38	0.3 , 0.3	0.30
4	4.5	0.6 , 0.6	0.60
1	4.5	0.4 , 0.4	0.40
1	17	0.6 , 0.4	0.50
1	86	1.9 , 1.7	1.80

Table 6.18. Total weight loss/impingement velocity data at the two nozzle diameters after 4 hours exposure time.

6.3.2.1.2. *Weight Loss due to the Pure Erosion component.*

As usual this was obtained in experiments in which the specimen was cathodically protected and the results are presented in Table 6.19. These display a fundamental difference between Marinel and Cu-10%Ni in that the pure erosion rates are clearly extremely low for Marinel.

Nozzle Diam.(mm)	Velocity (m/s)	Pure Erosion Weight Loss (mg)	Average Pure Erosion Weight Loss (mg)
4	2.38	0.0 , 0.0	0.00
4	4.5	0.0 , 0.0	0.00
1	4.5	0.0 , 0.0	0.00
1	17	0.1 , 0.1	0.10
1	86	0.3 , 0.3	0.30

Table 6.19. Weight loss values due to the erosion component after 4 hours exposure time.

6.3.2.1.3. *Weight Loss due to the Direct Corrosion component.*

Similar to the tests on Cu-10%Ni, the typical anodic polarisation curves shown in Figure 6.55a. and Figure 6.55b. display a substantial negative shift in E_{corr}, (to between –280 to –307mV), at all impingement velocities compared to static conditions and also a much greater difference between the anodic polarisation curves at the various velocities than is apparent in the 30 minutes exposure tests, (Figure 6.13a. and Figure 6.17b.).

Table 6.20. gives the instantaneous corrosion rates after 4 hours as calculated by the Tafel extrapolations, involving the normal correction procedure for the anodic curve. Also shown are the total amounts of material loss due to direct corrosion for the whole time period of the 4 hours obtained from the area under the graph of instantaneous corrosion rates versus times from experiments involving 30 minutes and 4 hours exposures.

Nozzle Diam.(mm)	Velocity (m/s)	Direct Corrosion current density ($\mu A/cm^2$)	Direct Corrosion current density ($\mu A/cm^2$) – Average	Instantaneous Direct Corrosion Weight Loss (mg/h)	Direct Corrosio Weight Loss (m
Static	0	0.6 , 0.6 , 0.5	0.56	0.003	0.010
4	2.38	13.0 , 13.0	13.00	0.072	0.176
4	4.5	6.5 , 6.5	6.50	0.036	0.135
1	4.5	8.0 , 8.0	8.00	0.044	0.177
1	17	17.0 , 15.0	16.00	0.088	0.264
1	86	50.0 , 50.0	50.00	0.278	0.687

Table 6.20. Weight loss values due to the direct corrosion component after 4 hours erosion corrosion.

The corrosion rate of Marinel clearly increased with velocity when a 1mm nozzle was employed. This expected trend was not evident from the more-limited experiments with a 4mm nozzle with which the corrosion rate at the comparable velocity of the 4.5m/s was lower than for a 1mm nozzle – as was also obtained in the previously presented 30 minutes tests, (Table 6.6.). At these times of 4 hours, the corrosion rates of Marinel are generally greater than for Cu-10%Ni, (Table 6.10.).

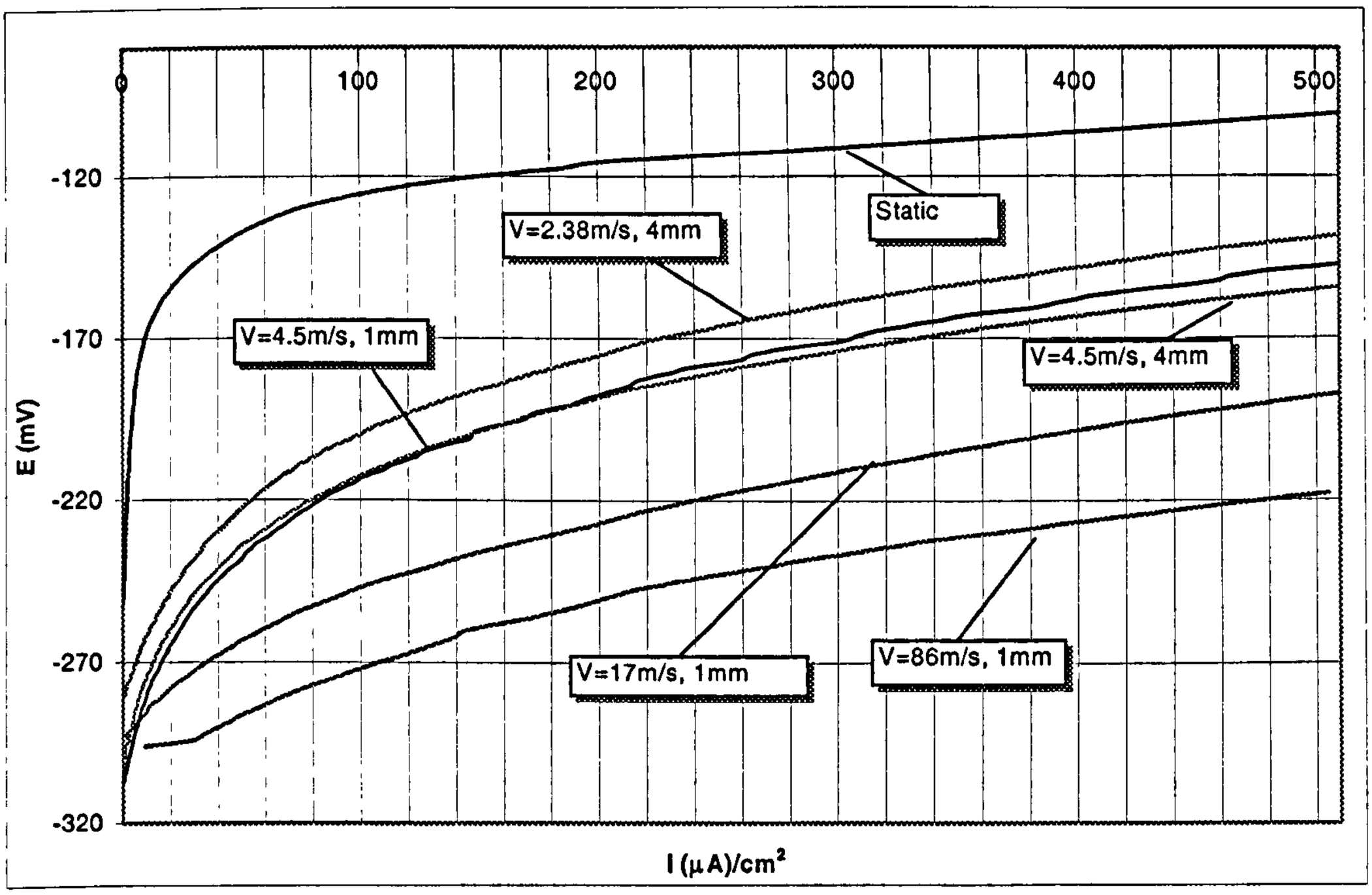

Figure 6.55a. Anodic polarisation tests of Marinel upon an initial exposure of 4 hours under the impinging jet.

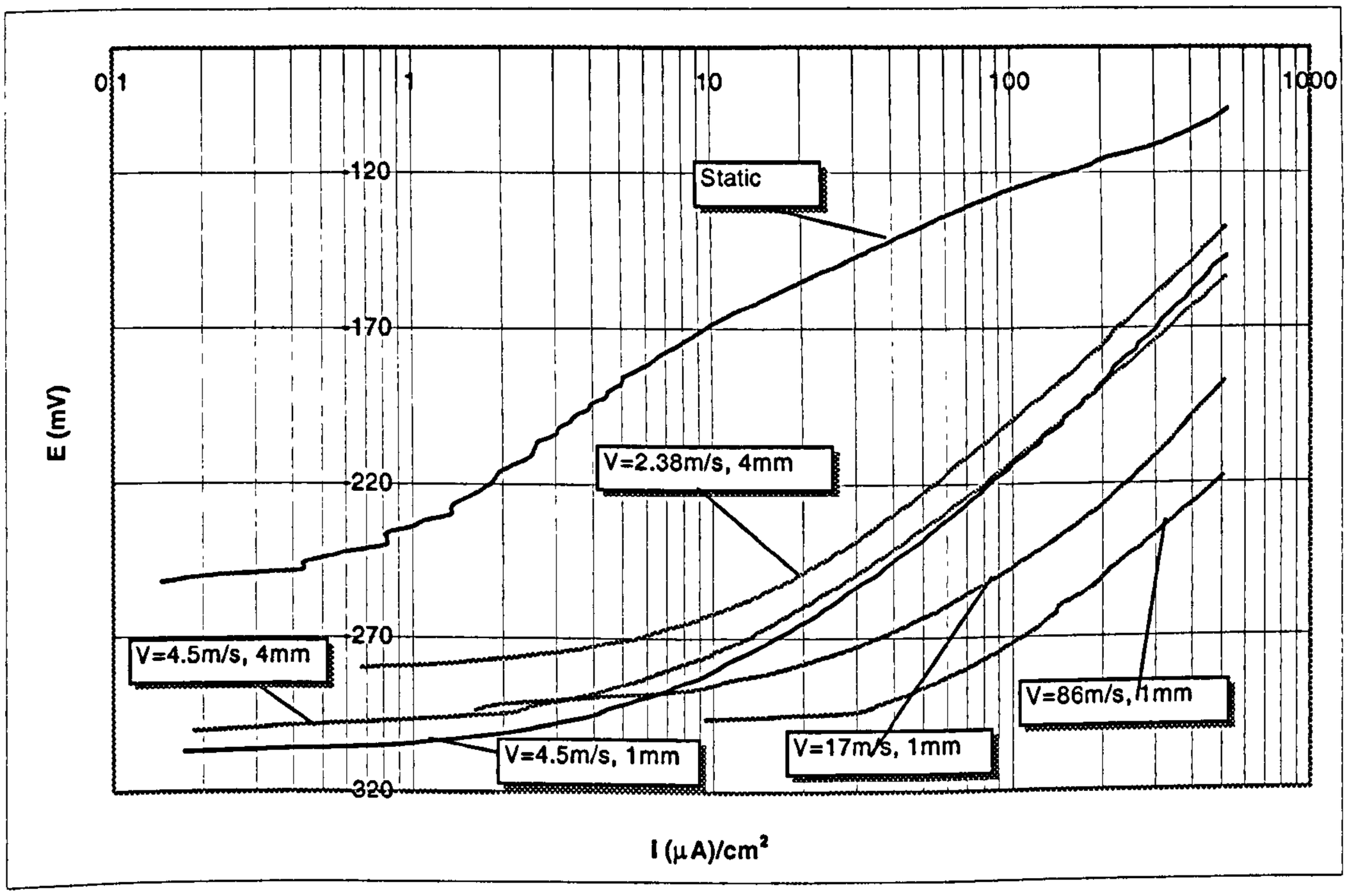

Figure 6.55b. Anodic polarisation tests of Marinel upon an initial exposure of 4 hours under the impinging jet.

6.3.2.1.4. *Remarks on the effect of velocity on erosion-corrosion for 4 hours.*

Table 6.21. shows the weight loss values due to erosion, corrosion and indirect corrosion (synergy).

Nozzle Diam.(mm)	Velocity (m/s)	Average Total Weight Loss (mg)	Average Pure Erosion Weight Loss (mg)	Average Pure Corrosion Weight Loss (mg)	Average Synergy (mg)
Static	0	0.01	~	0.01	~
	%		~	100	~
4	2.38	0.30	0.00	0.18	0.12
	%		0	59	41
4	4.5	0.60	0.00	0.14	0.46
	%		0	23	77
1	4.5	0.40	0.00	0.18	0.22
	%		0	44	56
1	17	0.50	0.10	0.27	0.13
	%		20	51	27
1	86	1.80	0.30	0.69	0.81
	%		18	37	45

Table 6.21. Weight loss values due to erosion, corrosion and indirect corrosion (synergy) effect, after 4 hours exposure time.

The erosion corrosion attack is clearly demonstrated by corrosion (direct + indirect via synergy) processes. Nevertheless, erosion phenomena are not negligible via those facilitated by corrosion (i.e. synergy) at low impingement velocities and significant pure erosion damage at higher velocities.

6.3.2.2. *Effect of time on erosion corrosion.*

The same protocol was employed as for the analogous study on Cu-10%Ni, namely focusing on the velocity of 17m/s, (with the 1mm nozzle) and undertaking experiments for 4, 8, 48 and 72 hours, together with a limited study, involving experiments for 4 and 8 hours, at a velocity of 86 m/s, (with the 1mm nozzle).

6.3.2.2.1. Total Weight Loss.

Table 6.22. shows the total weight loss/exposure time data, and the greater weight losses at the higher velocity are quite clear.

Whilst, at both velocities, an increased exposure time period resulted in an increased total weight loss, it is evident that the rate of material loss was decreasing with the passage of time.

Time (hours)	Velocity (m/s)	Total Weight Loss (mg)	Average Total Weight Loss (mg)
4	17	0.6 , 0.4	0.50
8	17	0.9 , 0.7	0.80
48	17	2.0 , 2.0	2.00
4	86	1.9 , 1.7	1.80
8	86	2.4 , 2.6	2.50

Table 6.22. Total weight loss/exposure time data.

6.3.2.2.2. Weight Loss due to the Pure Erosion component.

As was observed in the 4 hours tests on this material (Table 6.19.), the contribution of the pure erosive component to the total damage, (found on cathodically protected specimens), was very small especially at the lower velocity, (Table 6.23.).

Time (hours)	Velocity (m/s)	Pure Erosion Weight Loss (mg)	Average Pure Erosion Weight Loss (mg)
4	17	0.1 , 0.1	0.10
8	17	0.2 , 0.2	0.20
48	17	0.2 , 0.2	0.20
4	86	0.6 , 0.6	0.60
8	86	0.7 , 0.7	0.70

Table 6.23. Weight loss values due to the erosion component.

6.3.2.2.3. Weight Loss due to the Direct Corrosion component.

Figure 6.56a-b. and Figure 6.57a-b. show the typical anodic and cathodic polarisation curves generated from tests in 3.5% NaCl solution after the various time exposures. Evidently a substantial negative shift in E_{corr}, (to between -279 to–300mV), appeared at all impingement velocities compared to static conditions, (Figure 6.55a.). The instantaneous corrosion rates expressed in mg/h as calculated by the "Tafel extrapolation" method, and the direct corrosion weight losses expressed in mg as obtained by the "area under the graph" method, are shown in Table 6.24. The results show considerably higher corrosion rates at the greater velocity and a decreasing instantaneous corrosion rate at 8 hours compared to 4 hours for both velocities. In the longer running experiments at 17m/s, the measured instantaneous corrosion rate was lower again at 48 hours but exhibited a significant increase at 72 hours. These time dependencies were studied further by mean of linear-polarisation type experiments, the results of which are described in section 6.3.2.2.5.

Time (hours)	Velocity (m/s)	Direct Corrosion current density ($\mu A/cm^2$)	Direct Corrosion current density ($\mu A/cm^2$) – Average	Instantaneous Direct Corrosion Weight Loss (mg/h)	Direct Corrosion Weight Loss (mg)
4	17	15.0 , 17.0	16.0	0.090	0.26
8	17	7.0 , 7.0	7.0	0.039	0.52
48	17	6.3 , 5.5	5.9	0.033	1.74
72	17	10.0 , 10.0	10.0	0.056	2.78
4	86	50.0 , 50.0	50.0	0.280	0.69
8	86	40.0 , 40.0	40.0	0.224	1.74

Table 6.24. Weight loss values due to the direct corrosion component.

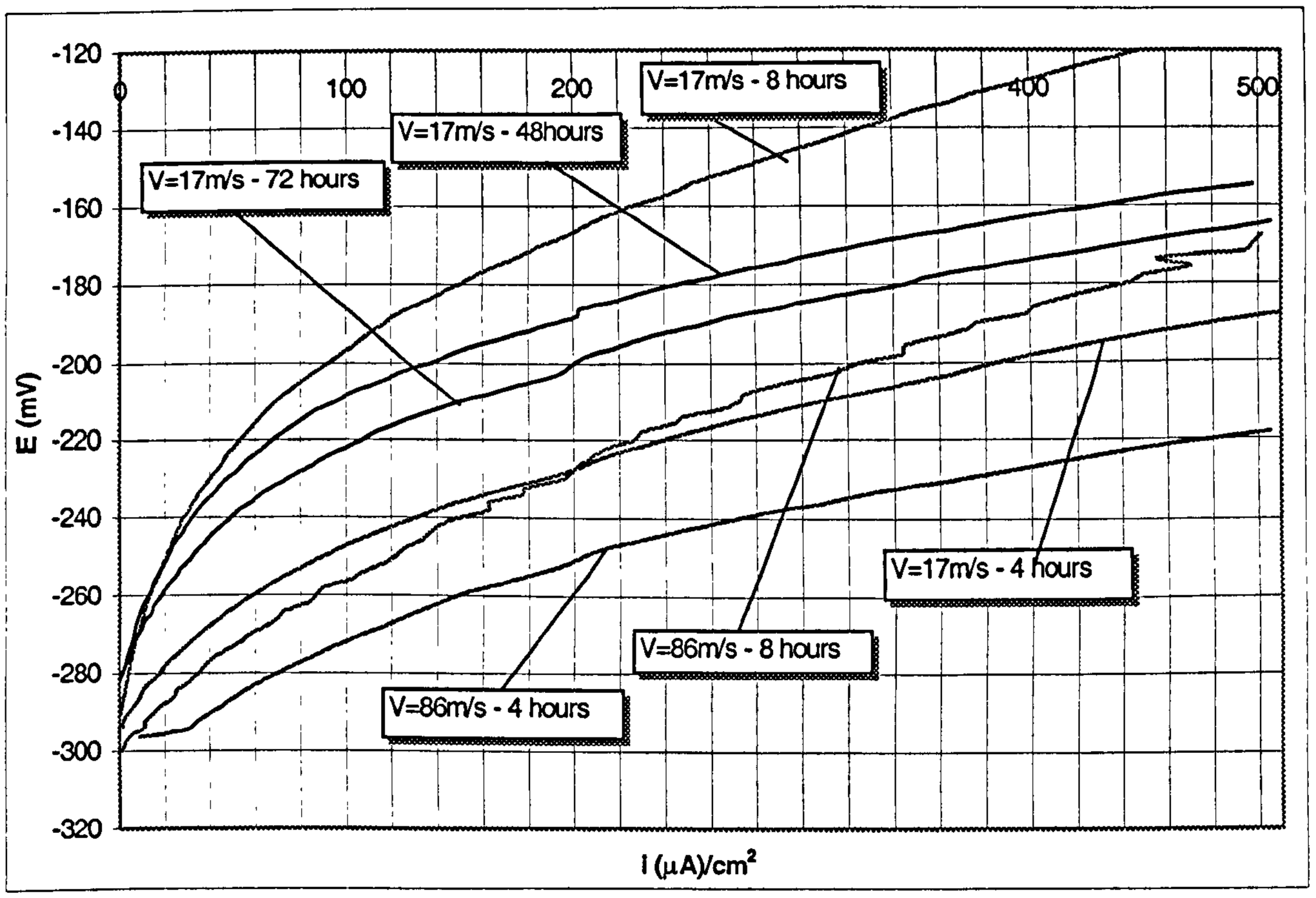

Figure 6.56a. Anodic polarisation curves of Marinel upon exposures of 4, 8, 48 and 72 hours under impinging velocities of 17m/s and 86m/s.

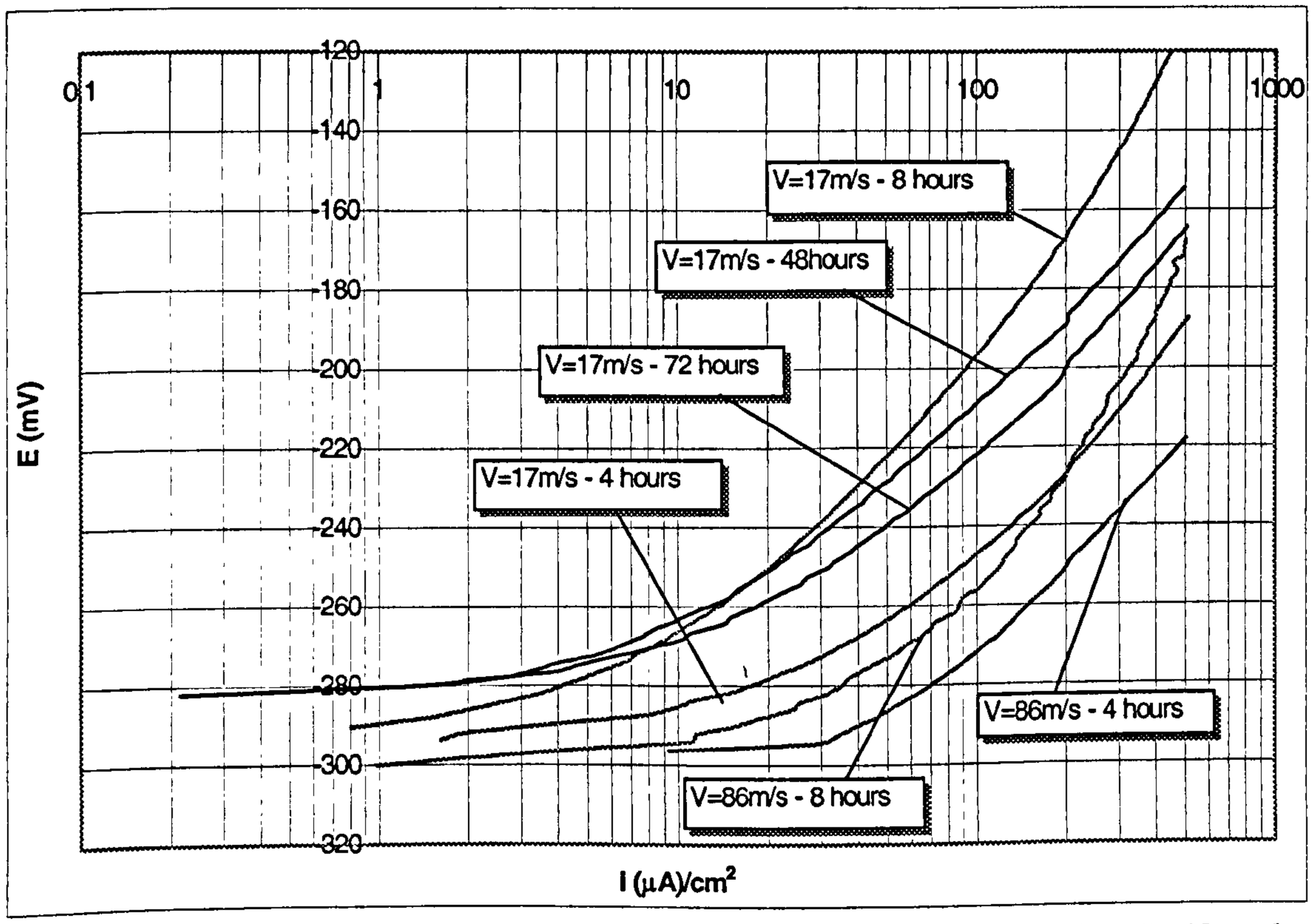

Figure 6.56b. Anodic polarisation curves of Marinel upon exposures of 4, 8, 48 and 72 hours under impinging velocities of 17m/s and 86m/s.

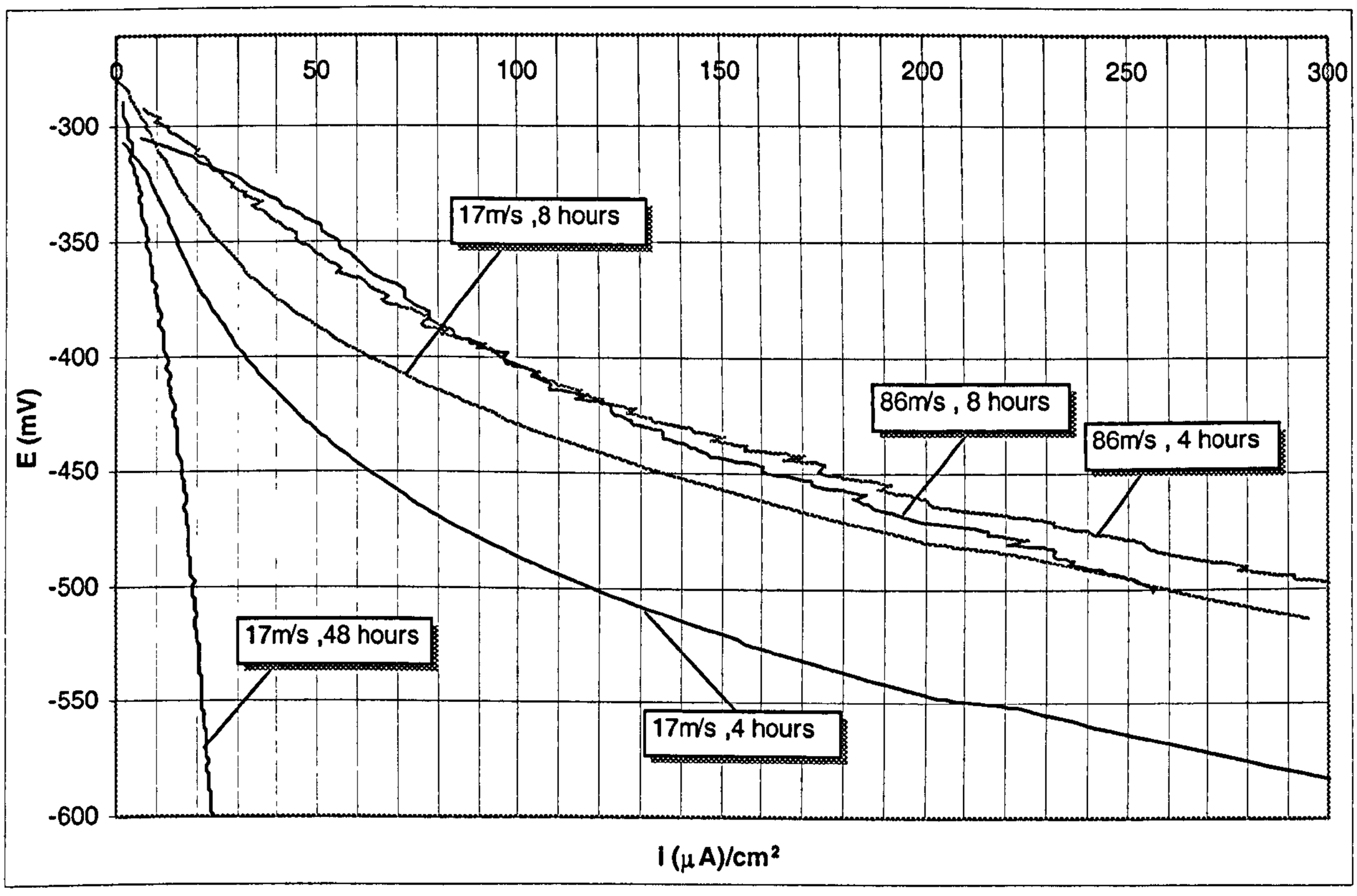

Figure 6.57a. Cathodic polarisation curves of Marinel upon exposures of 4, 8 and 48 hours under impinging velocities of 17m/s and 86m/s.

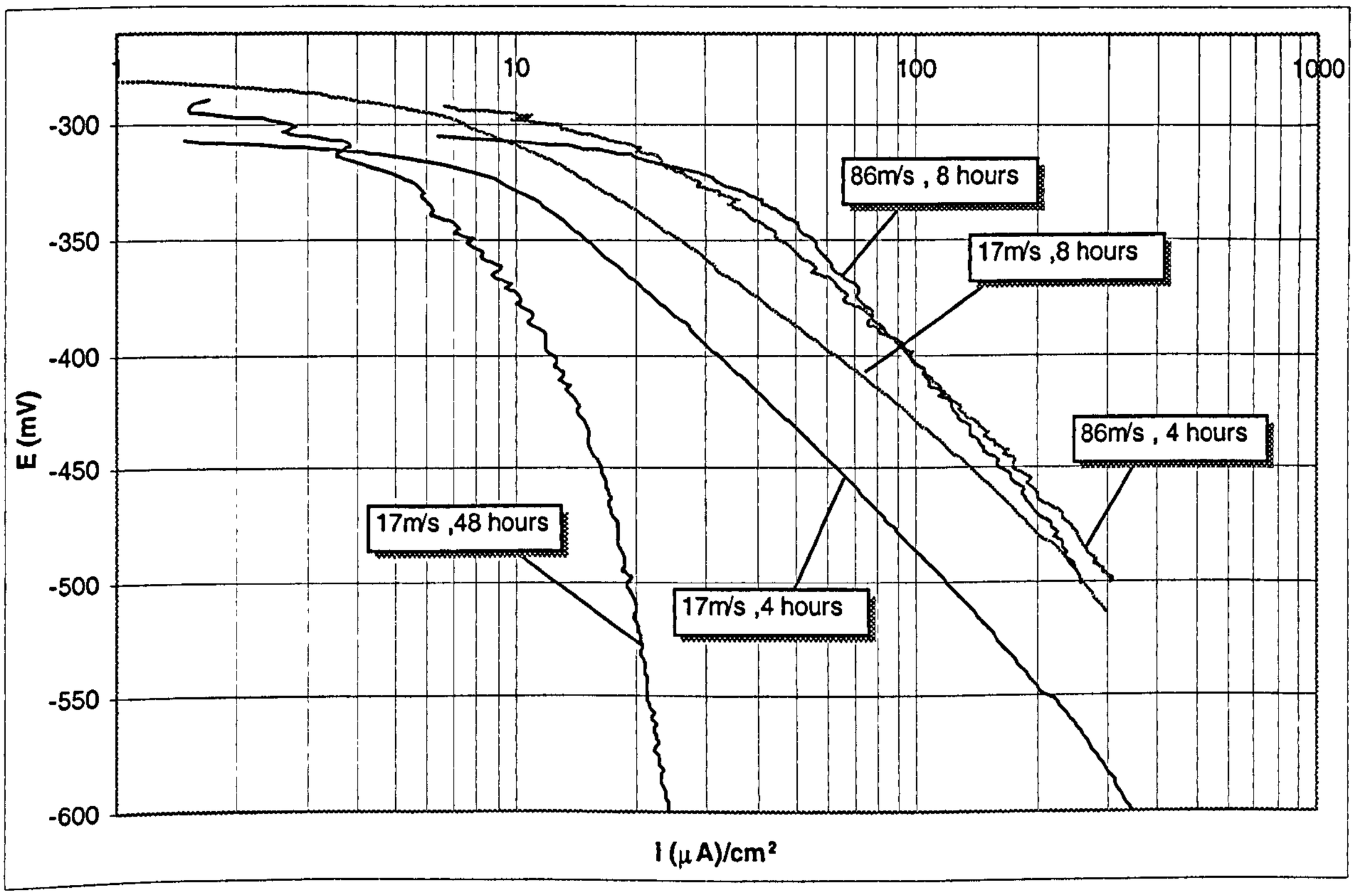

Figure 6.57b. Cathodic polarisation curves of Marinel upon exposures of 4, 8 and 48 hours under impinging velocities of 17m/s and 86m/s.

6.3.2.2.4. Remarks on the effect of time on erosion-corrosion process.

Table 6.25. shows the weight loss values due to erosion, corrosion and indirect corrosion (synergy).

Time (hours)	Velocity (m/s)	Average Total Weight Loss (mg)	Average Pure Erosion Weight Loss (mg)	Average Direct Corrosion Weight Loss (mg)	Average Synergy (mg)
4	17	0.50	0.10	0.26	0.14
	%		20	52	28
8	17	0.80	0.20	0.52	0.08
	%		25	65	10
48	17	2.00	0.20	1.74	0.06
	%		10	87	3
4	86	1.80	0.60	0.69	0.51
	%		33	38	29
8	86	2.50	0.70	1.74	0.06
	%		28	70	2

Table 6.25. Weight loss values due to erosion, corrosion and indirect corrosion (synergy) effect.

What is clear is that the dominant contributor to overall erosion-corrosion damage is the pure direct corrosion and the influence of this parameter increases with time. The synergy is appreciable at short times but later becomes almost negligible. There is also a significant contribution from pure erosion at the higher velocity.

6.3.2.2.5. Linear polarisation type tests.

In order to obtain more data to assist in the evaluation of trends in corrosion rate with time, a series of linear polarisation type monitoring exercises was undertaken at times of 30 min, 2, 4, 8, 16, 24, 32, 48, and 72 hours, at 17m/s. Figure 6.58a. and Figure 6.58b. show the resulting anodic polarisation curves for the 22mV anodic scans on duplicate specimens.

Table 6.26. shows the average values of E_{corr}, R_p' and $1/R_p'$ for Marinel at the different time exposures, and the duplicate specimen results and average values of $1/R_p'$ are also presented as a function of time in Figure 6.59a-b.

It is apparent that the time dependence of corrosion rate is complex as was indicated by the i_{corr} data, (Table 6.24.), which actually agree very well with the trends in Figure 6.59b.

Another interesting feature is that, as Table 6.26. reveals, the trends in E_{corr} match those of $1/R_p'$.

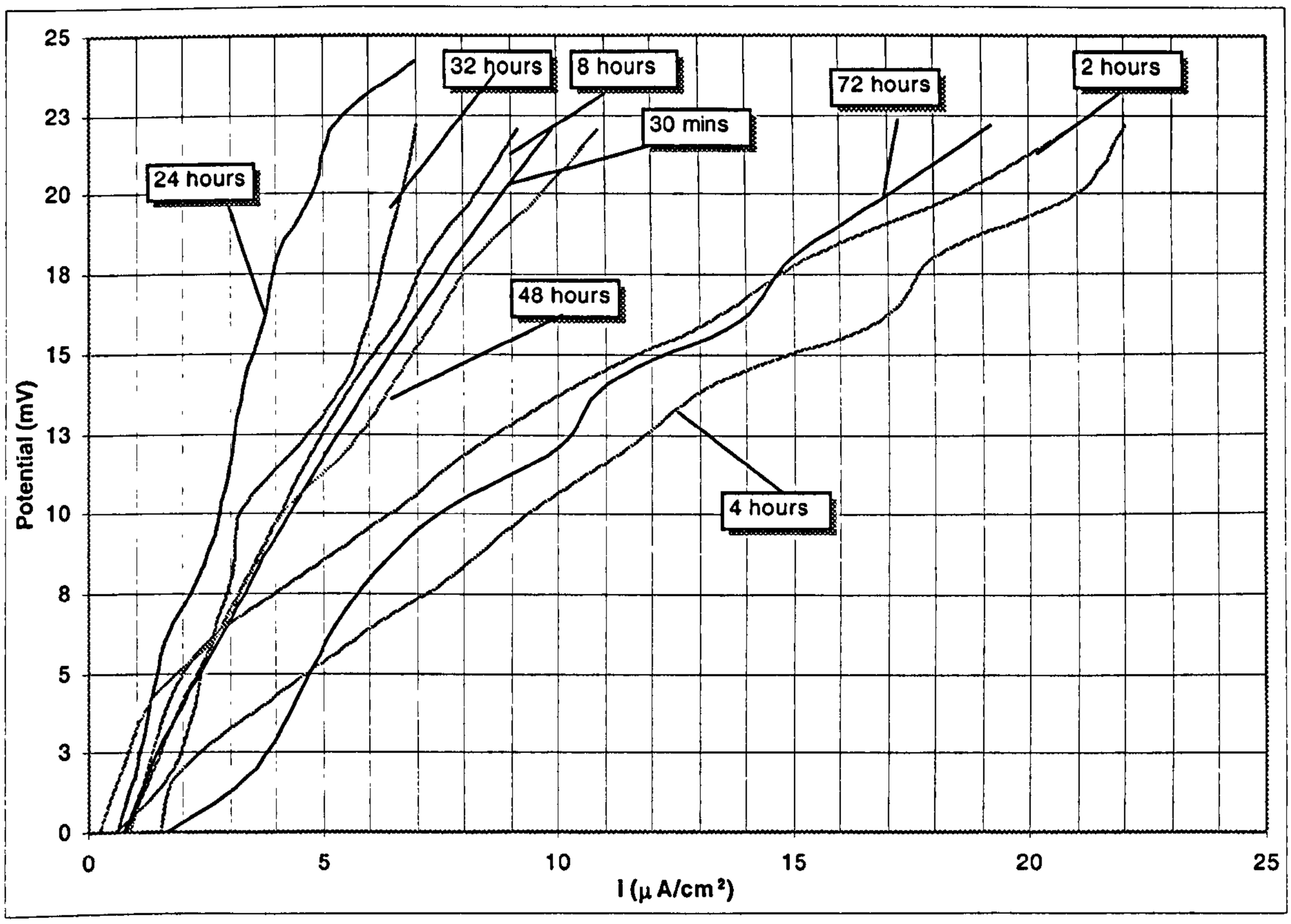

Figure 6.58a. Anodic polarisation curves of the specimen of Marinel, for an increase by 22mV to the value of E_{corr}, upon exposures of 30mins, 2, 16, 24, 32, 48 and 72 hours under impingement velocity of 17 m/s.

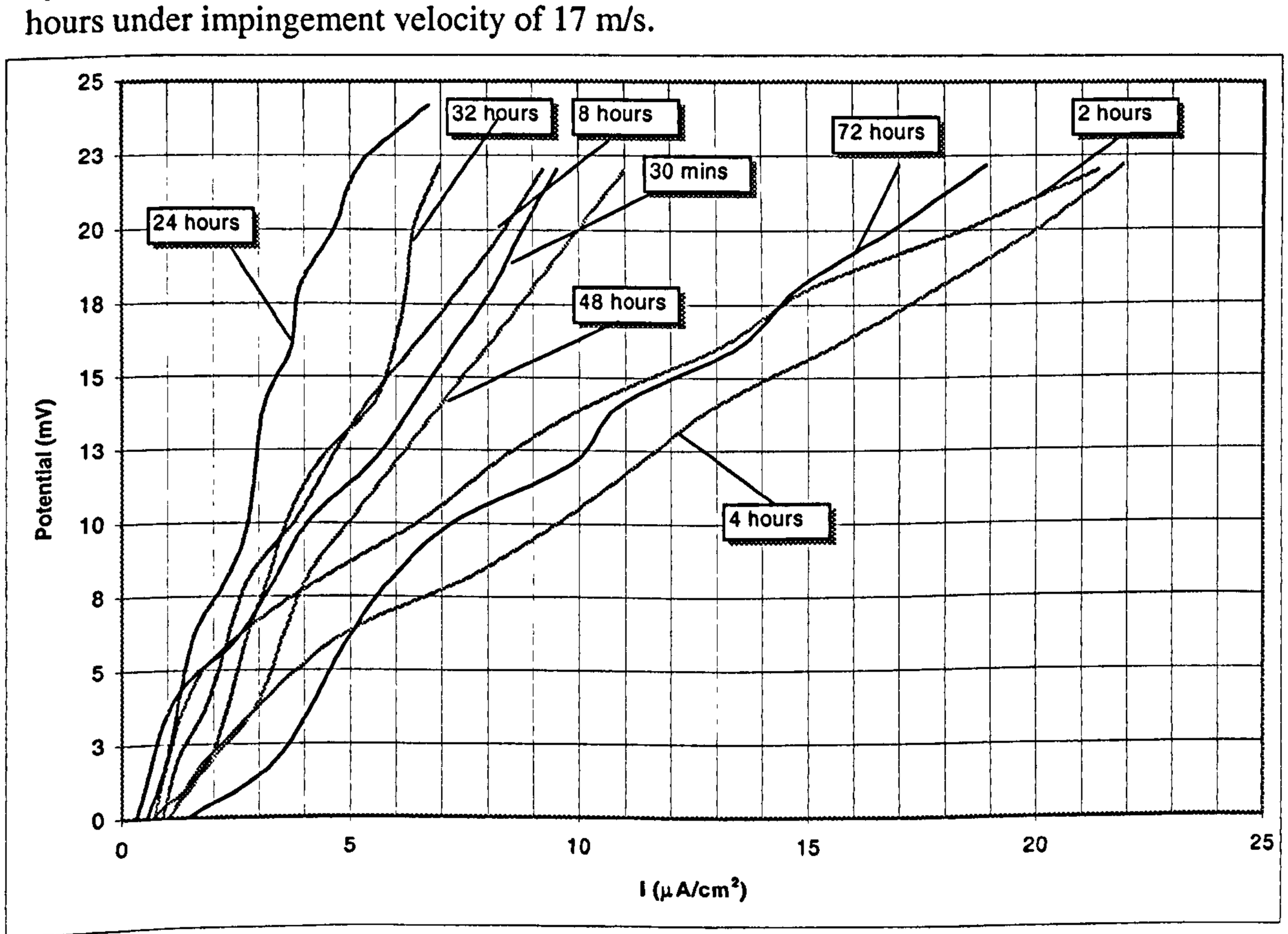

Figure 6.58b. Anodic polarisation curves of the specimen of Marinel, for an increase by 22mV to the value of E_{corr}, upon exposures of 30mins, 2, 16, 24, 32, 48 and 72 hours under impingement velocity of 17 m/s.

Time (hours)	Average E_{corr} (mV)	Average $R_p^{'}$ $(KOhm*cm^2)$	Average $1/R_p^{'}$ $(1/(KOhm*cm^2))$
½	-288.017	2.395	0.417
2	-301.179	0.989	1.012
4	-299.535	1.001	0.999
8	-301.346	2.624	0.381
16	-295.479	4.345	0.230
24	-284.971	4.310	0.232
32	-282.971	4.132	0.242
40	-283.109	4.005	0.249
48	-300.803	2.020	0.495
72	-306.514	1.243	0.804

Table 6.26. The average values of E_{corr}, $R_p^{'}$, $1/R_p^{'}$ for Marinel at different time exposures, for an increase by 22mV to the value of E_{corr}.

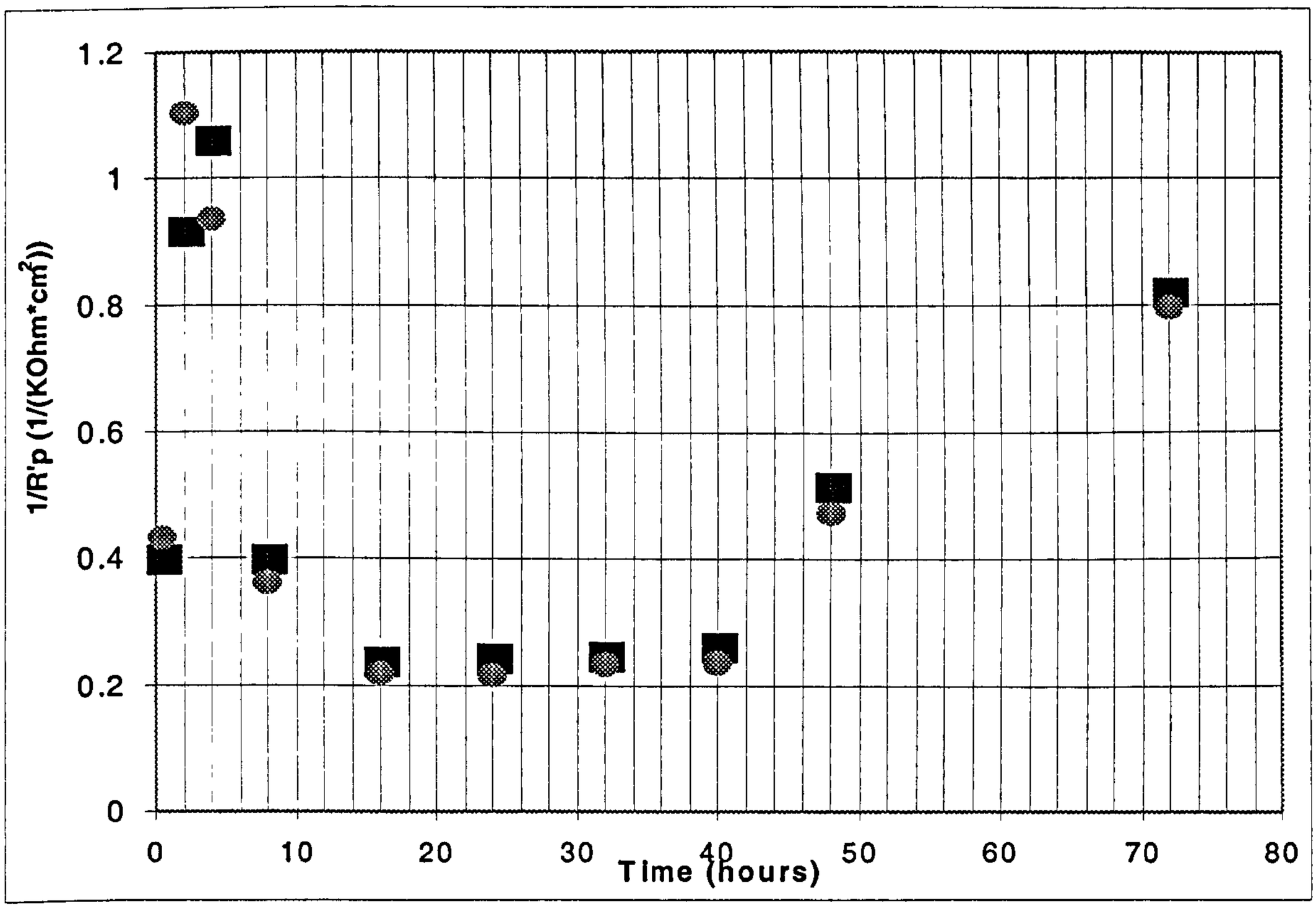

Figure 6.59a. $1/R_p'$ values vs. Time curve for the specimen of Marinel under impingement velocity of 17 m/s.

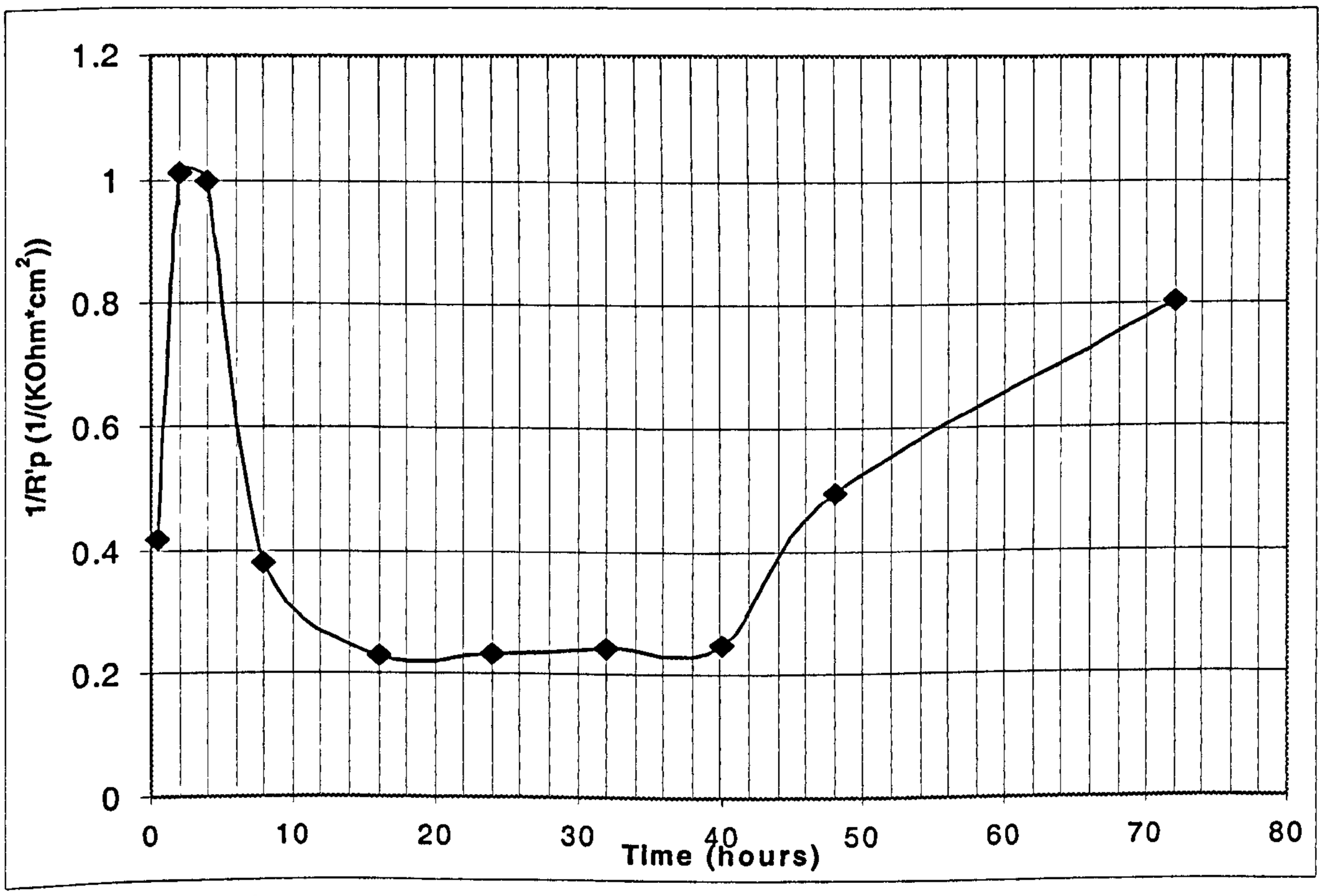

Figure 6.59b. $1/R_p'$ average values vs. Time curve specimen of Marinel under impingement velocity of 17 m/sec.

6.3.2.3. *Effect of anodic polarisation on erosion corrosion.*

In order to study the effect of the anodic polarisation on erosion corrosion behaviour of Marinel, the electrode potential of the specimen was maintained at a potential of -100 mV, while the specimen was subjected to impingement conditions at 17m/s, for time periods of 1 and 8 hours, (recall from Table 6.26. that the natural E_{corr} values under these conditions were about –290mV). During the time of the anodic polarisation test the produced corrosion current I, was measured using an external ammeter and the total weight loss was obtained by weighing the specimen before and after the impingement tests to an accuracy of 0.1mg. Duplicate experiments for each situation were conducted.

As the multistat output was continuously adjusted to maintain the potential at a value of –100mV, the corresponding I/t relationship followed a plot like the one presented Figure 6.60., which shows the typical curves generated for a Marinel specimen after exposure for 1 and 8 hour under an impinging jet at 17m/s.

The measured corrosion current values were transformed to weight losses by using Faraday's Law, and as a consequence the I/t plot was re-plotted to mg/t curves like the one in Figure 6.61.

In order to obtain the total amount of material loss due to direct corrosion for the whole time period, the area under the instantaneous weight losses versus time graph, (e.g. Figure 6.61.), was calculated. The contribution due to the erosion and the synergetic components was calculated by the usual formula:

Erosion+Synergy = Total weight loss – Direct corrosion weight loss.

Table 6.27a-b. show the total weight losses and those due to the direct corrosion and due to the erosion+synergy component, after 1 and 8 hours respectively.

Obviously the results state that upon an exposure of 8 hours under the impinging jet, a decrease in the rates of the total weight loss and the direct corrosion weight loss was detected, while the rate of the weight loss due to the erosion and the synergetic components, remains constant.

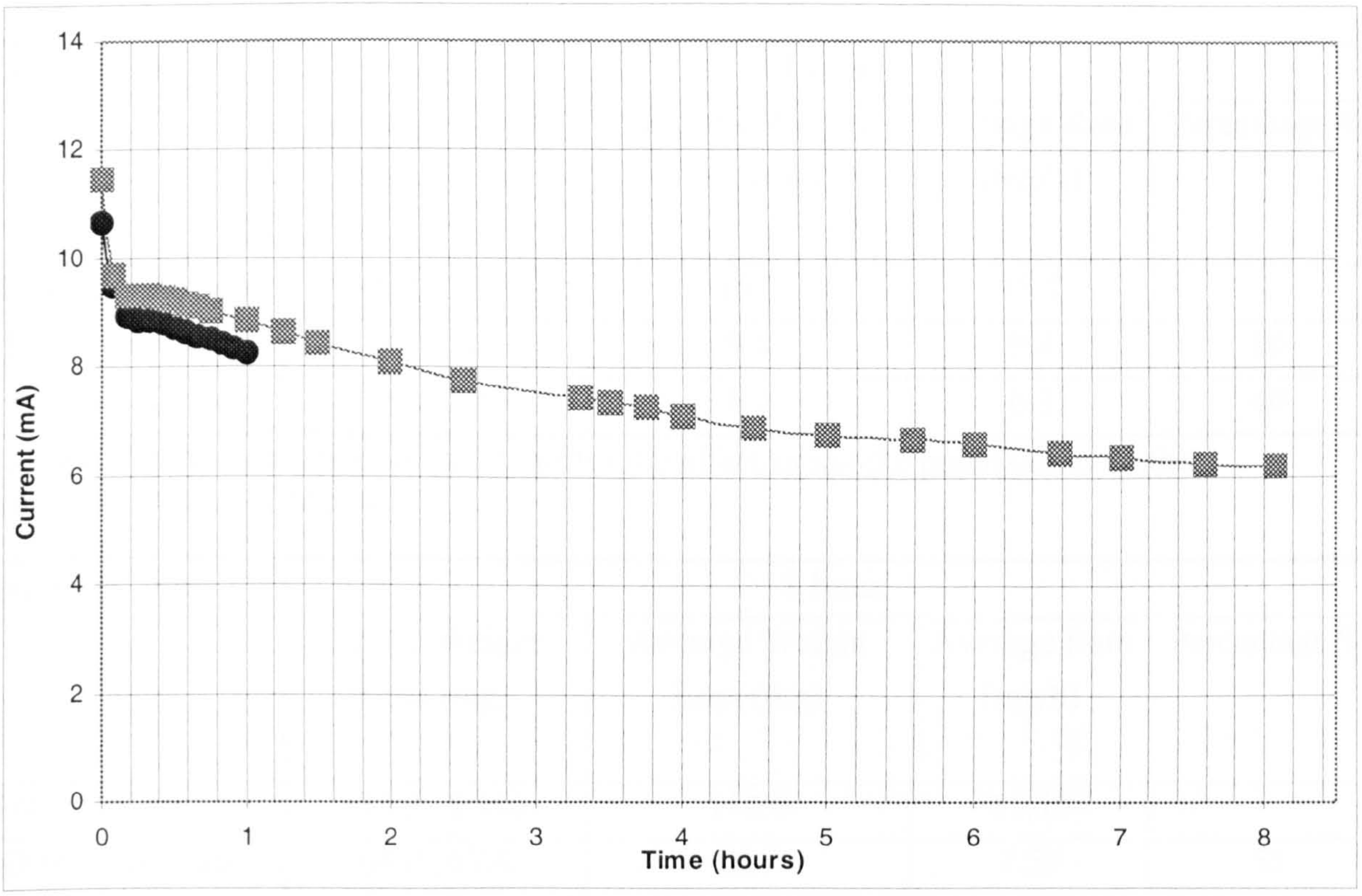

Figure 6.60. Current vs. Time curve for the effect of anodic polarisation on Marinel upon exposures of 1 and 8 hours under impinging velocity of 17m/s.

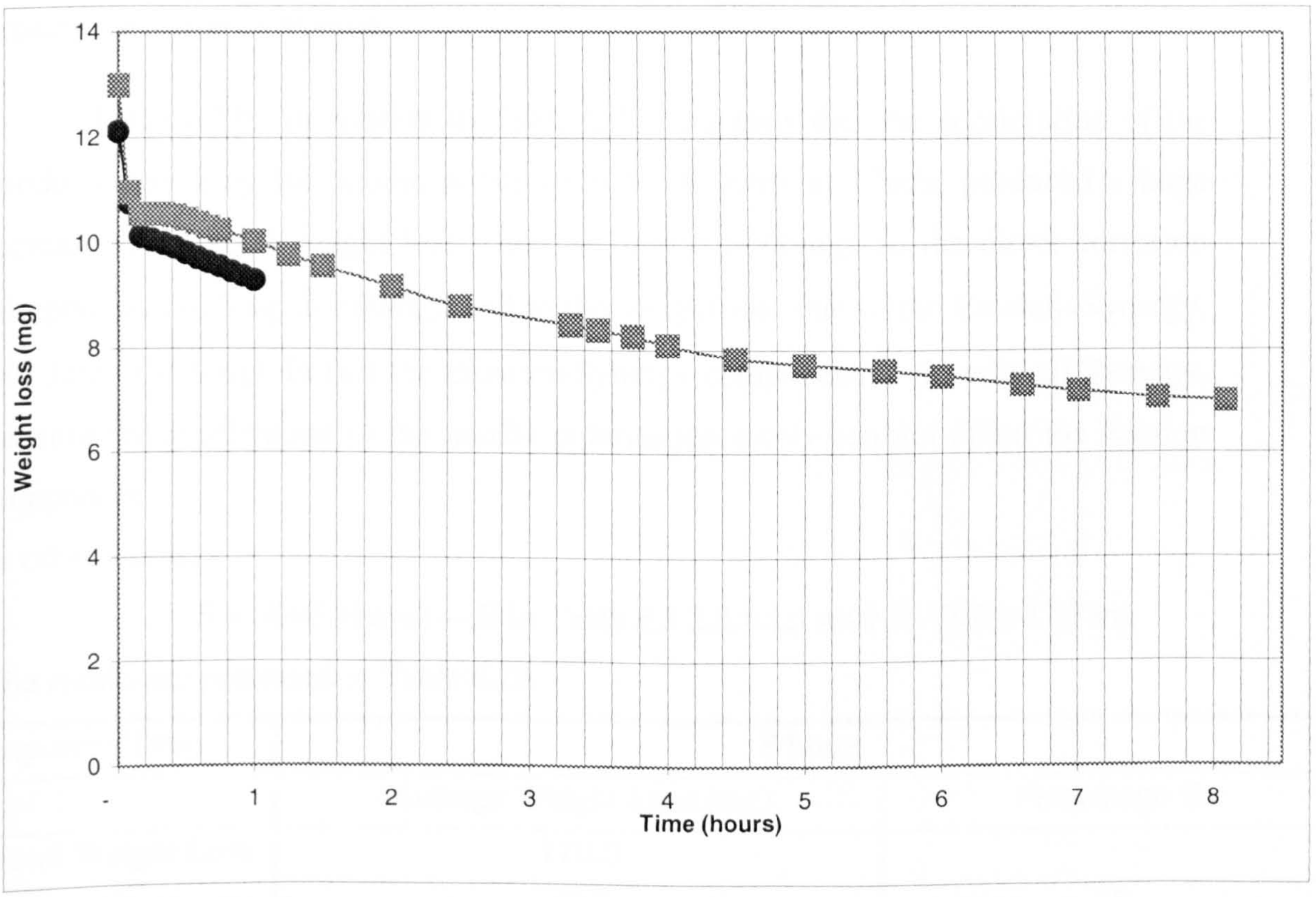

Figure 6.61. Weight losses vs. Time values for the effect of anodic polarisation on Marinel upon exposures of 1 and 8 hours under impinging velocity of 17m/s.

Exposure Time	**1 hour**			
	Actual Weight Loss (mg)	Average Weight Loss (mg)	Average Rate (mg/h)	Percentage %
Total Weight Loss	16.7 , 14.6	15.7	15.7	
Direct Corrosion	10.0 , 8.9	9.4	9.4	60
Erosion + Synergy	6.68 , 5.68	6.3	6.3	40

Table 6.27a. Weight losses after 1 hour for the effect of anodic polarisation on the erosion corrosion of Marinel.

Exposure Time	**8 hour**			
	Actual Weight Loss (mg)	Average Weight Loss (mg)	Average Rate (mg/h)	Percentage %
Total Weight Loss	113.2 , 106.8	110.0	13.75	
Direct Corrosion	64.0 , 57.4	60.7	7.59	55
Erosion + Synergy	49.2 , 49.4	49.3	6.16	45

Table 6.27b. Weight losses after 8 hours for the effect of anodic polarisation on the erosion corrosion of Marinel.

Table 6.27b. in relation to Table 6.25., suggests that the acceleration of the anodic reaction by the anodic polarisation for 8 hours at 17m/s, produced a huge increase to the total weight loss value, (<1mg to >100mg), to the direct corrosion component, (≈0.5mg to ≈60mg), and to the weight loss due to the Erosion+Synergy, (≈0.3mg to ≈50mg). In fact the Erosion+Synergy component is virtually all Synergy, because the acceleration of the anodic polarisation surely can not affect the Erosion component.

In other words,

$$S = (E+S \text{ above}) - (E \text{ in Table } 6.3.2.2.4.1.) = 49.3 - 0.2 = 47.3 \text{ mg}$$

The results are presented in Table 6.28.

Exposure Time	**8 hour**	
	Average Weight Loss (mg)	Percentage %
Total Weight Loss	110.0	
Direct Corrosion	60.7	55
Erosion	0.2	2
Synergy	47.3	43

Table 6.28. Weight losses after 8 hours for the effect of anodic polarisation on the erosion corrosion of Marinel.

6.3.2.4. *Microscopical examination.*

6.3.2.4.1. Low Impinging Velocities (2.38m/s, 4.5m/s).

V = 2.38m/s, Exposure time = 4 hours.

Specimens exposed to erosion-corrosion conditions without any electrochemical intervention, (relevant photographs labelled "T.W.L.").

With the unaided eye, two distinct zones were apparent, (Figure 6.62). There was a central deep-blue coloured region of about 8mm diameter. The remainder of the specimen had a red-brown coloured film on the surface.

Figure 6.63. shows that the film in the zone directly under the jet was relatively thick but discontinuous. The red-brown film at the outside area, Figure 6.64., is clearly thicker than on Cu-10%Ni, Figure 6.27. This difference between the two metals suggests that the effect of hydrodynamics produce thicker films on Marinel. Both films on Marinel, (at the centre and the outside zone), were of an acicular nature. Evident under the outer film and also in the regions between the thicker film in the directly-impinged zone was an etched structure with some white particles. These Ni/Nb particles are evident everywhere even direct under the jet, Figure 6.65.

Specimens subjected to continuous cathodic protection, (relevant photographs labelled "C.P.").

These specimens appeared to be completely unaffected by the test; i.e. no evidence of any damage or surface films, Figure 6.66.

Specimens subjected to erosion-corrosion with final anodic polarisation, (relevant photographs labelled "A.P.").

The final anodic polarisation appeared to have generated a more extensive film for both areas; under the jet and further outside.

V = 4.5m/s, 4mm nozzle, Exposure time = 4 hours.

Specimens exposed to erosion-corrosion conditions without any electrochemical intervention.

These conditions produced a similar surface appearance as found at 2.38m/s with the slight exception that the central zone, covered with the patchy film, Figure 6.67., was of larger diameter, 10mm, (as opposed to about 8 mm at the lower velocity). As Figure 6.68. suggests the more continuous film covering the rest of the surface is not quite as thick as the patchy film at the centre. Figure 6.69. and Figure 6.70 show at high magnification the central and the outer zones respectively with some light particles and some comets.

Specimens subjected to continuous cathodic protection.

As for the 2.38m/s specimens, Figure 6.71. demonstrates a negligible attack, which agrees with the weight loss (Table 6.19.) results, and proves that the Marinel is very largely unaffected under cathodic protection conditions at these low velocities.

Specimens subjected to erosion-corrosion with final anodic polarisation.

The final anodic polarisation appears to have produced a partial black film under the jet, generally similar to that on unpolarised specimens, but there is evidence of more etching attack at the uncovered regions. This is evident in Figure 6.72. which also reveals an array of light-coloured particles, which may consist of pits, or film nuclei, or precipitate particles. The rest of the surface had a film on the surface not quite as thick as the patchy film in the centre.

V = 4.5m/s, 1mm nozzle, Exposure time = 4 hours.

Specimens exposed to erosion-corrosion conditions without any electrochemical intervention.

With this nozzle size, there were three regions apparent on the specimen; a central zone of approximately 4mm diameter; an intermediate zone of approximately 15mm diameter with a further outside zone. These are shown in the left specimen in Figure 6.74.

Under the microscope the central zone structure consisted of discontinuous film, identical to the central region on the 4mm nozzle, (Figure 6.67.), the intermediate region comprised a more continuous but thinner film identical to the outer region of the 4mm nozzle, Figure 6.68. The outer zone appeared unattacked except of pits some of which were associated with comets, Figure 6.73.

Specimens subjected to continuous cathodic protection.

With the unaided eye there was no evidence of corrosion attack, right specimen in Figure 6.74. Under the microscope the appearance of the surface was very similar to the 4mm nozzle, Figure 6.71, but some shallow pits scattered randomly all over the specimen..

Specimens subjected to erosion-corrosion with final anodic polarisation.

The specimen was very similar to that produced in the test with the 4mm nozzle.

6.3.2.4.2. High Impinging Velocities (17m/s, 86m/s).

V = 17m/s, Exposure time = 4 hours.

Specimens exposed to erosion-corrosion conditions without any electrochemical intervention.

With the unaided eye a structure of different zones of attack was not distinctly evident, but under the microscope a complex picture of different types of film formation was apparent. In the centre of the specimen the etched structure can be seen but is clearly covered by a general thin film, Figure 6.75.. Additionally in some parts of the centre, there are white acicular, Figure 6.76. features which seem to represent another film. Yet another feature in the centre was the black patches and particles, some of which are also evident in Figure 6.76., but these patches were more acicular towards outside the directly impinged zone, Figure 6.77.. The outer region of the specimen was covered by a darker patchy film, Figure 6.78., in between which the visible etched structure was still visible.

Specimens subjected to continuous cathodic protection.

Like all the previously-described, cathodically protected specimen of Marinel, there was no evidence of corrosion attack but pits randomly distributed everywhere.

Specimens subjected to erosion-corrosion with final anodic polarisation.

There were very similar to the unpolarised specimens except more severe etching attack under the jet between the black film patches, and also more severe etching attack at the outer region.

V = 17m/s, Exposure time = 8 hours.

Specimens exposed to erosion-corrosion conditions without any electrochemical intervention.

With the unaided eye, two distinct zones were evident; a central lighter region, approximately 11 mm diameter, surrounded by a darker region, Figure 6.79. The surface was very similar to the 4-hour specimen, with a more continuous black film outside the jet, Figure 6.80., but the etched structure was evident through this film, Figure 6.81.. Also present in the outer regions were some light-colour needles, Figure 6.82., passing through the more-general darker film. Figure 6.82, also shows the NiNb particles This demonstrates that these are not associated with any particular type of film.

In the region directly under the jet, there were needles Figure 6.80., and also discreet patches, Figure 6.83., of a black film in between, which there appeared to be a thinner, transparent film through which the etched structure was visible, Figure 6.83..

Analysis done on several particles on this specimen after the test, (Figure 6.84, Figure 6.85.), showed similar concentrations of Ni and Nb and lower concentrations of Cu, as in the as-received polished specimen. The analysis demonstrating this more clearly was:

Copper - %	Nickel - %	Niobium - %	Chromium - %
14.1	54.0	20.2	0.67

Table 6.29. Chemical analysis of a light particle after 8 hours impinging at 17m/s.

These particles were also evident on the polished as-received specimens as shown on Figure 5.3. and Table 5.7. Obviously the corrosion process serves to 'decorate' the particles.

As Figures 6.84. demonstrates the particles at the grain boundaries may make material vulnerable to integranular corrosion, but no evidence of that was found.

A further interesting observation of these particles, was that some of them appear to have a "duplex" structure. One such particle is shown in Figure 6.86., and spot analyses on the core and the rim of the particle are shown below at Table 6.30. Clearly it

is apparent that the constitution of these particles may vary somewhat. [Note: Actually Figure 6.86. and the two analyses were obtained on a Marinel specimen after 4 hours at 2.38m/s, but have been included here to support the comparison with Figure 5.3 and Table 5.7].

	Copper - %	Nickel - %	Niobium - %	Chromium - %
Core	3.7	38.0	55.6	1.1
Rim	5.1	56.2	32.2	0.5

Table 6.30. Chemical analysis of a duplex particle after 4 hours impinging at 2.38m/s.

Specimens subjected to continuous cathodic protection.

As normal, there was no corrosion attack evidence except pits everywhere. Figure 6.87., shows the areas outside the directly impinged zone and clearly some pits have comet's tails.

Specimens subjected to erosion-corrosion with final anodic polarisation.

The structure of the samples subjected to the final anodic polarisation appeared very similar to the unpolarised specimens, except more severe etching under the jet between the black patches, Figure 6.88..

V = 17m/s, Exposure time = 48 hours.

Specimens exposed to erosion-corrosion conditions without any electrochemical intervention.

The surface under the microscope displayed some clear hydrodynamics effects. The central region was covered by a multicolour - red, yellow, blue, green – film. Where the film has been removed, the etched structure of the substrate is more evident, Figure 6.89.. Also some white particles were apparent. Figure 6.90. shows the intermediate zone

covered by a red film with a very slight evidence of the grain structure and some possible evidence, (in the form of discreet dark spots), of pitting initiation underneath the film. The pitting initiation was less evident further outside, area which was covered by a thicker dark red brown film.

In order to obtain more information about the attack, the specimen was mounted in cross-section, but such examination confirmed that there was no evidence of intergranular attack.

Specimens subjected to continuous cathodic protection.

There was no evidence of corrosion attack, but pitting over the entire surface.

Specimens subjected to erosion-corrosion with final anodic polarisation.

This specimen looked very similar to the total weight loss specimen covered by a discontinuous dark film through which the etched structure can be seen, Figure 6.91. – very similar to the 6.81). There was also clear evidence of pits, more abundant at the centre, but some present also at the outside, Figure 6.92, Figure 6.93, Figure 6.94.

These pits were quite deep as can be indicated by the degree of out of focus in Figure 6.94., and with the clear implication that they did not form solely during the final brief anodic polarisation.

V = 86m/s, Exposure time = 4 hours.

Specimens exposed to erosion-corrosion conditions without any electrochemical intervention.

There was a number of different zones of attack after exposure under these conditions. Under the microscope it was difficult to detect any difference in the microstructure related to the different zones apparent to the unaided eye, and this observation was supported by the surface profile result which demonstrated no significant roughening, (Figure 6.95). The roughness value for the entire surface, R_a, was 0.06μm,

while the roughness value for the entire surface of an as-received polished specimen was R_a=0.02μm. Most of the surface appeared with a much more continuous but thinner yellow-black film, compared to the 17 m/s samples, Figure 6.96. At high magnification the etched structure underneath the film and pits were revealed, Figure 6.97..

Specimens subjected to continuous cathodic protection.

Big changes appeared compared to the previous conditions. There was some corrosion attack under the jet with a discontinuous black film, Figure 6.98.. Outside the jet, very mild etching appeared.

Specimens subjected to erosion-corrosion with final anodic polarisation.

Figure 6.99 displays a thicker multicolour film – red, green, blue, yellow – under the jet, but as Figure 6.100 suggests, a more mild attack with some light particles apparent at the outside area and the etched structure is visible underneath a thinner greenish film.

V = 86m/s, Exposure time = 8 hours.

Specimens exposed to erosion-corrosion conditions without any electrochemical intervention.

With the unaided eye there was some evidence of non-uniform hydrodynamics zones, Figure 101. The damage seems to be similar over the entire surface, i.e. no hydrodynamics effects on the damage, Figure 6.102, with a higher roughness value for the entire specimen R_a=0.16μm, than after 4 hours. This is in clear contrast to the situation in Cu-10%iNi, where the damage is clearly concentrated in the central regions and is more severe. Under the microscope, the central region was similar to the 4-hour specimen but with a thicker yellow film under the jet, (i.e. fairly continuous film), Figure 6.103.. At the centre of the specimen, directly under the jet, the grain structure under the

film can be seen, Figure 6.104.. At the outer region i.e. outside the directly impinged zone, the surface is subjected to intense attack underneath the thick film, Figure 6.105..

The roughening under the jet is slightly greater than elsewhere with a value, R_a=0.20μm, Figure 106.

Specimens subjected to continuous cathodic protection.

Several hydrodynamics rings appeared, Figure 6.101.. Figure 6.107. shows a discontinuous film under the jet, R_a=0.15μm ,but at high magnification, Figure 6.108., the grain structure at the uncovered bits is almost apparent. The outside area looks like a ring which was covered by a thick yellow film, R_a=0.09μm, as demonstrated in Figure 6.109.. Further outside the etched structure is visible, Figure 6.110..

Specimens subjected to erosion-corrosion with final anodic polarisation.

Like under continuous cathodic protection conditions several hydrodynamics rings appeared. A discontinuous film was evident under the jet, Figure 6.111., but severe pitting attack was revealed at high magnification, Figure 6.112.. Figure 6.113. shows a ring zone covered by a thick yellow film, R_a=0.22μm, with a more continuous black film just outside. The etched structure with severe pitting covered the rest of the surface, Figure 6.114..

6.3.2.4.3. Acceleration of the Anodic reaction by the Anodic Polarisation,

(relevant photographs labelled "A.R.")

V = 17m/s, Exposure time = 1 hour.

The entire surface was covered by a black yellow film. Figure 6.115. and Figure 6.116., show the etched structure and some pits, which showed up everywhere. Conclusively the surface roughening was almost uniform over the entire surface, R_a=0.33μm.

V = 17m/s, Exposure time = 8 hour.

The damage was more severe than for 1 hour. The entire surface was covered by a thicker black yellow film and as Figure 6.117 demonstrates at high magnification, the surface appears to be almost amorphous. Figure 6.118 shows significant surface roughening over the entire surface, R_a=0.69μm, but with a slight indication that the roughening is greater at the central regions, R_a=0.77μm, than at the outside. Indeed the roughness over the whole surface was so great that it was impossible to obtain good general focus with the light microscope, (Figure 6.118).

When the specimen was mounted in cross-section and examined under the microscope, no evidence of significant intergranular attack was found.

Figure 6.62. Marinel, V=2.38m/s – 4mm nozzle, 4 hours, T.W.L. Two distinct zones were apparent.

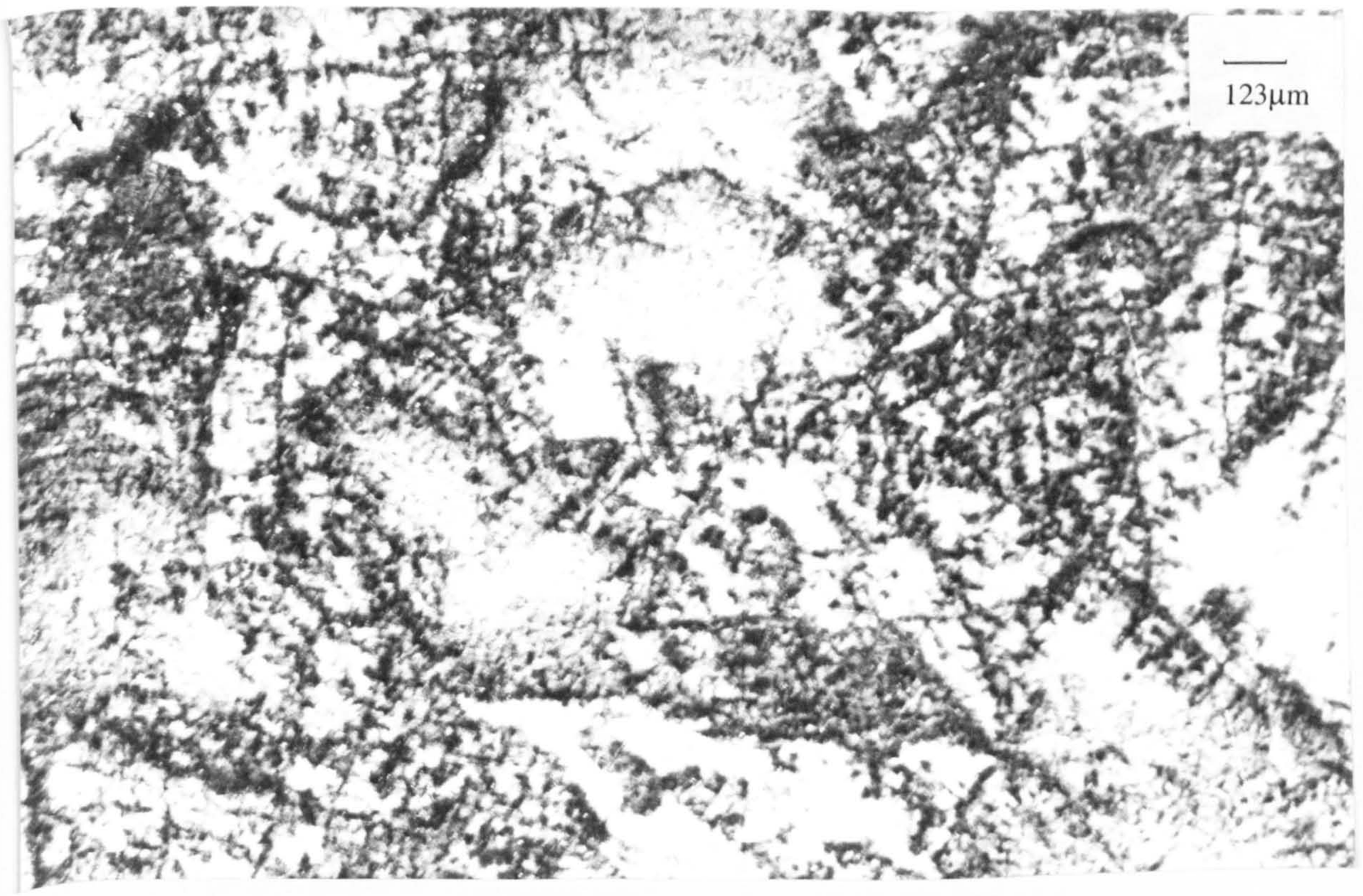

Figure 6.63. Marinel, V=2.38m/s – 4mm nozzle, 4 hours, T.W.L. The thick but discontinuous film directly under the jet.

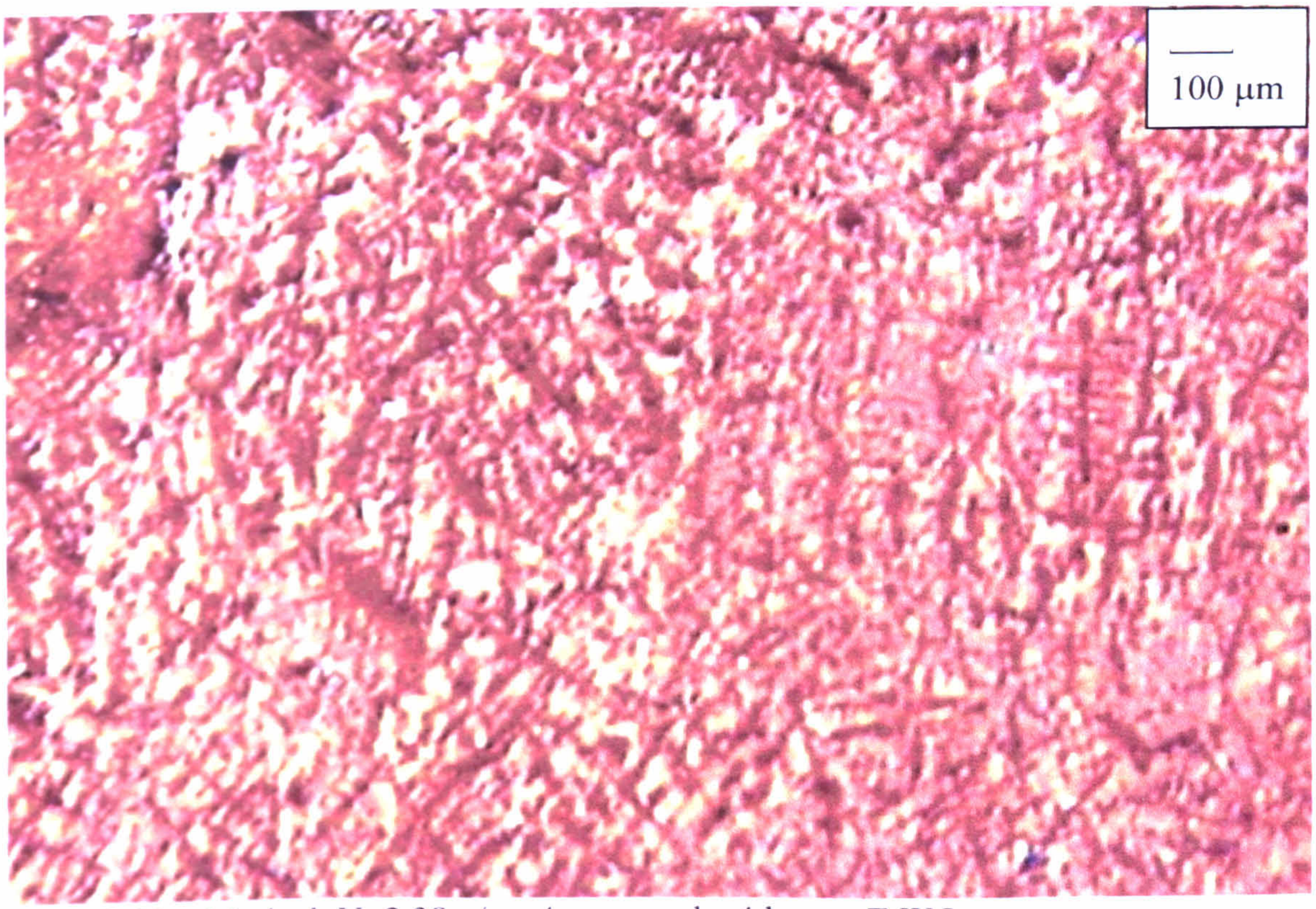

Figure 6.64. Marinel, V=2.38m/s – 4mm nozzle, 4 hours, T.W.L.
The red-brown film which covered the outside area.

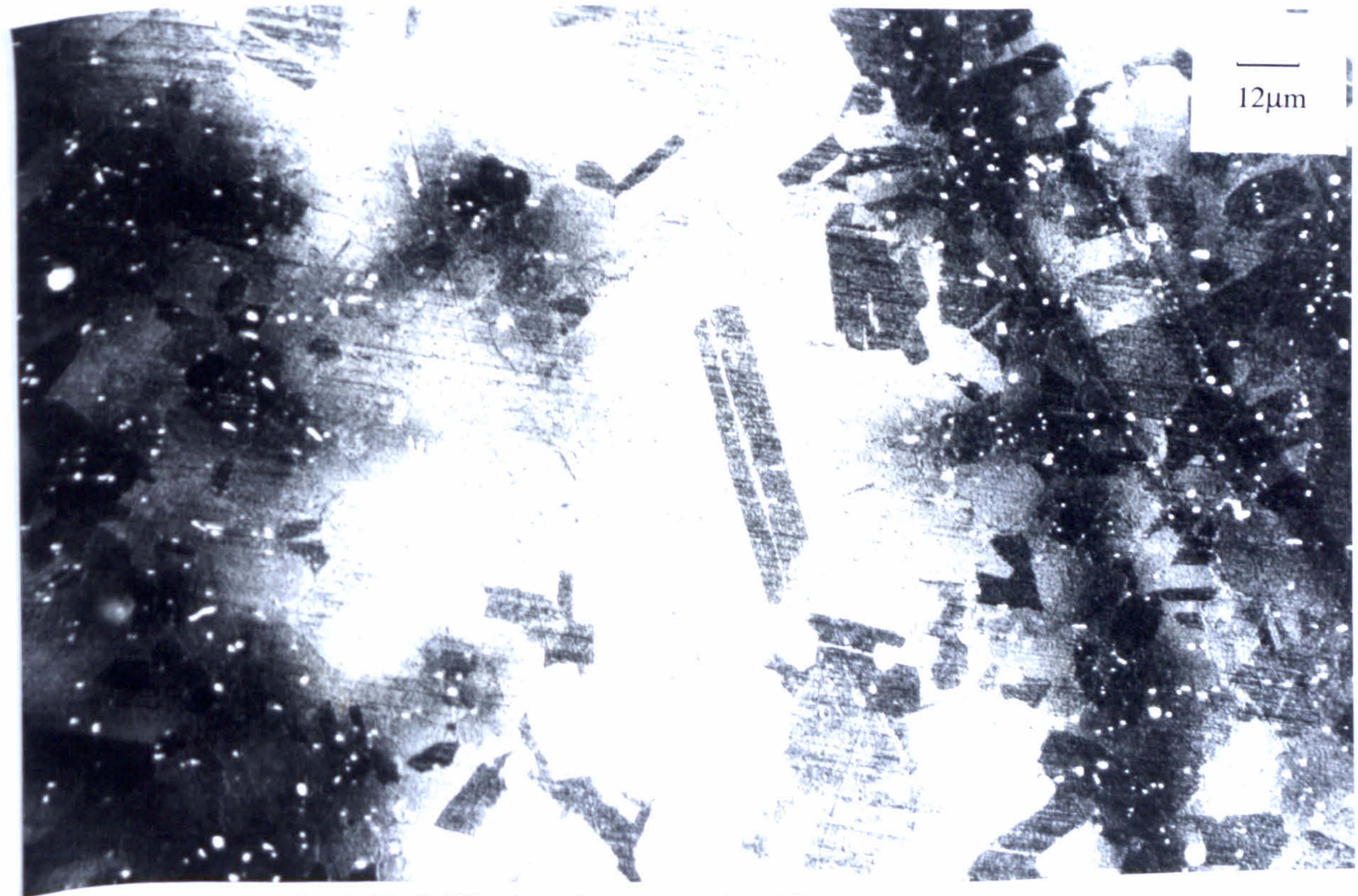

Figure 6.65. Marinel, V=2.38m/s – 4mm nozzle, 4 hours, T.W.L.
The Ni/Nb particles are evident even direct under the jet.

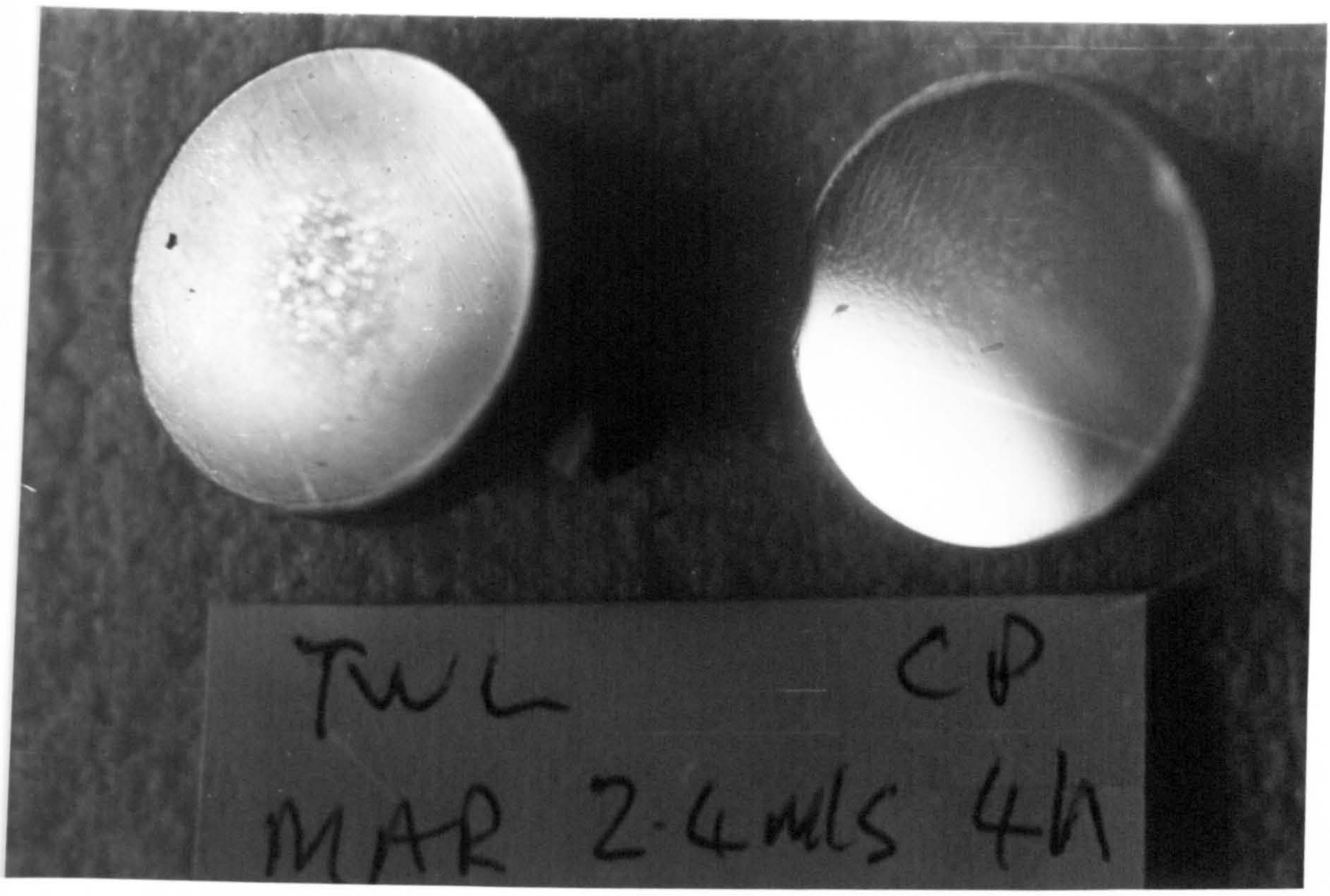

Figure 6.66. Marinel, V=2.38m/s – 4mm nozzle, 4 hours, C.P.
No evidence of damage. T.W.L. at the left, C.P. at the right.

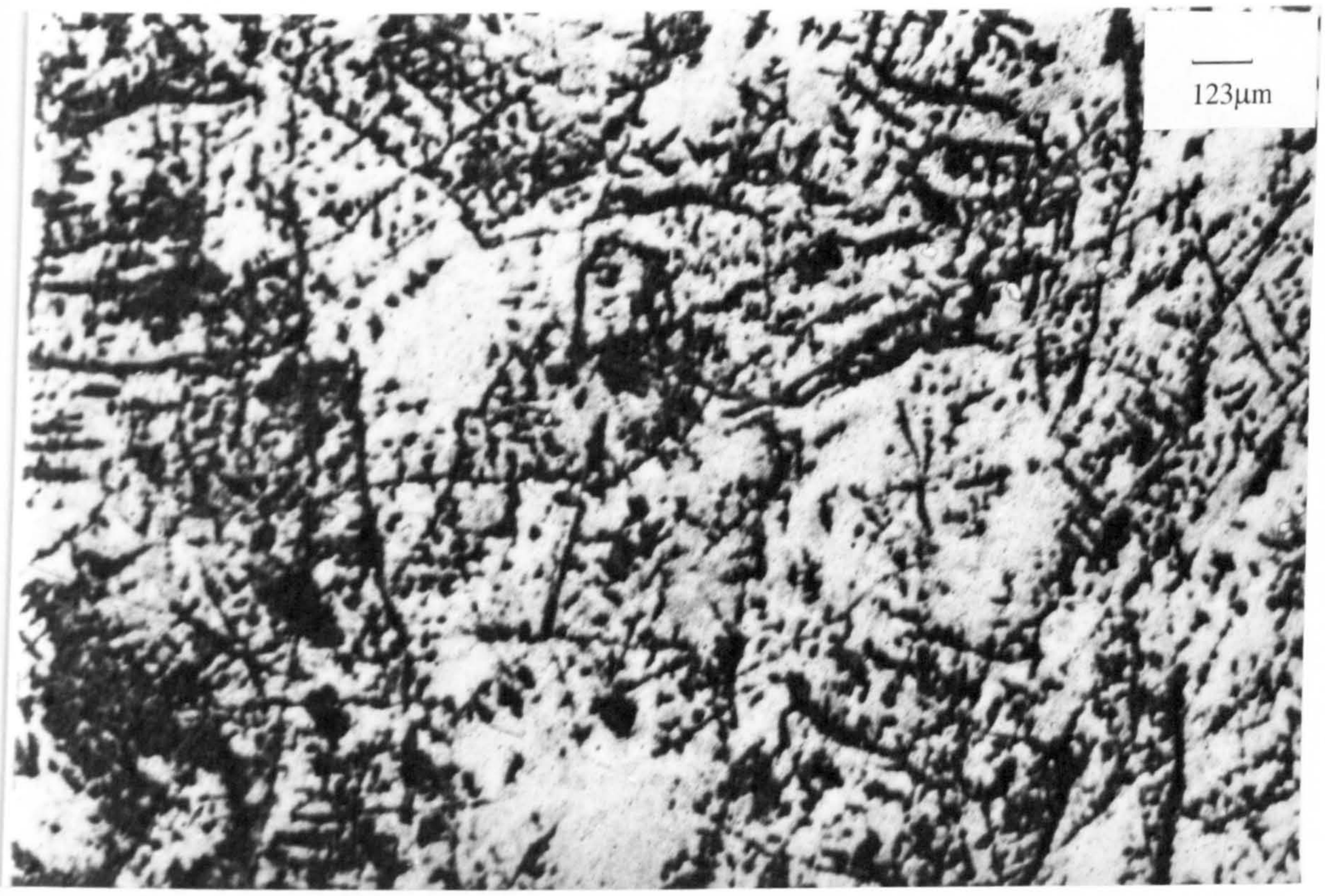

Figure 6.67. Marinel, V=4.5m/s – 4mm nozzle, 4 hours, T.W.L.
A patchy film covered the central zone.

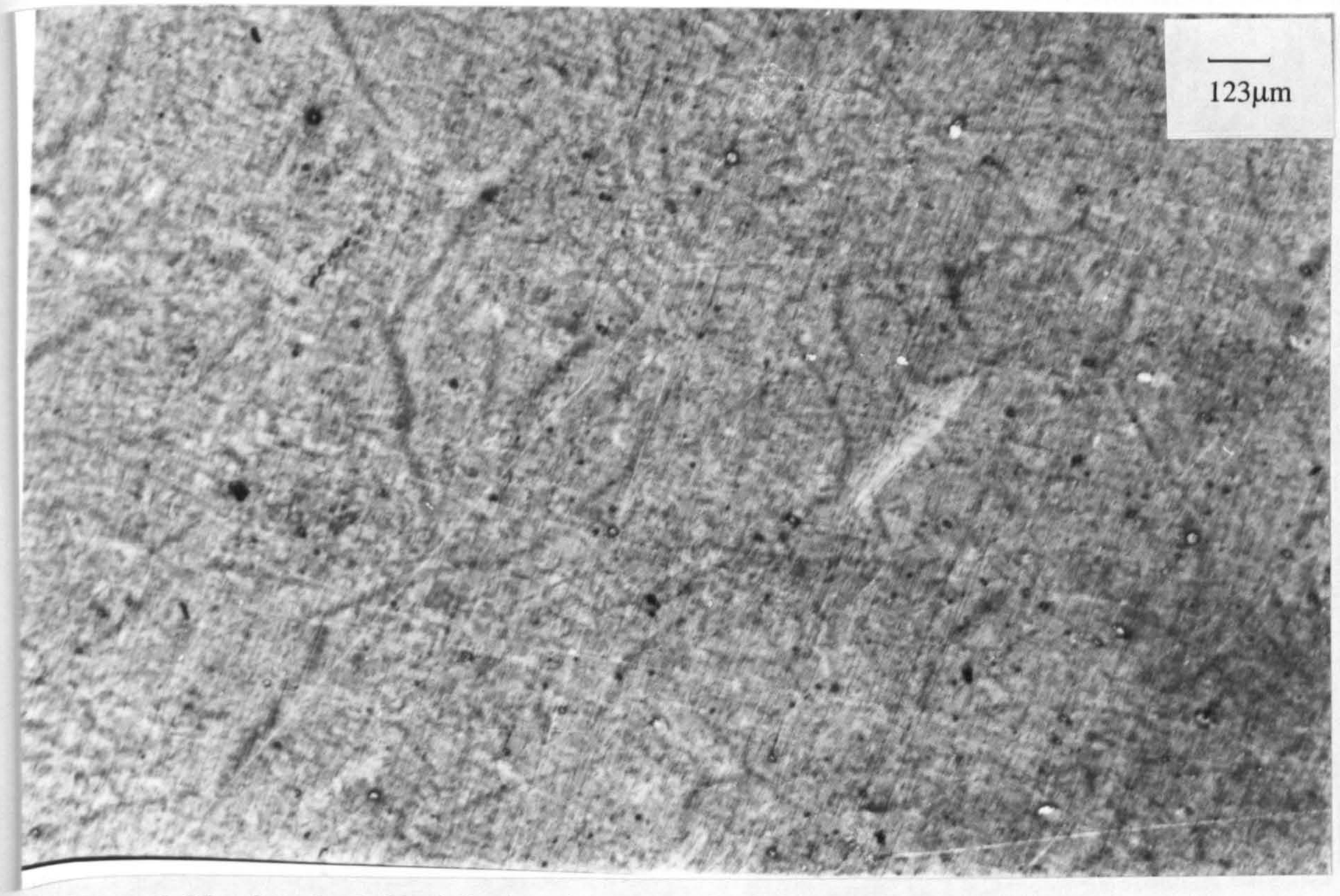

Figure 6.68. Marinel, V=4.5m/s – 4mm nozzle, 4 hours, T.W.L.
A patchy film, (not as thick as at the centre), covered the outside area.

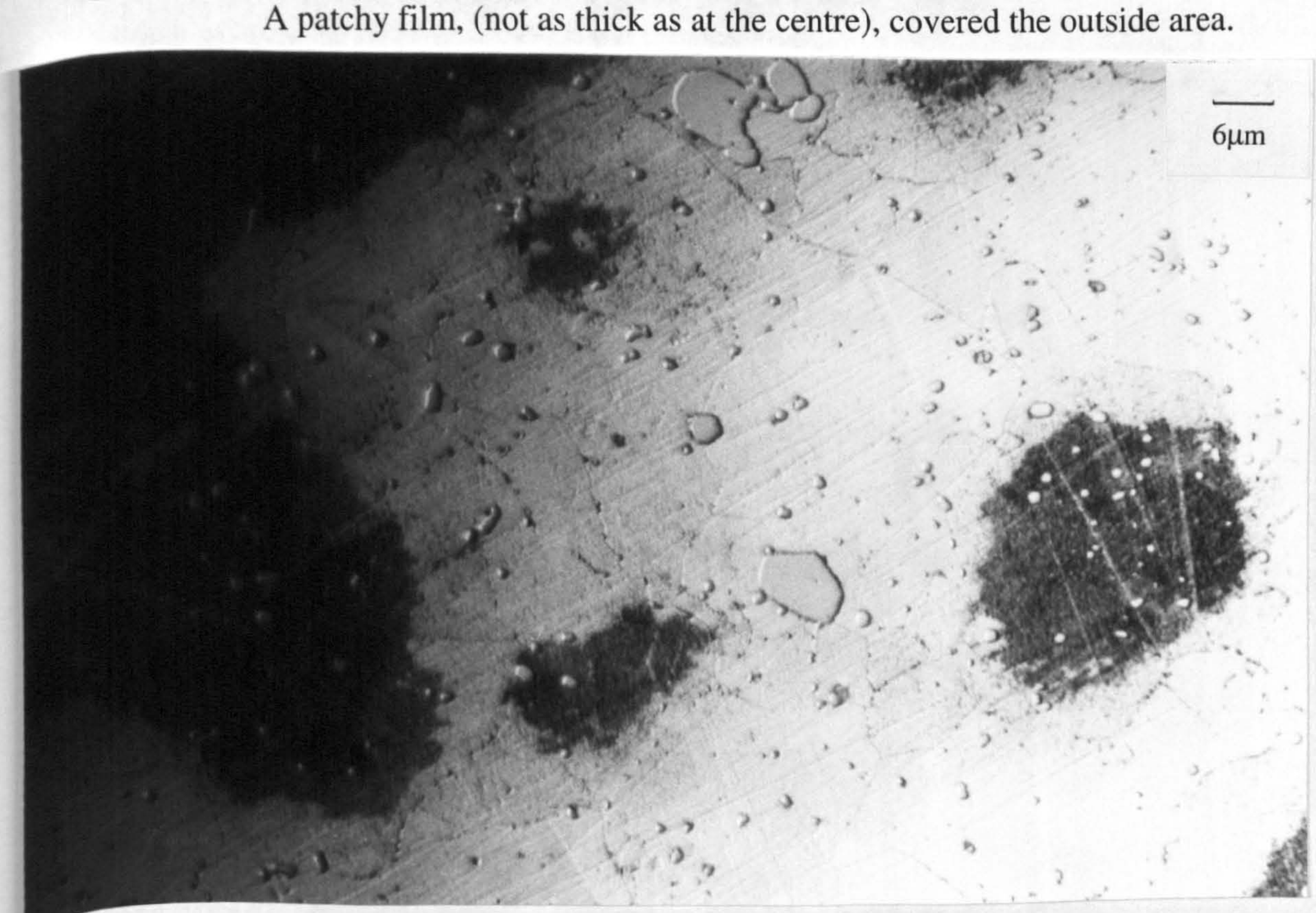

Figure 6.69. Marinel, V=4.5m/s – 4mm nozzle, 4 hours, T.W.L.
At high magnification the central zone.

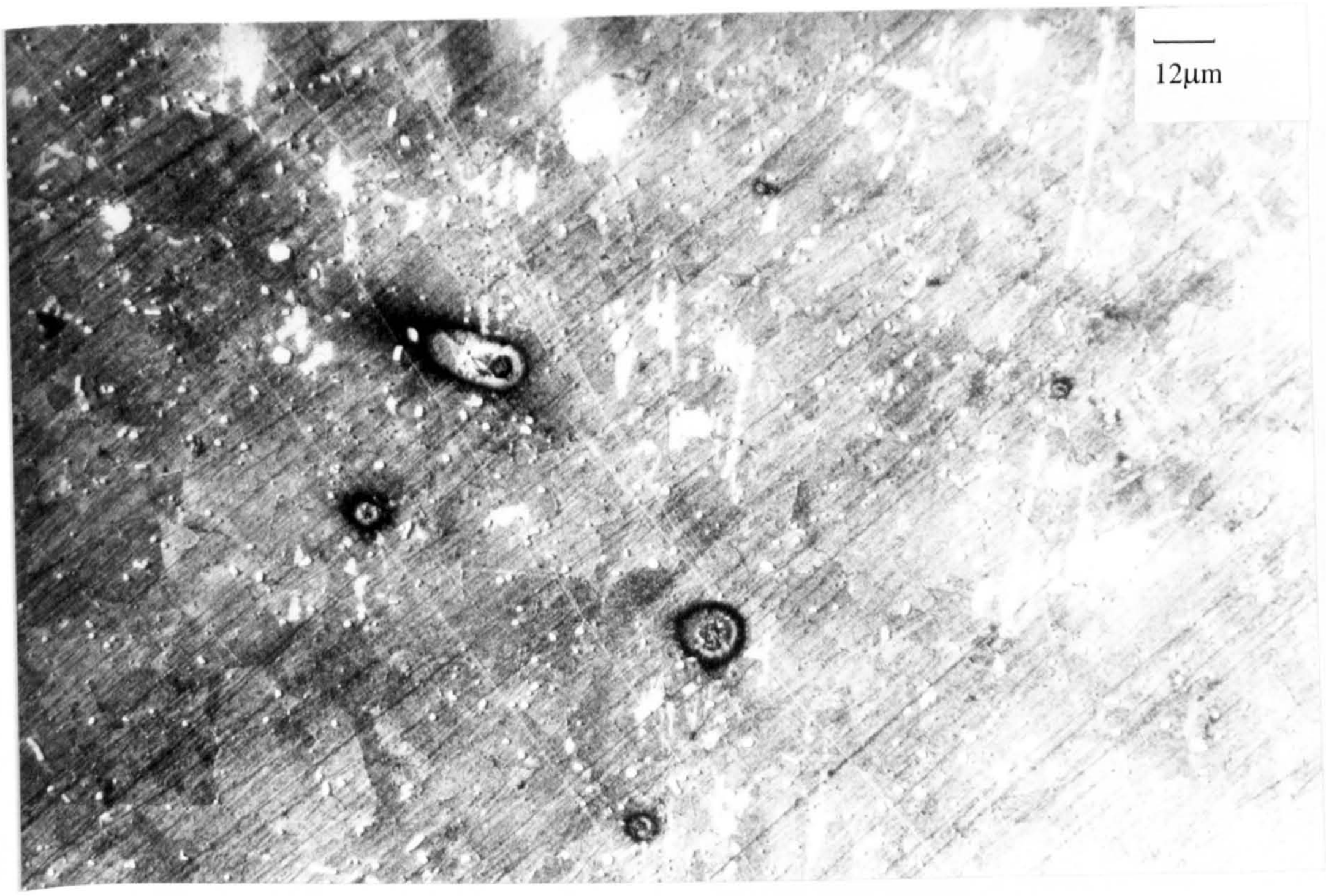

Figure 6.70. Marinel, V=4.5m/s – 4mm nozzle, 4 hours, T.W.L.
At high magnification the outside zone.

Figure 6.71. Marinel, V=4.5m/s – 4mm nozzle, 4 hours, C.P.
Negligible attack on the surface of the specimen.

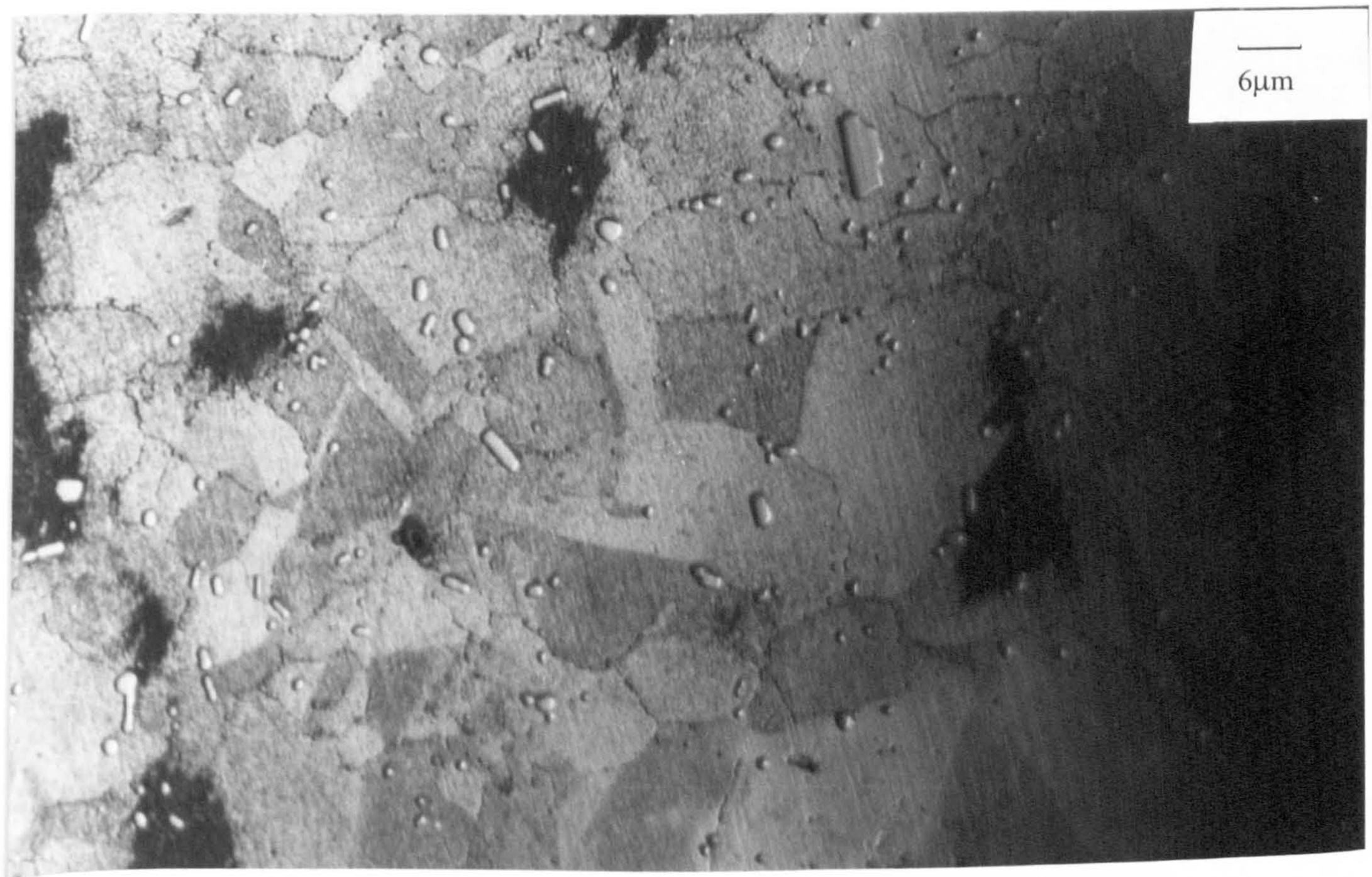

Figure 6.72. Marinel, V=4.5m/s – 4mm nozzle, 4 hours, A.P.
Partial black film under the jet. Etching attack at the uncovered regions.

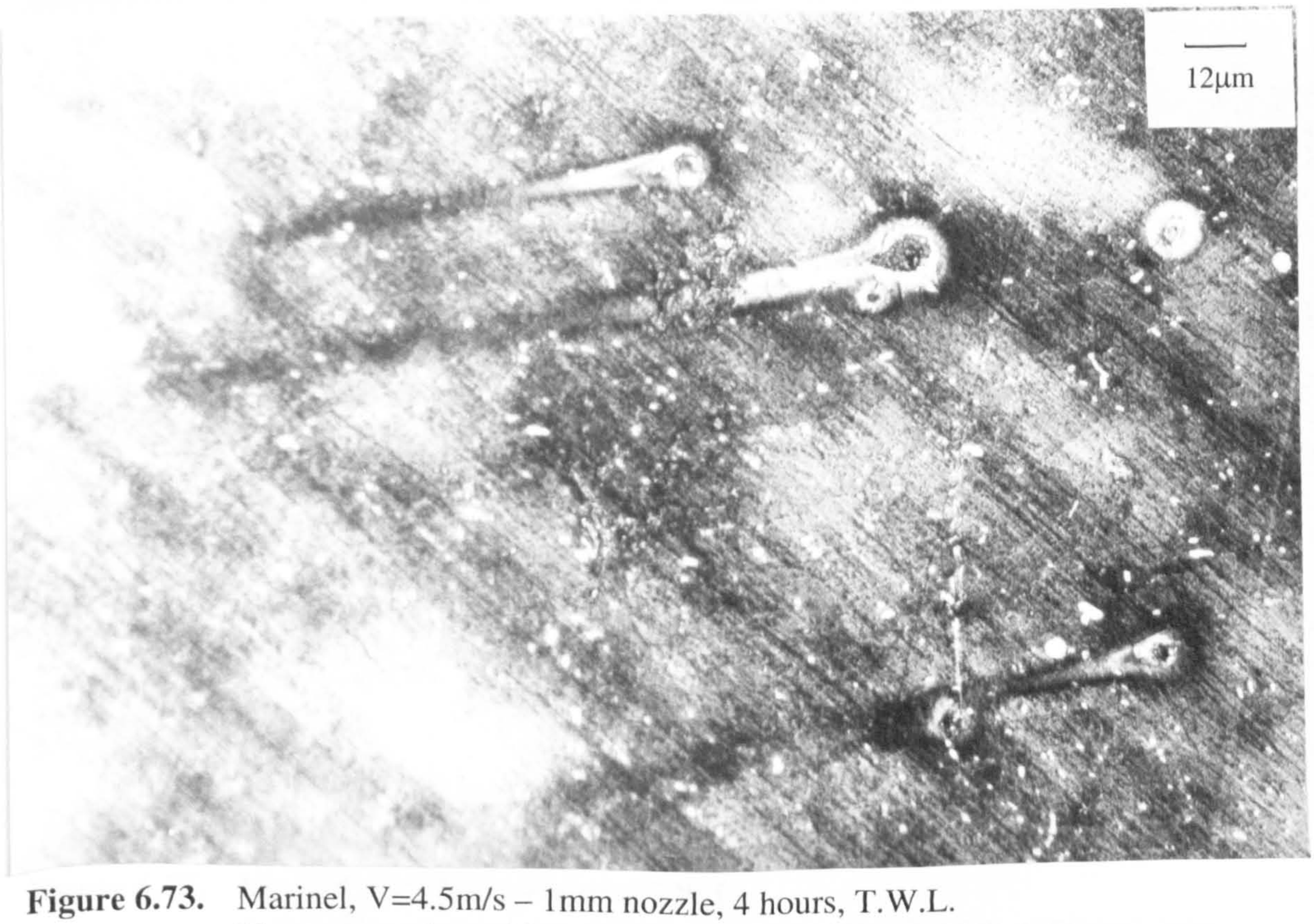

Figure 6.73. Marinel, V=4.5m/s – 1mm nozzle, 4 hours, T.W.L.
The outer region with some pits and comets.

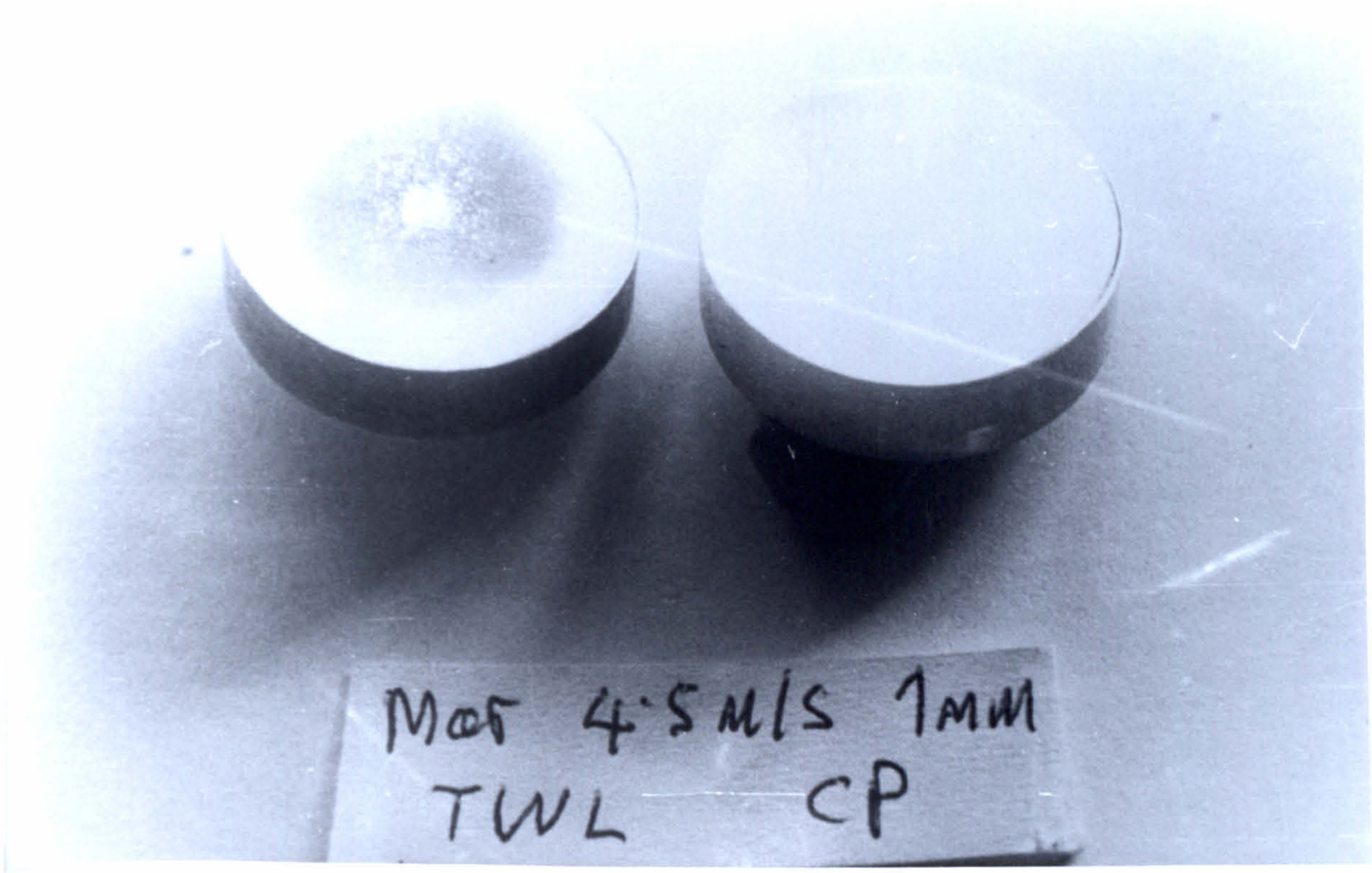

Figure 6.74. Marinel, V=4.5m/s – 1mm nozzle, 4 hours, T.W.L., C.P.
The left specimen is the T.W.L., and the right the C.P. specimen.

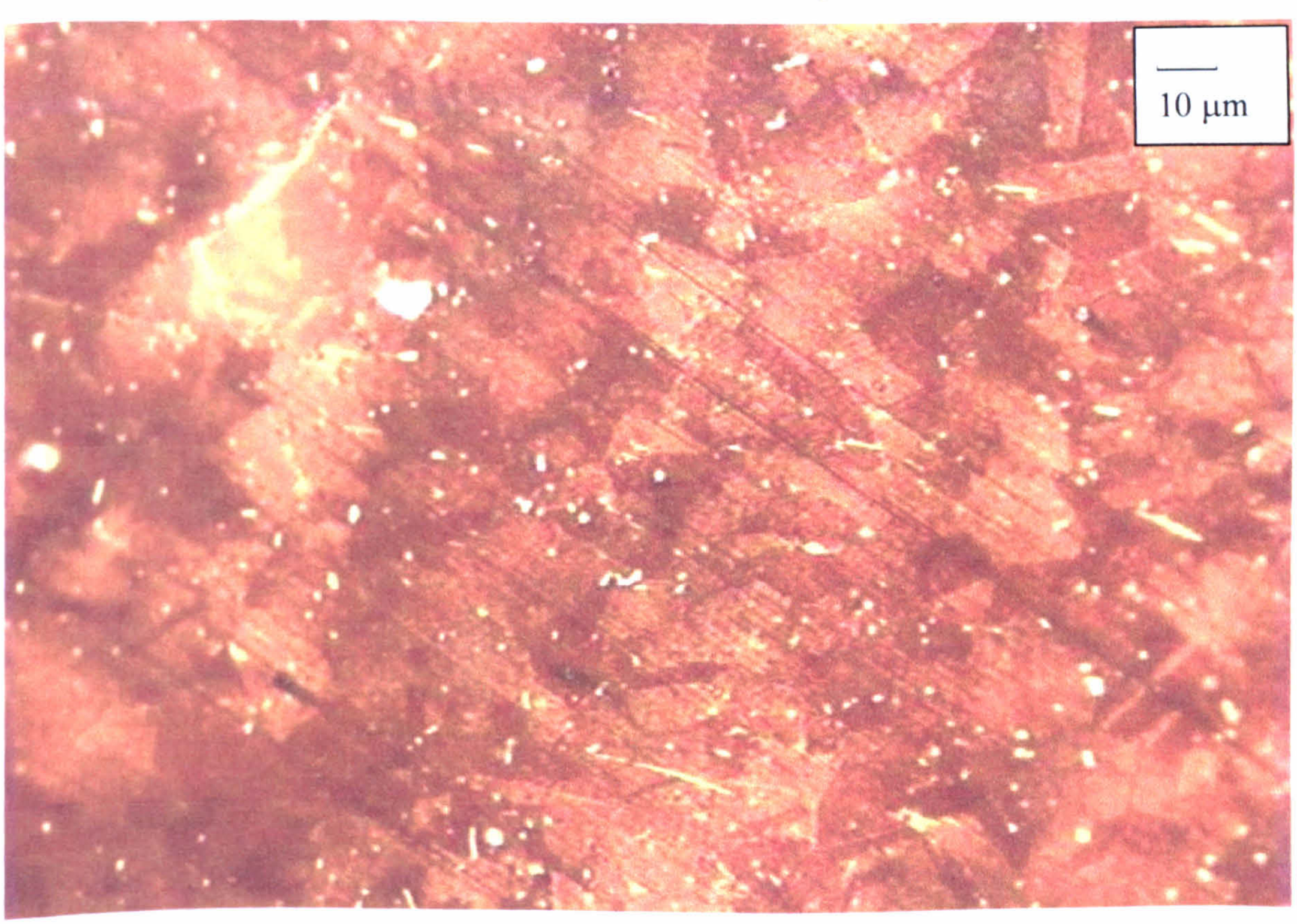

Figure 6.75. Marinel, V=17m/s, 4 hours, T.W.L.
A thin film covered the etched structure at the directly impinged zone.

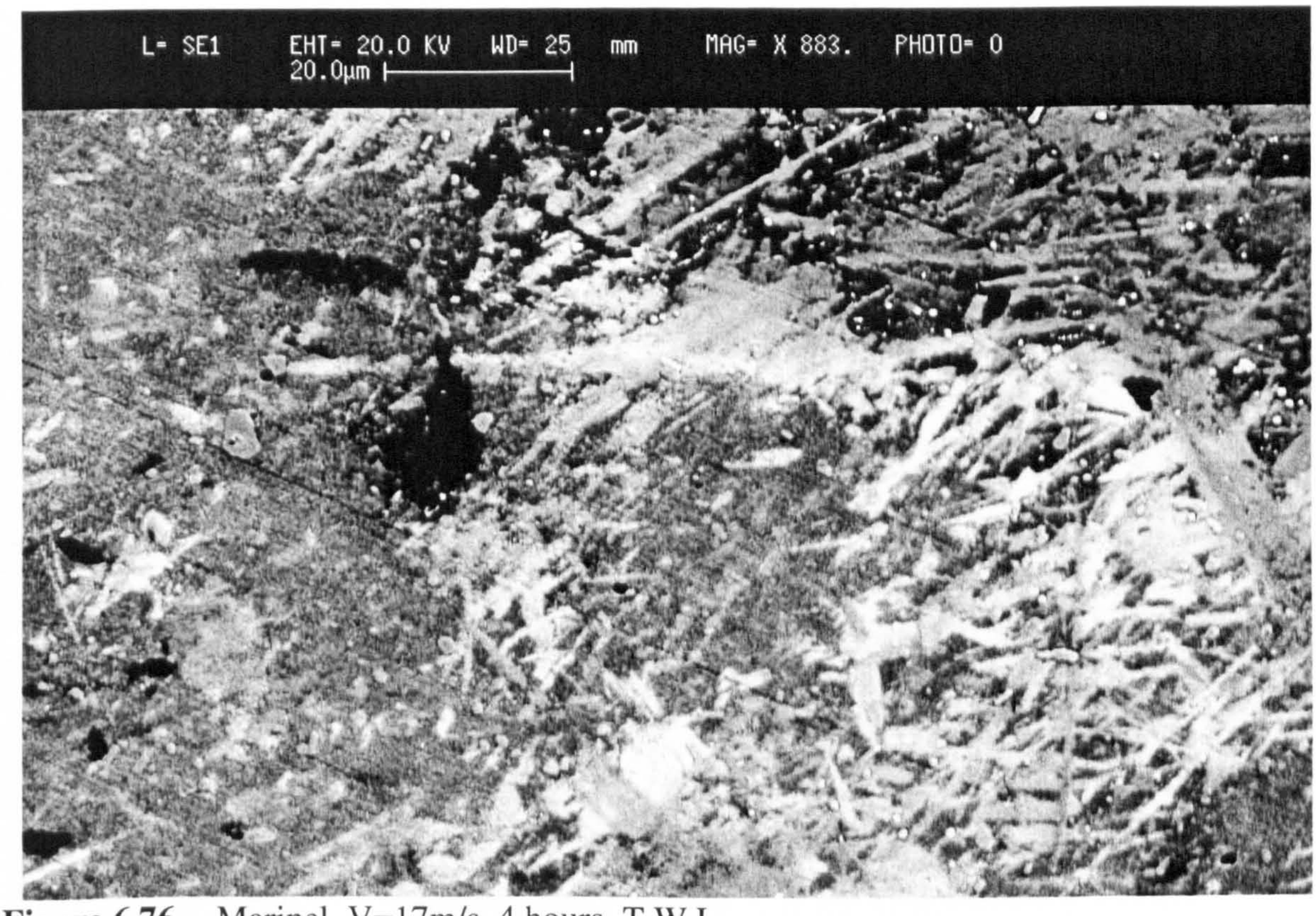

Figure 6.76. Marinel, V=17m/s, 4 hours, T.W.L.
At the centre some white acicular features, which represent another film.

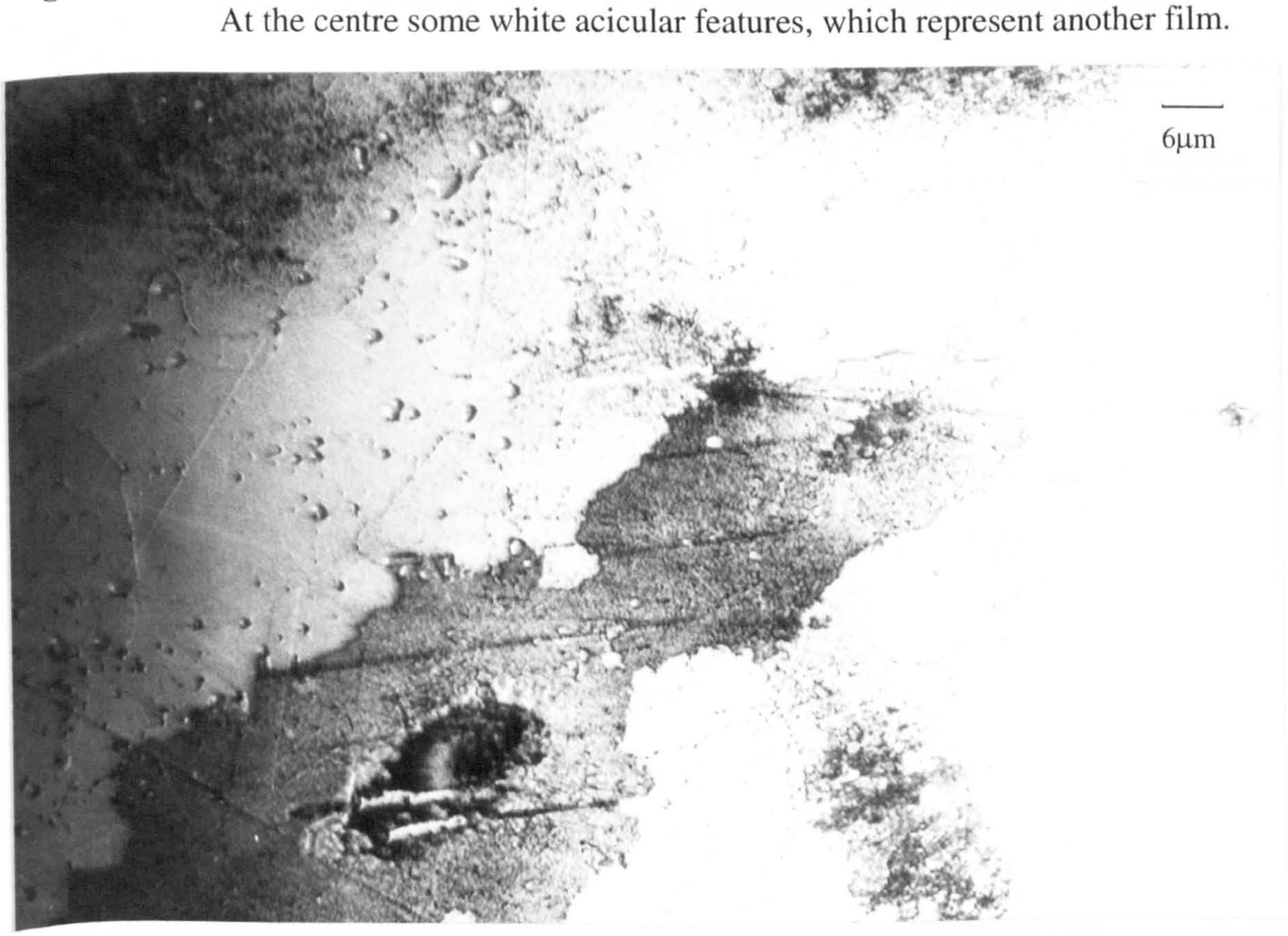

Figure 6.77. Marinel, V=17m/s, 4 hours, T.W.L.
Some black patches and particles at the centre.

Figure 6.78. Marinel, V=17m/s, 4 hours, T.W.L.
The darker patchy film at the outer regions with the etched structure.

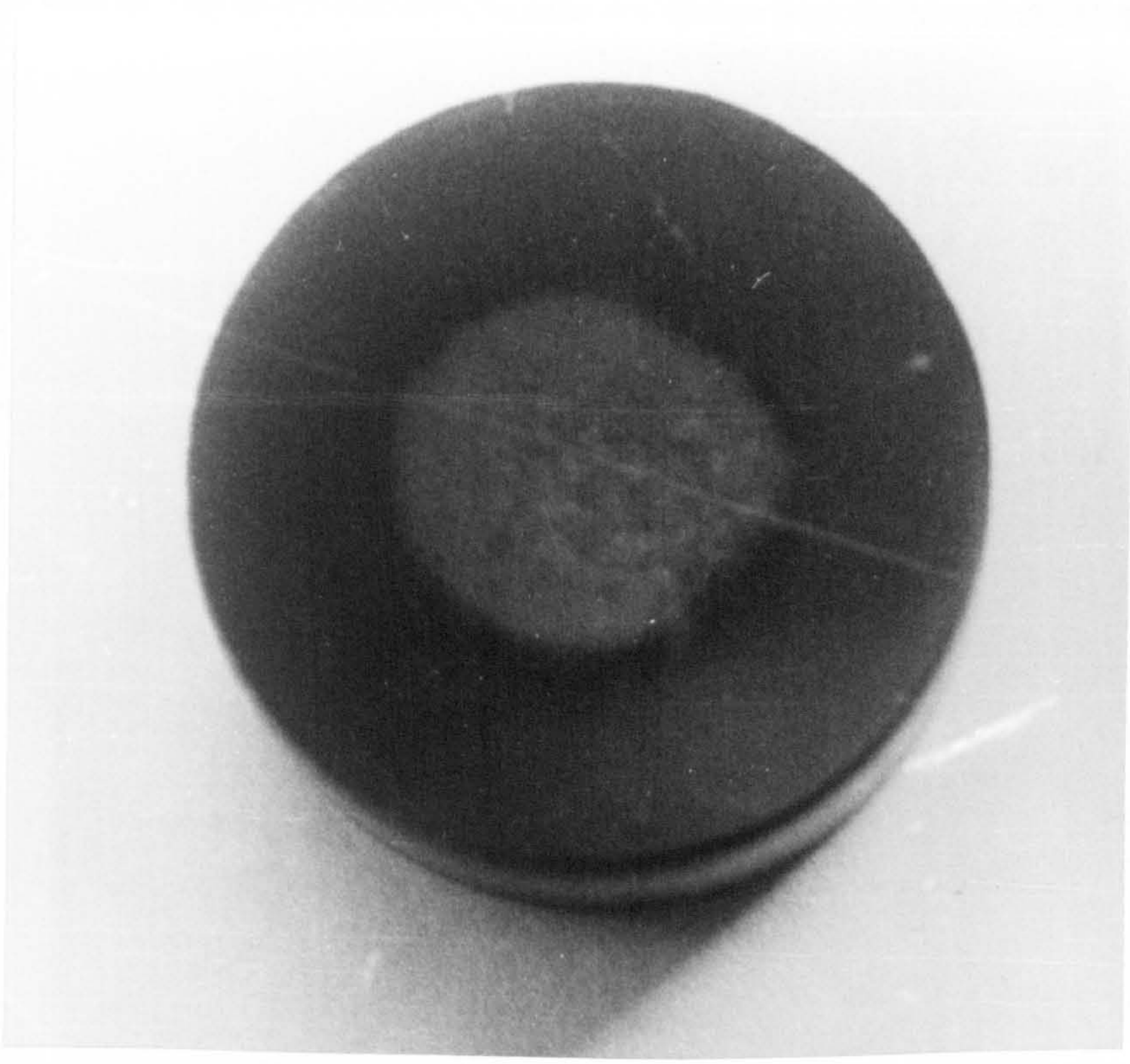

Figure 6.79. Marinel, V=17m/s, 8 hours, T.W.L.
Two clear hydrodynamic zones.

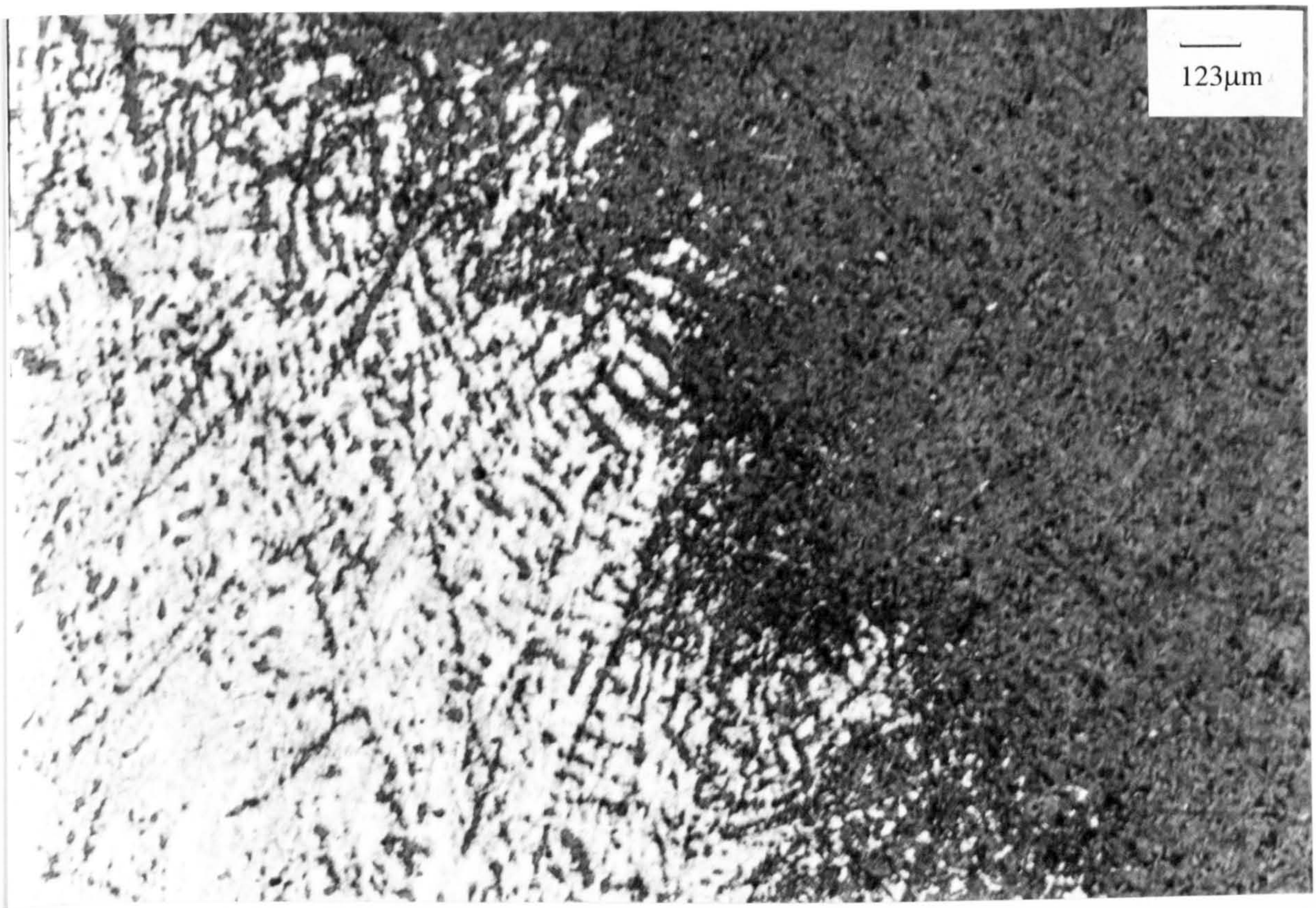

Figure 6.80. Marinel, V=17m/s, 8 hours, T.W.L.
A more continuous black film on the right, outside the jet.

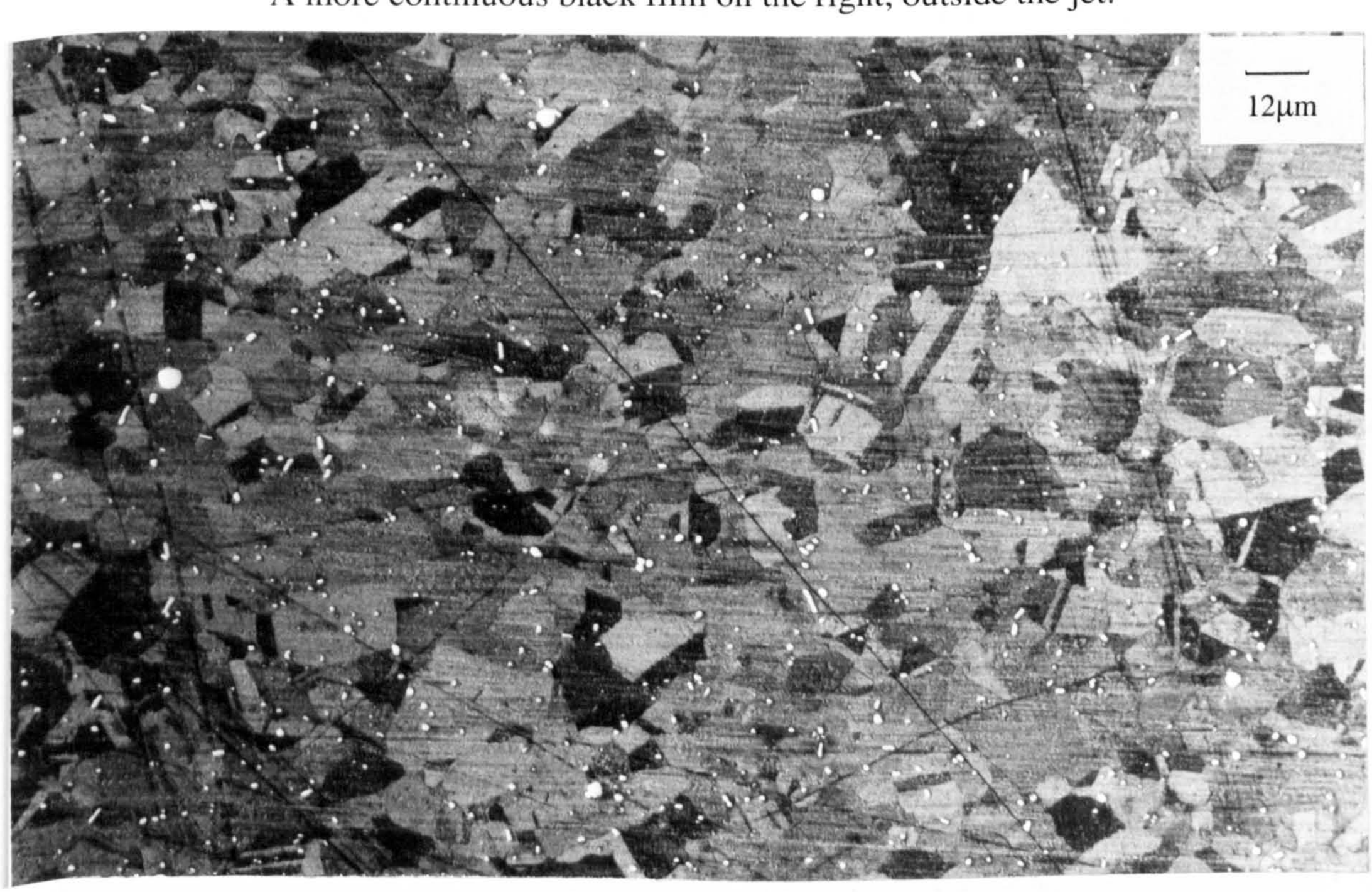

Figure 6.81. Marinel, V=17m/s, 8 hours, T.W.L.
The etched structure evident underneath the black film outside the jet.

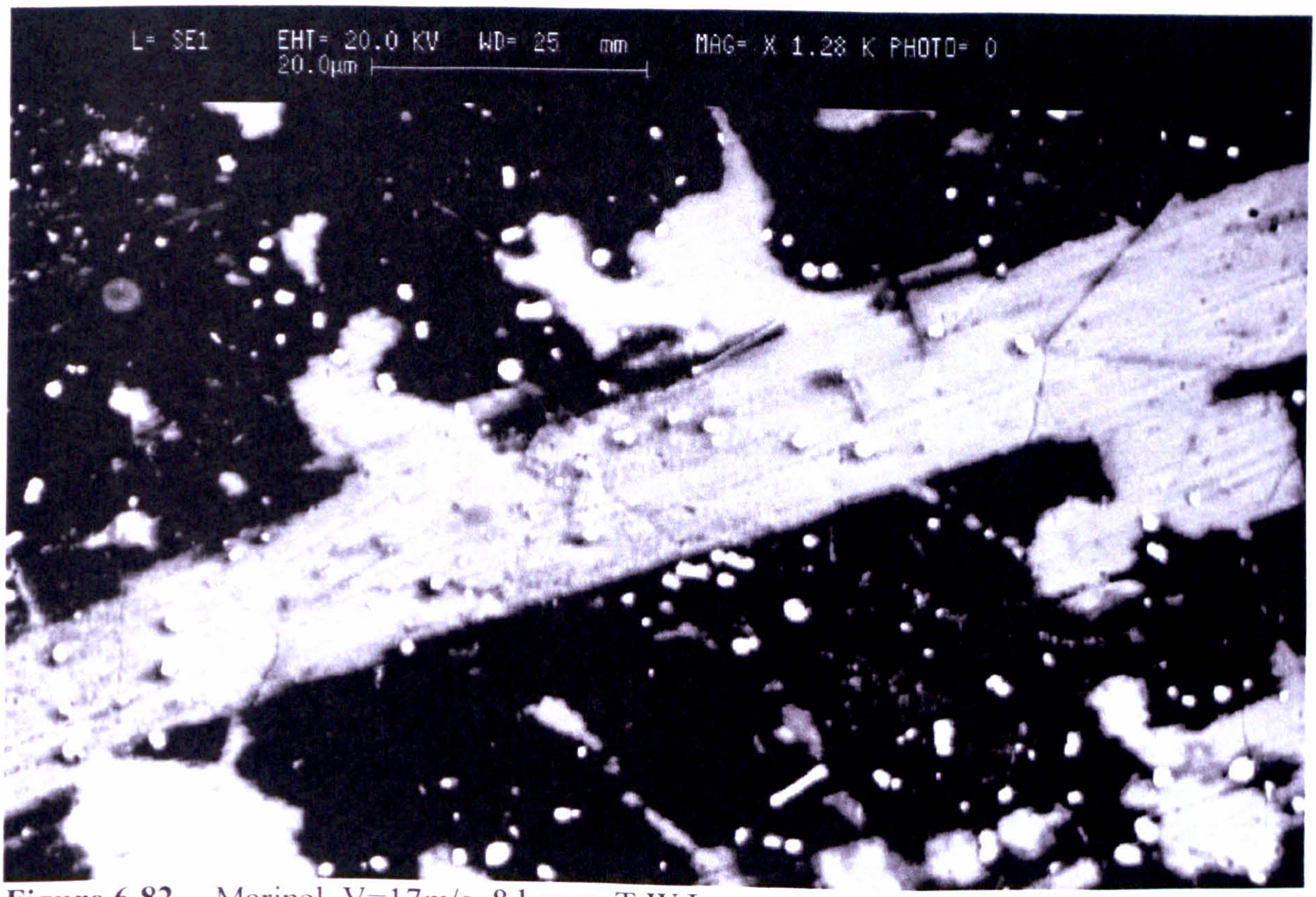

Figure 6.82. Marinel, V=17m/s, 8 hours, T.W.L.
Some Ni/Nb particles in both light needles and dark 'matrix'.

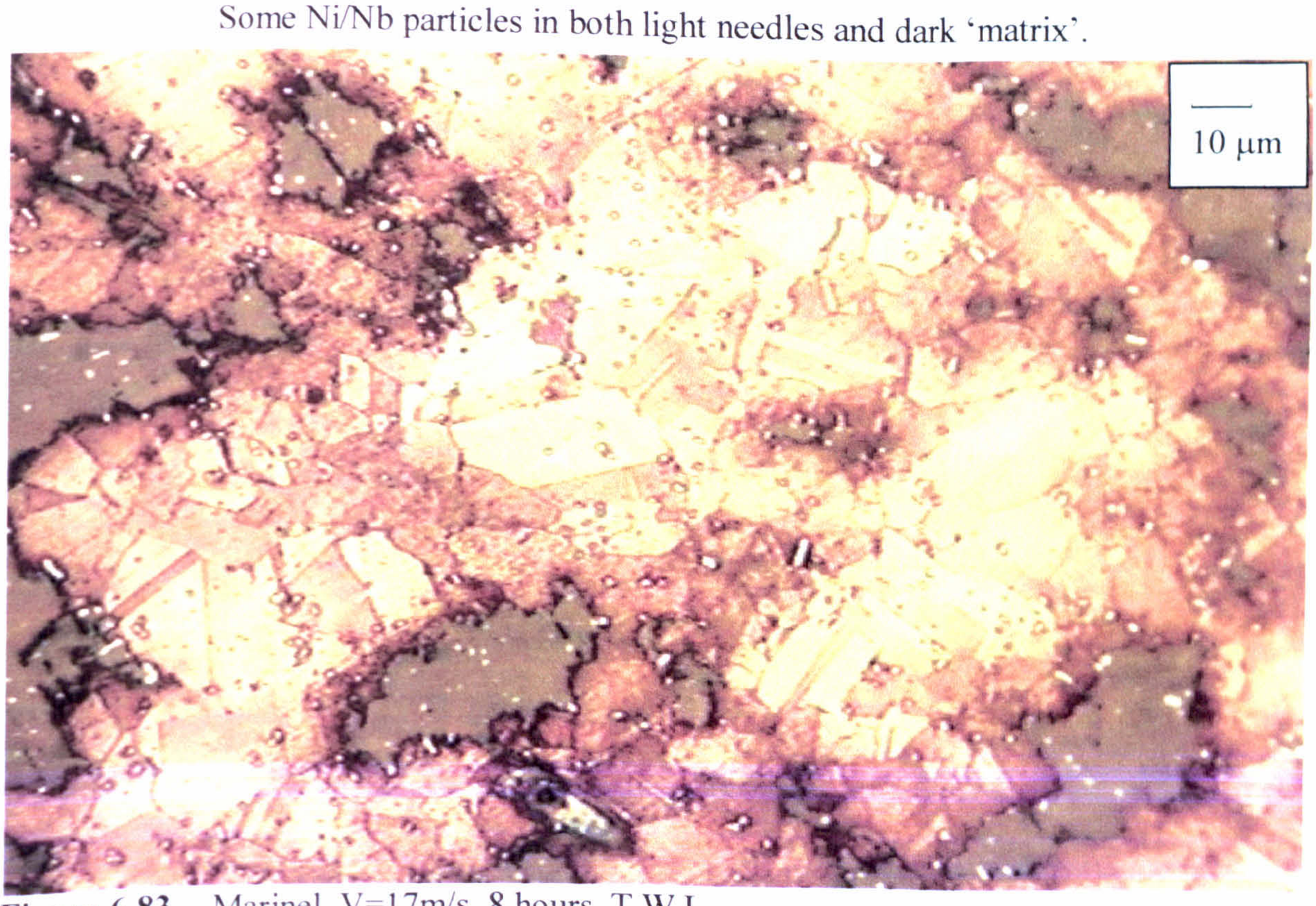

Figure 6.83. Marinel, V=17m/s, 8 hours, T.W.L.
A thin transparent film direct under the jet.

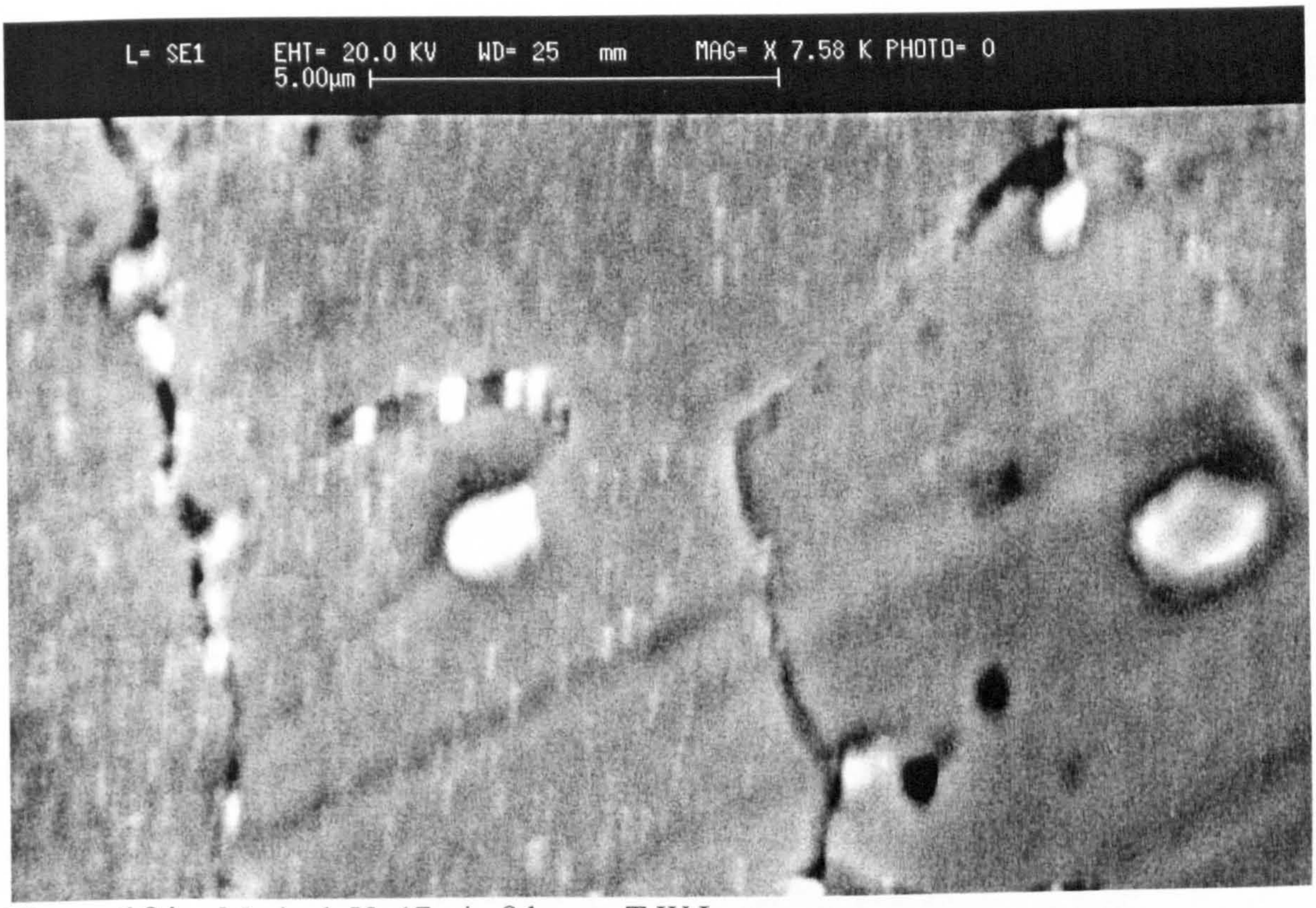

Figure 6.84. Marinel, V=17m/s, 8 hours, T.W.L.
Some Ni/Nb particles, at the grain boundaries.

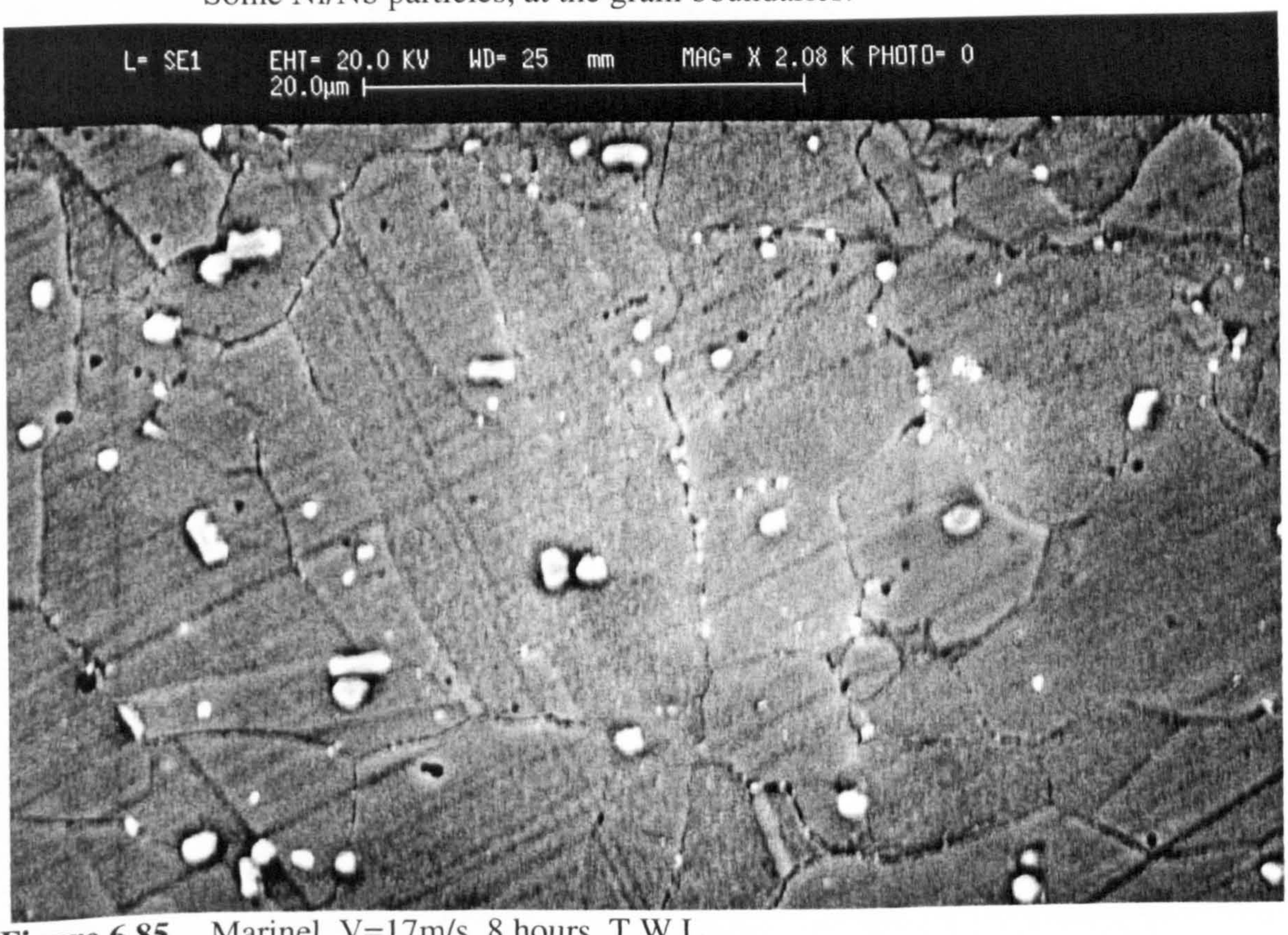

Figure 6.85. Marinel, V=17m/s, 8 hours, T.W.L.
Some Ni/Nb particles.

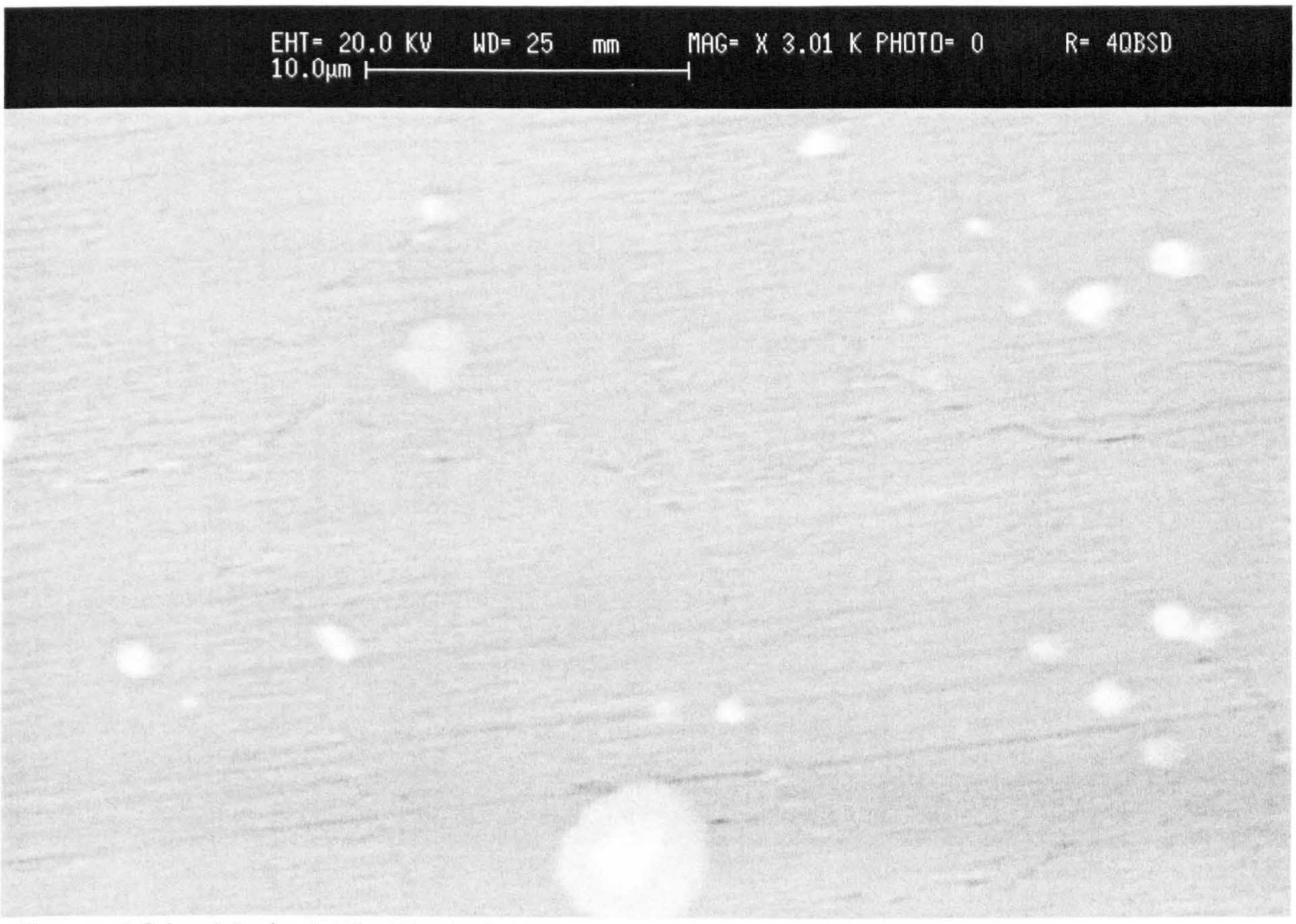

Figure 6.86. Marinel, V=17m/s, 8 hours, T.W.L.
A particle with a "duplex" structure at the bottom of the Figure.

Figure 6.87. Marinel, V=17m/s, 8 hours, C.P.
The area outside the directly impinged zone with some pits and comets.

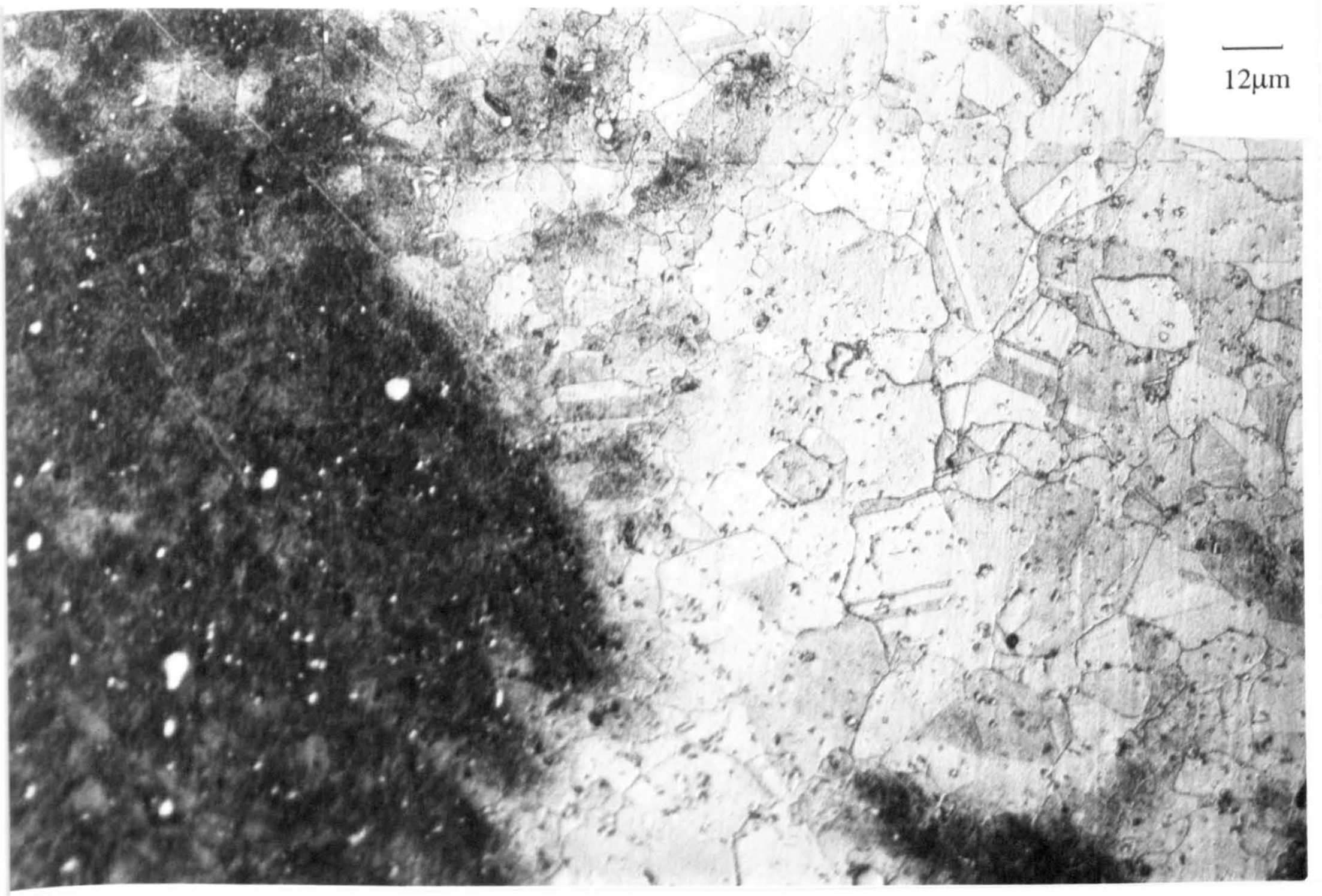

Figure 6.88. Marinel, V=17m/s, 8 hours, A.P.
More severe etching under the jet, between the black patches.

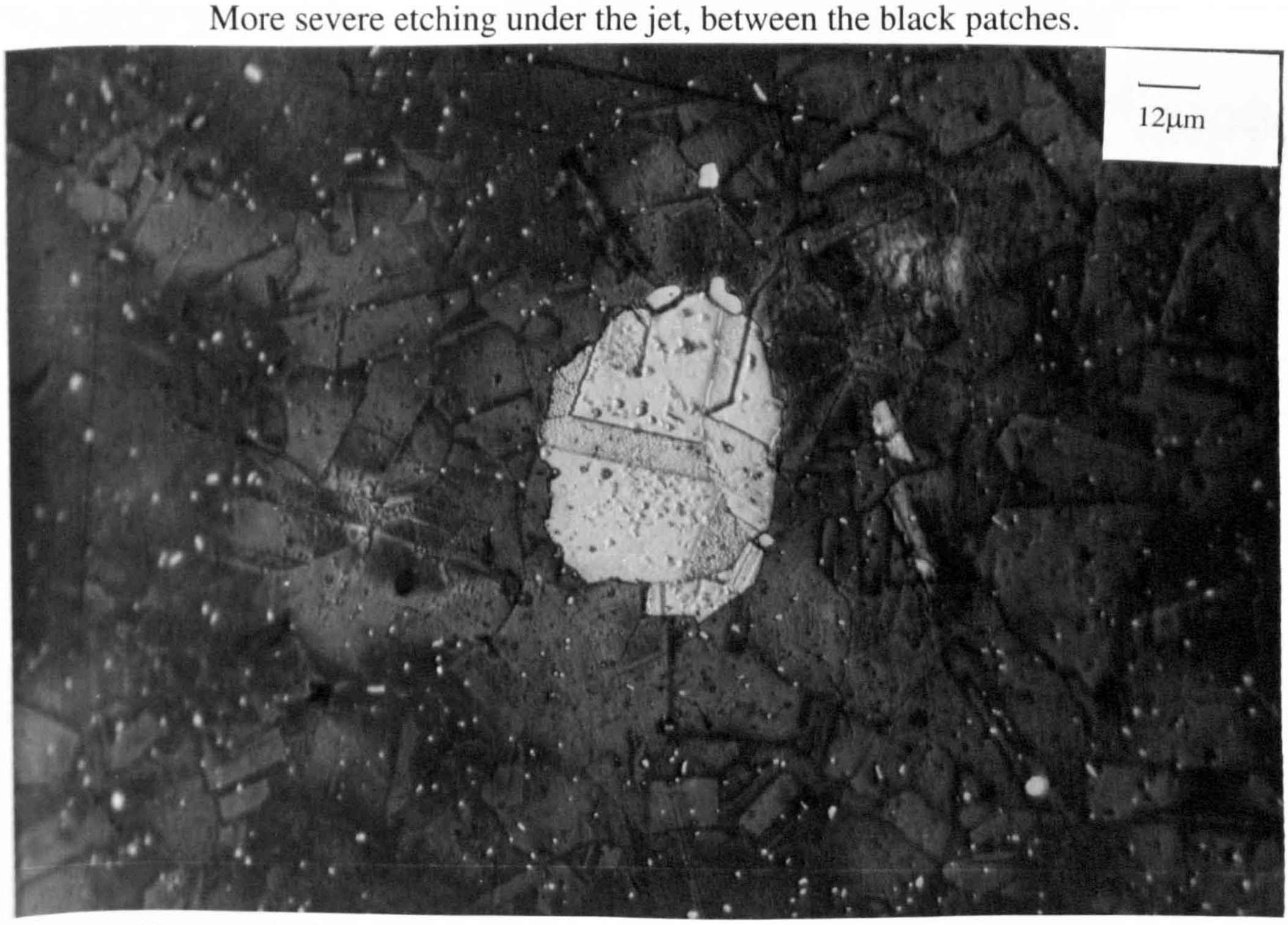

Figure 6.89. Marinel, V=17m/s, 48 hours, T.W.L.
The etched structure of the substrate.

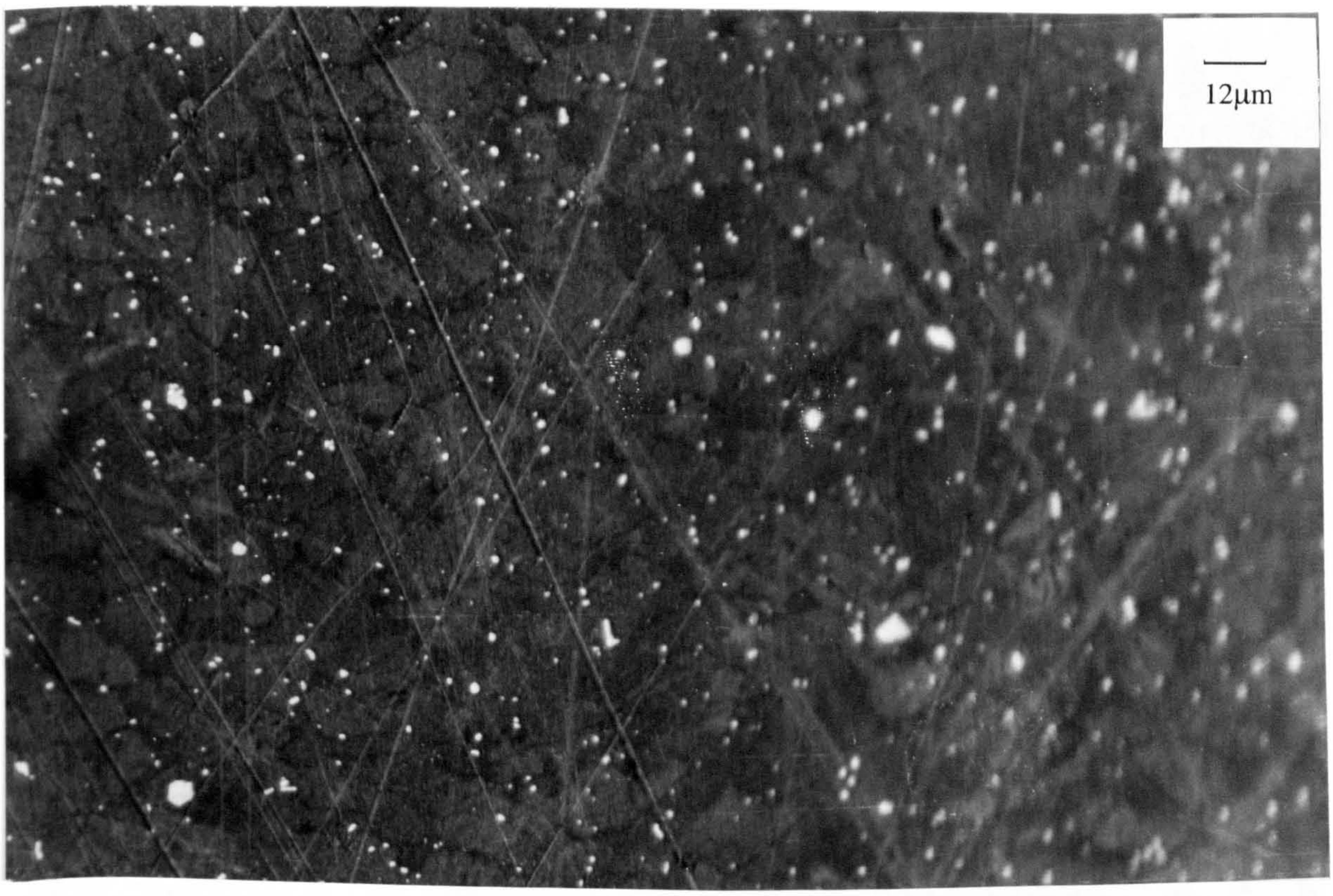

Figure 6.90. Marinel, V=17m/s, 48 hours, T.W.L.
Some Ni/Nb particles at the intermediate zone. Possible pitting initiation.

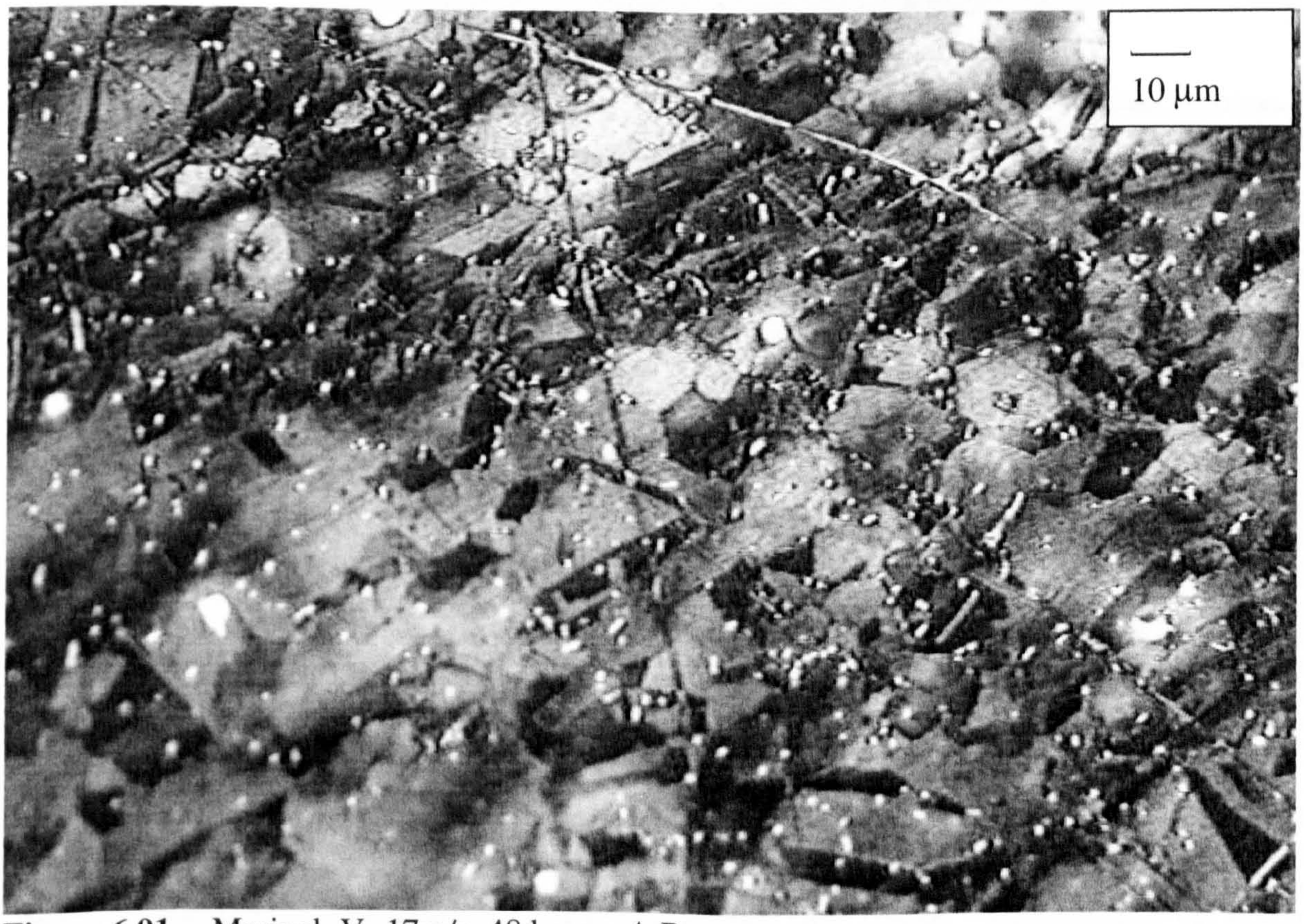

Figure 6.91. Marinel, V=17m/s, 48 hours, A.P.
A transparent dark film over the outside, with the etched structure.

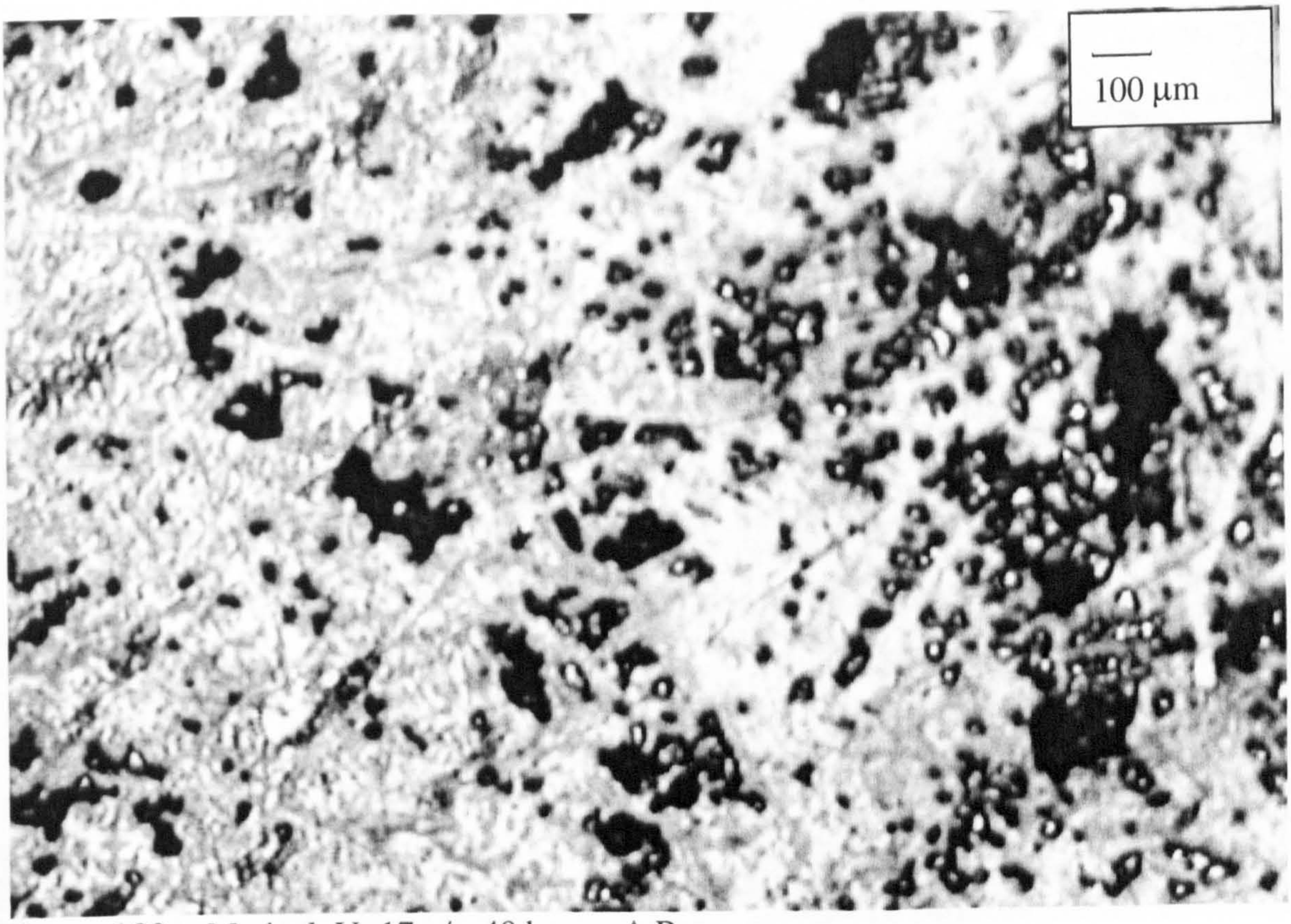

Figure 6.92. Marinel, V=17m/s, 48 hours, A.P.
Some pits at the centre.

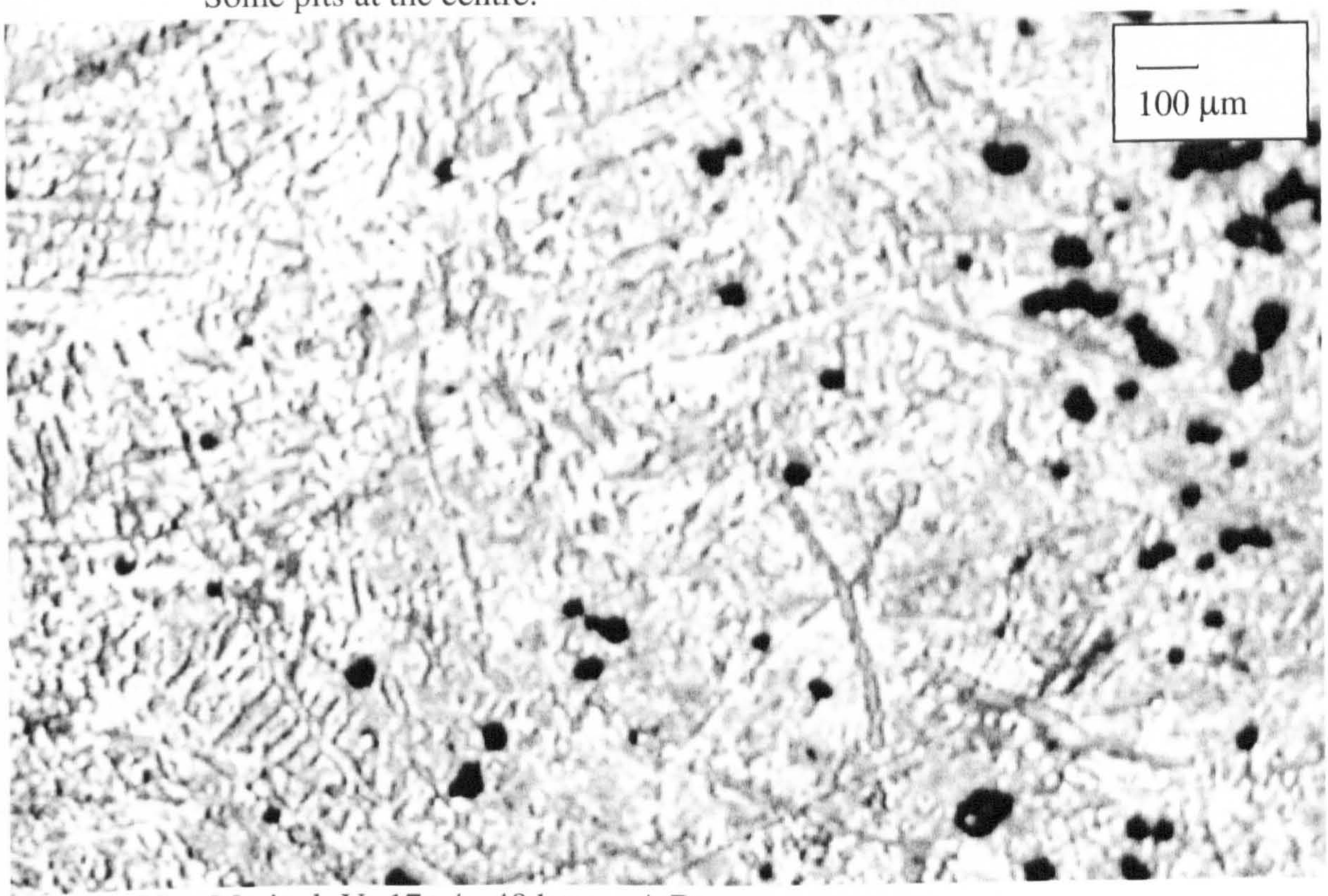

Figure 6.93. Marinel, V=17m/s, 48 hours, A.P.
Some pits at the intermediate zone.

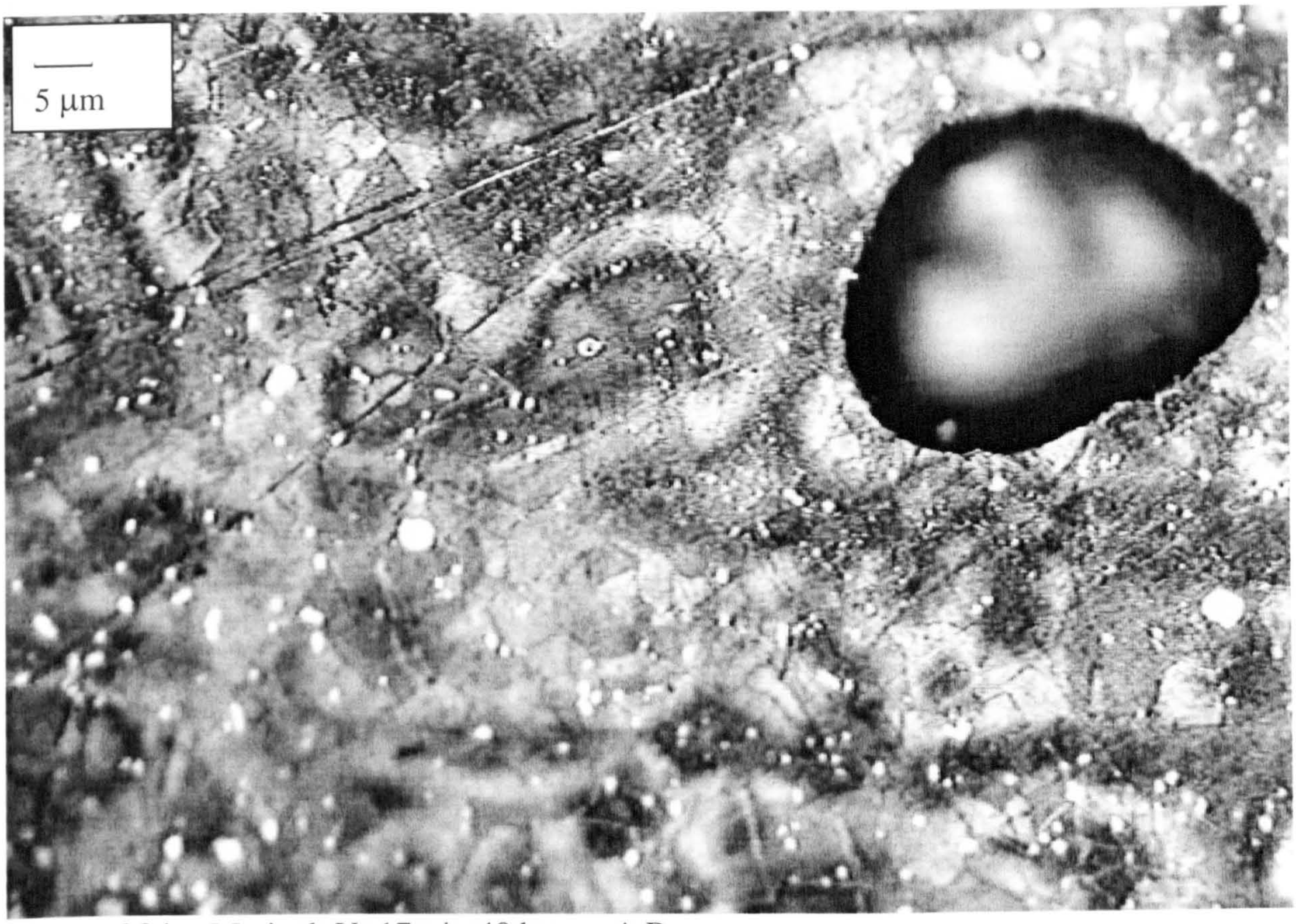

Figure 6.94. Marinel, V=17m/s, 48 hours, A.P.
Some pits at the outside with a deep one out of focus.

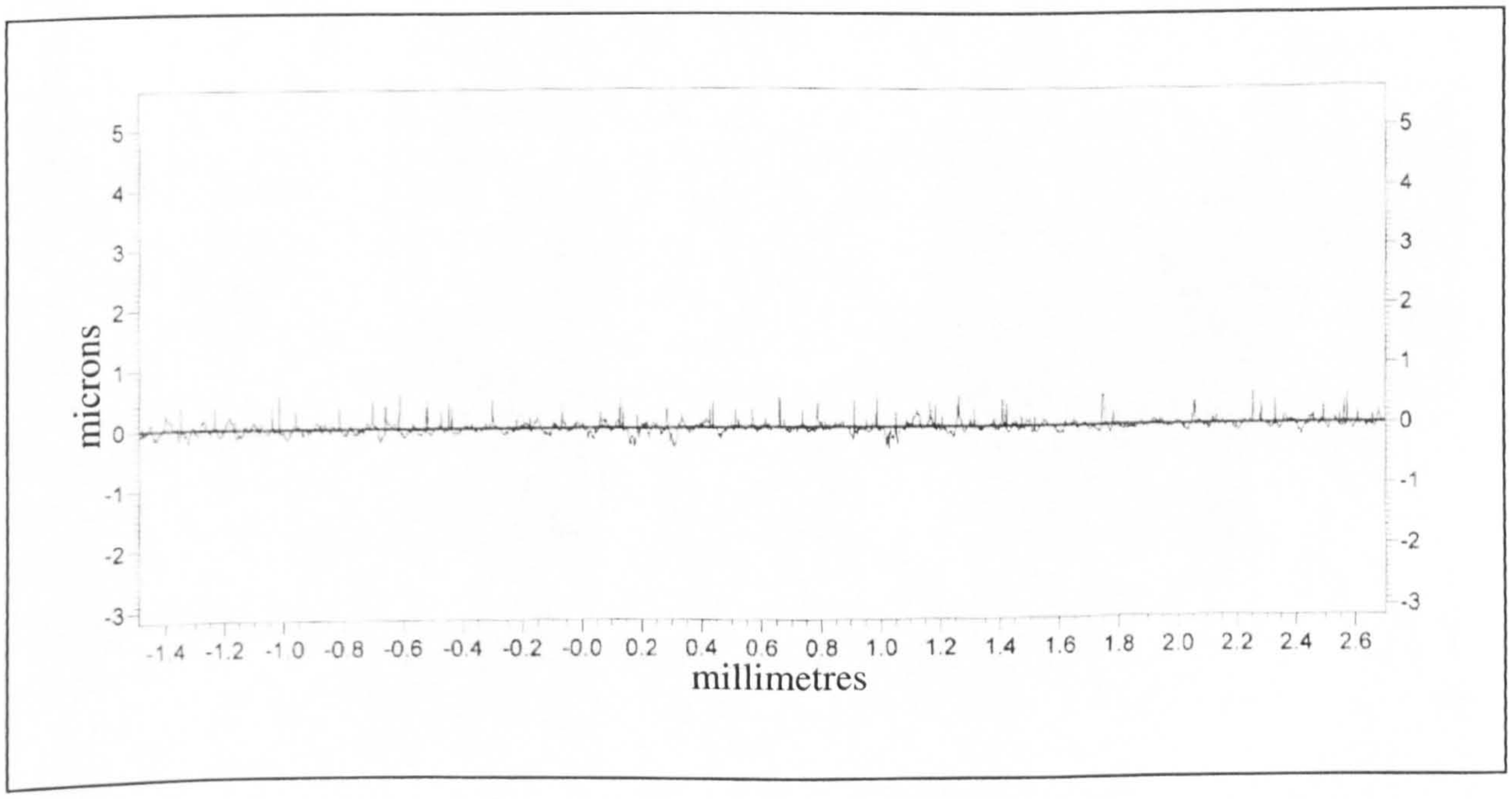

Figure 6.95. Marinel, V=86m/s, 4 hours, T.W.L.
Surface profile with R_a=0.06µm for the entire surface.

Figure 6.96. Marinel, V=86m/s, 4 hours, T.W.L.
The more continuous but thinner film that covered the whole surface.

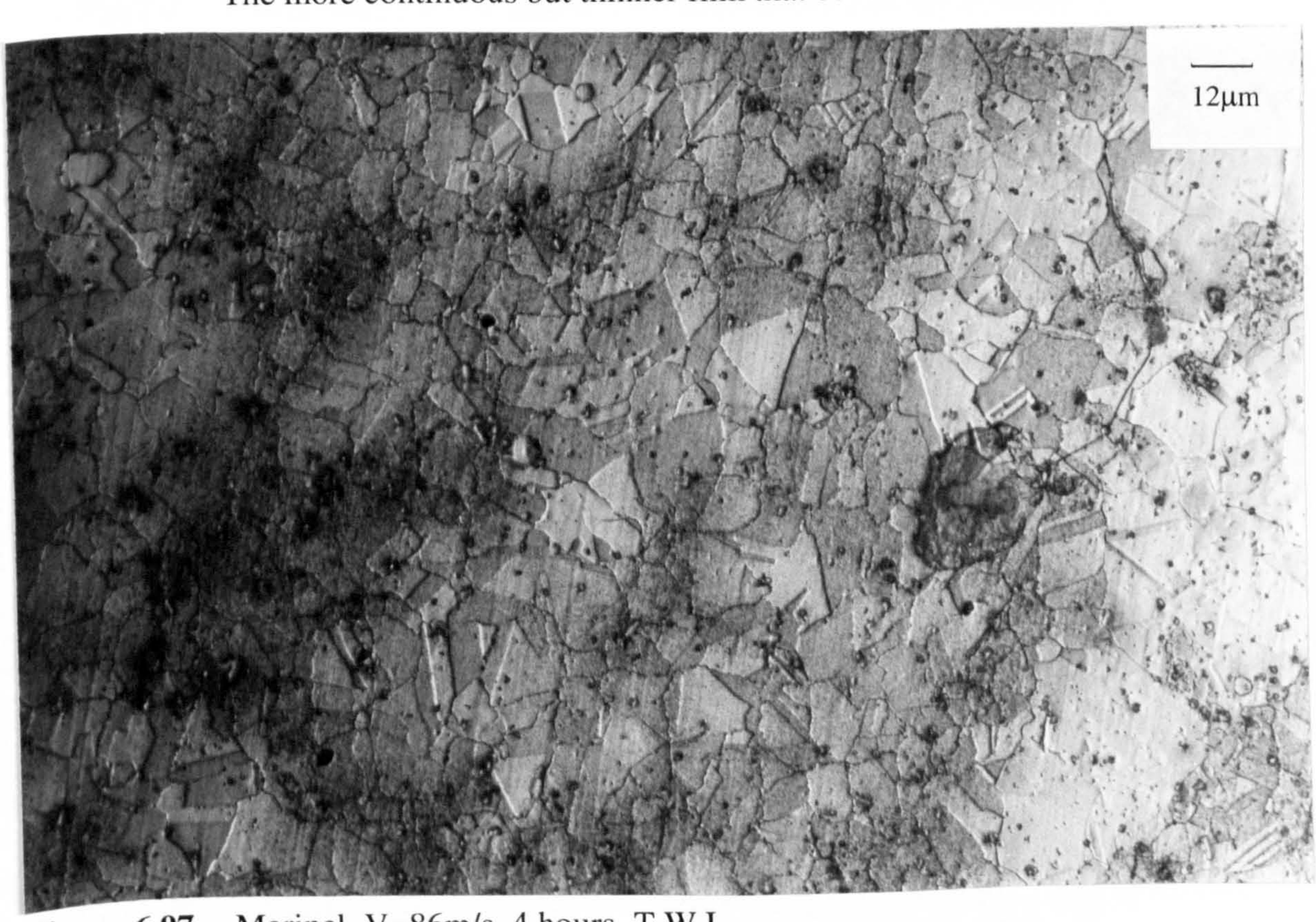

Figure 6.97. Marinel, V=86m/s, 4 hours, T.W.L.
The etched structure underneath the film directly under the jet.

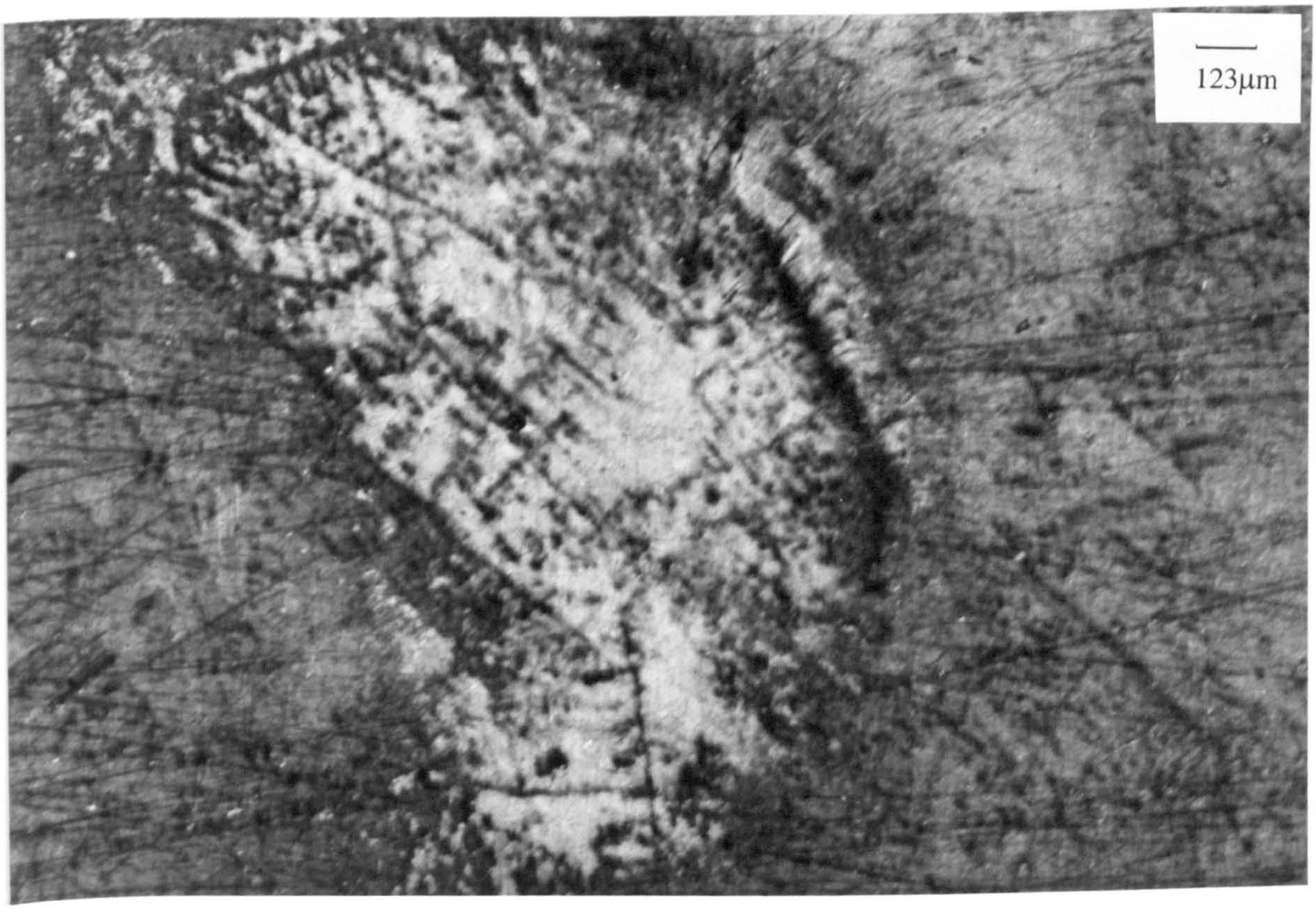

Figure 6.98. Marinel, V=86m/s, 4 hours, C.P.
Under the jet some attack, with a discontinuous black film.

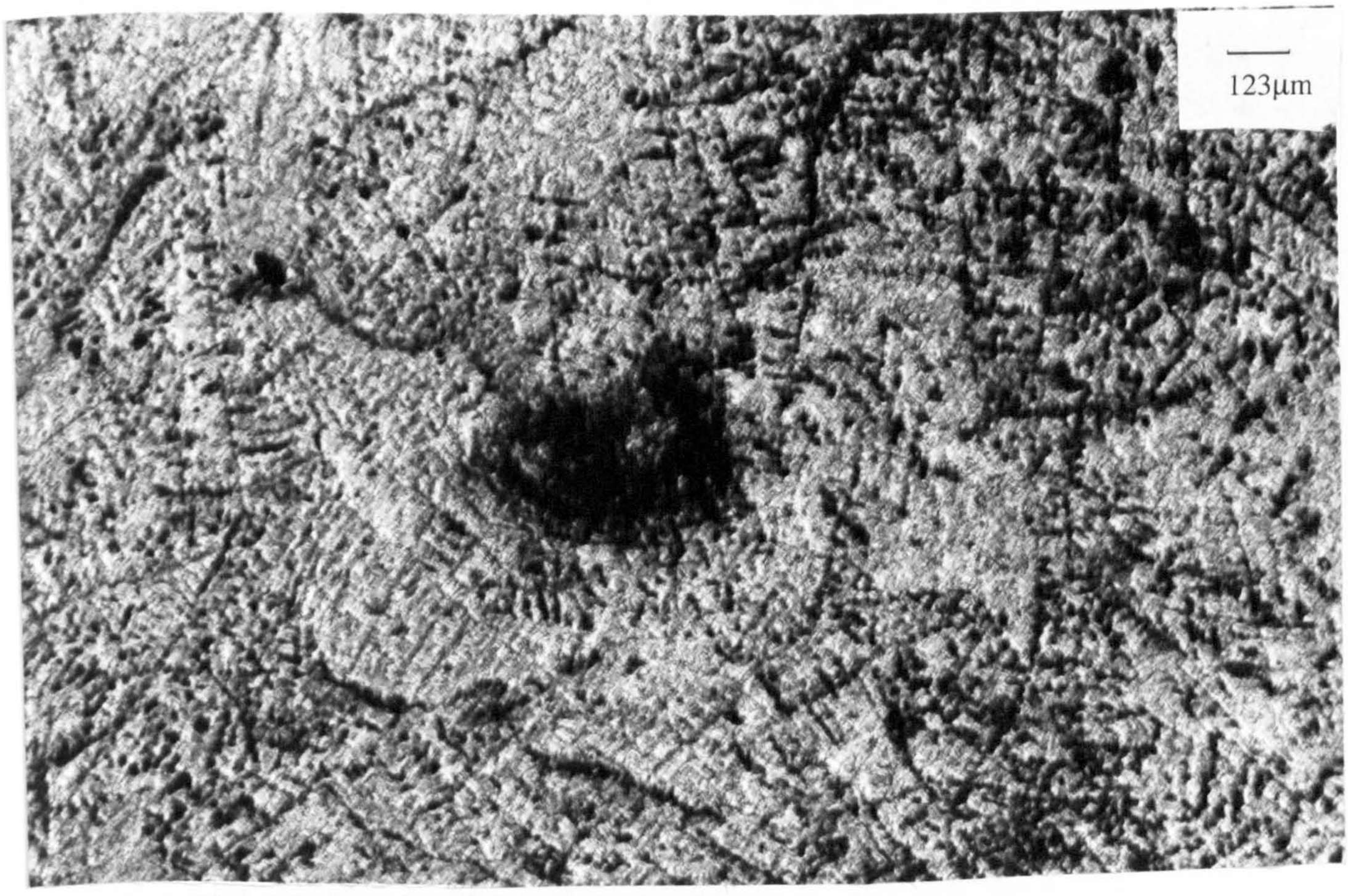

Figure 6.99. Marinel, V=86m/s, 4 hours, A.P.
The thicker multicolour film under the jet.

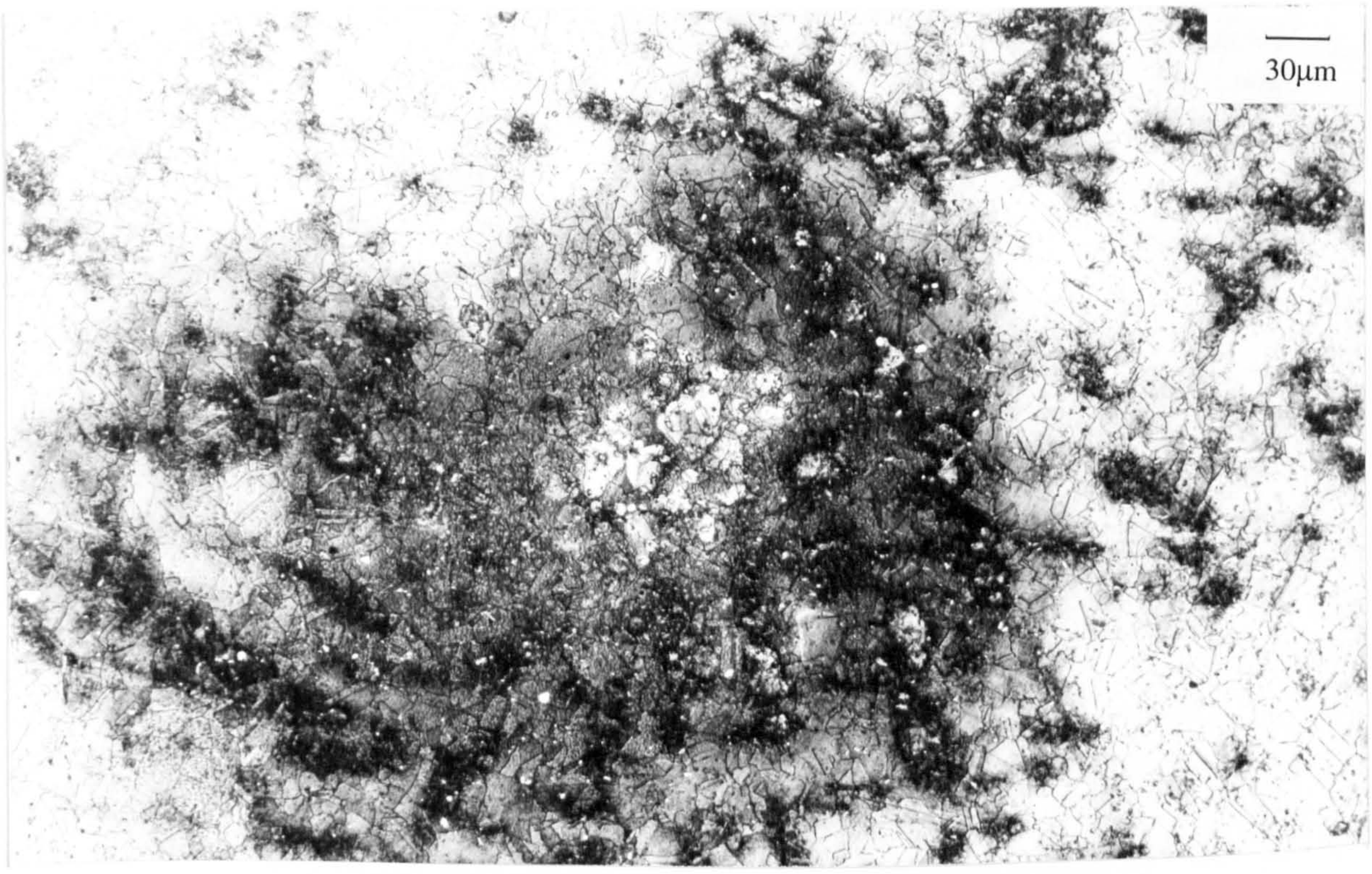

Figure 6.100. Marinel, V=86m/s, 4 hours, A.P.
More mild attack with some Ni/Nb particles at the outside area.

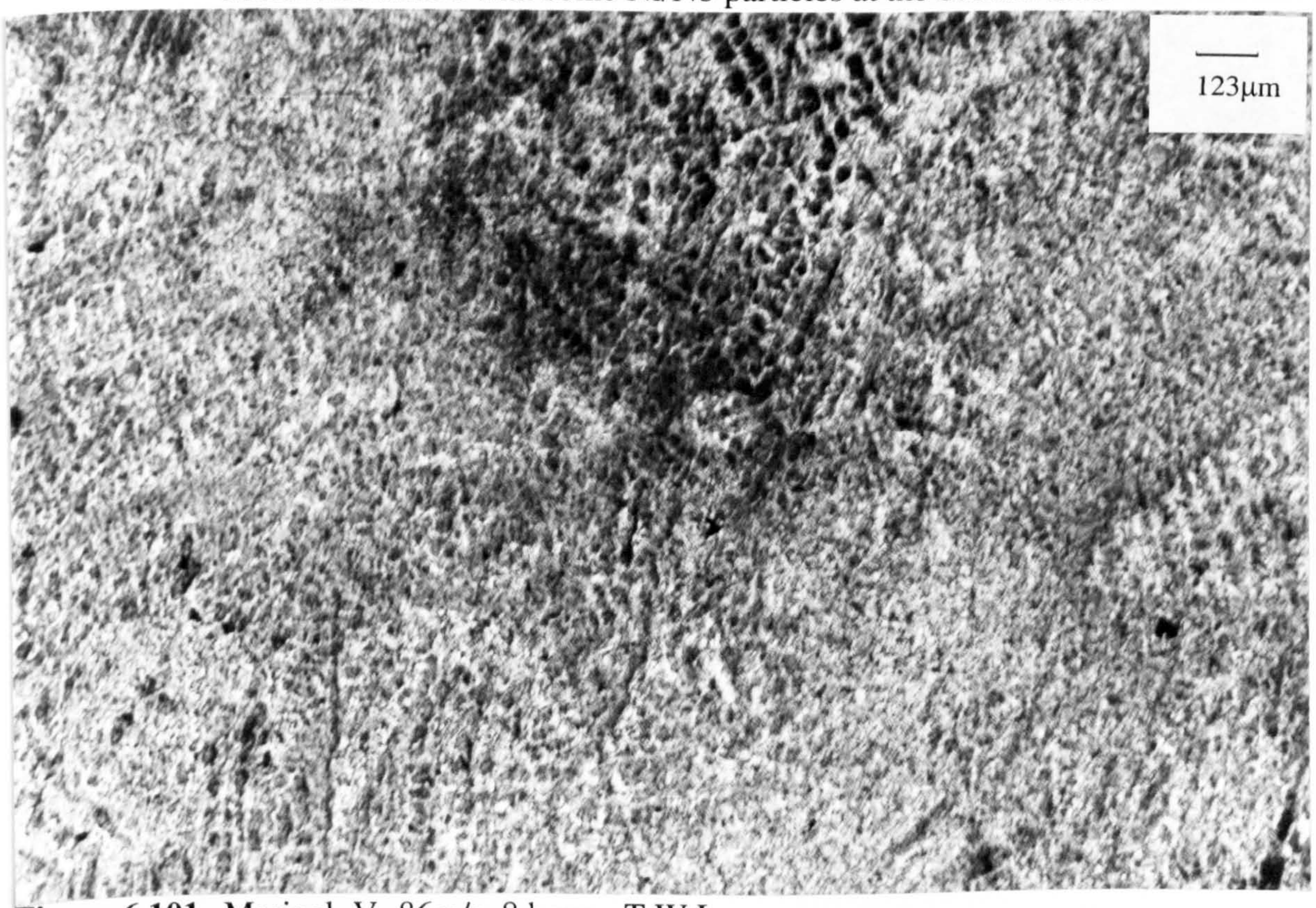

Figure 6.101. Marinel, V=86m/s, 8 hours, T.W.L.
At the left is the T.W.L. specimen, with the C.P. at the right.

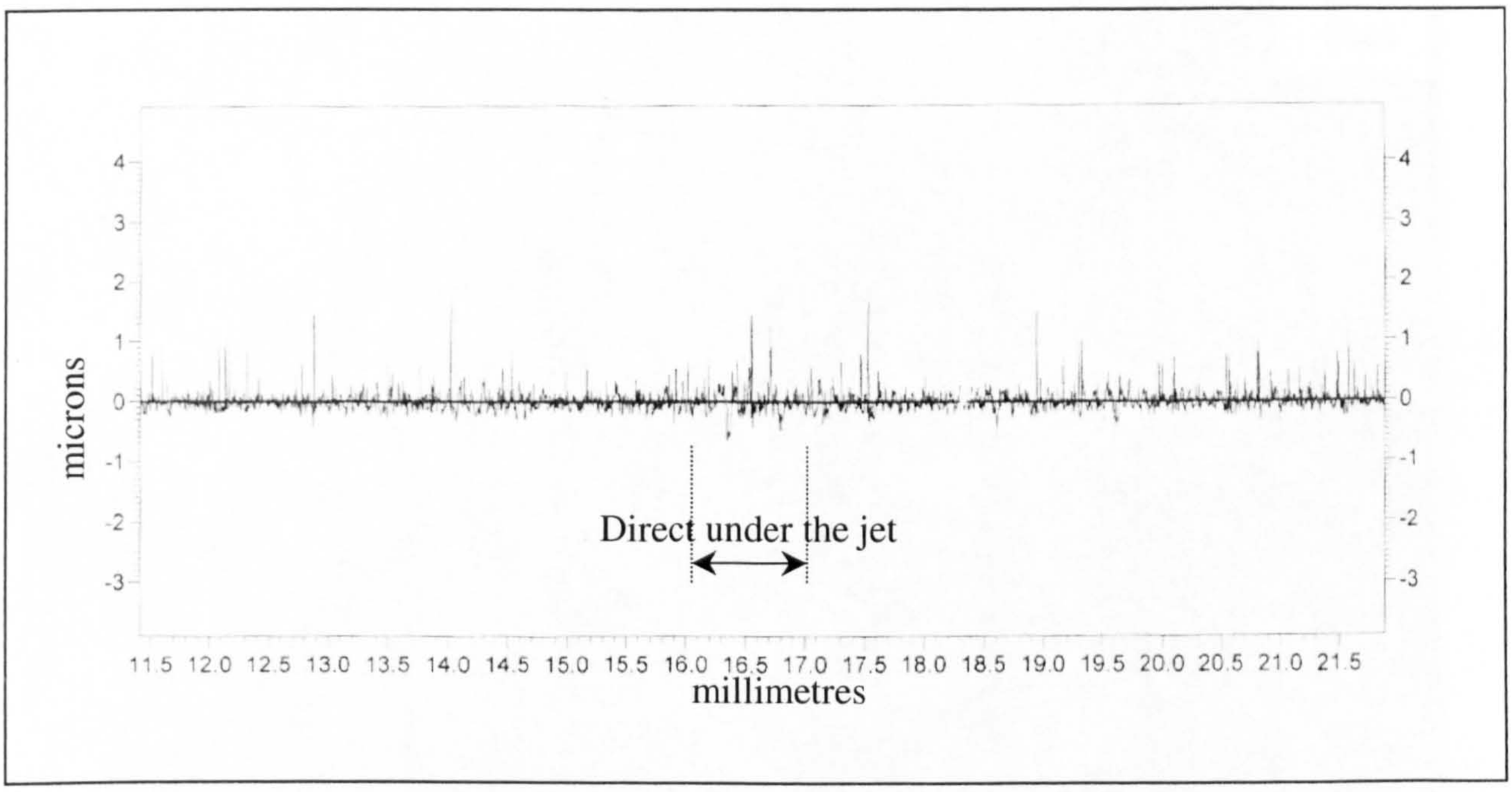

Figure 6.102. Marinel, V=86m/s, 8 hours, T.W.L.
Surface profile with R_a=0.16μm for the entire surface.

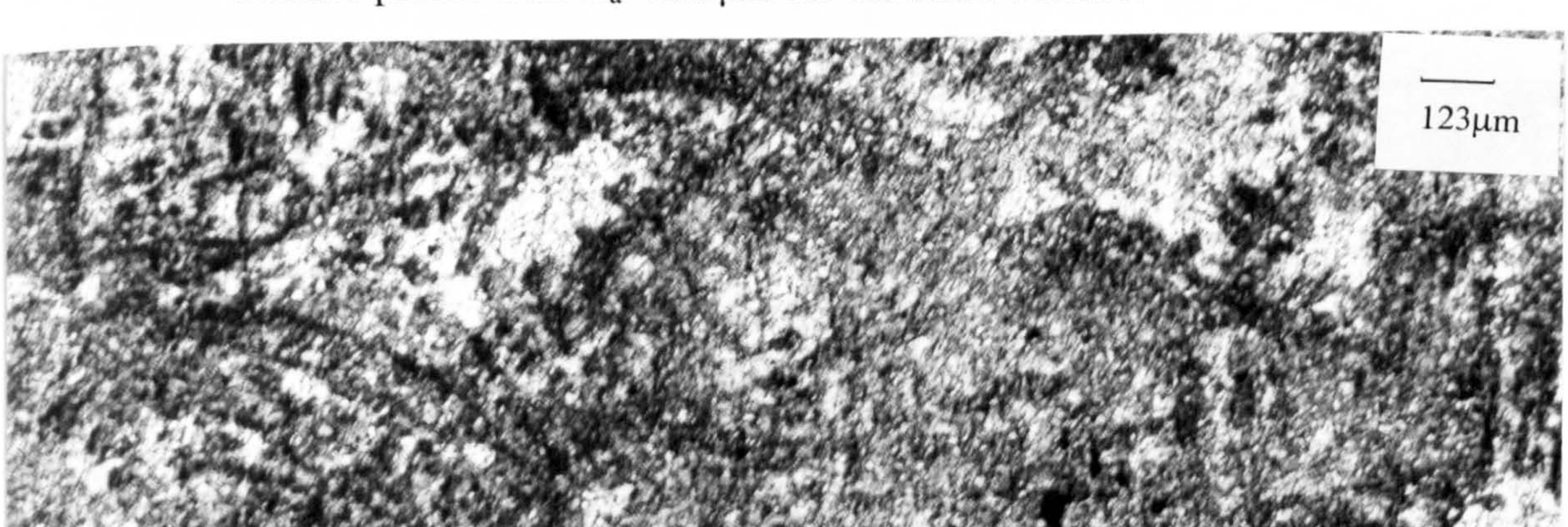

Figure 6.103. Marinel, V=86m/s, 8 hours, T.W.L.
Central region of the specimen, with a thick yellow film.

Figure 6.104. Marinel, V=86m/s, 8 hours, T.W.L.
The grain structure is evident under the jet.

Figure 6.105. Marinel, V=86m/s, 8 hours, T.W.L.
Intense pitting attack underneath the thick film outside the central zone.

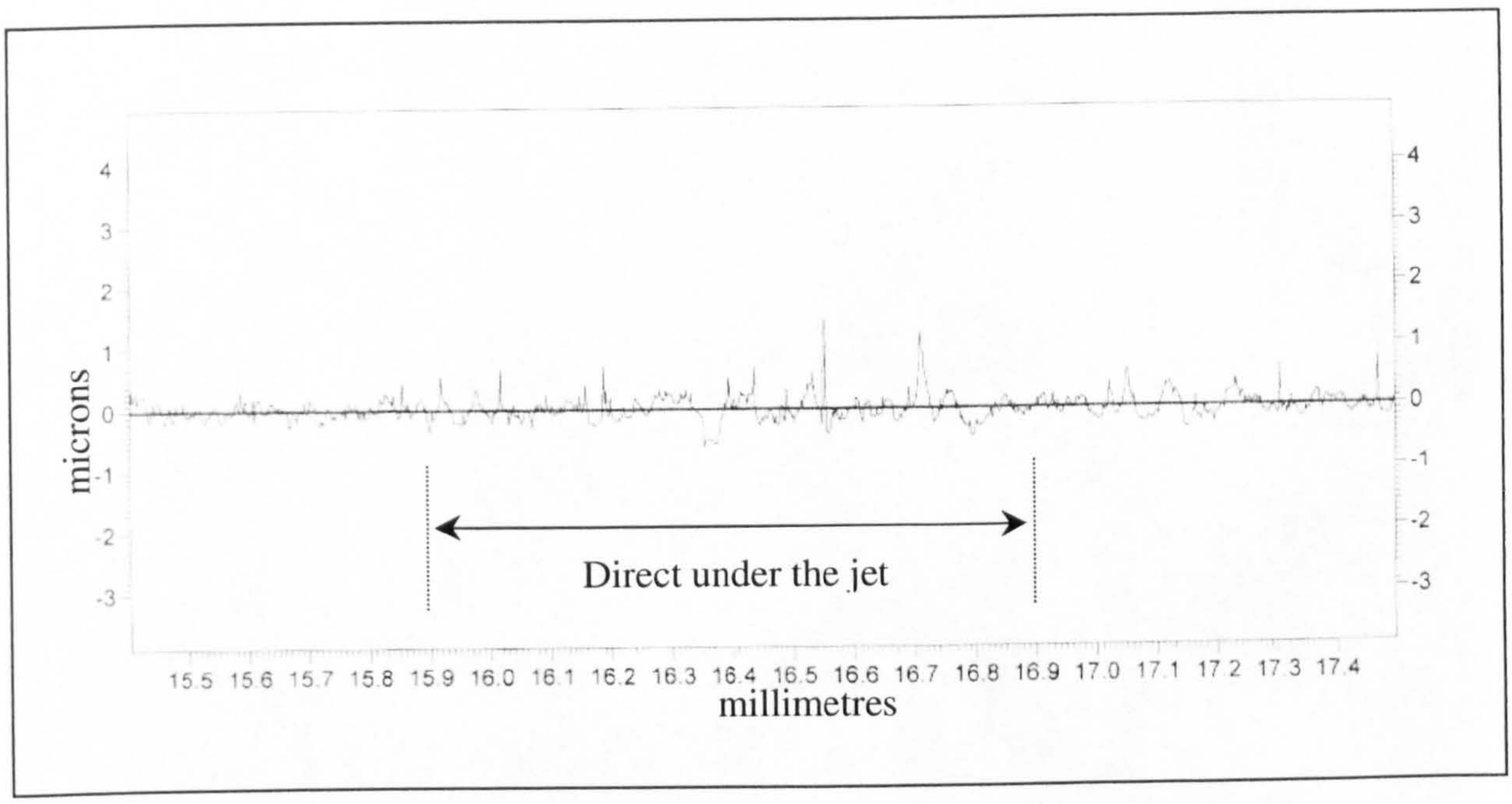

Figure 6.106. Marinel, V=86m/s, 8 hours, T.W.L.
Surface profile under the jet with R_a=020μm.

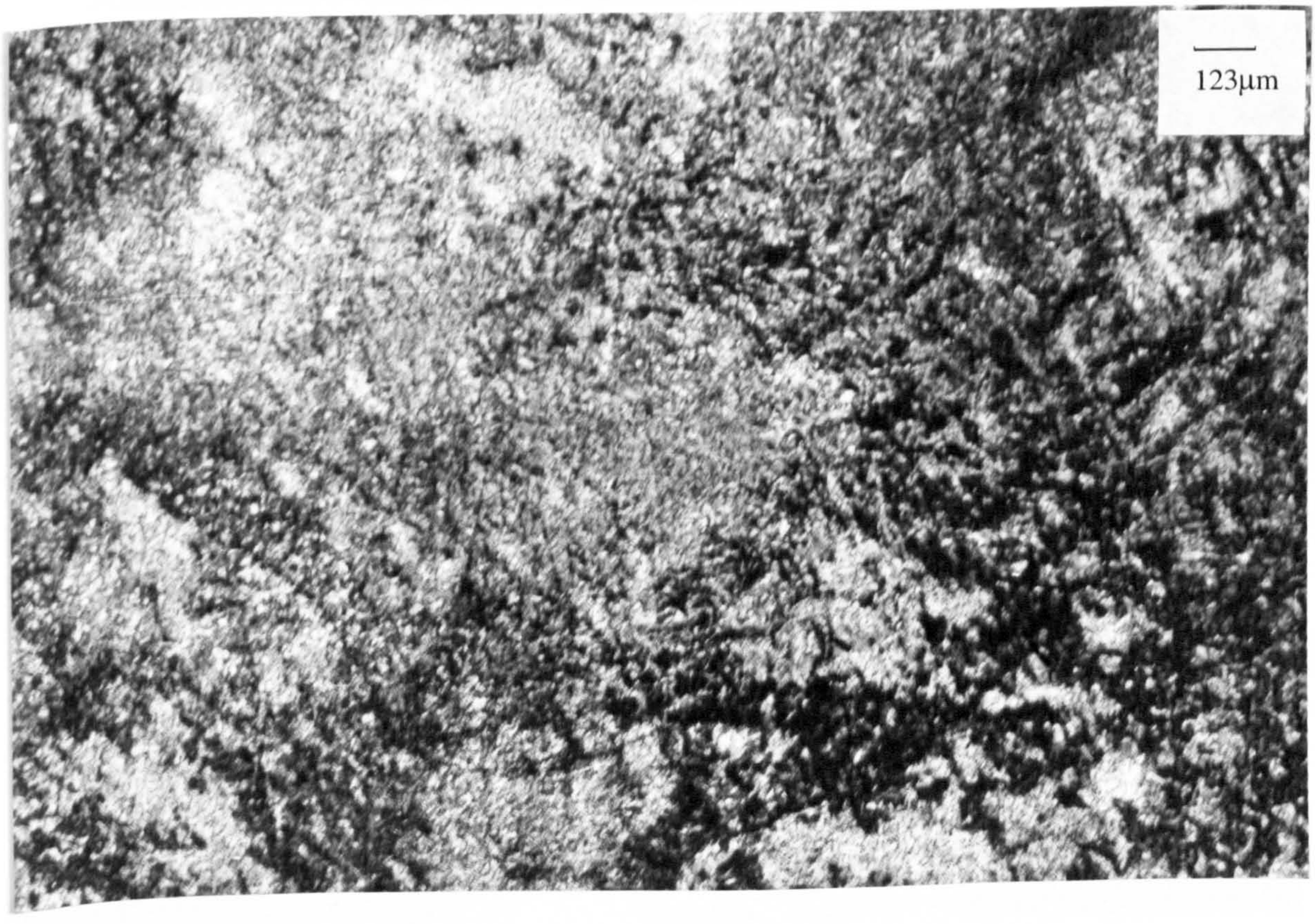

Figure 6.107. Marinel, V=86m/s, 8 hours, C.P.
A discontinuous film under the jet.

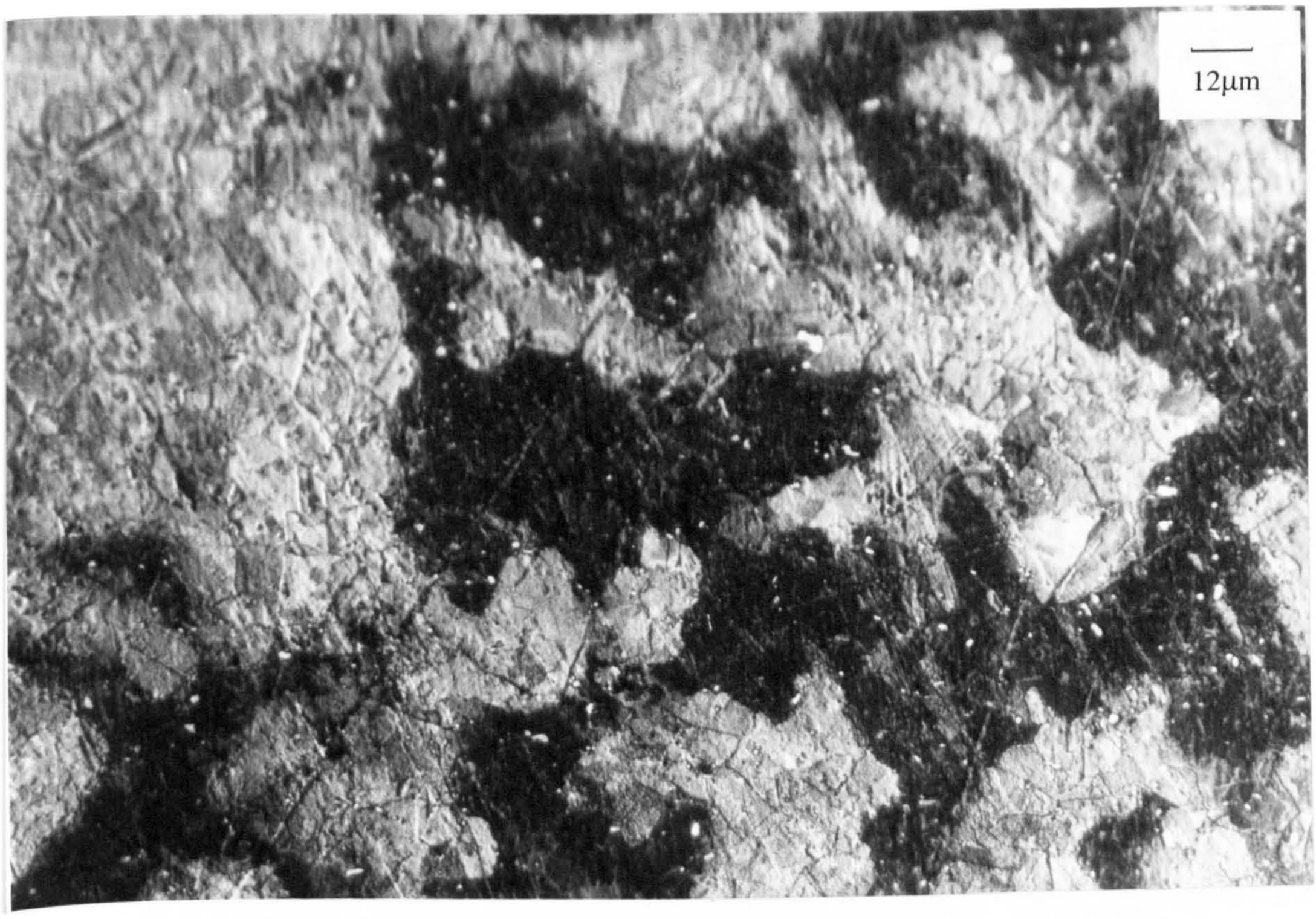

Figure 6.108. Marinel, V=86m/s, 8 hours, C.P.
The grain structure at the uncovered bits is almost apparent under the jet.

Figure 6.109. Marinel, V=86m/s, 8 hours, C.P.
The outside area looks like a ring at the left of the Figure.

Figure 6.110. Marinel, V=86m/s, 8 hours, C.P.
The outside area was covered by a thick yellow ring.

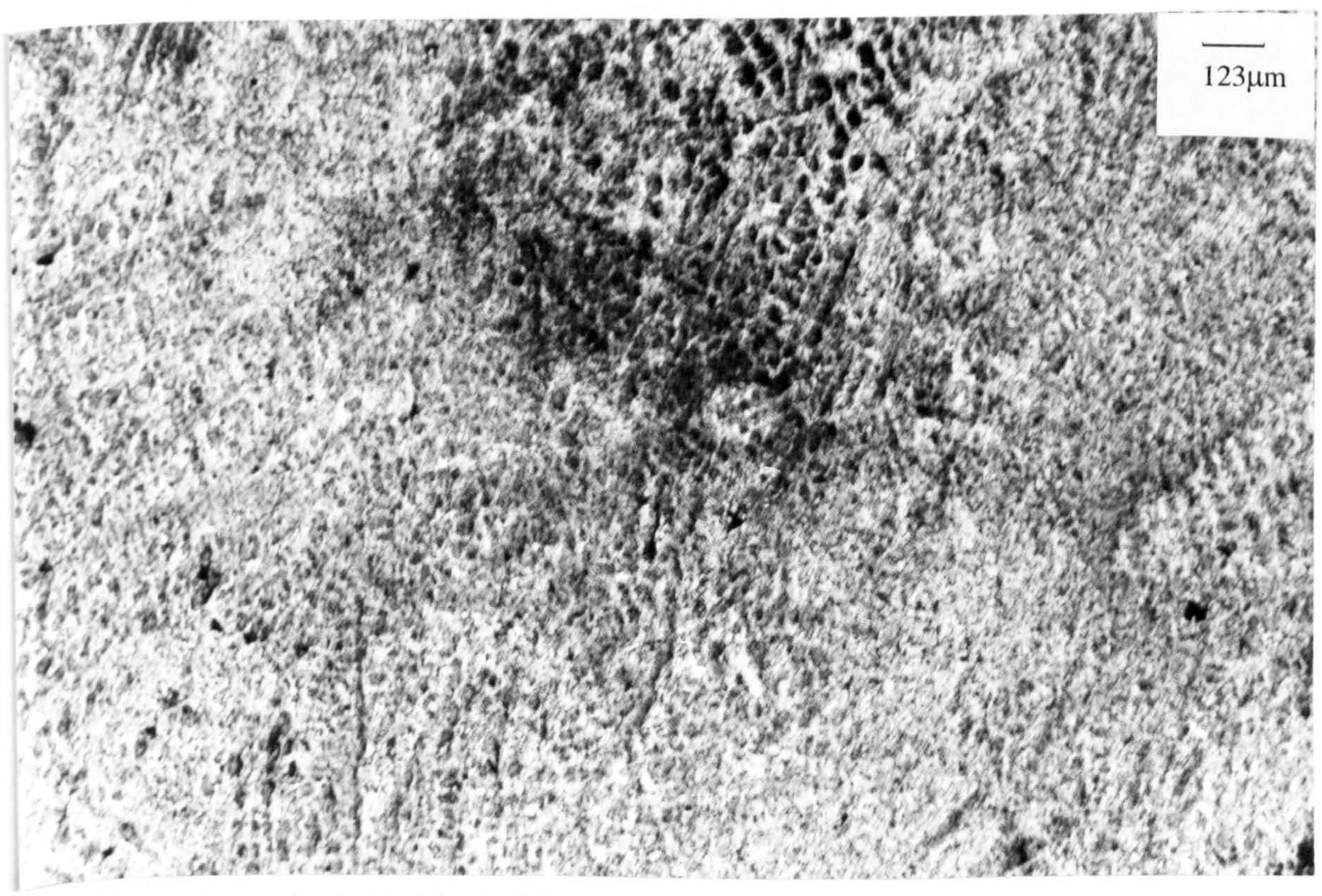

Figure 6.111. Marinel, V=86m/s, 8 hours, A.P.
A discontinuous film was evident under the jet.

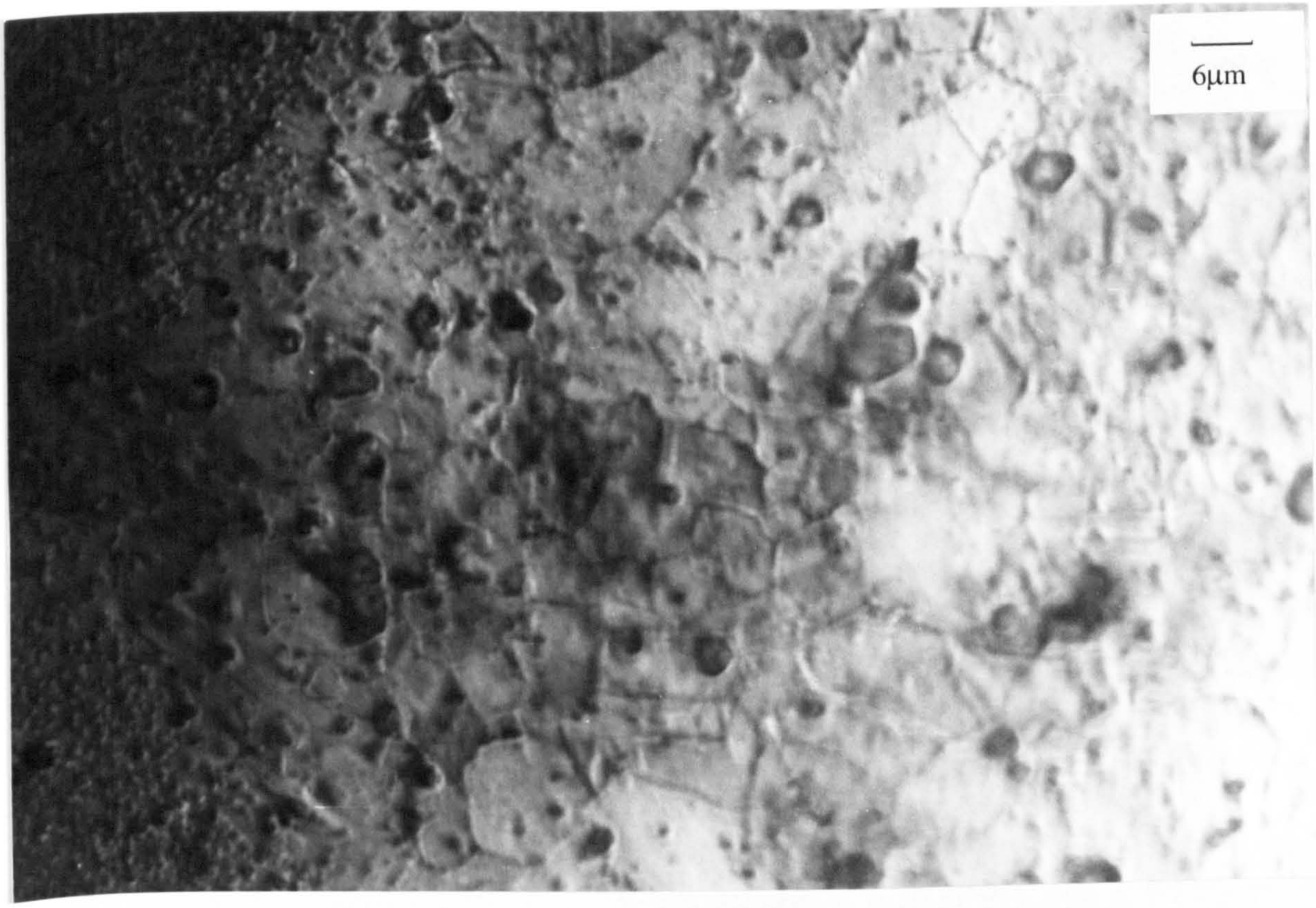

Figure 6.112. Marinel, V=86m/s, 8 hours, A.P.
Under the film of above Figure, severe pitting was revealed at high mag.

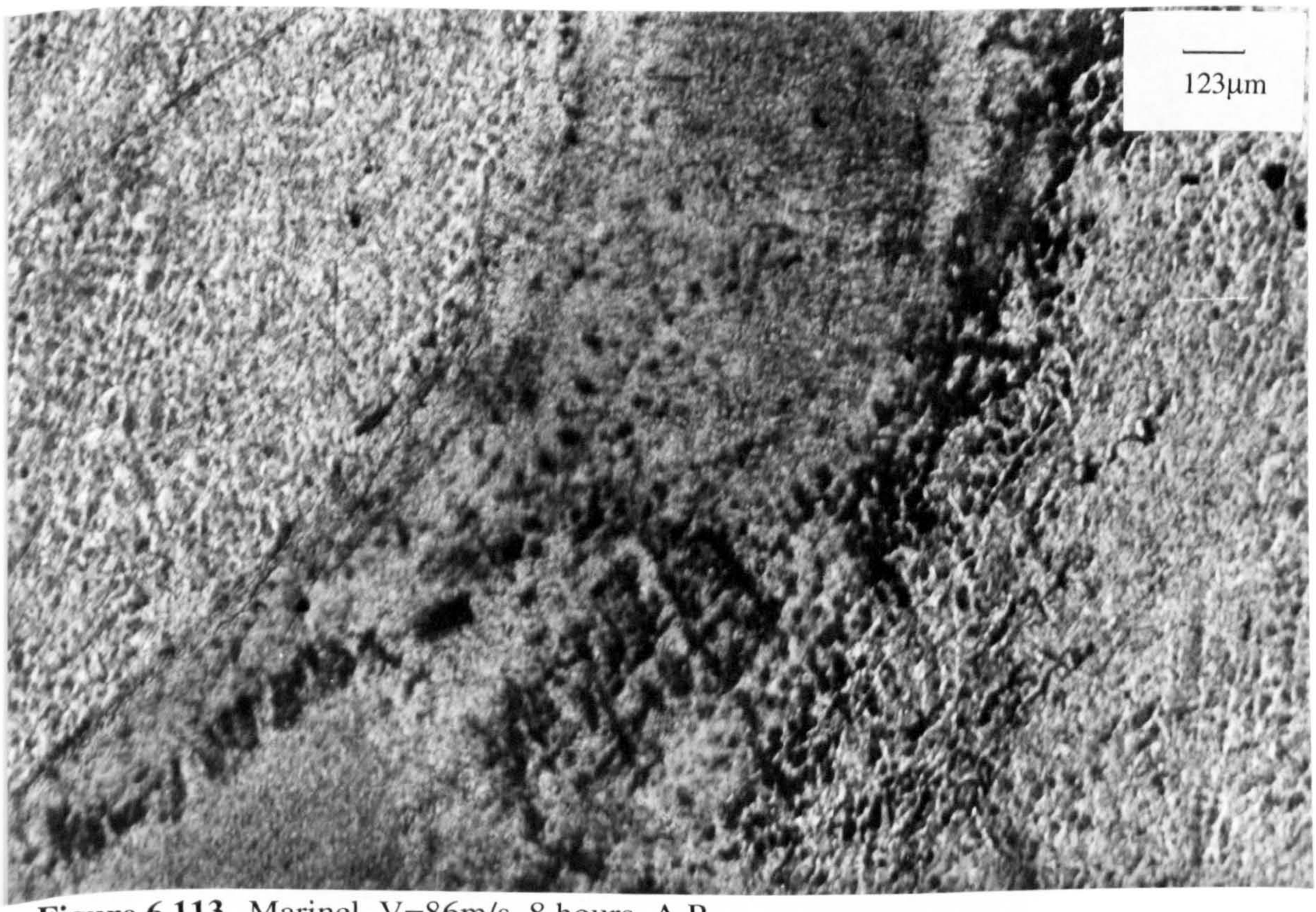

Figure 6.113. Marinel, V=86m/s, 8 hours, A.P.
A ring zone covered by a thick yellow film.

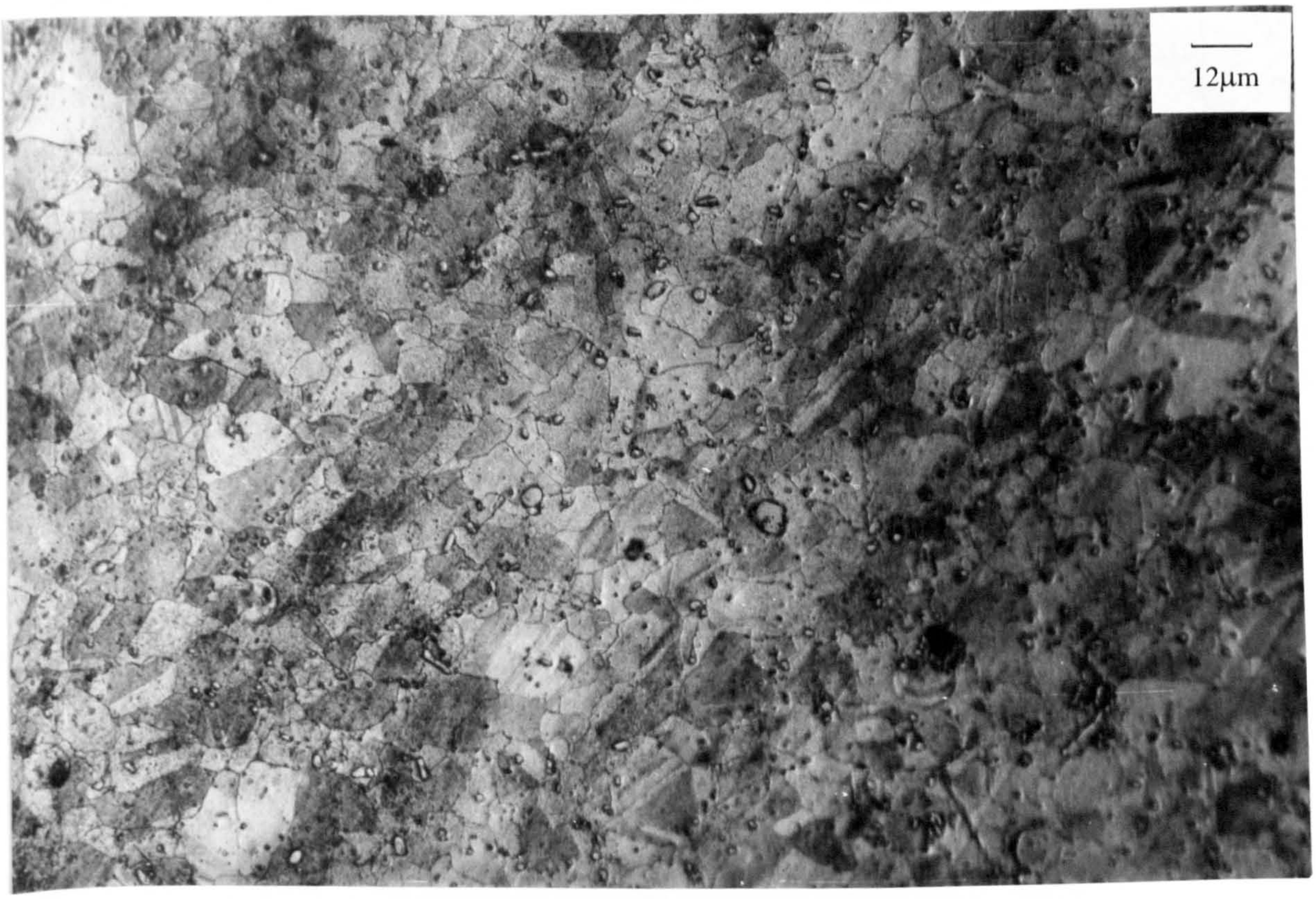

Figure 6.114. Marinel, V=86m/s, 8 hours, A.P.
The etched structure with severe pitting covered the rest of the surface.

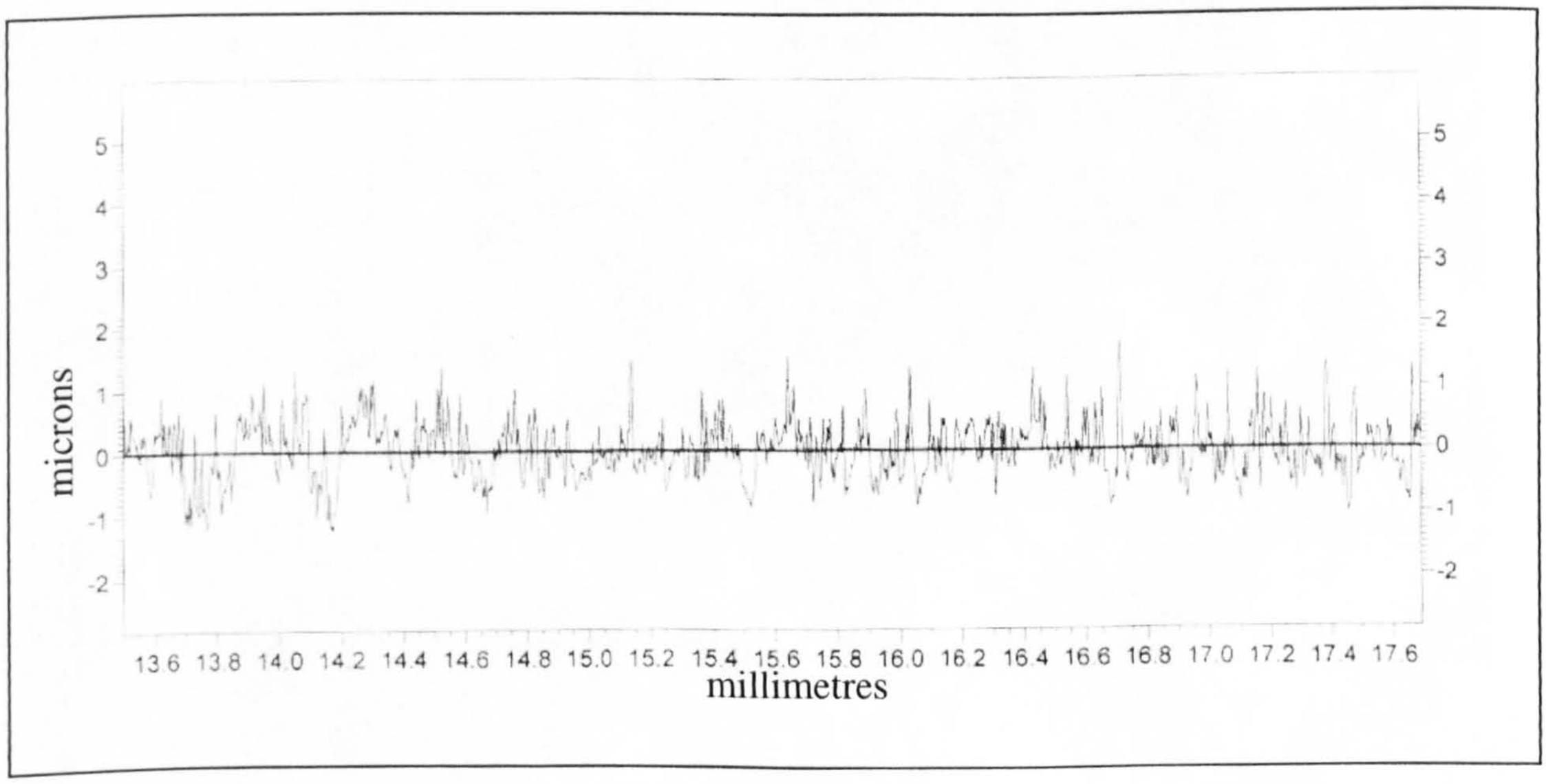

Figure 6.115. Marinel, V=17m/s, 1 hours, A.R.
Surface profile for the entire surface with R_a=0.33μm.

Figure 6.116. Marinel, V=17m/s, 1 hours, A.R.
The etched structure with some pits were evident everywhere.

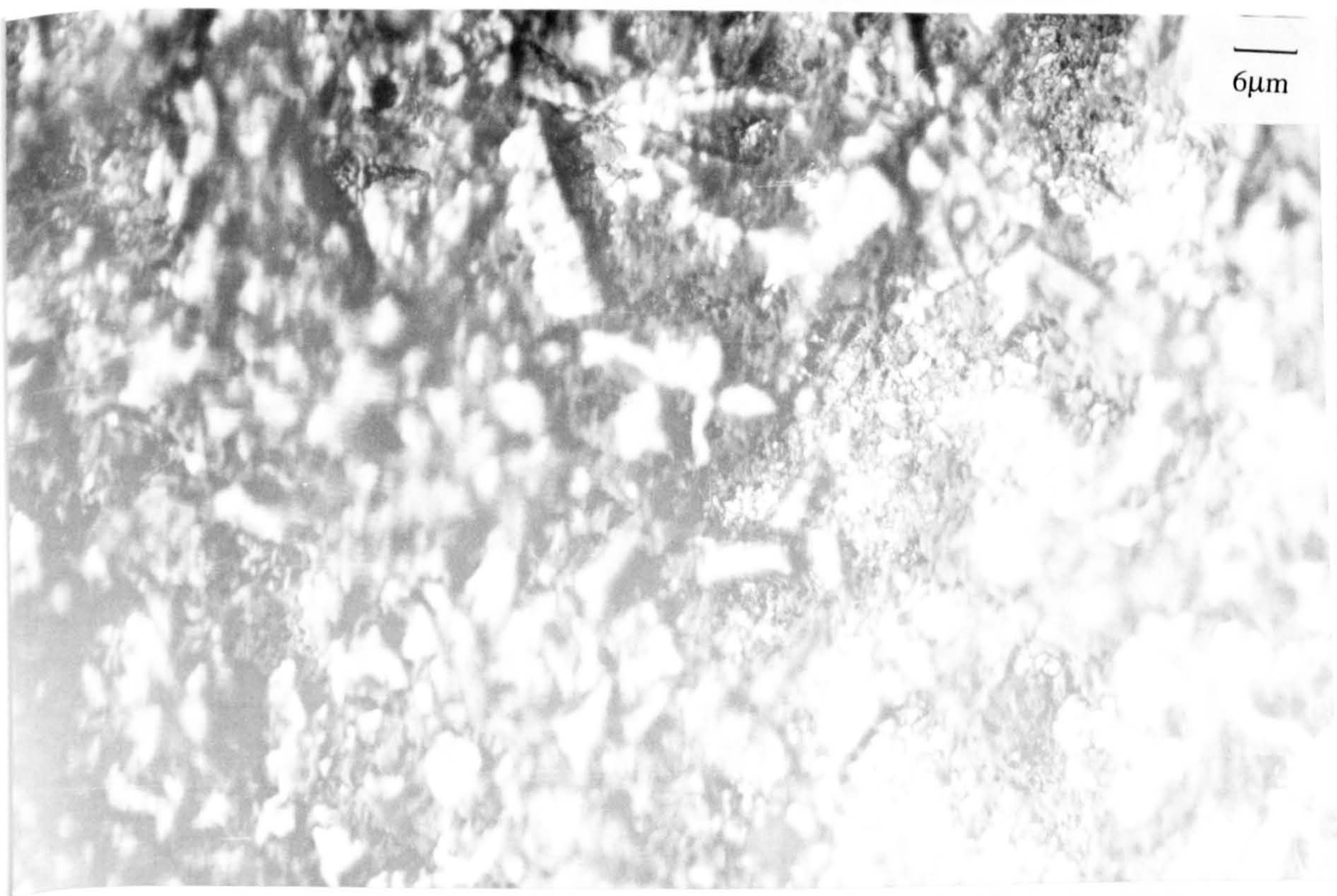

Figure 6.117. Marinel, V=17m/s, 8 hours, A.R.
A thicker black-yellow film covered the entire surface.

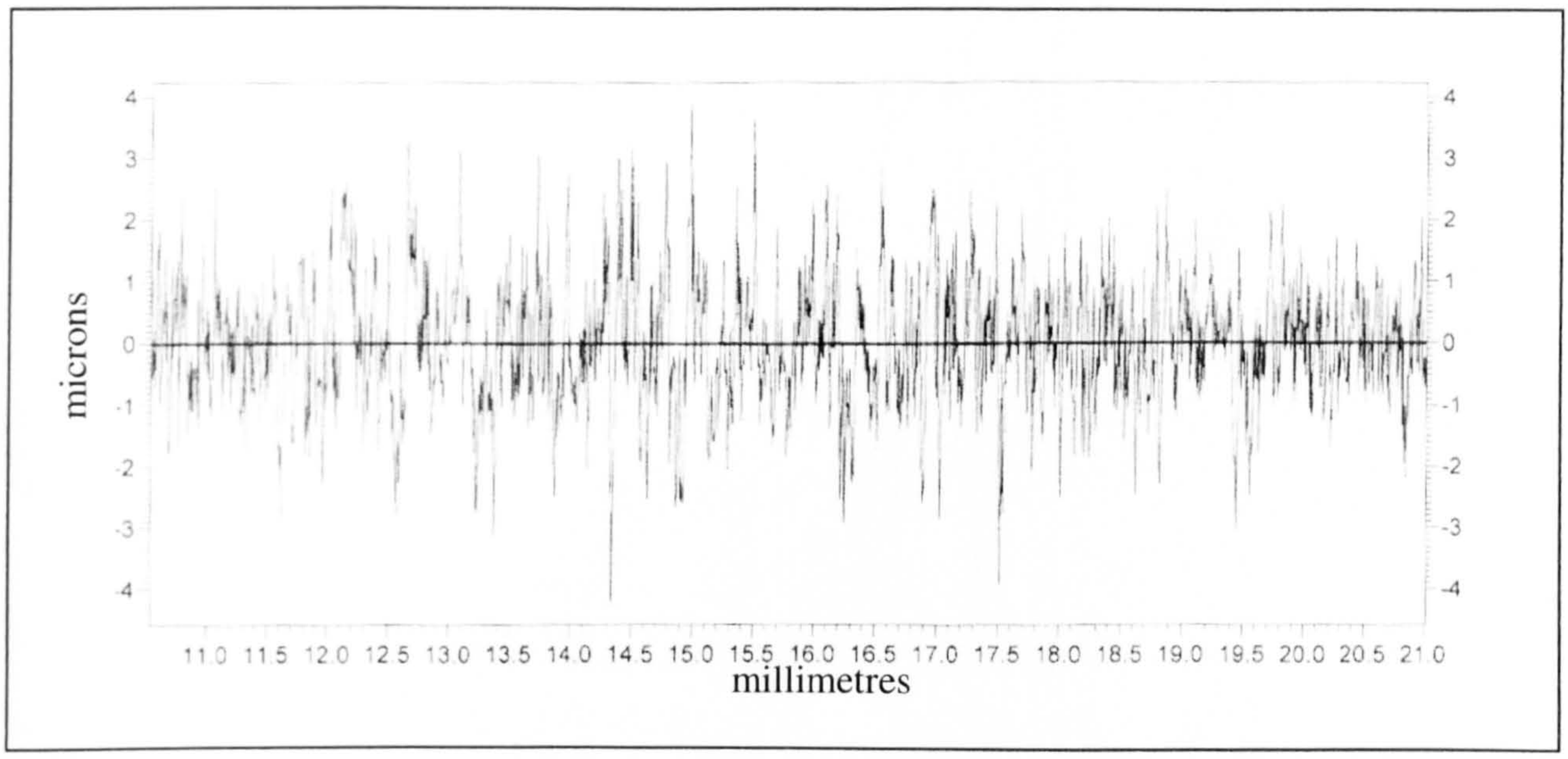

Figure 6.118. Marinel, V=17m/s, 8 hours, A.R.
Surface profile with R_a=0.69μm for the entire surface.